Investigation of Thermally Assisted OSL phenomenon in oxide based phosphors for their application in Radiation Dosimetry.

By

Anuj Soni

Enrolment No: PHYS01201104009

BHABHA ATOMIC RESEARCH CENTRE, MUMBAI

A thesis submitted to the
Board of Studies in Physical Sciences

In partial fulfillment of requirements
for the Degree of

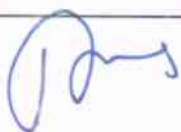**DOCTOR OF PHILOSOPHY**

Of

HOMI BHABHA NATIONAL INSTITUTE

May, 2015

Homi Bhabha National Institute

Recommendations of the Viva Voce Board

As members of the Viva Voce Board, we certify that we have read the dissertation prepared by **Anuj Soni** entitled **"Investigation of thermally assisted OSL phenomenon in oxide based phosphors for their application in Radiation Dosimetry"** and recommend that it may be accepted as fulfilling the dissertation requirement for the Degree of Doctor of Philosophy.

Chairman- Prof. A. K. Mohanty		Date: 22/05/11
Examiner- Prof. P.D. Sahare		Date 22/05/15
Guide- Prof. S. K. Gupta		Date: 22/5/15
Co-Guide -Dr. D. R. Mishra		Date: 22/05/2015
Member 1- Prof. Y. S. Mayya		Date: 22/5/15
Member 2- Prof. D Bahadur		Date: 22/5/15

Final approval and acceptance of this dissertation is contingent upon the candidate's submission of the final copies of the dissertation to HBNI.

We hereby certify that we have read this dissertation prepared under our direction and recommend that it may be accepted as fulfilling the dissertation requirement.

Date: 22th May 2015
Place: Mumbai

Dr. D.R. Mishra
Co-Guide

Dr. S.K Gupta
Guide

CERTIFICATE

I hereby certify that I have read this dissertation prepared under my direction. All the suggestions made by one of the referees in his evaluation report have been incorporated and the referee has approved these changes. Therefore, I recommend that this dissertation may be accepted as fulfilling the requirement for the Degree of Doctor of Philosophy.

Date: **Dr. S. K. Gupta**

Place: **(Convener)**

STATEMENT BY AUTHOR

This dissertation has been submitted in partial fulfillment of requirements for an advanced degree at Homi Bhabha National Institute (HBNI) and is deposited in the Library to be made available to borrowers under rules of the HBNI.

Brief quotations from this dissertation are allowable without special permission, provided that accurate acknowledgement of source is made. Requests for permission for extended quotation from or reproduction of this manuscript in whole or in part may be granted by the Competent Authority of HBNI when in his or her judgment the proposed use of the material is in the interests of scholarship. In all other instances, however, permission must be obtained from the author.

Anuj Soni

DECLARATION

I, hereby declare that the investigation presented in the thesis has been carried out by me. The work is original and has not been submitted earlier as a whole or in part for a degree/diploma at this or any other Institution / University.

Anuj Soni

LIST OF PUBLICATIONS

International Journal

1. B.C. Bhatt, **Anuj Soni**, G.S Polymeris, D.K Koul, D.K Patel, S.K. Gupta, D.R. Mishra, M.S. Kulkarni. Optically stimulated luminescence (OSL) and thermally assisted OSL in Eu^{2+} -doped $BaSO_4$ phosphor. *Radiation Measurements, 64, (2014) 35-43.*

2. D.R.Mishra, A.S. Bishnoi, **Anuj Soni**, N.S Rawat, B C Bhatt, M. S. Kulkarni and D.N. Sharma. A Versatile Laser Based Non- Linear stimulation OSL Reader System. *Nucl. Instr. Meth. in Phys. Rese. B. (2014). (Article in press)*

3. **Anuj Soni**, D.R. Mishra, B.C. Bhatt, M.S. Kulkarni, D.N. Sharma. OSL and thermally assisted OSL in dental enamel for its possible application in retrospective dosimetry. *Radiation and Environmental Biophysics (2014). DOI 10.1007/s00411-014-0554-5.*

4. N.S. Rawat, B. Dhabekar, M.S. Kulkarni, K.P. Muthe, D. R. Mishra, **Anuj Soni**, S. K. Gupta, D.A. R. Babu. Optimization of CW-OSL parameters for improved radiation dose detection threshold in α-Al_2O_3:C. *Radiation Measurements (2014), (Article in press).*

5. **Anuj Soni**, D.R. Mishra, B.C. Bhatt, S.K. Gupta, N.S. Rawat, M.S. Kulkarni, D.N. Sharma. Thermally Assisted OSL: A potent tool for improvement in minimum detectable dose and extension of dose range of α-Al_2O_3:C. *Geochronometria 40, (2013).258-265.*

6. **Anuj Soni**, D.R. Mishra, B. C. Bhatt, S. K. Gupta, M.S Kulkarni and D.N Sharma. Improvement in Dose Threshold of α-Al_2O_3:C using Thermally Assisted OSL. *Radiation Measurements, 49, (2013) 67-72.*

7. **Anuj Soni,** D.R. Mishra., B. C. Bhatt, S. K. Gupta, N. S Rawat, M.S Kulkarni and D.N Sharma. Characterization of Deep Energy Level Defects in α-Al_2O_3:C using Thermally Assisted OSL. *Radiation Measurements, 47(2), (2012), 111-120.*

8. **Anuj Soni,** D.R.Mishra, M.S.Kulkarni, K. P Muthe, S.K.Gupta, D.N. Sharma. Low Temperature TL Studies on Commercial and Developed α-Al$_2$O$_3$:C; *Radiation Protection and Environment. 34, (2011), 29-31.*

9. D.R. Mishra**, Anuj Soni.**, N. S. Rawat, M.S. Kulkarni, B. C. Bhatt and D.N. Sharma, Method of measuring thermal assistance energy associated with OSL traps in α-Al$_2$O$_3$:C phosphor. *Radiation. Measurement. 46, (2011), 635-642.*

Conference papers

1. **Anuj Soni,** D.R. Mishra., B. C. Bhatt, S. K. Gupta, M.S. Kulkarni and D.N Sharma, 2011. *Effect of UV light on the deeper traps of α-Al$_2$O$_3$:C using TA-OSL.* Proceedings of National Conference on Luminescence and its Applications (ICLA-2012)

2. **Anuj Soni,** D.R. Mishra., B. C. Bhatt, S. K. Gupta, M.S Kulkarni and D.N Sharma. *Improving Dose Threshold of α-Al$_2$O$_3$:C using Thermally Assisted OSL.* Proceedings of National Conference on Luminescence and its Applications (ICLA-2012).

3. D. K. Koul, G. S. Polymeris and **Anuj Soni**, 2014. *Response of OSL of natural quartz to firing: A case study.* International Conference on Luminescence and ESR Dosimetry (LumiDoz 8) 26-28 August 2014 ANKARA, TURKEY.

Anuj Soni

Dedicated to my Parents

and Wife

ACKNOWLEDGEMENTS

CONTENTS

SYNOPSIS

Detection and measurement of radiation are of importance for the safety of individuals working in radiation environment and general public in order to undertake appropriate protective measures. Utilization of facilities generating radiation is critically dependent on its precise and accurate assessment at various locations e.g. radiotherapy departments and nuclear power plants. This need together with the mounting societal anxiety about the harmful effects of radiation, impose very stringent requirements on the phosphors used for dosimetry typically carried out using thermoluminescence (TL) and optically stimulated luminescence (OSL) of phosphors techniques.

TL has been traditionally used for dosimetry but in recent years, OSL has emerged as an attractive alternative. OSL is the optical release of radiation induced meta-stable trapped charges (electrons and holes) in crystalline semiconductors/insulators and subsequent emission of luminescence, while in case of TL trapped charges are released by heat. OSL is a versatile technique with some inherent advantages like fast readout, option of multiple readouts, optical resetting of trapped charges and freedom from thermal quenching resulting in paradigm shift from TL to OSL dosimetry worldwide. However, it has few limitations such as requirement of light tight conditions and light induced bleaching.

Thermally assisted OSL (TA-OSL) is the phenomenon of phonon coupling with trapped charges in OSL process at elevated temperatures. It includes any combination (linear, non-linear, and isothermal) of thermal and optical stimulation (TL+OSL), depending on the application and the defect of the phosphor characterized. For example, it can be the combination of constant optical stimulation with linear heating or constant optical stimulation at elevated temperature and so on. We may note that, every OSL may be called TA-OSL in the sense that it is carried out at

some readout temperature (typically room temperature) i.e., the combination of thermal and optical stimulation are always applied on the material. The dependence of the optical excitation probability on temperature (> room temperature) has been reported in the literature and mostly assigned to the so-called thermal assistance leading to more signal as compared to that at room temperature (RT) [1, 2, 3]. In general, the vibration energy of the trapped electrons increases on heating the material which in turn assists the optical photons to de-trap the electrons resulting in increase of photoionization cross-section and hence the OSL signal.

Anion deficient α-Al$_2$O$_3$:C is one of the most important ultra sensitive OSL material with TL sensitivity of 40-60 times of TLD 100; with effective atomic number ($Z_{eff} \approx 10.2$) relatively close to that of tissue ($Z_{eff} \approx 7.4$). The temperature dependence of photoionization cross-section and TA-OSL in commercial α-Al$_2$O$_3$:C OSL phosphor has been reported [1]. On the other hand, the existence of deep energy level defects in α-Al$_2$O$_3$:C have been reported and studied by photo-transferred TL (PTTL) and optical absorption methods [4]. In the current work, efforts have been made to understand the mechanism of TA-OSL in various phosphors (by measurements at different temperatures) and to enhance the dosimetric properties compared to OSL. The effect of phonon coupling on photoionization cross-section of OSL active traps in α-Al$_2$O$_3$:C (and other phosphors) at different energy levels (low, intermediate and deep energy level defects) has been thoroughly investigated. Several advantages of TA-OSL have been demonstrated including: (a) the applicability of α-Al$_2$O$_3$:C for high dose dosimetry upto 10 kGy for applications such as food irradiation compared to 10 Gy using conventional constant wave OSL (CW-OSL), (b) possibility of multiple readout, (c) ability to re-assess dose from α-Al$_2$O$_3$:C phosphor which is inadvertently exposed to light, a feature also useful for retrospective/accident dosimetry and (d) reduced minimum detectable dose (MDD) of Al$_2$O$_3$:C by a factor of 2. The

technique has stretched the dose response and hence the application of α-Al_2O_3:C in both low as well as high dose dosimetry.

TA-OSL studies have also been carried out on other OSL phosphors ($BaSO_4$:Eu^2, Dental Enamel, Quartz) to establish the wider applicability of the technique for enhancing their performance. In particular, quartz which is generally being used for geological dating application has been studied for accident dosimetry using fired samples. The developed instrumentation infrastructure facilities/reader system such as Laser based non-linear TA-OSL (NL-TA-OSL) system can be of great importance for carrying the advanced research in study of TL/OSL phosphors and low temperature TL/OSL facilities have provided useful information on the shallow defects of OSL phosphors and TL phenomenon in biological materials such as leaf, algae etc. Elevated temperature bleaching setup has enabled rapid bleaching of OSL phosphors while high power optical bleaching can be used for biological samples. The work may be extended to next generation OSL phosphors having deeper/thermally disconnected traps.

The research work carried out and compiled here in the form of thesis has been published in peer reviewed journals. An overview of the thesis contents grouped under eight chapters is as follows:

Chapter 1. Introduction

The chapter begins with an introduction of Luminescence phenomenon including details specific to TL and OSL. An overview of popular TL/OSL phosphor materials (viz. fluorides, silicates and oxides) used in radiation dosimetry is presented. Oxide based materials that are subject of present study i.e. α-Al_2O_3:C, $BaSO_4$:Eu^{2+} etc. have been discussed in detail.

Chapter 2. Formulation of TA-OSL theory and its experimental verification

The chapter begins with the theoretical formulation of newly suggested method to determine temperature independent (pre-exponential) and temperature dependent part of photo-ionization TA-OSL cross-sections. The theory has been verified by numerical simulations and experimental validation using most popular OSL phosphor α-Al$_2$O$_3$: C. Temperature dependence of cross section showed Arrhenius nature. The chapter also brings out other aspects of the TA-OSL phenomenon in dosimetry traps of grade α-Al$_2$O$_3$: C, which will be helpful in further extending the applicability of α-Al$_2$O$_3$: C in radiation measurements. Thermal assistance energy (E_A) and photo-ionization cross-section of α-Al$_2$O$_3$:C associated with TA-OSL have been determined by simultaneous stimulation with continuous 470 nm light and linearly increasing temperature.

Chapter 3. Extension of dose response of α-Al$_2$O$_3$:C

This chapter describes the formalism of a novel experimental technique to access the signal from deep traps of α-Al$_2$O$_3$:C without heating the sample to temperatures higher than 400 $^{\rm o}$C and limiting the readout time up to 120s. The linearity of the integrated TA-OSL signal from deep traps has been measured as a function of absorbed dose for the first time and found to be linear up to 10 kGy. The measured TA-OSL signal can be used to extend the applicability of α-Al$_2$O$_3$:C OSL phosphor for accidental/retrospective dosimetry in harsh conditions of light exposure and temperatures such as fire accident as well as for high dose dosimetry. Thus the technique has overcome the limitation of OSL of requirement of dark conditions. Using the technique, nature of deep traps was also identified. Theoretical approach and numerical simulations carried out to devise this technique have been presented. Temperature dependence model for α-Al$_2$O$_3$:C have been proposed to explain the TA-OSL mechanism from deep traps. TA-OSL measurements have been used to identify the nature of these deep energy level defects in α-Al$_2$O$_3$:C and also to evaluate their TA-OSL parameters. Advantages of the technique along with its limitations are

also addressed. Effect of photon energy on the TA-OSL characteristics of α-Al$_2$O$_3$:C to determine optimum photon energy and analysis temperature have also been carried out. Comparison of TA-OSL characteristics on commercial and BARC developed α-Al$_2$O$_3$:C revealed that BARC material has higher concentration of deeper defects. In addition, elevated temperature bleaching setup has been developed for its application in the fast resetting of deep traps of OSL phosphor.

Chapter 4: Improvement in MDD of α-Al$_2$O$_3$:C

This chapter illustrates the influence of electron-phonon interaction on the shape of the OSL decay curve of α-Al$_2$O$_3$:C and improvement in its minimum detectable dose (MDD) using TA-OSL. The MDD of phosphor depends on the standard deviation of the background signal which affects the signal-to-noise ratio. Theoretical formulation of signal to noise ratio analysis in CWOSL and the effect of readout temperature on the dose threshold have been presented. Numerical simulations have been carried out to explain the measured temperature and CW-OSL intensity dependence of decay constant and thus the Photo-ionization cross section. The standard deviation of the background signal reduces at lower stimulation light intensity while the readout time increases. Further, measurement at higher temperature enhances the OSL signal with faster decay due to the temperature dependence of photo-ionization cross-section. To achieve the same decay constant and more signal, the temperature of measurement was raised. As a result of lowering the stimulation intensity at higher temperature (85 ^{o}C), the standard deviation in the background signal reduces and signal increases which in turn improves the overall dose threshold of α-Al$_2$O$_3$:C by 1.8 times. In addition, optimization of OSL parameters for improvement in dose detection threshold in α-Al$_2$O$_3$:C has also been carried out. It was revealed that best S/N ratio in OSL mode is achieved when signal is integrated and acquired for initial few seconds only, thus

obviating the need of extracting complete OSL signal that takes much longer time. This provides fast throughput and multiple assessment of dose using α-Al$_2$O$_3$:C. This finding has inherent simplicity and can be deployed for OSL based countrywide personnel monitoring and other radiological applications.

Chapter 5: Development of low temperature TL/OSL reader

This chapter focuses on the effect of temperature on photo-ionization cross-section at low temperatures dose measurements that may be important if ambient temperature is low. In this context, low temperature TL/OSL reader has been developed to study the photoionization cross-section of OSL active traps at low temperatures and to determine the role of shallow traps in environmental and online OSL dosimetry. This includes electronics hardware for data acquisition as well as software. The system can record TL from (-125 to 300 °C) with programmable heating rate of 0.1 K/s to 1 K/s. It also enables OSL measurements such as CW-OSL, NL-OSL, TA-OSL and linearly modulated OSL (LM-OSL) with built in low temperature X-ray irradiation facility. Using this system, TL/OSL studies of α-Al$_2$O$_3$:C have been carried out that showed the existence of low temperature (-8$^{\text{o}}$C) OSL sensitive peak, suitable for online radiation dosimetry. It is found that at very low temperatures, conventional dosimetric traps in α-Al$_2$O$_3$:C act as deeper traps in regard with their respective photoionization cross-section. The studies suggest that the readout protocol of the OSL dosimeter based on α-Al$_2$O$_3$:C phosphor must consider the calibration temperature of the OSL dosimeter. The low temperature TL studies on commercial and indigenously developed α-Al$_2$O$_3$:C samples reveal that the vacuum annealing in graphite ambience of α-Al$_2$O$_3$ single crystals leads to the formation of same types of defects as in case of commercial α-Al$_2$O$_3$:C single crystals.

Chapter 6: Universality of TA-OSL in OSL phosphors

TA-OSL technique has been investigated on various OSL phosphors such as $BaSO_4:Eu^{2+}$, Dental Enamel $(Ca_{10}(PO_4)_6(OH)_2)$, Al_2O_3:Si Ti, Al_2O_3: Mg, Y and Mg_2SiO_4 :Tb to ascertain its wider applicability. The temperature dependence of OSL on $BaSO_4:Eu^{2+}$ showed that integrated TA-OSL signal increases with stimulation temperature between 50 and 250 ^{o}C, while between 260 and 450 ^{o}C the signal intensity decreases. This behavior is seen to arise from competing effects of thermal assistance (activation energy E_A= 0.063 ± 0.0012 eV) and depletion of trapped charges. The increase of OSL at elevated temperature can be employed for enhancing the sensitivity of phosphor for radiation dosimetry. Apart from this, the phosphor has been thoroughly characterized using photoluminescence (PL), pulsed-OSL (P-OSL), TL, CW-OSL, LM-OSL and NL-OSL techniques. The phosphor is found to be 6 and 4 times more sensitive than $CaSO_4$: Dy and α-Al_2O_3:C, respectively, in TL mode. However, its OSL sensitivity is 75 % of α-Al_2O_3:C. It was concluded that its high sensitivity and fast luminescence lifetime can be used for imaging applications similar to that of $CaSO_4$:Dy and LiF:Mg,Cu,P in TL mode, and of BaFBr: Eu in PL/OSL mode.

Similarly, TA-OSL studies on dental enamel showed that integrated TA-OSL and thus OSL signal increases with readout temperature between 100 and 250 ^{o}C due to the temperature dependence of OSL. The thermally assisted energy (E_A) associated with this increase in signal is found to be 0.21 ± 0.015 eV. This increase of OSL at elevated temperature can be employed for enhancing the sensitivity of dental enamel for ex-vivo measurements in retrospective dosimetry. Similar to $BaSO_4:Eu^{2+}$, dental enamel was thoroughly characterized using various Luminescence based techniques for better understanding of the defects. In addition, Al_2O_3: Si, Ti and Al_2O_3: Mg, Y OSL phosphors were also studied using TA-OSL for their application in radiation dosimetry.

Chapter 7: Laser based NL-TA-OSL measurement system

A novel method called Pulse Frequency Modulated Stimulation (PFMS) has been developed for providing increasing optical stimulation (non linear or linear) for different TA-OSL studies. In this method, short pulses of laser (10 kHz range) are used for optical excitation of the sample and frequency of pulses is controlled to generate average optical stimulation with desired time dependence. Short pulses are generated by chopping of light (at different frequency) from continuous wave (CW) Nd-YAG laser. Actual power at each frequency is also calibrated with a photodiode. The developed system was used to study the TA-OSL characteristics using various combinations of stimulation profiles and the results are in agreement with conventional techniques of varying time dependence of light intensity.

Chapter 8: Summary and Conclusions

This chapter presents summary of the thesis. Temperature dependence of photo-ionization cross-section and determination of thermally assisted energy level in OSL has revealed wealth of information. The theory of TA-OSL has been formulated and its various parameters have been theoretically simulated and experimentally verified. The novel technique has stretched the dose response and hence the application of α-Al_2O_3:C in both low as well as high dose dosimetry. Low temperature TL/OSL reader has been designed and developed to study the TA-OSL at low temperatures. Many other materials have been studied to explore wider applicability of TA-OSL technique. The chapter concludes with some of the aspects of the studied materials that are yet to be explored, setting the tune for the future work.

References

1. McKeever, S .W.S., Bϕtter-Jensen, Agersnap Larsen, N, and Duller, G.A.T. *Radiation Measurements 27 (1997) 161-170.*

2. Spooner, N. A. *Radiation Measurements. 23, (1994) 593-600.*

3. Chruścińska, A. *Radiation. Measurements. (2010) 45, 991-999.*

4. Akesrold, M.S., and Gorelova, E.A. *Radiation Measurements 21 (1993) 143-146.*

LIST OF FIGURES

A- B - ςC is resultant net TA–OSL.

along with TL heating at 4 k/s.

(Activation Energy (E_A)) of second deep trap $= 0.4857 \pm 0.0132$ eV.

dosimetric peak starts giving signal at 95 °C onwards. Inset figure shows the luminescence efficiency measured using elevated temperature CW-OSL vs temperature, which reveals decrease in luminescence efficiency from 120 °C onwards. Region (25 to 100 °C) - No thermal quenching, region (100 to 120 °C)- negligible thermal quenching, region (120 to 250 °C) - dominating thermal quenching.

to be 4 times more sensitive to α-Al_2O_3:C.

chosen in order to verify the quality of the fitting. (Inset shows the same in normal scale.)

three TL peaks at 112, 210 and 390 °C respectively.

variable stimulation active time $\tau_p(t)$ and constant f_m.

and TBP (l) for fixed final intensity of 8 mW/ cm^2 and time 1000s at 500 mGy absorbed dose.

LIST OF TABLES

Chapter 1

Introduction

1.1 Motivation and Background

Detection and measurement of radiation are of importance for the safety of individuals working in radiation environment and general public in order to undertake appropriate protective measures. Utilization of facilities generating radiation is critically dependent on its precise and accurate assessment at various locations e.g. radiotherapy departments and nuclear power plants. This need together with the mounting societal anxiety about the harmful effects of radiation, impose very stringent requirements on the phosphors used for dosimetry typically carried out using thermoluminescence (TL) and optically stimulated luminescence (OSL) of phosphors techniques. These techniques will be discussed in this chapter. OSL has advantages over TL but

also has few limitations such as requirement of light tight conditions and light induced bleaching. Photo-ionization cross-section being the key parameter to judge the dosimetric viability of an OSL phosphor, in this work, its dependence on temperature in case of α-Al_2O_3:C and various other phosphors has been extensively investigated using Thermally assisted OSL (TA-OSL). It has advantages under certain conditions and involves the phenomenon of phonon coupling with trapped charges in OSL process at elevated temperatures. We may note that, every OSL may be called TA-OSL in the sense that it is carried out at some readout temperature (typically room temperature).

The dosimetric traps of α-Al_2O_3:C show sub-linear dose response for doses > 1Gy and hence put limitations for high dose applications like accidental dosimetry and dosimetry for food irradiation. Thus, if a method becomes available to exploit and reliably measure the information from the deep traps using the conventional TL/OSL reader, new vistas in the field of luminescence dosimetry may emerge to overcome the limitations of OSL for α-Al_2O_3:C in high dose dosimetry. In addition certain novel experimental techniques which have been specifically devised for improvement of the dose response and hence the application of phosphors have been presented and they constitute an important ingredient of this research work. It has also lead to the development of low temperature TL/OSL faculty which can boost the R & D work for better understanding of the defects in the materials.

1.2 Luminescence Phenomena

The phenomenon of luminescence is the property of certain materials to emit light in the visible or near visible region when excited with radiation. The materials and substances that are capable of emitting light in the visible range are termed 'luminescent'. The wavelength of the emitted light is characteristic of the luminescent material. Unlike natural radioactivity, luminescence

does not occur spontaneously, but, generally requires energy to induce emission. The excitation can be caused by ultraviolet light, ultraviolet light, X-ray, gamma ray, electrons, or alpha particles, all of which can deposit energy in the material that is subsequently re-emitted in the form of visible light. The ability to store the radiation energy is an important property of certain phosphors for their application in luminescence dosimetry and is generally associated with the presence of impurity atoms (activators) and the structural defects in the luminescent material. A wide variety of natural and synthetic materials like minerals, sediments, crystals, chemical substances, biomaterials etc. are known to possess luminescence properties. However, not all are efficient enough to be put to practical use. The more efficient materials are those, which are prepared in laboratories and have a specific chemical composition. These materials exhibit a degree of reproducibility and reliability in their performance, which qualifies them for practical applications.

The luminescence phenomena are given specific names based on the type of radiation used to excite the emission from the luminescent material. Hence, we have radioluminescence (excitation by nuclear radiation), photoluminescence (excitation by optical / ultraviolet light), and cathodoluminescence (excitation by electron beam). In addition to the excitation by radiation, luminescence can also be generated by chemical energy (chemiluminescence), mechanical energy (triboluminescence), electrical energy (electroluminescence), biochemical energy (bioluminescence), sound energy (sonoluminescence), pressure (piezoluminescence), etc. Other accompanying effect that results in bright light is incandescence. It is exhibited when the material is very hot; the light from the tungsten filament lamp or a burning piece of coal are examples of incandescence. The heating of an object to such a high temperature strongly agitates the atoms and, by collision with the neighboring atoms, results in the excitation and emission of

light. At temperatures < 600 °C, this radiation is in the far infrared (which is invisible) but, at higher temperatures, shifts to the visible region.

1.3 Classification of Luminescence

Depending upon the time elapsed between the excitation and light emission, luminescence is termed as fluorescence and phosphorescence. Both phenomena have their own importance and are used extensively in a variety of applications.

In general, luminescence emission (see Fig. 1) can be explained by the transfer of energy from radiation to the electrons of the solid, thus exciting the electrons from the ground state E_g to an excited state E_e (transition (i) in Fig. 1.1a). The emission of luminescence photon takes place when an excited electron returns to its ground state (transition (ii)). The emission of light takes place a characteristic time τ_c after absorption of the radiation. The luminescence can thus be classified into fluorescence in which $\tau_c < 10^{-8}$ second and phosphorescence in which $\tau_c > 10^{-8}$ second.
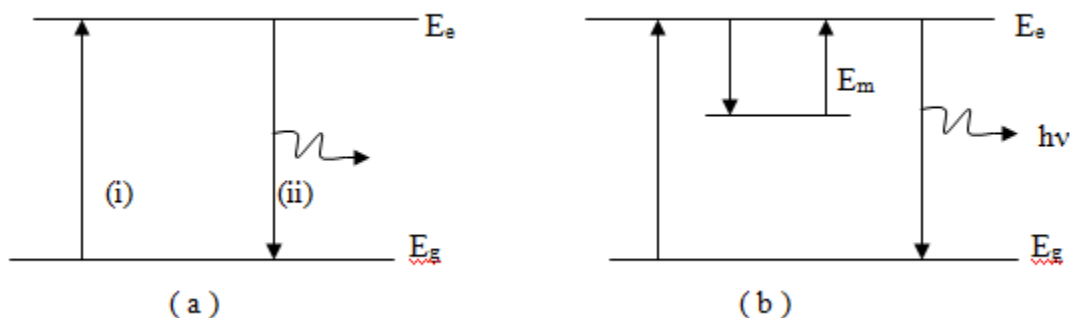
Figure 1.1: *Energy transitions involved in the production of (a) fluorescence and (b) phosphorescence.*

1.3.1 Fluorescence

The term fluorescence can be used to denote the spontaneous emission in which light emission persists to around 10^{-8} s after the source of excitation is switched off. Fluorescence emission

persists as long as the excitation is continued and stops immediately after termination of radiation. The decay time (τ_c) of the fluorescence is determined by the probability of the transition from an excited state to the ground state and is independent of temperature.

1.3.2 Phosphorescence

The phosphorescence emission continues for some time even after the excitation is removed and can be divided into short-period ($\tau_c < 10^{-4}$s), and long period ($\tau_c > 10^{-4}$s).   Practically, the only way to distinguish between fluorescence and phosphorescence is to study the effect of temperature upon the decay of luminescence as later exhibits strong temperature dependence.

The delay between excitation and light emission in this type of luminescence can be from minutes to more than 10^{10} years therefore it can be used in solid-state dosimetry for measurement of ionizing radiation. This ability to store the radiation energy is generally ascribed to the presence of activators (i.e. impurity atoms and structural defects) and is central to luminescence based radiation dosimetry which is realized through the phenomena of TL and OSL and is described in the following sections.

1.4.   Thermally Stimulated Luminescence (TL)

Thermally stimulated luminescence, usually termed thermoluminescence (TL) is the process in which a TL phosphor previously excited by ionizing radiation emits light while it is being heated. The light emitted is due to the recombination of charges trapped at metastable defect sites within the TL lattice, and its intensity is proportional to energy absorbed by the phosphor as a result of its previous exposure to ionizing radiation (ultraviolet, nuclear, cosmic rays). The excitation energy remains "frozen-in" at a relatively lower temperature in a TL material until heating stimulates its release in the form of light. As exposure of the material to radiation at room temperature leads to a progressive build-up of trapped electrons proportional to the

absorbed dose (holes are trapped in an analogous way) TL material functions as an integrating detector.

The trapping centers are levels between the conduction and valence bands. Normally, charges trapped in the phosphor lattice will remain there for periods ranging from fraction of a second to years or even hundreds of thousands of years at the ambient temperatures. This length of time is a function of sample temperature. Heating enhances de-trapping rate resulting in recombination and emission of photons in the visible region. The emitted light can easily be detected by a photomultiplier and associated electronic equipment. TL has been used extensively to measure ionizing radiation doses since the early 1950s [1].

1.4.1. Theory of Thermoluminescence

Let us assume that the TL signal is caused by the thermal release of electrons from a single type of trap, at a depth E from the bottom of the conduction band. The escape probability for a single electron per second is given by

$$p = s \exp(-E/kT)$$

(1.1)

Where s is the frequency factor, E trap depth (activation energy), k is the Boltzmann constant and T is the absolute temperature. If the trap is deep enough it will be inactive (stable) at typical environmental temperature, but will release electrons at elevated temperatures. As the temperature of the sample is raised, the recombination rate increases initially and reaches a maximum as more trapped electrons are released. Subsequently, emission decreases as the trapped carriers are depleted. Thus, the resulting TL curve (light intensity versus temperature) will be a single peak. The peak shape and the temperature T_m at which maxima occurs depend not only on the trap specific parameters such as E and s but also on the heating rate, the radiation dose and the order of kinetics. Several types of traps with different activation energies usually

result in several TL peaks. If the sample is kept at a constant temperature, the resulting luminescence is called phosphorescence due to isothermal decay of charge carriers. The different models of TL are discussed in the following.

1.4.2. Randall-Wilkins Model

Randall-Wilkins [2] in 1945 proposed a one trap one recombination (OTOR) model for thermoluminescence based on the following assumptions: i) once the electron/hole is freed from its trap the probability of its re-trapping is negligible compared to the probability of recombination, ii) the population density of the electrons in the conduction band (n_c) is negligible compared to the number of trapped electrons (n) i.e. that there is no buildup of charge carriers in the conduction band, iii) luminescence intensity at any temperature is directly proportional to the rate of de-trapping of charge carriers. If n is the concentration of filled traps at time t, then during heating, the intensity of TL with time is proportional to the rate of change of population density of trapped electrons, and can be given by

$$I(t)\alpha - \frac{dn}{dt}$$

The escape probability for a single electron per second is given by

$$p = s\exp(-E/kT)$$

$$\frac{dn}{dt} = -np = -ns\exp(-E/kT)$$

(1.2)

Where, E is the activation energy (eV), s is the frequency factor or attempt to escape factor (s^{-1}) and k is the Boltzman's constant (eV K^{-1}). The negative sign indicates that the population density of trapped electrons n decreases with time or temperature. Assuming linear heating rate of $\beta = dT/dt$, and substituting it equation (1.2) and on subsequent integration, we obtain

$$n = n_0 \exp[-\frac{s}{\beta} \int_{T_0}^{T} \exp(-E/kT)dT]$$

(1.3)

where, n_0 is the number density of trapped electrons (m^{-3}) which is dependent on the radiation dose, , T_0 is the starting temperature, $T(t)$ is temperature at any time t. The intensity of thermoluminescence $I(T)$ at the temperature T in Randall-Wilkins model is,

$$I = -\frac{dn}{dt} = n_0 s \exp(-E/kT) \exp\left[-\frac{s}{\beta} \int_{T_0}^{T} s \exp\left(-\frac{E}{kT}\right)dT\right]$$

(1.4)

It is seen that the intensity builds up as T increases, reaches a maximum value at T_m and then falls with further heating of the sample. At $T = T_m$, $dI/dT = 0$, and we obtain the condition of maxima of TL peak as

$$\frac{\beta E}{kT_m^2} = s e^{-E/kT_m}$$

(1.5)

Equation (1.5) indicates that a) at constant heating rate β we observe shift in T_m (peak temperature) towards higher temperature as E increases or s decreases, b) for a given trap (ie constant E & s), T_m shift towards higher temperature as β increases.

1.4.3. Garlick-Gibson Model

TL glow curves obtained from the solution of Randall-Wilkins equation are of first order (no retrapping and the TL glow curve falls relatively faster than in case of retrapping). Absence of retrapping is an ideal assumption as during heating the release of electrons makes traps empty and therefore the possibility of retrapping exists. Garlick and Gibson [3] in 1948 proposed a new model, which takes into account the retrapping of conduction band electrons during the TL measurement. For simplicity they assumed the retrapping and recombination probabilities to be equal:

$$I = -\frac{dn}{dt} = \frac{n^2}{N}p = \frac{n^2}{N}s\exp(-E/kT)$$

(1.6)

$$I = \frac{n_0^2 s \exp(-E/kT)}{N[1 + \frac{n_0 s}{\beta N}\int_{T_0}^{T}\exp(-E/kT)dT]^2}$$

(1.7)

Where N is occupancy index. The intensity of TL in Garlick-Gibson model is proportional to n^2, implying that the order of kinetics is two. It may be noted that a second order glow curve has increased possibility of retrapping as compared to the first-order case (i.e., the light emission is delayed). Generally TL glow curves obtained by Garlick-Gibson model are symmetric compared to Randall-Wilkins model.

1.4.4. Model for General order kinetics

The situations in which retrapping and recombination probabilities are not equal, the TL peaks are found to follow general-order kinetics. In such situations, the order of kinetics is neither one nor two but between one and two or greater than two. May and Partridge [4] in 1964 proposed an empirical relation representing general order TSL kinetics for such situations

$$I = n^b s'\exp(-E/kT)$$

(1.8)

Where, s' has dimensions of $m^{3(b-1)}\text{s}^{-1}$ and b is defined as the general order parameter and is not necessarily one or two. However, s' does not have much physical significance and the dimensions of s' change with the kinetic order. A more logical form of the general order kinetics is given by recasting of the general order kinetic equation as proposed by Rasheedy [5]

$$I = -\frac{dn}{dt} = \frac{n^2}{N}p = (\frac{n^b}{N^{b-1}})s\exp(-E/kT)$$

(1.9)

which clearly reduces to the first and second-order kinetics equations for $b = 1$ and $b = 2$. The advantage of the Rasheedy's proposal on general-order model of TL is that the difficulty encountered in the interpretation of *s* in May and Partridge model is removed.

1.4.5. Limitations of TL

From the standpoint presented so far, it is evident that TL properties of materials are intimately linked with the defect structure. The emission from a phosphor depends on the activator. The trapping details, however, are normally decided by defects and impurities of another kind. Control of such defects is an integral part of development of a dosimetry grade phosphor. Further, the collective stability of these defects with respect to temperature decides the reliability of the dose related information and thereby governs its performance as a phosphor. TL efficiency of certain materials exhibits a sharp reduction at elevated temperatures due to the dominance of non-radiative relaxations at elevated temperatures. This reduction in TL efficiency, namely thermal quenching, effectively hinders their application as dosimetric phosphor.

Heating of a sample is intrinsic to the process of TL and hence is inevitable. Moreover, it is essential to frequently subject a TL phosphor to additional heat treatments for its reuse. These heat treatments are specific to a particular material. The heat treatment especially the cooling rate may upset the defect structure and markedly influence the location, size as well as the shape of the peak and thereby the performance of a phosphor. Therefore it is necessary maintain a precise heating profile at each and every stage of TL process. Apart from these complications, the heating of a phosphor, in the long run, compromises the chemical integrity of the phosphor and limits its reusability. These deficiencies call for an appropriate solution in terms of stimulation and next portion of this chapter relates to such a technique which is based on a more convenient mode of stimulation named- *light*.

1.5 Optically Stimulated Luminescence (OSL)

In OSL process, light stimulates the release of these electrons and holes from these trapping centers, resulting in electron/hole recombination and excitation of luminescence centers in the crystal. Schematic representation of OSL process is illustrated in fig. 1.2 that depicts its use in the detection and measurement of ionizing radiation. The three stages involved in the OSL process being:

a) **Excitation** in which the OSL phosphor is exposed to ionizing radiation leading to excitations and ionizations and therefore the generation of electron/hole pairs across conduction and valence band. Subsequently, these electron/hole pairs has probability of getting trapped at defects in the crystal lattice, the energy levels for which are represented by the short horizontal lines in the band gap, in between the valence and conduction bands (Fig. 1.2a).

b) **Latency period** characterized by a metastable concentration of trapped electrons and holes (fig. 1.2b). If trap depth/potential wells associated with the trapping centers are sufficiently deep, then the thermally induced escape probability of the trapped charges is negligible at room temperature. This relatively stable concentration of trapped electrons and holes is related to the energy absorbed by the crystal during the excitation process, that is, to the absorbed dose of radiation; it represents latent information about the radiation field.
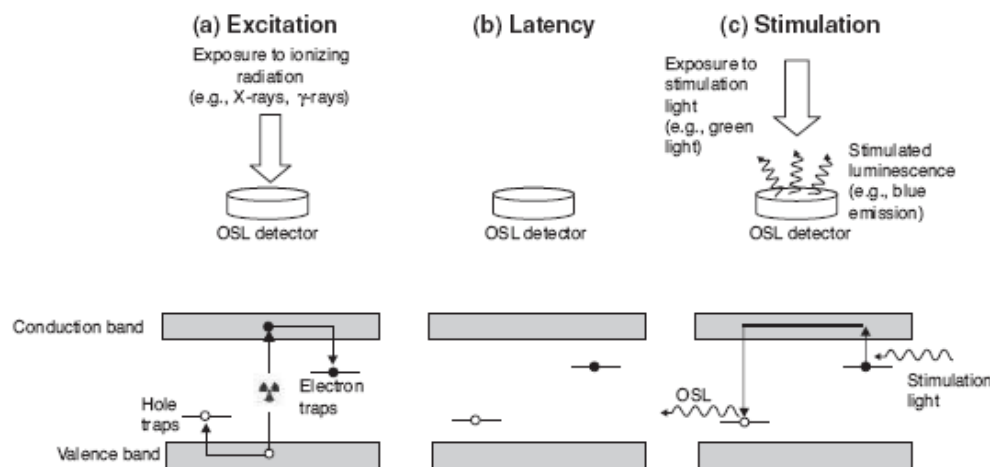
Figure 1.2. Different stages involved in the OSL process: (a) excitation of the OSL detector by ionizing radiation creating free electrons (•) and holes (∘); (b) latency period characterized by a metastable concentration of electrons and holes captured at defects in the crystal and (c) stimulation of the detector with light [6]

c) **Stimulation** by light that is eventually used to read information stored in the OSL detector (fig. 1.2c). Here a photon of wavelength λ_{stim} (e.g., green light) stimulates the electron to the conduction band. As the electron is free to move in the delocalized conduction band (but within the confines of the crystal/solid), the electron may reach and recombine with the trapped hole that creates a defect in the excited state, which on radiative relaxation to the ground state emits a photon of wavelength λ_{OSL} (e.g., blue light)[6].

Earlier OSL, was not extensively used in radiation dosimetry due to the lack of good luminescent material having high OSL sensitivity and poor post irradiation fading characteristics. However, the introduction of α-Al_2O_3:C phosphor about twenty years ago as a highly sensitive dosimetric material has attracted many researchers to work on its applications in radiation dosimetry based on the OSL technique. The potential of OSL for radiation dosimetry has been reviewed by Bøtter-Jensen and McKeever [7]. Another mode of stimulation being "Delayed OSL" (DOSL) was also

suggested for radiation dosimetry that involves optical stimulation for the transfer of trapped charge carriers from deeper to shallow traps and then monitors the phosphorescence at room temperature [8]. Phosphors such as BeO [9], $CaSO_4$:Dy [10] were used in this mode, but they exhibited low sensitivity. In a photo-transfer thermoluminescence (PTTL) technique, the irradiated samples are illuminated with suitable light to transfer charges from deeper traps to record the TL [11].

1.5.1. *Theory of OSL*

1.5.2. *Stimulation Modalities*

The OSL technique provides fine control over the stimulation process, the degree of control depending on the particular light source. Optimization of the readout process involves not only choice of stimulation wavelength, but also determination of the best modulation and duration of the stimulation intensity. Several approaches have been proposed for the OSL readout to take advantage of this degree of control.

1.5.2.1. *Continuous wave OSL (CW-OSL)*

The simplest OSL readout approach consists of stimulating the detector with light of constant intensity, a modality known as continuous-wave OSL (CW-OSL). In this case, discrimination between OSL and stimulation light is based only on wavelength separation. Therefore, it is essential that the transmission band of the detection filters does not overlap with the spectrum of the stimulation light, which is determined by the light source and optical filters used in front of it. One monitors the intensity of the luminescence as a function of time resulting in a characteristic luminescence-versus-time curve. The integral of the luminescence-versus-time curve is thus related to the trapped charge concentration, which in turn, is proportional to the initial dose of the absorbed radiation. CW-OSL is the most widely used stimulation method in dosimetry and luminescence dating due to its simplicity and frequently satisfactory performance.

Mathematical description of CW- OSL

We assume here once again one-trap/one-center model for mathematical simplification in our further discussion. One can assume quasi-equilibrium condition and the rate of change of electron population in conduction band is negligibly small as compared to the rate of change of optically stimulated depleted trapped electron concentration, i.e.

$$\frac{dn_c}{dt} << \frac{dn}{dt}, \frac{dm}{dt} \quad and \; n_c << n, \, m$$

Where, n_c and n are the concentrations of electrons in conduction band and OSL active traps respectively, m is the concentration of holes in recombination traps. Therefore, OSL intensity, I_{OSL} is proportional to rate of depleting OSL active electron traps, i.e.

$$I_{OSL} = -\frac{dn}{dt} \tag{1.10}$$

Let us consider that electrons of concentration *n* are trapped at a localized state until stimulated into the conduction band by absorption of photons (of energy hv_{ex}). The freed electrons are then able to recombine at trapped holes centers m via conduction band, producing OSL with intensity I_{OSL}. If '*f* 'is optical excitation rate (s^{-1}) of optical released charges, under no re-trapping of optically released charge carriers, i.e. first-order kinetics, equation (1.10) can be written

$$I_{OSL} = -\frac{dm}{dt} = -\frac{dn}{dt} = nf \tag{1.11}$$

The *f* can be expressed in terms of photo-ionization cross-section "$\sigma(\lambda)$" (cm^2) of trap level and stimulating light flux "$\phi(\lambda)$" (no. of photons/cm^2/sec) as

$$f = \sigma(\lambda)\phi(\lambda) \tag{1.12}$$

For a given stimulation wavelength, $\sigma(\lambda)$ remains constant for the given trap level if we keep stimulation flux constant with respect to time as $\phi(\lambda) = \phi_o(\lambda)$.

Therefore equation (1.12) can be written as

$$f = f_o = \sigma(\lambda)\,\phi_o(\lambda) \tag{1.13}$$

Incorporating equation (1.13) in equation (1.11), we get

$$I_{OSL} = -\frac{dm}{dt} = -\frac{dn}{dt} = nf_o \tag{1.14}$$

$$\frac{dn}{dt} = -nf_o \implies n = n_0 e^{-f_0 t} \tag{1.15}$$

Here n_o is initial number of trapped charges at time t = 0. Incorporating equation (1.15) into (1.14) gives following CW-OSL equation

$$I_{OSL} = n_o f_o e^{-f_o t} = I_o e^{-f_o t} \tag{1.16}$$

Where, I_o is initial CW-OSL intensity. The plot of equation (1.16) is a well-known exponential decay function with decay constant f_o (s^{-1}) as shown in Fig 1.3.
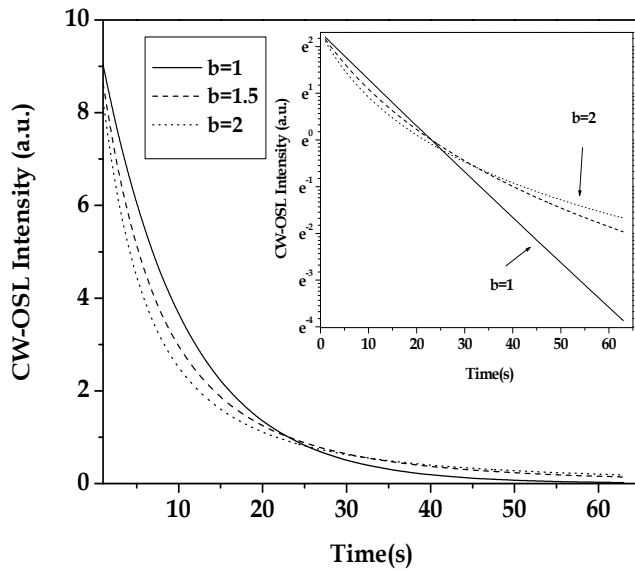
Fig. 1.3: *Variation in CW-OSL intensity curve with change in order of kinetics during readout. Inset shows the same in log Y axis scale. Inset gives the same in log scale for Y axis.*

15

However, in case of re-trapping of released charge carriers, i.e., general-order kinetic model, for the rate of recombination equation (1.14) gets modified as [12]

$$^{b}I_{OSL} = -\frac{dn}{dt} = f_{o} \frac{n^{b}}{n_{o}^{b-1}}$$

(1.17)

Where *b* (a dimensionless positive number) is kinetic order. The solution of above equation (1.17) can be derived as

$$^{b}I_{OSL} = f_{o}n_{o} \left[1 + (b-1)f_{o} t \right]^{\frac{b}{b-1}}$$

(1.18)

Where, *b> 0, b ≠ 1.*

The plot of equation (1.18) for change in order of kinetics has been shown in (Fig.1.3) for same initial number of trapped charges $n_{o.}$ The (Fig.1.3) highlights the effect of non-first order kinetics on CW-OSL curve. The inset figure shows (natural log scale plot) that the CW-OSL intensity decay is no longer linear for non 1st order kinetics.

1.5.2.2.   Pulsed OSL (POSL)

Despite the simplicity of the CW-OSL technique, the need to completely remove the scattered stimulation light often requires the use of optical filtration that ends up reducing significantly the intensity of the measured OSL signal. This problem is more critical the smaller the wavelength separation between the stimulation light and the OSL emission band becomes.

In some situations, particularly low-dose measurements, it may be advantageous to use additional temporal discrimination between the stimulation light and the OSL emission instead of extra optical filters. This can be done using a pulsed light source and a gated detection system that detects the OSL signal only in the period between the stimulation pulses, when there is no scattered light. If the intensity of the scattered stimulation light is too high, it may be necessary to gate the PMT, that is, to switch the PMT high voltage off during stimulation and back on in the period between the

stimulation pulses. However, the most practical approach is to use optical filtration to reduce the scattered light to a safe level, avoiding PMT damage, while gating only the photon counter to detect only the pulses arriving in between the stimulation pulses. This approach avoids the drastic measure of turning the PMT high-voltage on and off, improving the stability (and probably the durability) of the reader. This OSL readout modality is called pulsed OSL (POSL) [6].

The applicability of POSL for dosimetry using Al_2O_3:C detectors was first explored by Markey et al, in 1995 [13], and further demonstrated in subsequent publications [14, 15]. Fig. 1.4 illustrates a POSL scheme in which short laser pulses are used to stimulate the detector at a frequency of 4000 Hz, that is with one laser pulse every 250 µs (Fig. 1.4a). The photon counter gate is open during a 220 µs interval in between the laser pulses (Fig. 1.4b), which means that only the PMT counts arriving in this time interval are counted.
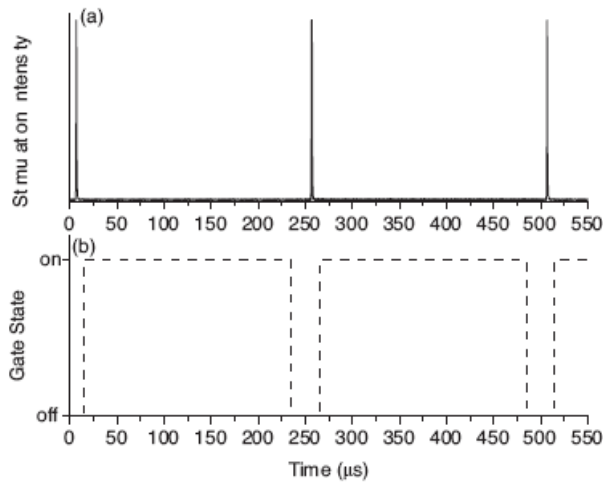
Figure 1.4. Schematics of the POSL readout scheme, showing (a) the optical stimulation pulses and (b) the gate state of the photon counter used to count the photons arriving at the PMT only between the stimulation pulses. The pulse frequency in this example is 4 kHz [6].

This temporal discrimination depends of course on the lifetime of the luminescence centers responsible for the OSL signal, which is the characteristic time scale in which the excited centers relax to the ground state once recombination takes place. If the luminescence lifetime is shorter than the stimulation pulse duration, the luminescence centers decay immediately after recombination and, consequently, the OSL emission occurs only during stimulation. In this case, the OSL intensity in the periods between laser pulses is negligible and the POSL technique is not effective. However, when the luminescence lifetime is significantly longer than the stimulation pulses, a significant fraction of the luminescence centers decays after the stimulation pulse is over, producing OSL in the period between stimulation pulses [6].

The use of pulsed OSL presents several opportunities in radiation dosimetry. Since millisecond pulses are all that is required to read the OSL signal a very rapid readout of radiation doses becomes possible. Also multiple readout of one sample is feasible since the signal is not depleted in one reading at same rate as in CW-OSL mode. Since the emission is not detected while the pulse is on, this arrangement can extend the range of stimulation wavelengths that may be used. The pulse widths of a few milliseconds, and powers ranging from 10 mW to 2 W, have been used successfully to measure OSL in Al_2O_3:C. It was also demonstrated that the shorter the excitation pulse, the greater is the amount of light emitted after the pulse compared with that emitted during the pulse [16]. The high sensitivity and point-by-point rapid OSL readout features also allow use of the method for imaging the distribution of the dose over large area detectors [17].

1.5.2.3.   *Linearly Modulated OSL (LM-OSL)*

In the LM-OSL mode, the stimulating light intensity at the sample position is increased linearly from zero to a maximum as a function of time to obtain the OSL curve. The OSL output is observed to increase steadily and reaches its maximum peak value (OSL peak), after which the OSL intensity

decreases non-linearly to zero due to depletion of charge carriers. This method is useful for distinguishing between OSL originating from different traps. For a material having more than one type of OSL traps, LM-OSL technique yields a series of OSL peaks as a function of read-out time. Each peak corresponds to a different trap, with traps having largest photo-ionization cross-section (σ) emptying first. In LM-OSL, from the knowledge of ramp rate, one can determine the photo-ionization cross-section at the wavelength used in the experiments. This technique has been applied to a variety of materials including quartz and sapphire.

Mathematical description LM-OSL

In LM-OSL method, the OSL output is observed to increase initially linearly as stimulation intensity increases, reaches a maximum value with respect to time, after which the OSL intensity decreases non-linearly to zero [12]. The time at which the luminescence intensity reaches its peak value is dependent on the variation of stimulating intensity ramp rate γ ($Wcm^{-2}s^{-1}$) (expressed in terms of photon fluence rate, i.e. photons $cm^{-2}s^{-2}$) with respect to time and photo-ionization cross-section σ of the trap. The traps with different photo-ionization cross-sections result in multiple peaks in LM-OSL curve. One can assume quasi-equilibrium condition i.e, the rate of change of electron population in conduction band is negligibly small as compared to the rate of change of optically stimulated depleted trapped electrons concentration. Considering the linear variation of stimulating light flux $\phi(t)$ as

$$\phi(t) = \phi(\lambda, \gamma, t) = \gamma t \qquad (1.19)$$

Now re-writing the optical excitation rate in f(t), the LM-OSL case can be written as

$$f(t) = \sigma(\lambda)\phi(t) = \sigma \gamma t \qquad (1.20)$$

The LM-OSL intensity can be given as

$$I_{LM} = -\frac{dn}{dt} = f(t)\, n = \sigma\, \gamma\, n\, t \tag{1.21}$$

Solution of above differential equation will be

$$I_{LM} = \sigma\, \gamma\, n_o\, t\, e^{-\left(\frac{\sigma\gamma}{2}\right)t^2} \tag{1.22}$$

The above equation gives the LM-OSL intensity under no re-trapping of optically released charges, i.e. 1ˢᵗ order of kinetics. Fig. 1.5 shows the plot of equation (1.22) for 1ˢᵗ order, 2ⁿᵈ order and general order kinetic.
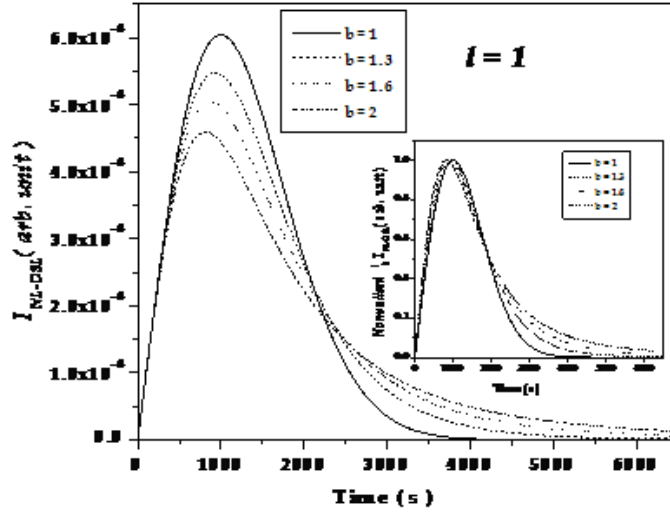
Figure 1.5. Variation of LM-OSL intensity under first and general order kinetics. Inset figure shows the normalized LM-OSL intensity.

The condition for OSL intensity maximum can be obtained by applying the condition of maximum to equation (1.22), we get

$$\left(\frac{dI_{LM}}{dt}\right)\bigg|_{t=t_{max}} = 0 \qquad \Rightarrow \qquad t_{max} = \frac{1}{\sqrt{\sigma\gamma}} \tag{1.23}$$

Where, t_{max} is the time required to reach the maximum in OSL intensity curve. As we can see from equation (1.23) that the photo-ionization cross-section comes in the denominator, for a fixed γ, the different photo-ionization cross-sections associated with various trap levels results in distinct OSL peaks in LM-OSL intensity curve. This is why this technique is extensively used to estimate the possible photo-ionization cross-sections associated with OSL active trap levels in luminescent material. The value of LM-OSL intensity at t_{max} can be given by incorporating equation (1.23) into (1.22) as

$$I_{LM-\max} = n_o \sqrt{\sigma\gamma}\ e^{-\frac{1}{2}} \tag{1.24}$$

From this equation it can be seen that the value of peak maximum increases with increase in photo-ionization cross-section, as well as with increase in value of intensity ramp rate γ.

In case of re-trapping of optically stimulated charges we have LM-OSL intensity ($^{b}I_{LM}$) as

$$^{b}I_{LM} = -\frac{dn}{dt} = f\ \frac{n^b}{n_o^{b-1}} = \sigma\ \gamma\ t\ \frac{n^b}{n_o^{b-1}} \tag{1.25}$$

The solution of above differential equation gives

$$n = n_0 \left[1 + (b-1)\ \frac{\sigma\ \gamma\ t^2}{2} \right]^{b/1-b} \tag{1.26}$$

Where, $1<b\leq2$.

Incorporating equation (1.26) into (1.25) we get,

$$^{b}I_{LM} = \sigma\ \gamma\ n_0\ t^2 \left[1 + (b-1)\ \frac{\sigma\ \gamma\ t^2}{2} \right]^{b/1-b} \tag{1.27}$$

This is the equation representing the LM-OSL intensity under general order kinetics. Re-trapping decreases the value of peak intensity and LM-OSL peak occurs in shorter time but shows extended

tail in time domain due to delay in depopulating the OSL active traps and relatively longer time is taken in recording complete OSL signal with increase in order of kinetics.

The time required to reach peak of LM-OSL intensity $^b t_{max}$, can be derived by equating first derivative to be zero i.e.

$$\left(\frac{d\,^b I_{LM}}{dt} \right) \Bigg|_{t=^b t_{max}} = 0$$

$$\Rightarrow \quad ^b t_{max} = \left(\frac{2}{\sigma\,\gamma\,(b+1)} \right)^{\frac{1}{2}} \tag{1.28}$$

The increase in order of kinetics brings OSL peak in shorter time. The value of peak intensity can also be derived by incorporating equation (1.28) into equation (1.27) as

$$^b I_{LM-max} = n_0 \sqrt{\frac{2\sigma\,\gamma}{b+1}} \quad \left(\frac{2b}{b+1} \right)^{\frac{b}{1-b}} \tag{1.29}$$

From equation (1.35), it is evident that increase in order of kinetics decreases the value of peak intensity.

1.5.2.4. *Non-linear OSL (NL-OSL)*

While applying OSL, the traditional way of stimulating phosphor is continuous wave (CW)-OSL mode, where the stimulation intensity is held constant with respect to time and decay of OSL signal is recorded. The decay constant of such CW-OSL curve under 1st order of kinetics contains direct information about photo-ionization cross-section of traps participating in OSL phenomenon. The other OSL technique is the Linearly Modulated (LM)-OSL, in which the intensity of stimulation at sample increased linearly with respect to time. This leads to multiple OSL components in LM-OSL curve corresponding to different photo-ionization cross-sections of the different traps participating in LM-OSL phenomenon. The LM-OSL method provides very useful information about different

22

active OSL traps along with order of kinetics [18]. The advantage of LM–OSL is obvious over CW-OSL, as the latter gives non-exponential complex decay function under very closely spaced active OSL traps having different values of photo-ionization cross-section as well as for the traps obeying non-first order of kinetics. Therefore LM-OSL technique is generally used for probing information about active OSL traps, having very close value of photo-ionization cross-sections. Mishra et al. [19] have theoretically formulated more generalized approach to Non-Linear–OSL phenomenon. Also, recently, Bos and Wallinga [20] presented a mathematical description of OSL signal under linearly, hyperbolically, exponentially and reciprocally increasing, stimulation intensity for an one-trap one recombination-center model assuming charge transfer by 1st order kinetics. In the present work, by using non-linearly modulated (particularly for parabolic profiles) OSL, we have established that NL-OSL technique provides better signal to noise ratio compared to LM-OSL technique. The extended dose linearity associated with traps having relatively larger photo ionization cross-section in α-Al$_2$O$_3$:C phosphor has also been demonstrated using NL-OSL technique.

4.5.1. Theory of NL-OSL

Using one trap one recombination center model and considering first-order kinetics, the relation for the non-linear stimulation modulation OSL (NL-OSL) intensity is given by [19]

$$I_{NL-OSL} = n_0 \, \sigma \, \gamma' t^l e^{-\left(\frac{\sigma\gamma'}{l+1}\right)t^{l+1}} \tag{1.30}$$

Where γ′ is a constant related to stimulation flux by the relation

$$\phi(\lambda) = \phi(\lambda, t, l) = \gamma' t^l \tag{1.31}$$

and 'l' is the parameter that can take values in the range $0 < l < \infty$ (like 0.1, 0.5, 1, 2…, etc). The value of l will determine the power of light modulation in the time domain, for example, l=1 will

produce linear light modulation (LM) and l=2 will lead to parabolic, non-linear light modulation.

This parameter γ' is related to stimulation flux rate at any instant of time by the relation

$$\gamma = \frac{d\varphi}{dt} = \gamma' l t^{l-1} \tag{1.32}$$

Thus l can be termed as Time Base Power (TBP) of light modulation [19]. We can express the stimulation excitation rate f by the relation

$$f = \sigma(\lambda)\gamma' t^l \tag{1.33}$$

The time required to reach the maximum value of $I_{NL\text{-}OSL}$ intensity can be obtained by applying condition of maximum intensity, which gives

$$_1^l t_{max} = [1/\sigma\gamma']^{\frac{1}{l+1}} \tag{1.34}$$

Where $_1^l t_{max}$ is the time required to reach peak intensity in NL-OSL curve for TBP being 'l' for first-order kinetics. Considering general- order kinetics and solving NL-OSL equation, we get the NL-OSL intensity for given values of l and b as

$$_b^l I_{NL-OSL} = \sigma\gamma' n_0 t^1 \left[1 + (b-1)\frac{\sigma\gamma' t^{l+1}}{l+1}\right]^{b/(1-b)} \tag{1.35}$$

Equation (1.35) represents OSL intensity under non-linear light modulation for the general-order kinetics (i.e. b > 0 and $b \neq 1$). The time required to reach the maximum $_b^l t_{max}$ can be obtained by taking the time derivative of equation (1.35) and equating it to zero, we get

$$_b^l t_{max} = \left[\frac{l(l+1)}{\sigma\gamma'(b+l)}\right]^{\frac{1}{l+1}} \tag{1.36}$$

Increase in the order of kinetics will decrease the value of $_b^l t_{max}$ i.e. the OSL peak will appear in a shorter time, for both LM- and NL $-$ OSL processes. It is found that the value of $_b^l I_{NL\text{-}OSL\text{-}max}$

24

decreases with an increase in the order of kinetics for a given value of *'l'*. On the other hand, for a given value of the order of kinetics ${}_{b}^{l}I_{NL-OSL-\max}$ is found to increase with increase in *'l'*. This is expected in order to conserve the total area under all NL-OSL curves for same value of n_o (dose). Apart from this an increase in the order of kinetics results in a stretching of the LM-OSL curve in the time domain into a long tail [18].
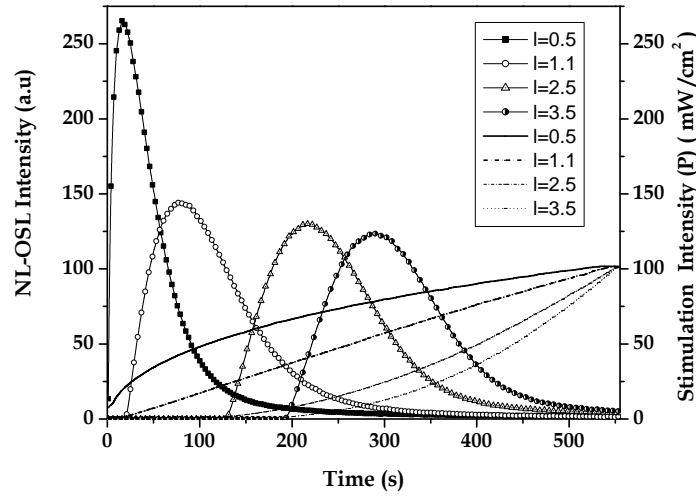
Fig.1.6. NL-OSL curves recorded for various value of TBP "l", for fixed final intensity and fix time.

1.6. Merits of OSL

The OSL is comparatively recent technique as an alternative to the TL and has significant advantages over the TL technique for various reasons, which have led to its increasing popularity in radiation dosimetry applications. OSL is normally measured at room temperature, which simplifies the design of the equipment and thus results in instrumental simplicity. The OSL dosimetry is becoming a serious contender to TL dosimetry due to its operational ease. The OSL readout method is fully optical in nature. In the routine OSL readout, heating of the sample is not required like in the case of TL, where a reliable and reproducible heating profile needs to be maintained for every TL read out (however, some additional advantages may be gained by performing the OSL at slightly

elevated temperature discussed in coming chapters). The avoidance of heating removes the problems due to thermal quenching (i.e. reduction in efficiency of luminescence as the temperature of the sample increases due to non radiative relaxations of charges) of luminescence efficiency of the phosphor and thus a significant increase in sensitivity is achieved. Since the material does not need to be heated during readout, it allows the extension of OSL material to neutron dosimetry through use of "plastic" material (as the matrix with which, the neutrons upon interaction produce knock-on protons) is possible.

Further, this all optical nature also allows remote measurement of doses which has immediate application in space dosimetry. The expansion of the exploration program of US, Asian and EU Space Agencies is leading to an increased exposure of astronauts to space radiation. Thus the customized monitoring of space radiation has acquired a high priority. In this regard, the change in certain OSL parameters is being actively used to identify and differentiate such particles involved in the space dosimetry. In several case studies, connected with such space radiation experiments, OSL has been used effectively. Thus the OSL technique offers active as well as passive space dosimetry option which can cater to such advance level radiation monitoring.

The all-optical nature together with high sensitivity of OSL has been once again proved itself beneficial to the medical dosimetry as well. In the diagnostic applications of radiation, OSL has been used with significant success in dose imaging systems. Application of OSL in this area has helped medical physicists and Oncologists to work out an irradiation plan which is efficient as well as effective. The high sensitivity of OSL also leads to the multiple readout of the same sample unlike in TL, which can be read only once, and second or repeated readouts are not possible. In OSL technique, one has a fine control over the degree to which the traps can be emptied by varying the intensity and wavelength of stimulation light. Because, it is not necessary to stimulate all the

trapped charges in order to obtain sufficient luminescence signal, with an appropriate choice of stimulation wavelength and power, the dose can be reanalyzed multiple times subject to material sensitivity. In dating and retrospective dosimetry, repeated measurements on the same sample are the basic necessity, where all necessary measurements for estimating the dose are made on a single sub-sample. In short, the lower detection limits (nGy), convenient optical stimulation, short readout time (~ ms), optical erasing of the dose, high dynamic dose range (7 order), high sensitivity, dose imaging, optical fiber based on-line remote dosimetry are some of the advantages of OSL over the TL technique.

1.7 Phosphors for OSL dosimetry

Sulfides were one of the earliest material systems to be investigated as a prospective OSL phosphor for dosimetric application [21]. In this pioneering attempt, various sulfides after irradiation were stimulated using IR light and the emitted light was used as a guide to monitor the dose received. The follow-up efforts however were reported almost a decade later which involved many sulfides (MgS, CaS, SrS) and included SrSe doped with rare earth elements like Ce, Sm, Eu [22,23]. Although these materials possessed high sensitivity to radiation, the fact that they could be read even with IR stimulation implied that their dosimetric traps were not deep and as a result these phosphors exhibited a significant fading at room temperature. Further, these phosphors also have a very high effective atomic number causing OSL response to be strongly photon energy dependent thus preventing their use in personnel monitoring.

The first report on Sulfides was immediately followed by a study in which BeO samples exposed to X-rays were stimulated by 410 nm light to cause emission of UV light. This emission was attributed to the presence of doubly occupied electron traps [24]. Although this system possesses an ever needed attributes namely near tissue equivalence, wide separation between emission and

excitation wavelengths and low cost, its toxicity has discouraged its large scale application. In the recent past, phosphors like $YAG:Ce^{3+}$, Tb^{3+}, C, $BaSO_4:Eu^{2+}$, BaFBr: Eu too have been reported to possess high OSL sensitivity.

1.7.1 Nano Phosphors

Commercial TL and OSL dosimeters providing high sensitivity and low fading have been designed on the basis of characterization and availability in large quantities of these materials and put to successful operation. However, the dose range of these traditional phosphors is normally not over 100 Gy, while higher doses need be measured in technological and medical applications (e.g. sterilization of medical products, irradiation of food products, etc.). In this connection, various nanophosphors have been synthesized and studied for their possible application in radiation dosimetry. Nanophosphors present a type of phosphors consisting of particles 10-100 nm in size, which include nanopowders, pressed compacts, nanoceramics, thin films on substrates, nanopowder coatings of different thickness, etc. [25]

Nanophosphors, such as $CaSO_4:Dy$ and $BaSO_4:Eu$, were prepared by Sahare and coworkers [26-30] who studied their TL characteristics with the objective of their application in radiation dosimetry. TL sensitivity of nanocrystalline phosphors, at low doses, was found to be much less than that of their bulk analogues. But the dose vs. TL response of these nanophosphors did not saturate up to the studied dose of $5 - 20$ kGy. Most of these nanophosphors were prepared by chemical co-precipitation method. It is reported that TL glow curves of the nanophosphors show multiple peaks compared to their bulk analogues, and TL maxima of the dosimetry peak appear shifted relative to the main dosimetric peak in polycrystalline phosphors. Nanophosphors of LiF:Mg,Cu,P and $Ba_{(0.97)}Ca_{(0.03)}SO_4:Eu$ may be useful for dosimetry of high LET beams[29,30].

Blair et al. have investigated TL and OSL properties of Al_2O_3 nanophosphors for their possible application in radiation dosimetry [31]. The nanophosphors were prepared using solution combustion synthesis (SCS) method; use of urea as fuel resulted in a phosphor with more desirable characteristics. However, TL and OSL sensitivity of the nanophosphor was about 1/100th of the commercial Al_2O_3:C TL/OSL phosphor. Nanophosphor showed multiple TL peaks compared to the Al_2O_3:C phosphor and its dose vs. OSL response was similar to that of the commercial phosphor. Kortov [32] has reported that nanoceramics can be used up to the maximum of 30 kGy as compared to the useful dose range up to 10 Gy for the bulk Al_2O_3:C. For nanoparticles, increase in surface to volume ratio would lead to formation of high concentration of surface defects, including F-type surface centres. The appearance of multiple peaks in nanophosphors has also been related to high concentration of surface trapping centres/defects. Specific causes of low luminescence efficiency are not known. For nanophosphors, after gamma or beta irradiation, spontaneous recombination losses may occur, which result in less storage in terms of trapping in metastable states. This could be one of the reasons for observing less intense TL peak in nanophosphor than in their bulk analogues at relatively low doses. Increase in surface defects may lead to increase in non-luminescent relaxation processes. Kortov[25] explained the higher radiation resistance of nanophosphors (which is also the reason for extended dose response) as due to efficient sinking and annihilation of defects at nanograin boundaries; as a result, accumulation of defects in nanomaterial is retarded. Previous works [33, 34] showed that degree of crystallinity and the presence of impurities, including OH- groups, are detrimental to luminescence efficiency in nanophosphors. In this context it is interesting to note that nanosheet $CaSO_4$:Mn [35], having an average thickness of 35 nm, synthesized by hydrothermal method, gives TL sensitivity eight times higher than that of LiF:Mg,Cu,P(GR-200) commercial phosphor

hot-pressed chips (about 200 times that of LiF:Mg,Ti(TLD-100)). Nanocrystalline phosphor gives three TL peaks at 485, 504 and 526K, compared to a prominent TL peak at about 373K in polycrystalline phosphor. Its dose response was linear up to 7 Gy, before leading to saturation at higher doses. This indicates that the method of synthesis used plays an important role in determining the characteristics of nanophosphor.

Soft tissue equivalence (Z_{eff} =7.4) of diamond (Z=6) and its chemical stability make it an attractive material for dosimetry, particularly for medical applications. Chemical vapor deposited (CVD) polycrystalline diamond films exhibited a prominent TL peak at about 280 °C with linear dose response up to 20 Gy. However, the synthesis process and growth conditions can strongly influence the TL signal in CVD diamond. Recently, nanodiamond films grown from Tequila using pulsed-liquid injection chemical vapor deposition(PLICVD) technique has been reported to be promising for the high-dose dosimetry [36]. Nanodiamond thin films show TL glow curve with peaks at 170 and 350 °C. The dose response of these films was reported to be linear in the dose range 100 to 1600 Gy. However, direct comparison of TL sensitivities of CVD polycrystalline diamond and nanodiamond films is not readily available in the published literature. Thus, nanophosphors could find many potential applications in the field of radiation dosimetry, such as low-energy beta dosimetry, high-LET dosimetry, and high-dose dosimetry for technological applications.

1.7.2. Bulk Phosphors

1.7.2.1 BaSO$_4$:Eu^{2+}

Rare earth (RE)-doped alkaline earth sulphates based TL materials have been studied since 1970. Of these, CaSO$_4$ doped with dysprosium gained special attention due to its high sensitivity to radiation and is being used as a personal dosimeter for the radiation workers. Many attempts

were made to improve the sensitivity of this phosphor. RE-doped $BaSO_4$ phosphors are studied

for its thermoluminescence (TL) properties by various groups [37, 38]. Europium-doped $BaSO_4$

was found to have better dose linearity and TL sensitivity than presently used $CaSO_4$:Dy

phosphor. These studies employed materials synthesized by methods such as re-crystallisation,

co-precipitation and solid-state diffusion at high-temperature sintering etc [39, 40]. Gonzalez et

al. [41] have reported recently that $BaSO_4$:Eu crystals prepared by the crystallization technique

were found to be three to four times more sensitive than $CaSO_4$:Dy. But the dosimetric peak

appears at 175 °C, which results in more fading during post-irradiation storage at ambient

climatic conditions. The studies present the TL characteristics of $BaSO_4$:Eu^{2+} phosphor prepared

through the new, simple, high-temperature solid-state diffusion technique, which is three to four

times more sensitive than the $CaSO_4$: Dy TL phosphor. Though, $BaSO_4$:Eu^{2+} has been

thoroughly studied for its application in radiation dosimetry, its OSL and TA-OSL response was

not reported so far. Therefore, it's OSL and TA-OSL properties have been investigated and

described in detail in chapter 6.

1.7.2.2 Mg_2SiO_4:Tb

Mg_2SiO_4:Tb is an attractive thermoluminescent material because of its high sensitivity to

gamma-rays and chemical stability [42, 43, 44]. It was first introduced by a Japanese group [45,

46]. The phosphor was subsequently produced on commercial scale and marketed by Kasei

Optonix Ltd., Japan. Recently, Prokic and Yukihara have reported development of ultra-high TL

sensitive Mg_2SiO_4:Tb. Mg_2SiO_4:Tb has been synthesized by sintering technique under the

reaction between the stoichiometric amounts of MgO and SiO_2 with the addition of optimal

Tb_4O_7 activator concentration of about 12 mg atoms Tb per mole of Mg_2SiO_4 [44]. It was

sintered for 1h at 1660 °C in air under extremely slow heating rate in an electric furnace. Finally

the polycrystalline phosphor was crushed and sieved in the grain sizes between 75 and 200 μm. After cold pressuring of polycrystalline material with pellets of 4mm diameter and 0.8mm or 0.4 mm thickness, they were sintered under the same conditions like during the preparation of the crystalline phosphor. The sintered TLD pellets are opaque and very hard. The phosphor has a simple glow curve with main TL peak at about 210 °C and very low fading. Its TL sensitivity is reported to be 110 times that of LiF:Mg,Ti (TLD-100), with a detection threshold of 1μGy. Mittani et al., 2008 have reported optically stimulated luminescence and TL of this phosphor [47]. In OSL mode, the minimum detectable dose was estimated to be 30-50 μGy. Its dose response was linear up to studied dose of 5 Gy. Thus, it can be a potential phosphor for radiation dosimetry. A detailed TL and TA-OSL study has been carried out in the present work and described in chapter 6.

1.7.2.3 α-Al$_2$O$_3$

But so far none of these phosphors has qualified the criterion of successful commercialization. In this regard, an opening was provided by TLD-500 i.e. α-Al$_2$O$_3$:C. Originally this phosphor was developed by Urals Polytechnic Institute, Russia as a TL phosphor. However, the truth that this phosphor needs to be protected from exposure to light during its post-irradiation storage coupled with a masterly insight that the very vulnerability of dosimetric information to ambient light is going to make it quite amenable to dose readout by optical stimulation, lead a group at Oklahoma State University to reveal that Al$_2$O$_3$: C can as well be used as a very sensitive OSL phosphor for radiation dosimetry [48]. This material besides being exceptionally stable in thermal, chemical and mechanical terms also has a large cross-section for a broad band of stimulation wavelength (450 nm to 555 nm). Further, the lifetime of the emission from Al$_2$O$_3$:C is 35 ms which is long enough to render it appropriate to optical stimulation in the form of pulses whose widths are typically 100 ns.

The phosphor α-Al_2O_3:C has been found to be so well suited to OSL applications that currently, more than 1.5 million dosimeter badges based on α-Al_2O_3:C are in routine use for personnel and environmental monitoring.

1.7.2.3a Crystal Structure

For dosimetric purposes, only α modification of Al_2O_3 (corundum) is used, either in single or in polycrystalline form. The crystal structure of α-Al_2O_3 is rhombohedral with the unit cell containing two molecules of Al_2O_3. The large O^{2-} ions are on a slightly distorted close-packed hexagonal sub lattice with smaller Al^{3+} ions occupying two out of three sites on layers between the oxygen layers. Each Al atom is bonded to six O in the form of a distorted octahedron and each O is bonded to four Al atoms in the form of a distorted tetrahedron. There are two short Al-O bonds of 1.846 Å and four longer bonds of 1.985 Å (Fig. 1.7a). Each O also has twelve second-nearest-neighbor O atoms with distance of separation ranging from 2.524 to 2.869 Å.
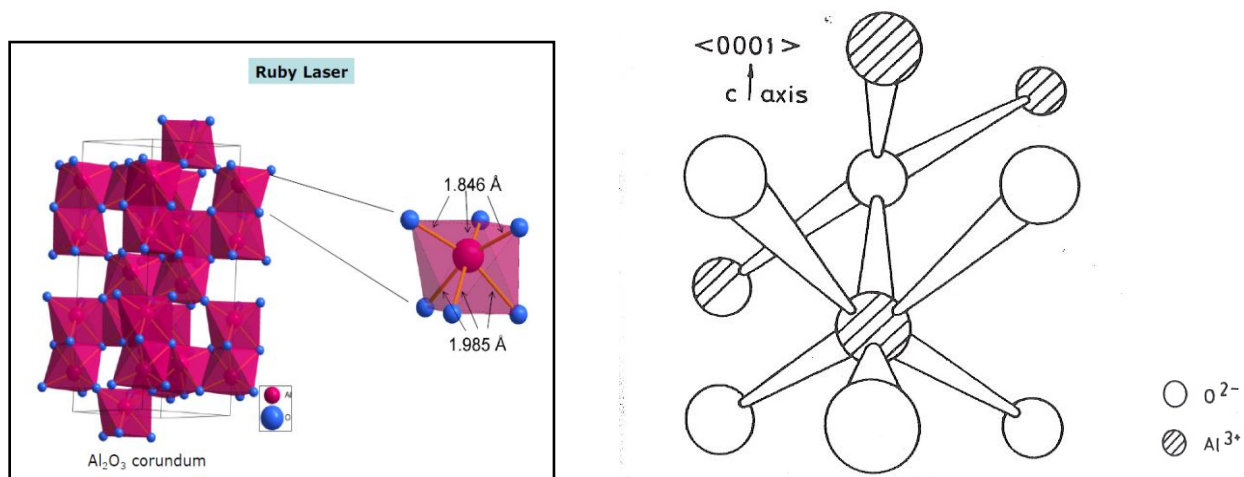
Figure 1.7a. Crystal Structure of α-Al_2O_3 b). Schematic representation of the α-Al_2O_3 lattice showing positions of Al^{3+} and O^{2-} atoms.

The structure can also be viewed as a stacking of alternate layers of O and Al atoms in the a-b plane of an equivalent hexagonal cell triple the size of the rhombohedral primitive cell. In the cation layer, half of the Al atoms are actually slightly above and the other half slightly below the plane (Fig. 1.7b). Even the highly pure Al_2O_3 crystal contains some impurities, of which the 3d series transition metals (TM) play an important role in the TL phenomenon. The impurity ions such as Cr^{3+}, substitute normally for Al^{3+} ions, not exactly occupying an Al site, but slightly displaced from it. It should also be noted, that there is a considerable proportion of covalent bonding in Al_2O_3, having an effect even more expressed on the energy levels and wave functions of substitutional TM ions than of the host Al^{3+} ion.

Though the band gap of Aluminum oxide (Al_2O_3), 9.5 eV is not as large as its Fluoride companions, it has a peculiar type of bonding. Its constituent atom Al is unique in the respect that, although technically a metal, it is not located in the left portion of the periodic table where regular i.e. alkali metals are positioned but rather towards right and borders on being a semimetal. Since its position in the periodic table is closer to oxygen than many of the other metals the difference in their electro-negativities is relatively less and bonds between aluminum and oxygen are not purely ionic but somewhere in between ionic and covalent. Moreover, Al ion has a high charge of +3 and a very small radius and thus a large charge density which makes it a strongly polarizing cation. Hence Al^{3+} ion is able to distort the electron cloud of the oxide ion i.e. it attracts the donated electrons toward itself therefore causes existence of a net effective electron density *between* the aluminum ion and oxygen anion and ensures that these electrons stay shared. This introduces a substantial covalent character in the bonding which further enhances the strength of the bonds. As a result its lattice energy is singularly large i.e. 15916 kJ/mol. Therefore a lot of energy is required to break these bonds causing the melting point of Al_2O_3 to be as high as 2080 °C.

Such a large lattice energy of α-Al_2O_3 together with its large enough band gap and its density which due to a very closely packed crystal structure equals the maximum value admissible theoretically, makes the formation of ionic defects i.e. lattice vacancies and /or interstitial ions as well as that of electronic defects related to oxygen i.e. localized electrons and holes, very difficult [49].

As a desirable consequence, the population of native charge carriers in valence and conduction bands and thus the '*zero dose background*' in this host is kept low very effectively. Further the large differences between lattice energies and melting points of oxides and halides have a direct implication that the corresponding activation energies and temperatures for movement and thereby diffusion of these defects are appreciably larger in the case of former [50]. All these factors impart alumina an exceptional thermal and chemical stability and the unique ability to accommodate, retain and preserve the defect structures in a much more disciplined manner. Alumina therefore represents a classic opportunity and a model platform to visualize, prototype, implement and thereafter actually evaluate engineering of defects in such a manner that quest for phosphor with a predictable dosimetric performance dispenses its premise.

1.7.2.3b α-Al_2O_3 as TL/OSL host material

The initial attempt towards Alumina as a host material which dates back to 1957, did not involve any intentional doping but plain Alumina samples representing various crystal phases, degree of hydration and chemical purity. The magnitude of TL signal in synthetic sapphire which is highly crystalline phase of alumina i.e. α-Al_2O_3 was found to be relatively large but typical sensitivity of these samples was about a tenth of that of TLD 100 [51]. In 1967, studies related with effect of Chromium (Cr) on Al_2O_3 revealed TL emission around 400-450 °C in the red region of the visible frequency spectrum [52]. But the thermal noise associated with these temperatures interfered with the signal itself rendering emission spectrum inconvenient for reading. The studies carried out so far

were generally confined to samples acquired out of standard commercial alumina based products which were made for purposes other than dosimetry.

First step forward in improving the sensitivity of Al_2O_3 is due to the Indian scientists who methodically devised dopants Si and Ti using a technique known as flame synthesis which involved heating the mixtures with Oxygen-Burshane (N-Butane 60%, iso- butane 18%, propane 14%) flame. They could achieve a clear fivefold increase in sensitivity over TLD-100 [53]. The next attempt involved use of dopants Mg, Ti in Al_2O_3 and revealed the TL response to be linear between 1 mGy and 10 kGy [54]. In the same year i.e. 1980 it was reported that single crystals of alumina grown in Molybdenum crucible could successfully measure doses as low as 0.1 mGy and the reason to this was ascribed to the presence of impurities Ti and Mo [55]. These attempts were however based on an approach that typically reflected a traditional mindset namely an emphasis on substitutions at cationic site.

The lateral thinking that the connection of anionic deficiencies in oxides with emissive properties too deserves to be investigated, lead Kortov and colleagues at Ural State Technical University Russia to identify the decisive role of oxygen vacancies in shaping up the luminescent properties of Zirconium oxide initially [56] and then about a decade later in Al_2O_3 [57]. The notion that led to the extension of these studies from ZrO_2 to Al_2O_3 was formed on the results of TL and **thermally stimulated exo-electron emission** (TSEE) studies**.** Earlier investigations on α- Al_2O_3 doped with Chromium had revealed that occurrence of TL was synchronous with TSEE and this was not merely accidental but they shared an intimate connection not only with each other but also with the presence of defects i.e. color centers. In TSEE a sample that has been exposed to radiation earlier is heated. The trapped electron thus gets liberated and subsequently gets localized at another trap. This diffusion continues unless and until it recombines with a hole (mostly a trapped one). The energy of

recombination is then imparted to a third electron and may cause to its transition to the states above vacuum level. Thus electron- hole recombination leads to TSEE. Likewise in TL, the first stage i.e. liberation of trapped electron to conduction band is initiated thermally; therefore activation energy of TSEE corresponds to thermal activation energy of traps. Like in TL, this description of process is equally applicable even when trapped charge carrier is a hole.

The probability of this mode of relaxation increases significantly if the impurity is positioned nearby. Thus in order to increase the TL sensitivity the necessary condition is to ensure simultaneous existence of hole and electron traps in sufficiently large concentration. It is possible to realize such condition in Al_2O_3 by doping with Mg. Here Al^{3+} is substituted by Mg^{2+} which causes formation of hole trap centers and oxygen vacancies which compensate for excess negative charge. In the case of doping Alumina with Mg, vide *two-center Auger emission'* formalism it was observed that, TSEE was accompanied by F center emission regardless of the polarity of the thermally liberated charge carrier i.e. hole or electron. This provided a valuable insight to Kortov, Akselrod and their colleagues that Oxygen vacancies in the form of F and F^+ centers act as traps as well as emission centers and therefore are of key significance in so far as enhancement of TL sensitivity of alumina is concerned [58].

In a bid to further boost the concentration of oxygen vacancies Akselrod intentionally melt alumina in the ambience of *graphite*. The strongly reducing atmosphere provided by hot graphite ensures a low partial pressure of oxygen though $C + O_2 = CO_2 \uparrow$ and $2 C + O_2 = 2CO\uparrow$. The degree of difficulty in reduction of a particular metal oxide depends on the affinity of that metal for the oxide lattice, a property characterized by the standard free energy of formation for the oxide. The heat of formation of CO_2 is -94 kcal and that of CO is -26 kcal. Therefore, Reaction 1 is favored at temperatures lower than about 650 °C, whereas Reaction 2 is expected to dominate at higher

temperatures. Notably, reaction 1 only incurs a small change in volume and therefore the change in entropy is negligibly small. Reaction 2, in contrast, involves an increase in volume and thereby larger change in entropy as well [59]. This implies that carbon can theoretically remove oxygen from any oxide provided the temperatures are high enough. Fig.1 shows the energy level diagram representing the electronic transition involved in the photo-transfer process from various traps in α-Al_2O_3: C. It has the band gap of 9 eV. In this band gap, various defects have been reported such as shallow defects (ST), low temperature defect (LT), intermediate defect also called as main dosimetric defect (MDT) and two deeper defects (DT1 & DT2). The thermal trap depth of the main dosimetric trap has been reported as 1.24 eV, for low temperature defect is 0.81 eV and for shallow trap is 0.23 eV. However, not much information is available about the thermal trap depth of deeper defects. At room temperature (25 °C) the shallow defects are unstable and only the main dosimetric trap contributes to total OSL signal. The low temperature trap has been reported to be TL sensitive only so does not contribute to OSL. The recombination centers or the luminescence centers in this material are the F and F^+ centers. They are nothing but the –ive ion (Oxygen) vacancies trapped with two or one electron respectively and are located just above the valance band.
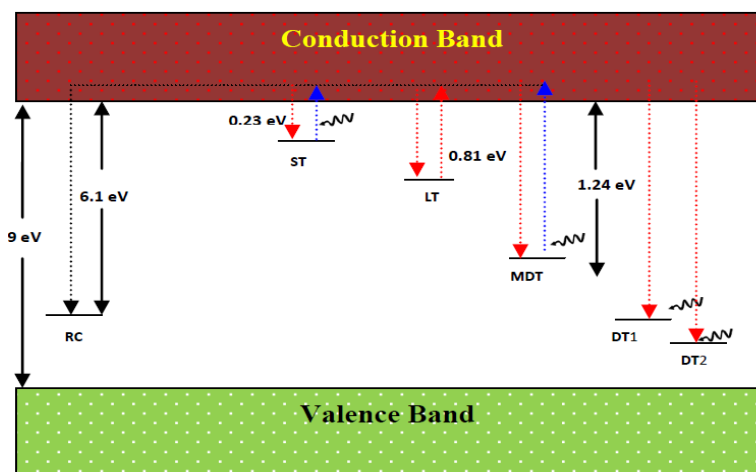
Fig. 1.8 Band diagram of α-Al₂O₃: C showing various energy levels.

1.9. Alternative approaches for preparation of α-Al$_2$O$_3$: C

Conventional method of synthesis of α-Al$_2$O$_3$: C uses Czochralski crystal growth. This 'single crystal' approach is expected to pose certain difficulties as crystal growth takes place at a specific temperature/growth rate and during the course of crystal growth, vacancies in the aluminum oxide melt have a tendency to drive forward as a result the defect concentration shows an increase along the growth axis and in the part of the crystal that solidifies last, the F center concentration is reported to be maximum. Therefore, in this mode of synthesis, it is not possible to manage the extent of incorporation of carbon into lattice and achieve homogeneity in nature and concentration of defects. As a result, dosimetric properties show undesirable variation across different regions of crystal [60]. Further, the crystal growth route is time consuming and needs expensive equipment. These factors increase the basic cost of the phosphor as well as overheads. The need to deal with these limitations of such a varied nature has prompted the successful development of a new low-cost 'polycrystalline' pathway for synthesis of this high performance multifunctional phosphor. Following are the techniques for synthesis of Al$_2$O$_3$: C which effectively generates dosimetrically relevant defects and that too in a manner which is straightforward and highly economical.

1.9.1. Post-Growth Thermal Impurification Technique (PGTI)

In PGTI method, commercially available grown plain single-crystal α-Al$_2$O$_3$ (size 10 mm × 10 mm and thickness 0.4 mm) were heated in a furnace in the presence of graphite at the temperatures ranging from 1100 to 1500 °C in the vacuum of ~10^{-6} Torr [61]. Since this new technique sets out to build the defects in an alumina crystal whose growth has already been carried out by processing it at elevated temperatures in a ambience of vacuum in the presence of carbon in the form of graphite, it is referred to as Post-Growth Thermal Impurification Technique (PGTI) described below, presented schematically in Fig. 1.9. This process is based on the concept of a measured

incorporation of impurities into solids by means of thermal diffusion whose speed and extent is well defined due to the fact that the temperatures involved are well below the melting point of solid, in particular alumina wherein diffusion is initiated at the surface of crystal and progressively expected to advance to its core. This technique is therefore anticipated to realize a slow and steady generation of defects and therefore is expected to enable the monitoring of thermal evolution of these defects vis-a-vis TL/OSL properties which is quite relevant in understanding the systematic of the mechanisms responsible to these properties.
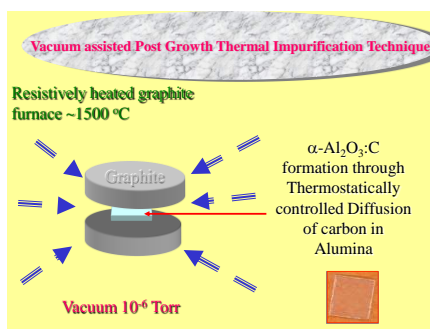
Figure 1.9. The schematic presentation of PGTI process for synthesis of α-Al₂O₃: C

The vacuum hot furnace consists of two units, one its main vacuum chamber and the other is its control unit as shown in Fig. 1.10. The single crystal along with the graphite powder was placed in the graphite crucible which was placed in the vacuum chamber. Uniform heating and cooling rates of 20 ºC/min were used. The samples were given a post-processing annealing treatment at 900 ºC for 10 min.

Control Unit

Vacuum Chamber

Inside view
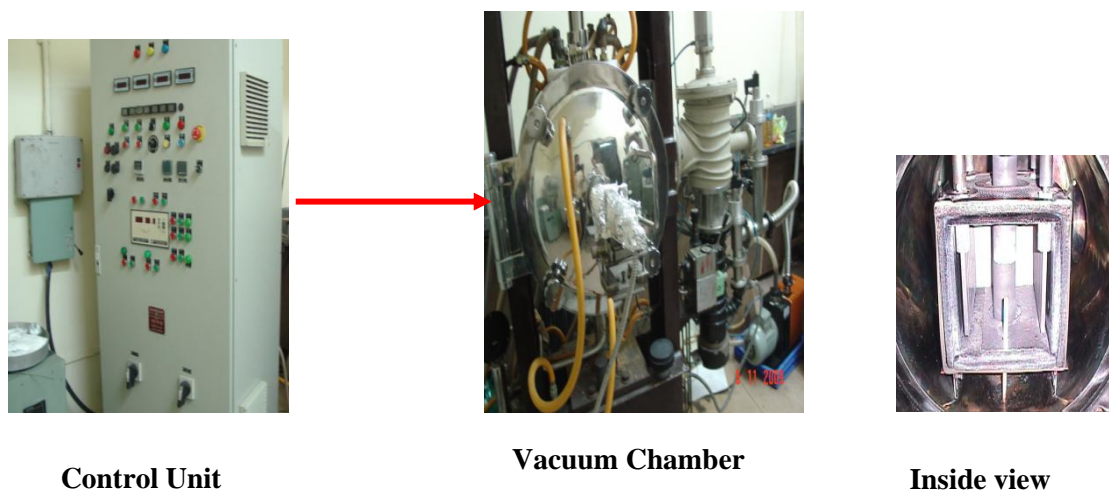
Figure 1.10. The vacuum hot furnace used for PGTI samples.

The α-Al_2O_3 crystals processed in vacuum at 1500 °C in presence of graphite for 90 minutes were found to possess excellent TL and OSL response. Hence the studies were mostly conducted for α-Al_2O_3 samples processed at 1500 °C for 90 minutes in presence of graphite.

1.9.2. Electron-gun Method

In the earlier technique for the synthesis of dosimetry-grade α-Al_2O_3:C, in which a pure α-Al_2O_3 crystal is heated to temperatures of 1500 ^{o}C in the graphite environment and vacuum allows better control over defect formation. However, the process depends on availability of single crystals of alumina as a necessary prerequisite.

In the conventional process for fabrication of OSL dosimeters, synthesized α-Al_2O_3:C single crystals are crushed to a powder using a ball mill. The TL sensitivity of powdered material has been found to be dependent on the grain size. Interestingly, the sensitivity increases with grain size and nearly saturates when the grain size is 80–100 mm [62]. This indicates that growth of single-crystalline material for dosimetry applications is not necessary and polycrystalline material with sufficient grain size may be an acceptable dosimetry material. Therefore, a process of melting

41

alumina powder in vacuum in the presence of graphite followed by cooling was envisaged as a possible simple process for preparation of dosimetry-grade alumina powder.

To confirm the feasibility of this concept, electron gun method was employed [63]. For this purpose, commercially available polycrystalline alumina powder of 99.99% purity (Make: Aldrich) was pressed into pellets of 10 mm diameter and 2 mm thickness at a pressure of 50 kg/cm^2. The sintered pellets were placed in the graphite crucible of electron gun (Hind High Vacuum make Model: EBG-PS-3 K) as shown in Fig. 1.11. The pellets were slowly heated to melting temperature (in 20 min.) and were maintained in molten state for 10 min. Subsequently, the material was cooled to room temperature in 5 min. The material so obtained was characterized for its crystalline, optical, and dosimetric properties.
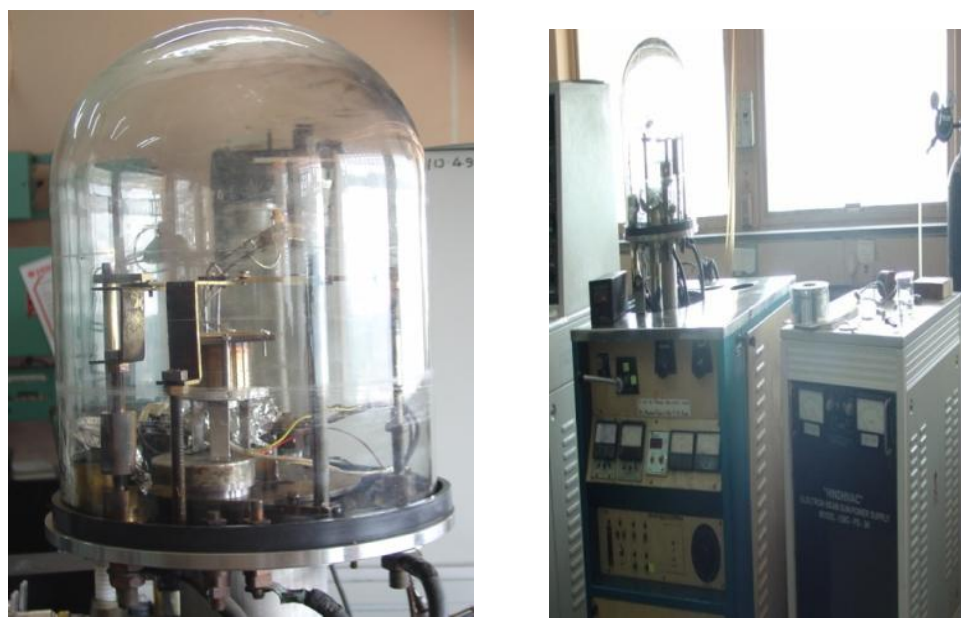
Figure 1.11. Electron gun evaporation system

1.9.3.   Melt Processing technique for Scaled up Synthesis of α-Al₂O₃:C

In this method, a stack of sintered pallets of polycrystalline alumina powder weighing ~50 gm was placed in a graphite crucible and then was melted in high temperature vacuum induction furnace depicted in Fig. 1.12 at 2000 ^{o}C at 10^{-6} Torr vacuum in a controlled manner. The furnace was cooled down to the room temperature after reaching the 2000 ^{o}C.

Figure 1.12. Inductively Heated Vacuum melting system

The processed α-Al₂O₃:C phosphor was characterized for its suitability as a viable OSL phosphor for large scale personnel and environmental monitoring applications. The TL and OSL sensitivity variation in all the processed batches of α-Al₂O₃:C is found be within ± 30% and three batches have sensitivities comparable to that of commercially available α-Al₂O₃:C phosphor (from Landauer Inc. USA). The material has shown negligible fading in both TL and OSL domain for a period of 3 weeks when compared to its TL and OSL output after 24 hours of exposure. The processed material showed very good linearity in the range 20 μGy to 5 Gy. The minimum measurable dose (MMD) is found to be 20 μGy (3σ).

1.10 Thermally Assisted OSL (TA-OSL)

Thermally assisted OSL (TA-OSL) is the phenomenon of phonon coupling with trapped charges in OSL process at elevated temperatures. Any combination (linear, non-linear, and isothermal) of thermal and optical stimulation (TL+OSL), depending on the application and the defect of the phosphor characterized, gives raise the TA-OSL phenomenon. For example, it can be the combination of constant optical stimulation with linear heating or constant optical stimulation at elevated temperature and so on. In other words, every OSL is TA-OSL in the sense that it is also taken at some readout temperature (room temperature) i.e., the combination of thermal and optical stimulation are always applied on the material. In OSL, the decay shape is dependent upon the sample, the absorbed dose, the illumination intensity and the temperature of readout. The dependence of the optical excitation probability on temperature is reported in the literature and mostly assigned to the so-called thermal assistance or to the presence of the shallow trap that is thermally depopulated at the temperatures of OSL measurement which leads to give more signal as compared to that at room temperature (RT). In general, the vibrational energy of the trapped electron increases on heating the material which in turn assists the optical photon to de-trap the electrons, which were inaccessible using optical stimulation alone. Thus, it increases the probability of interaction (i.e., photoionization cross-section) between incident photon and the trapped electron and hence the OSL signal.

1.10.1 Modes of Thermal Assistance re

The thermal assistance to the incident optical photon can be done by various ways. In general, the temperature dependence of OSL is complicated if a sample contains a significant number of shallow traps which become inactive as the temperature increases. When OSL measurements are carried out at RT, a long tail to the OSL curve is often observed. This can be attributed to the

influence of shallow traps which localize charges released during illumination and slowly release them again at a rate determined by the trap depth and the sample temperature. Since at low temperatures, where the half-life of the charge in the shallow traps is much longer than the decay time, a small OSL signal is obtained due to trapping in the low temperature traps. At high temperatures, where the trap lifetime is very small, a much increased OSL is obtained. After the initial increase the decay curve is approximately exponential initially, but departs from exponential at longer times. In this way shallow traps may slow down the OSL decay processes. Furthermore, shallow traps give rise to a temperature dependent OSL component since at higher temperatures they become less effective at trapping charge. Measurement at elevated temperature reduces the effect of the shallow traps considerably since these states cannot store any charge which is optically transferred to them from deeper traps. Similar observations may also be expected, however, from the d-a recombination model discussed above. Here excitation into an excited state leads to the overlap of the excited state wave functions and a thermally assisted hopping motion, leading to recombination, takes place. As discussed, this is thermally activated with an activation energy E_h [64].

Thermally activated process may also take place via a thermally assisted transition into the delocalized band. For example, OSL is observed from feldspars following illumination with infra-red light. At these wavelengths direct optical excitation from the deep trap into the conduction band is unlikely and thus a thermally assisted transition was postulated by Hütt et al. [65] in which the IR excites the electron into an excited state, from where it may be thermally excited into the delocalized band with a thermally activated probability which follows an $\exp\{-E_A/kT\}$ law. By monitoring the OSL obtained as a function of temperature an estimate was

obtained for E_A. In either of the above cases, the OSL is seen to be thermally activated, but the interpretation of the activation energy is quite different.

A detailed study by Poolton et al. [66] showed that the value of the measured thermal activation energy for OSL in feldspars is dependent upon the wavelength of the light used to stimulate the OSL. Even for green light stimulation small activation energy is obtained. The interpretation of this by Poolton et al. [66] was that the light stimulated the electrons into low lying band tail states, and the activation energy (E_H) represented a hopping motion through these tail states. Similar observations were made by Spooner for OSL in quartz stimulated by green light [67]. Spooner postulated the existence of an array of available states in the ground state of the trap. The upper levels of this array are accessed at higher temperatures, with activation energy, requiring a smaller optical energy to excite the charges into the delocalized bands. It should be recalled, however, that when stimulated with green light the charge is excited to the delocalized bands, and shallow traps in the material can also give rise to a thermally dependent OSL signal in these circumstances. The critical energy in this case is the shallow trap depth, E_t. Each of these processes is indicated schematically in Fig. 1.13.
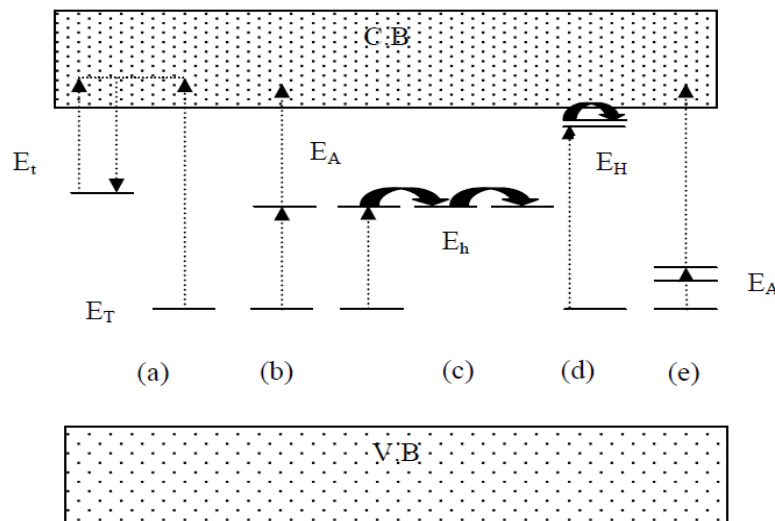
Fig.1.13. Schematic representation of the processes suggested to give rise to a temperature dependence for OSL production [68]. These include: (a) the effect of shallow traps [68]; (b) thermal assistance from an excited state [65]; (c) d-a hopping [64]; (d) band tail hopping [65]; and ground state excitation [67].

In case of Al_2O_3:C, the stimulation is not restricted to one particular wavelength, transition of charges from the deeper traps to the higher electronic states is unlikely, instead it moves to higher vibrational state of the same electronic state as a effect of temperature. The coming chapters will discuss the temperature dependence of photoionization cross-section of dosimetric traps, deeper traps and shallow traps of α- Al_2O_3: C separately in detail.

1.11. Summary

In this chapter we have presented an introduction of Luminescence phenomenon that includes the details specific to TL and OSL. α-Al_2O_3:C developed using different approaches was presented. We have also seen how the defects produced due to dopants can decisively improve sensitivity of a material system. Thus the dosimetric performance of a material critically depends on defect concentration, its nature and distribution throughout the host lattice. Consequently, studies of these defects assume critical importance as they not only offer important insights into the mechanism of their operation but also provide clues about prospective material systems which can be relevant to dosimetric applications. In the end, an introduction to the TA-OSL phenomenon and various modes of thermal assistance to charge transfer is presented. Next chapter deals with theoretical formulation of TA-OSL and its application on the dosimetric trap of α-Al_2O_3:C.

References:

1. Daniel, F., Boyd, C. A., Sanders, D. F. 1953. *Science* 117, 343.

2. Randall, J.T., Wilkins, M.H.F. 1945. *Proc. R. Soc.* A 184, 366.

3. Garlick, G.F.J., Gibson, A.F. 1948. *Proc. Phys. Soc.* 60 574.

4. May, C.E., Partridge, J.A. 1964. *J. Chem. Soc.* 40, 1401.

5. Rasheedy, M.S. 1993. *J. Phys.: Condens. Matter* 5, 633.

6.   Yukihara, E G. and McKeever, S. W. S. 2011. *A Jo*hn Wiley and Sons, Ltd., Publication*.

7. Botter-Jensen, L. and McKeever, S. W. S. 1996. *Radiat. Prot. Dosim.* 65 (1-4), 273.

8. Yoder, R. C. and Salasky, M. R. 1997. *Health Phys.*, 72, S18.

9. Rhyner, C. R. and Miller, W. G. 1970. *Health Phys.*, 18, 681–684.

10. Pradhan, S. and Bhatt, R. C. 1981. *Phys. Status Solidi A*, 68, 405–411.

11. Miller, S., Endres, G. R., McDonald, J. C., Swinth, K. L. 1988. *Radiat. Prot. Dosim.* 25, 201.

12. Bulur, E. 1996. *Radiat. Meas.* 26, 701.

13. Markey, B. G., Colyott, L. E. and McKeever, S. W. S. 1995. *Radiat. Meas.* 24, 457.

14. Akselrod, M. S. and McKeever, S. W. S. 1999. *Radiat. Prot. Dosim.* 81, 167.

15. McKeever, S. W. S. and Akselrod, M. S. 1999. *Radiat. Prot. Dosim.*, 84, 317.

16. McKeever, S. W. S., Akselrod, M. S. and Markey, B. G. 1996. *Radiat. Prot. Dosim.* 65, 267.

17. Akselrod, M. S., Agersnap Larsen, N. and McKeever, S. W. S. 2000. *Radiat. Meas.*, 32, 215.

18. Kitis, G. and Pagonis, V. 2008. *Radiat. Meas.* 43, 737.

19. Mishra, D.R., Kulkarni, M.S., Rawat, N.S., Muthe, K.P., Gupta, S.K., Bhatt, B.C., Sharma, D.N. 2008. *Radiat. Meas.* 43, 1177.

20. Bos, A. J. J. and Wallinga, J. 2009. *Physical Rev. B* 79, 195118.

21. Antonov –Romanovski, V.V., Keirum-Marcus, I.F., Proshina, M.S., Trapeznikova, Z.A. 1956. *Conf. of the Acad. Of Sciences of the USSR on the peaceful Uses of Nuclear Energy, Moscow, 1955, USAEC Report AEC-tr-2435* (Pt.1) 239.

22. Bräunlich, P., Schafer, D. and Scharmann, A. 1967. *Proc. International Conf. on Lum. Dosim. , USAEC* P. 57.

23. Sanborn, E.N. and Beard, E.L. ibid. P. 183.

24. Albrecht, H.O. and Mandeville, C.E. 1956. *Phys. Rev.* 101, 1250.

25. Kortov, V.S., 2010. *Radiat. Meas*. 45, 512.

26. Salah, N. et al., 2006. *Radiat. Meas*. 41, 40.

27. Salah, N. et al., 2007. *J. Lumin.*124, 357.

28. Salah, N. et al., 2009. *J. Lumin..*129, 192.

29. Lochab, S.P. et al., 2008. *J. Appl. Phys.* 104, 033520.

30. Sahare, P.D. et al., 2010. *J. Lumin.*130, 258.

31. Blair, M.W. et al., 2010. *J. Lumin.* 130, 825.

32. Jacobsohn, L.G. et al., 2008. *J. Appl. Phys.* 104, 424303.

33. Zych, E. et al., 2001. *Opt. Mater.* 16, 445.

34. Zahedifar, M. et al., 2011.*Appl. Radiat. Isot.*69, 1002.

35. Benabdesselam, M. et al., 1999. *Radiat. Prot. Dosim*. 84, 257.

36. Morales, J. 2010. *Radiat. Prot. Dosim.* doi:10.1093/rpd/ncp292.

37. Azorin, J, Furetta, C., Gutierrez, A., Gonzalez, P., 1991. Appl. Radiat. Isot. 42, 861-863.

38. Okamoto, Y., Kawaguchi, S., Kino, S., Miono, S., Kitajima, T., Misaki, A., Saito, T., 1986. Nucl. Instrum. Meth. Phys. Res. A243, 219-224.

39. Atone, M. S., Dhoble, S. J. And S. V. Moharil. 1993. Radiation effects and defects. 127, 225-230.

40. Madhusoodanan, U., Jose, M. T. and Lakshmanan, A. R. 1999. *Radiat. Meas*. 30, 65–72.

41. Gonzalez, P. R., Furetta, C., Calvo, B. E., Gaso, M. I.and Cruz-Zaragoza, E. 2007.*Nucl. Instrum. Methods Phys. Res. B.* 260, 685–692.

42. K. Ayyangar, A.R.Lakshmanan, Bhuwan Chandra and K. Ramdas, Phys. Med. Biol. 19, 665 (1974).

43. A.R. Lakshmanan and K.G.Vohra, Nucl. Instru. Meth. 159, 585 (1979).

44. M. Prokic and E. Yukihara, Rad. Meas. 43, 463 (2008).

45. T. Hashizume, Y. Kato, T. Nakajima, T.Toryu, H.Sakamoto, N.Kotera and S.Eguchi, Proc. Symp. In Radiation Detectors, IAEA-SM-143/11, Vienna, p.91 (1971).

46. T.Toryu, H.Sakamoto, N.Kotera and H. Yuruda, In Proc. Int. Conf. on Luminescence, Leningrad, USSR, pp. 685-689 (1973).

47. J.C.Mittani, M. Prokic and E.G.Yukihara, Rad. Meas. 43, 323 (2008).

48. Markey, B.G., Colyott, L.E. and McKeever, S.W.S. 1995. *Radiat. Meas.*24, 457.

49. Prescott, R. and Graham, M.J. 1992. *Oxid. Met.* 38, 233.

50. Popov, A.I., Kotomin, E.A., and Maier, J. 2010. *Nucl. Instrum. Methods. in Physics Research B* 268, 3084.

51. Rieke, J. F., Daniels, F. J. 1957. *J. Phys. Chem.* 61, 629.

52. Philbrick, C.R., Buckman, W.G. and Underwood, N. 1967. *Health. Phys.* 798.

53. Mehta, S.K. and Sengupta, S.1976. *Phys. Med. Bio.* 21, 955.

54. Osvey, M. and Biro, T. 1980. *Nucl. Instrum. Methods* 175, 60.

55. Kvapil, J., Vitamvas, Z., Perner, B., Kvapil, Jos, Maneck, .B., Admatez, O. and Kubelka, J. 1980. *Krist. Tech.* 15 859.

56. Kortov, V.S., Polezhaev, J.M., Gaprindashvily, A.I., Shaljapin, A.L.,. Nauk, Akd Izv. SSSR. 1975. *Ser. Neorg. Mater.* 11, 257.

57. Kortov, V.S. 1985. *Jpn. J. Appl. Phys.* 24, 65.

58. Kortov, V.S., Bessonova, T.S., Akselrod, M.S. and Milman, I.I. 1985. *Phys. Stat. Sol.(a)* 87, 629 .

59. Barker, J., Saidi, M.Y. and Swoyer, J.L. 2003. *Electrochem. Sol. Stat. Lett.* 6, 53.

60. Gimadova, T.L., Bessonova, T.S., Tales, I.A., Avvkumova, L.A. and Bodyachevsky, S.V. 1990. *Radiat. Prot. Dosim.* 33, 47.

61. Kulkarni, M.S., Mishra, D.R., Muthe, K.P., Singh, A., Roy, M., Gupta, S.K. and Kannan, S. 2005. *Radiat. Meas.* 29, 277.

62. Akselrod, M.S., Kortov, V.S. and Gorelova, E.A. 1993. *Radiat. Prot. Dosim.* 47, 159.

63. Muthe, K.P., Kulkarni, M.S., Rawat, N.S., Mishra, D.R., Bhatt, B.C., Singh, A., Gupta, S.K. *2008. J. Luminescence* 128 (3), 445-450.

64. Poolton, N.R.J., Botter-Jenson, L., Ypma, P.J.M. and Jonson, O. 1994. *Radiat. Meas*. 23, 551-554.

65. Hütt, G., Jaek, I., Tchonka, J., 1988. *Quaternary Sci. Rev*. 7, 381-385.

66. Poolton, N.R.J., Botter-Jenson, L., Jonson, O. 1995. *Radiat. Meas*. 24, 531-534.

67. Spooner, N. A., 1994. *Radiat. Meas*. 23, 593-600.

68. McKeever, S .W.S., Bϕtter-Jensen, Agersnap Larsen, N, and Duller, G.A.T. 1997. *Radiat. Meas.* 27, 161-170.

Chapter 2

Theoretical formulation of TA-OSL and its experimental verification

This chapter describes the theoretical formulation of newly suggested method to determine temperature independent (pre-exponential) and temperature dependent part of photo-ionization cross-sections. Further it describes the experimental validation of the formulated theory on the dosimetric (intermediate) traps of α-Al_2O_3:C to find the thermally assisted energy and photo-ionization cross-section associated with such traps.

2.1. Introduction

The temperature dependent nature of CW-OSL decay constant can be understood, by investigating the temperature dependence characteristics of photoionization cross-section (s) of

OSL trap, as the decay constant is product of former (i.e. s) and stimulation flux. Spooner (1994) has studied the temperature dependent nature of photo-ionization cross-section in quartz by taking elevated temperature isothermal CW-OSL measurements and suggested that the temperature dependence of photo-ionization cross-section follows Arrhenius nature [1]. It is suggested that the photo-ionization cross-section consists of basically of two parts e one is temperature independent and the other temperature dependent exponential term. Therefore, the value of photo-ionization cross-section measured at room temperature is the value of photo-ionization cross-section with thermal assistance of energy from 0 K to room temperature. In the present study, a new method has been suggested to determine the thermal assistance energy associated with OSL traps, which helps to determine the two distinct terms - temperature independent pre-exponential and temperature dependent part of photoionization cross-sections. The theoretical formulation of newly suggested method has been verified by numerical simulation and experimental validation using most popular OSL grade dosimeter α-Al$_2$O$_3$:C phosphor. The present chapter also brings out more detailed information about the phenomenon of Thermally Assisted (TA)-OSL in dosimetry traps of grade α-Al$_2$O$_3$:C, which will be helpful to extend the applicability of α-Al$_2$O$_3$:C in radiation dosimetry.

2.2 Theory of TA-OSL

Temperature dependence of photo-ionization cross-section is investigated by many researchers [1,2,3]. Spooner (1994) described this temperature dependence of photo-ionization cross-section effect in terms of thermal activation from a ground state to an intermediate excited state, with activation energy E_A, from where optical excitation to the delocalized band takes place (Fig. 2.1).
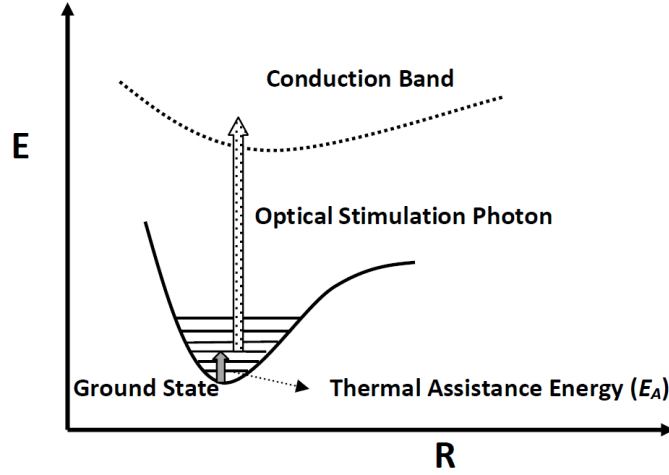
Fig. 2.1 Configuration coordinate diagram of trap level under thermally assisted optical stimulation.

The decay constant of CW-OSL curve was observed to follow Arrhenius law. This can also be expressed in terms of photo-ionization cross-section $\sigma(T,\lambda)$ as:

$$\sigma(T,\lambda) = \sigma_o(\lambda)\ e^{-\frac{E_A}{kT}} \tag{2.1}$$

Where k is the Boltzmann's constant and $\sigma(T,\lambda)$ is the photo ionization at temperature T (K) and stimulation wavelength (λ). The $\sigma_o(\lambda)$ is the a pre-exponential photo-ionization cross-section which is free from thermal perturbations. However, for optical transitions from deep traps to a parabolic delocalized band it can be expressed [4] as

$$\sigma_o(\lambda) = K\sqrt{E_o}\ \frac{(h\upsilon - E_0)^{3/2}}{h\upsilon(h\upsilon - \delta E_0)^2} \tag{2.2}$$

Where K is a constant, hυ is the energy of the stimulation light of wavelength λ, E_o is the optical ionization threshold energy for the trap, and δ is a constant ($\delta = 0.559$ for quartz; Alexander)[5]. Incorporating Eq. (2.1) into Eq. (1.13) given in chapter 1, we get:

$$f = \phi_o\ \sigma_o(\lambda)\ e^{-\frac{E_A}{kT}} = f_o(\lambda)e^{-\frac{E_A}{kT}} \tag{2.3}$$

54

2.2.1 Analysis under first-order kinetics

The assumption of first-order kinetics requires that the re-trapping of optically released charges

is negligibly small. Incorporating Eq. (2.3) in Eq. (1.11) of chapter 1, we get

$$I_{TA-OSL} = -\frac{dn}{dt} = n\,\phi_o\,\sigma_o(\lambda)\,e^{-\frac{E_A}{kT}} = n\,f_o(\lambda)\,e^{-\frac{E_A}{kT}} \tag{2.4}$$

Where, I_{TA-OSL} is the TA-OSL intensity.

Now consider the more dynamic approach to investigate the temperature dependence nature of

this Eq. (2.7) by incorporating linear increase in temperature (keeping stimulation intensity

constant) as

$$T = T_o + \beta\,t \tag{2.5}$$

Where T is the instantaneous temperature *in* Kelvin, T_o is start temperature in Kelvin. The β is

the heating rate (K/s) and t is the time (s). Further solving Eq. (2.4) for *n*, also incorporating Eq.

(2.5), we get

$$n = n_o e^{-\frac{f_o}{\beta}\int_{T_o}^{T} e^{-\frac{E_A}{kT'}} dT'} \tag{2.6}$$

Incorporating Eq. (2.6) in Eq. (2.4) and solving for I_{TA-OSL}, we get

$$I_{TA-OSL} = n_o\,f_o(\lambda)\,e^{-\frac{E_A}{kT}}\,e^{-\frac{f_o}{\beta}\int_{T_o}^{T} e^{-\frac{E_A}{kT'}} dT'} \tag{2.7}$$

Traditionally, OSL is recorded in time domain as luminescence intensity v/s time, so the Eq.

(2.7) can be rewritten in time domain as

$$I_{TA-OSL} = n_o\,f_o(\lambda)\,e^{-\frac{E_A}{k(T_o+\beta t)}}\,e^{-f_o\int_{0}^{t} e^{-\frac{E_A}{k(T_o+\beta t')}} dt} \tag{2.8}$$

Eq. (2.7) gives the TA-OSL intensity under 1st order of kinetics. The plot of numerically

generated OSL intensity is shown in Fig. 2 for input parameters being E_A = 0.241 eV, β = 2 K/s

and $\sigma_o(\lambda) = 2 \times 10^{-16}$ cm^{-2}, with CW-stimulation intensity $\phi_o = 33$ mW/cm^2 of 470 nm light. Eq. (2.7) seems to be similar to that for TL intensity for 1st order of kinetics at a given heating rate β (refer Eq. 2.9) except that the attempt to escape factor *(S),* also termed as frequency factor in the expression for TL intensity, has replace by f and thermal trap depth *(E)* by thermal assistance energy E_A in TA-OSL equation. The TL intensity equation can be expressed as (Chapter 1)

$$I_{TL} = n_o\, S\, e^{-\frac{E}{kT}}\, e^{-\frac{S}{\beta}\int_{T_o}^{T} e^{-\frac{E}{kT'}}\,dT'} \tag{2.9}$$

The temperature at which TA-OSL is maximum, can be derived from:

$$\frac{d}{dT}\left(I_{TA-OSL}\right)_{T=T_M} = 0 \tag{2.10}$$

This gives the condition as

$$\frac{E_A\beta}{kT_M^2} = \phi_o\,\sigma_o(\lambda)\, e^{-\frac{E_A}{kT_M}} \tag{2.11}$$

Where T_M is the absolute temperature in *(K)* at which TA-OSL intensity peak occurs. The shift in TA-OSL peak position (time and temperature domain) with heating rate β is shown in Fig. 2.3. For a given stimulation intensity, TA-OSL peak temperature T_M increases with heating rate β. But in time scale, TA-OSL peak occurs earlier with increase in heating rate. Also TA-OSL peak shift occurs earlier in time domain with increase in stimulation intensity ϕ_o (Fig. 4). Eqs. (2.7) and (2.11) are very useful for determining E_A and σ_o. As the initial part of the Eq. (2.7) can be considered to be dominated by 1st exponential factor term, the log of TA-OSL intensity v/s *1/kT* plot for initial part gives slope as E_A. Subsequently, Eq. (2.11) can be used for determining σ_o, as the φ_o.

Analysis under general-order kinetics (b≠1;b>1)

In this case, we assume probability of re-trapping of optically de-trapped charges. For second-order kinetics (i.e, $b = 2$) i.e. there is equal probability of re-trapping and recombination of the optically released charge carriers. However, a more general approach would be to consider general-order kinetics and solve TA-OSL equation (under constant stimulation and linearly increasing temperature), thus

$$^b I_{TA-OSL} = -\frac{dn}{dt} = \frac{n^b}{n^{b-1}} \phi_o \, \sigma_o(\lambda) \, e^{-\frac{E_A}{kT}} = \frac{n^b}{n^{b-1}} f_o(\lambda) e^{-\frac{E_A}{kT}}$$ (2.12)

Where $^b I_{TA-OSL}$ is the TA-OSL intensity for given value of ϕ_o and b. Solution of Eq. (2.12) gives the TA-OSL intensity in the case of general-order kinetics with respect to temperature as

$$^b I_{TA-OSL} = n_o \phi_o \, \sigma_o(\lambda) \, e^{-\frac{E_A}{kT}} \left[1 + (b-1) \frac{\phi_o \, \sigma_o(\lambda)}{\beta} \int_{T_o}^{T} e^{-\frac{E_A}{kT}} dT' \right]^{b/_{1-b}}$$ (2.13a)

This in time domain can be expressed as

$$^b I_{TA-OSL} = n_o \phi_o \, \sigma_o(\lambda) \, e^{-\frac{E_A}{k \, (T_o+\beta \, t)}} \left[1 + (b-1) \, \phi_o \, \sigma_o(\lambda) \int_{0}^{t} e^{-\frac{E_A}{k \, (T_o+\beta \, t)}} dt' \right]^{b/_{1-b}}$$ (2.13b)

Eqs. (2.13a) & (2.13b) represent TA-OSL intensity under constant light stimulation for the general-order kinetics (i.e. $b > 0$ and $b \neq 1$). Figs. 2.2 and 2.3 depict the numerically simulated TA-OSL intensity for various values the order of kinetics for fixed stimulation intensity. These Figs. 2.2 and 2.3 clearly show the effect of re-trapping (i.e. the order of kinetics) on the TA-OSL intensity curves. It is observed from Figs. 2.2 and 2.3 that as the order of kinetics increases the peak intensity decreases and the TA-OSL peak is obtained in a shorter time so as in temperature scale at lower temperature since heating rate β is constant.
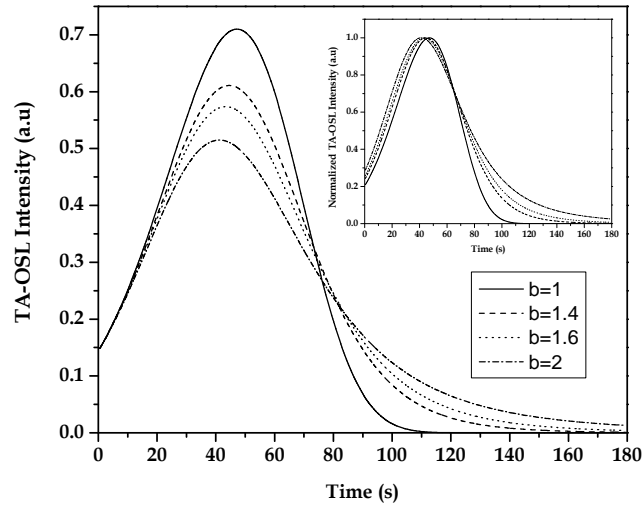
Fig. 2.2 Numerically simulated TA-OSL signal v/s time plot for various order of kinetics with β=2 k/s, E_A=0.241, $\sigma_o(\lambda) = 2 \times 10^{-16}$ cm^2 with stimulation intensity ϕ_o= of 33 mW/cm^2 of 470 nm light. The inset shows the corresponding normalized plots.
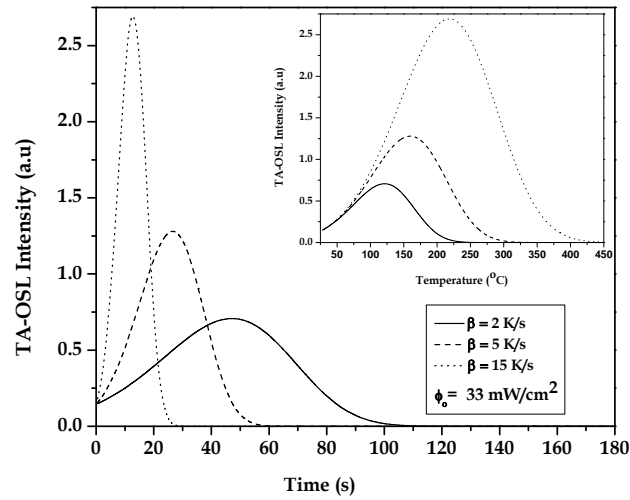
Fig. 2.3   Numerically simulated TA-OSL signal v/s time plot for various heating rates β with CW stimulation intensity ϕ_o = 33 mW/cm^2, E_A=0.241, and $\sigma_o(\lambda)$= 2 $\times 10^{-16}$ cm^2 of 470 nm light. The inset shows same numerically simulated TA-OSL signal against temperature for various heating rates.

The temperature at which maximum in TA-OSL intensity occurs can be derived by applying the following condition on Eq. (2.13a)

$$\frac{d}{dT}\left(^{b}I_{TA-OSL}\right)_{T=T_{M}} = 0 \qquad (2.14)$$

Solving Eq. (2.14), we get

$$\frac{\beta E_{A}}{kT_{M}^{2}} = b\,\phi_{o}\,\sigma_{o}(\lambda)\,e^{-\frac{E_{A}}{k\,T_{m}}}\left[1 + (b-1)\,\frac{\phi_{o}\,\sigma_{o}(\lambda)}{\beta}\int_{T_{o}}^{T_{M}}e^{-\frac{E_{A}}{k\,T'}}dT'\right]^{-1} \qquad (2.15)$$

The Eq. (2.15) gives the condition for maximum in TA-OSL intensity. Here also, as the order of kinetics increases, the TA-OSL peak will occur at lower temperature. The value of T_M also decreases with increase in value of stimulation intensity φ_o and σ_o (Fig. 2.4). Therefore, to get the TA-OSL peak in short time (temperature) one has to select higher values of heating rate and stimulation flux.
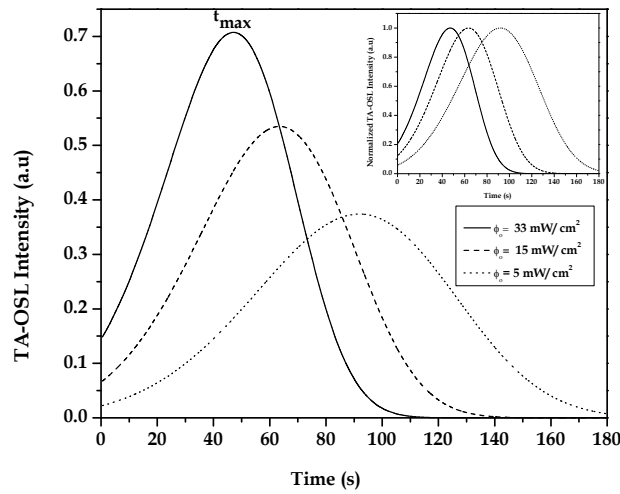
Fig. 2.4 Numerically simulated TA-OSL signal v/s time plot for various CW stimulation intensity ϕ_o with $\beta=2K/s$, $E_A=0.241$, $\sigma_o(\lambda)= 2 \times 10^{16}$ cm² of 470 nm light. The inset shows the normalized plots.

2.3 Experimental verification on α-Al$_2$O$_3$:C

2.3.1 Materials and Method

The OSL dosimetry grade single crystals α-Al$_2$O$_3$:C (5 mm dia. and 0.9 mm thick, Urals Polytechnique Institute, Russia.) were irradiated using a calibrated 5mCi, ^{90}Sr/^{90}Y beta source. The TA-OSL was recorded at room temperature for the irradiated samples in a laboratory developed integrated TL and OSL reader system [6] consisting of a high intensity blue light emitting diode (λ_p = 470 nm, $\Delta\lambda$ = 20 nm) cluster as a stimulating light source, transistor based high current LED driving circuit to drive LEDs. Before irradiation, the samples were optically bleached for 10 min at elevated temperature of 400 °C using 470 nm LED light source ~100 mW/cm^2 with GG 435 optical filter across it to cut off UV components in the blue LED spectrum. This bleaching removes hard to bleach OSL components which may interfere with TA-OSL measurements [7]. The UG-1 optical filter was used across the PMT to prevent the stimulating light from reaching the PMT.

2.3.2 Results and Discussion

2.3.2.1. Generation of Thermally Assisted (TA)-OSL signal

The dosimetry TL peak in α-Al$_2$O$_3$: C is reported to occur at ~182 °C along with low temperature ~54 °C [8]. To investigate the temperature dependent TA-OSL signal, we irradiated α-Al$_2$O$_3$: C dosimeter to a dose of 60 mGy. Apart from this, to avoid interference due to the low temperature (54 °C) TL peak during the TA-OSL measurements, all TL and OSL measurements were carried out at temperature ≥ 52 °C. Since the photo-ionization cross-section of OSL traps in α-Al$_2$O$_3$: C sample is sufficiently large to give CW-OSL signal even at stimulation intensity < 10 mW/cm^2 and as most of the OSL in α-Al$_2$O$_3$: C is contributed by the traps responsible for the from dosimetry TL peak, the week stimulation intensity (~6.3 mW/cm^2) has been used along with

linear heating of 3K/s to record TA-OSL measurements. All luminescence measurements have been recorded after the post irradiation periods of 5 min, as this allows room temperature phosphorescence decay from low temperature TL peak at 54 °C. Fig. 2.5, curve (A) shows the TA-OSL curve which consist of CW-OSL with thermal assisted component and TL signal consist of 182 °C peak. In order to separately investigate the presence of TA-OSL component from Fig. 2.5 curve (A), we separated OSL and TL contribution from curve (A). To do this, the sample was given elevated temperature optical bleaching of 10 mints at ~100 mW/cm^2 and followed by 60 mGy irradiation. The CW-OSL thus recorded at the elevated temperature of 54 °C with same stimulation intensity (i.e. 6.2 mW/cm^2) is shown in Fig. 2.5 curve (B).
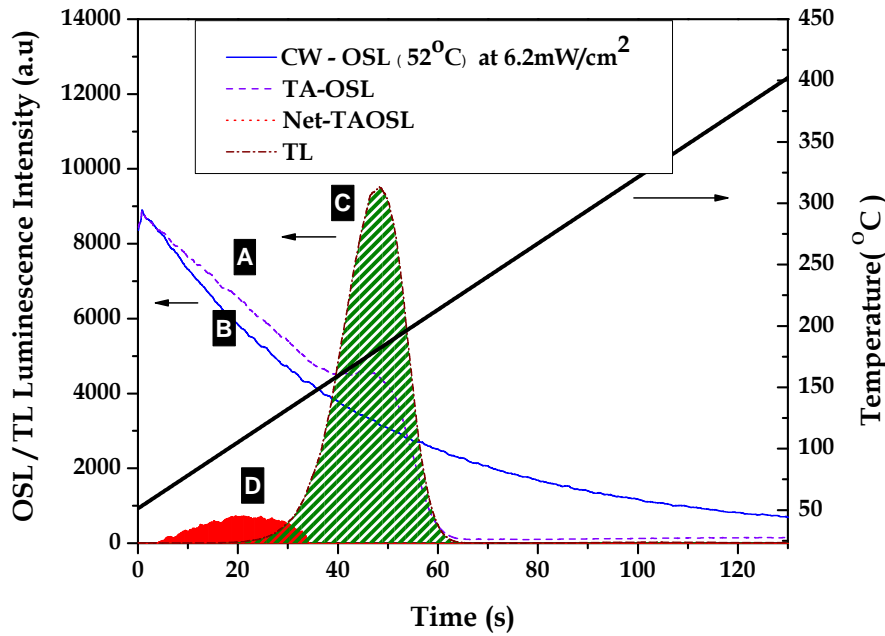
Fig. 2.5 The Curve (A) is TA-OSL signal recoded with CW stimulation and linear heating of 3K/s. Curve (B) is the CW-OSL recorded at 52 °C temperature with 6.2 mW/cm^2 stimulation light. The curve (C) is a TL glow curve recorded after irradiation with 60 mGy of β dose. Curve (D) is the subtraction of curves D= A- B - ςC is resultant net TA–OSL.

In the similar way, TL has been recorded (in absence of stimulated light) for same absorbed dose and with 3K/s heating rate as shown in Fig. 2.5 (C) showing dosimetry TL glow peak occurring at 182 °C. The net increase in TA-OSL signal curve (D) as compare to CW-OSL and TL, can be given as $D = A - B - \varsigma C$ as shown in curve Fig. 2.5 (D). The constant ς is the scaling factor which takes care of reduction in TL glow curve area due to simultaneous application of optical and thermal simulation during TA-OSL readout. Thus, the TL glow curve was multiplied by a factor ($\varsigma <1$) so that the resultant doesn't become negative. This factor was determined by numerically comparing the height of peak in curve B and C. It can be seen from Fig. 2.5 curve (A), that area of the 182 °C TL glow peak area recorded in absence of optical stimulation (Fig. 2.5, curve (C)) is larger compare to TL part visible in TA-OSL curve (A). The TA-OSL signal increases with increasing temperature as predicted by 1st exponential term in Eq. (2.7). However, at the relatively time the 2nd exponential term dominates and represents the decreasing part. As a result, a well-defined TA-OSL peak occurs in time as well as temperature domain as depicted from TA-OSL curve shown in Fig. 2.5 (Curve (D)).
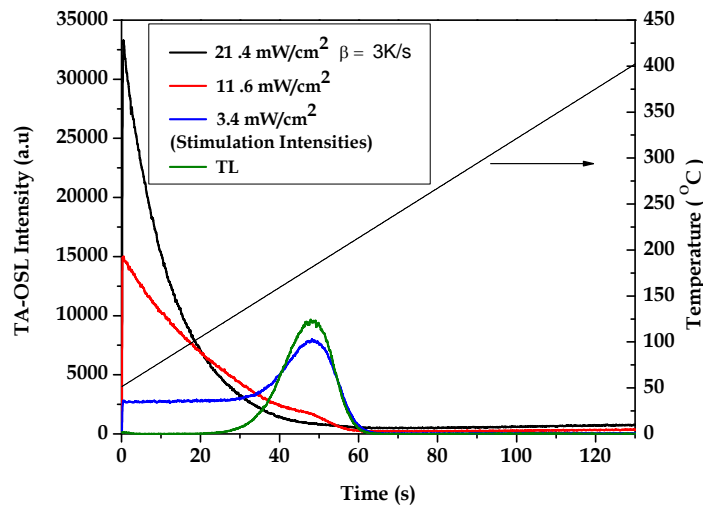
Fig. 2.6(a) TA-OSL curve for various CW stimulation intensities and fixed heating rate of $\beta = 3$ K/s.

Fig. 2.6 (a) shows the TA-OSL signal recorded for different CW stimulation intensities. Since in α-Al$_2$O$_3$:C, it is found that dominant OSL is coming from 182 °C TL peak, therefore with the increase CW optical stimulation intensity, the TA-OSL signal increases with consequent decrease in TL component. The shift in TA-OSL signal in time domain has been observed as predicted theoretically-experimental results are shown in Fig. 2.6 (b) for various stimulation intensity for an adsorbed dose of 60 mGy and a heating rate of 3K/s.
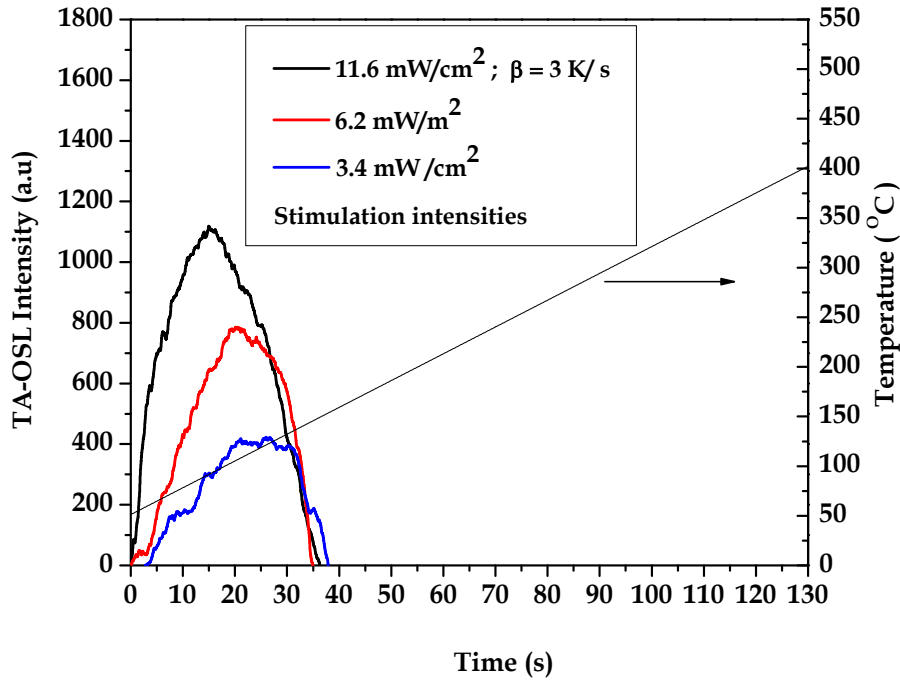
Fig. 2.6 (b) Net TA-OSL curve for various CW stimulation intensities and fixed heating rate of β = 3 K/s under CW for absorbed dose 60 mGy.

As expected by (see Eq. (2.11)), the TA-OSL peak was found to shift at higher temperature like the TL peak in temperature domain as shown in Figs. 2.7 (a) and 2.7 (b)
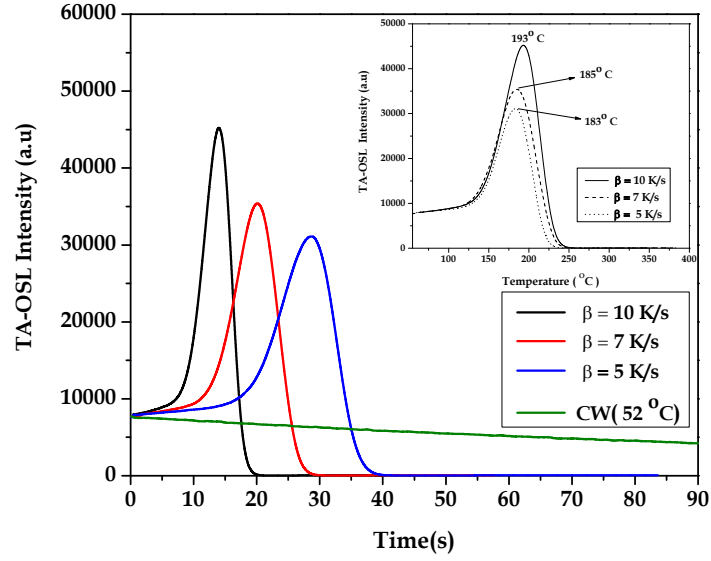
Fig. 2.7(a) TA-OSL curve for various heating rate under CW stimulation intensity of 3.7 mW/cm² @ 470 nm. Inset gives the corresponding curves in temperature domain.
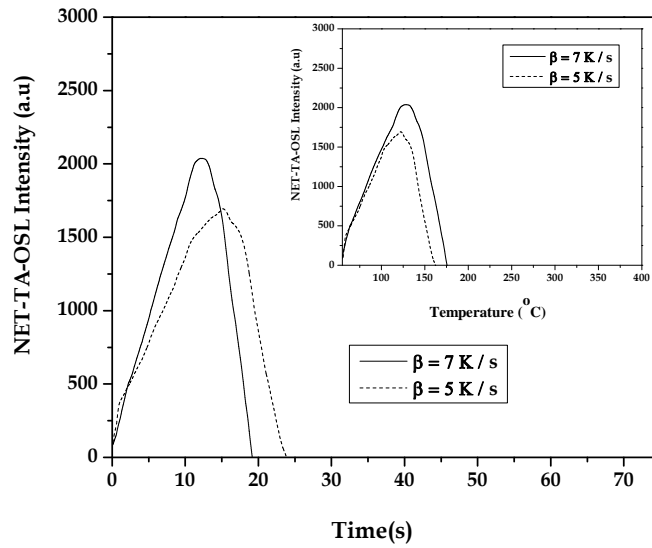
Fig. 2.7(b). Net-TA-OSL curve for heating rates 7 K/s and 5 K/s under CW stimulation intensity of 3.7 mW/cm² @ 470 nm. The inset gives the corresponding curves in the temperature domain.

2.3.2.2 Measurements of Thermally Assisted Energy and Pre-exponential factors of TA-OSL

The measurement of thermal assistance energy (E_A) and the pre-exponential photo-ionization cross-section $\sigma_o(\lambda)$ can be done in two steps. First, the determination E_A using the Eq. (2.7). Since the initial rising part of TA-OSL is governed by 1st exponentially increasing part of Eq. (2.7) and under week stimulation product of $n_o f_o$ can be assumed to remains nearly constant.
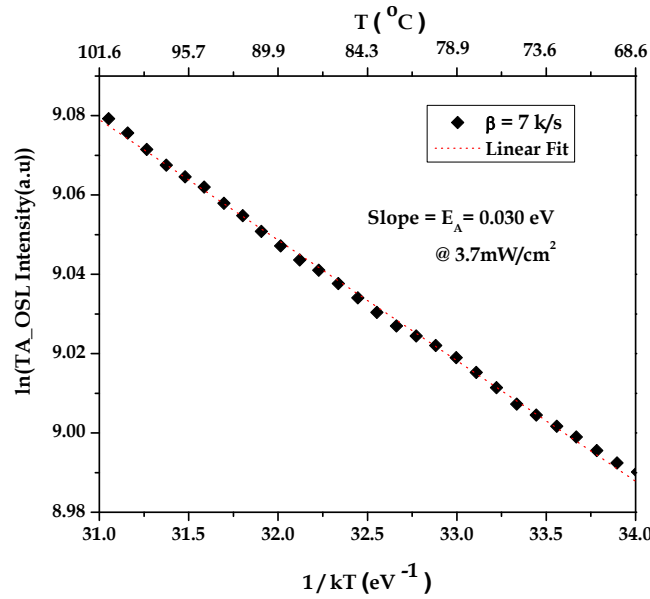
Fig. 2.8.   Natural logarithm TA-OSL intensity vs 1/ kT gives slope as thermal assistance every of OSL trap E_A for heating rate β = 7 K/s and CW stimulation of 3.7 mW/ cm² for various heating for absorbed dose of 60 mGy.

Therefore, under the weak stimulation assumption, the Eq. (2.7) can be expressed as

$$I_{TA-OSL} = B\,e^{-\frac{E_A}{k\,T}}$$

(2.16)

Where *B* is a constant and the plot of *ln(Integrated I(T)$_{TA-OSL}$)* v/s *1/kT* gives linear plot with slope as thermal assistance energy *(E$_A$)*. The Fig. 2.7a shows the CW-OSL recorded in at constant temperature of 52 °C for weak stimulation. The comparison of TA-OSL with CW-OSL

(at 52 °C) in Fig. 7(a) clearly shows the increasing intensity of TA-OSL signal with increase in heating rate. Since, less than 100 °C TL signal from main dosimetry TL peak in α-Al$_2$O$_3$:C does not interfere with TA-OSL signal, the rise in TA-OSL signal in initial part is purely due to exponentially increasing parts as given in Eq. (2.16). The plot of natural logarithm of integrated TA-OSL v/s *1/kT* for a heating rate of 7 K/s has been shown in Fig. 8 from 68 °C to 100 °C. The TA-OSL signal data above 100 °C has been not considered due to expected thermal quenching in α-Al$_2$O$_3$:C [7] and partial interference of TL signal generated due to dosimetry 182 °C TL peak. The slope of line *ln(Integrated I(T)$_{TA\text{-}OSL}$)* v/s *1/ kT* was found to be $E_A \approx$ 0.03 eV. With increases in heating rate the shift (time and temperature domain) occurs in TA-OSL peak as well as in dosimetry TL peak as shown in an inset graph of Fig. 2.7 (a). With increase in heating rate the shift (in time and temperature domain) occurs in TA-OSL peak as well as in dosimetry TL peak as shown in the inset to the Fig. 2.7(a). The value of σ (300K, 470nm) has been determined for α-Al$_2$O$_3$:C sample by varying the stimulation power and recording value of excitation rate at different stimulation power (flux φ (λ=470 nm)) as shown in Fig. 2.9. The slope of this line gives value of σ (300 K, 470 nm) and is found to be ~1.33 $\times$ 10^{-18} cm^2. Since the value of thermal assistance energy E_A has been already estimated using Fig. 2.8 and Eq. (2.16). Now incorporating the above determined values of E_A and σ (300 K, 470 nm) in Eq. (2.1), we get the value of pre-exponential factor as σ_o ~ 4.24 $\times$ 10^{-18} cm^2. Therefore, Eq.(2.1) can be rewritten as

$$\sigma(T, 470nm) = 4.24 \times 10^{-18} \, e^{-\frac{0.030}{k(300K)}}$$

(2.17)
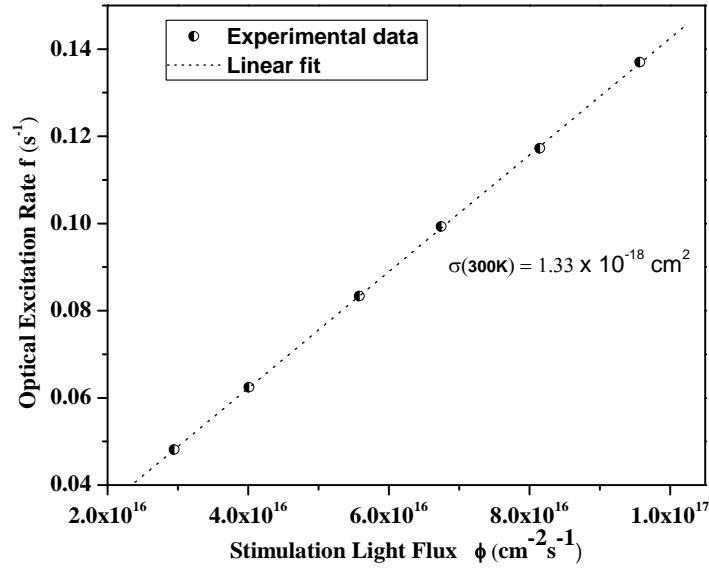
Fig.2.9 Optical excitation vs stimulation flux at room temperature for 470 nm of light slope of above line gives the value of photo-ionization cross-section at room temperature.

In the second method to determine the value of pre-exponential factor, we have taken the CW-OSL at different elevated temperatures for the irradiated α-Al_2O_3: C phosphor at stimulation power of 52 mW/cm^2 as shown in Fig.2.10 (a). The value of CW-OSL decay constant is found to increase with increase in temperature of CW-OSL measurements from 23 °C to 150 °C. The inset to Fig. 2.10(a) clearly shows increase in the value of photo-ionization cross-section associated with main OSL dosimetry trap in α-Al_2O_3: C phosphor. The thermal assistance energy responsible for this increase in value of photo ionization cross section can be determined independently using the following equation with incorporation of Eq. (2.1)

$$f(T,\lambda) = \phi_o(\lambda)\, \sigma(T,\lambda) = \phi_o(\lambda)\, \sigma_o(\lambda)\, e^{-\frac{E_A}{kT}} = f_o\, e^{-\frac{E_A}{kT}}$$

$$(2.18)$$
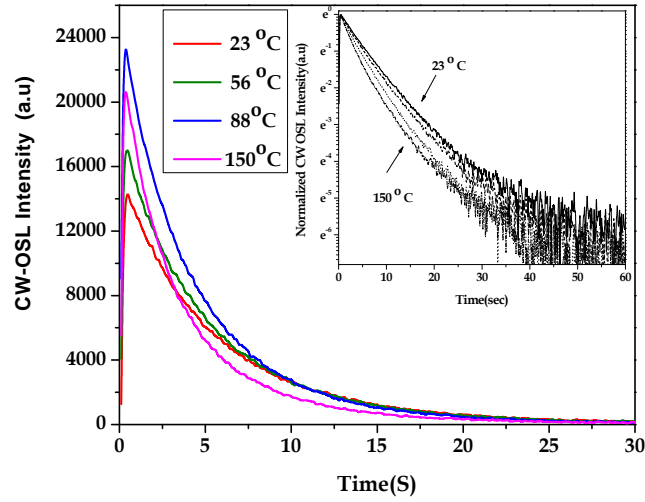
Fig. 2.10(a) The CW-OSL response at various elevated temperature for 60 mGy absorbed dose. The inset shows the normalized CW-OSL intensities.
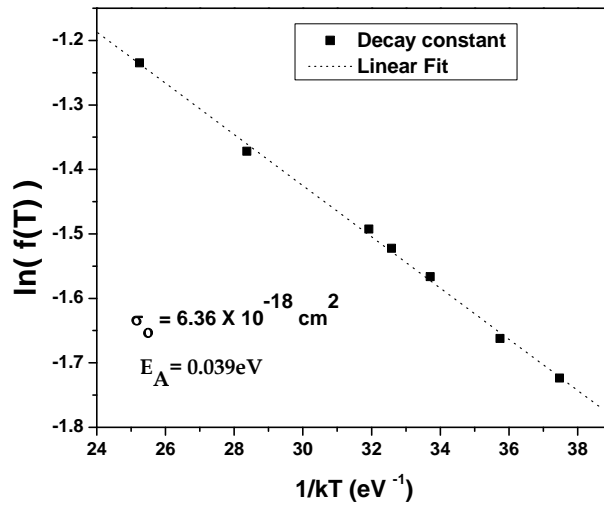
Fig. 2.10(b) Variation of excitation rate for 52 mW/cm² with 1/ kT gives slope as E_A and intersection as ordinate gives value of σ_o.

The natural logarithm of excitation at different temperature i.e. *ln(f(T,λ)) vs 1/kT* will give slope as thermal assistance energy (E_A) associated with OSL traps and intercept will give the value of

pre-exponential factor (σ_o). The Fig. 2.10 (b) shows the graph of *ln(f) v/s 1/kT* and the thermal

assistance energy associated with OSL traps is determined as $E_A \sim 0.039$ eV and pre-exponential

factor $\sigma_o \sim 6.36 \times 10^{-18}$ cm^2. The numerically simulated TA-OSL signal for α-Al$_2$O$_3$: C using

$E_A \sim 0.03$ eV and $\sigma_o \sim 4.24 \times 10^{-18}$ cm^2 under various stimulation intensities of 470 nm light with

3 K/s heating rate has been shown in Fig.2.11(a).
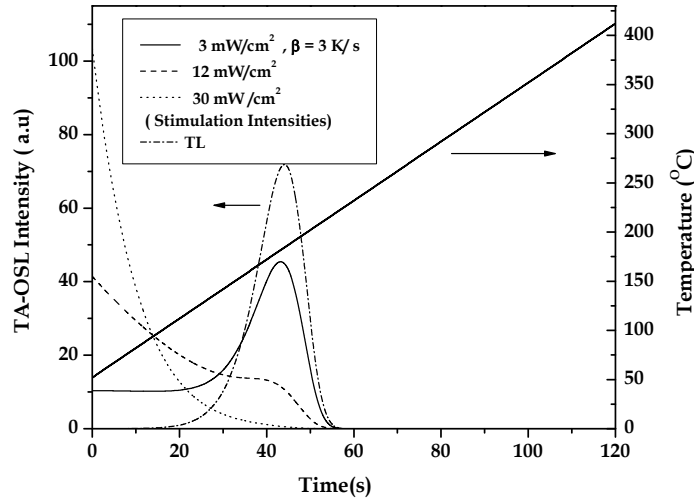
Fig. 2.11(a). TA-OSL curve numerically simulated for various CW stimulation intensities and fixed

heating rate of β= 3 K/s with E_A=0.03 eV, σ_o = 4.24 × 10^{-18} cm^2, E=1.1 eV and S= 2.5 × 10^{11} s^{-1}.

For this simulation, TL parameters have been taken for 1st order kinetics with trap depth (*E*)=*1.1 eV*

and frequency factor *S =2.5 × 10^{13} s^{-1}* (using initial rise method). The results curves of Fig. 2.11(a)

are in closely resembling the similar experimental measured curves shown in Fig. 2.6(a). In the

similar way, the effect of different heating rates on numerically computed TA-OSL using

experimentally determined values of E_A and σ_o has been shown in Fig. 2.11(b). The resultant curves

of Fig. 2.11(b) are in good agreement with experimentally measured TA-OSL curves shown Fig.

2.6(b) under similar conditions.
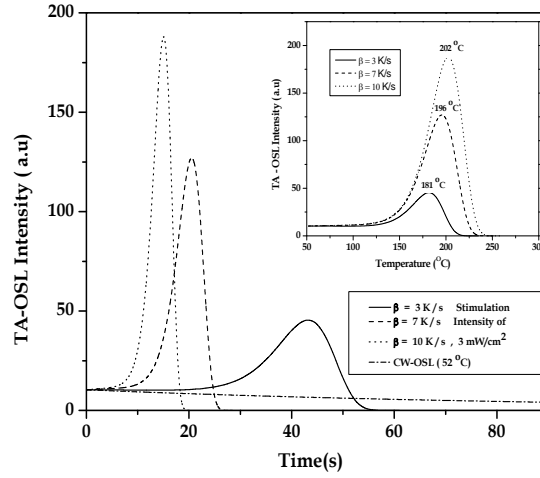
Fig. 2.11(b). TA-OSL curve numerically simulated for various heating rate and fixed CW stimulation intensities 3 mW/cm^2 with experimentally determine value of E_A=0.03 eV, σ_o = 4.24 $\times$ 10^{-18} cm^2, E=1.1 eV and S= 2.5 $\times$ 10^{11} s^{-1}. Inset figure shows the temperature domain plot of TA-OSL signal.
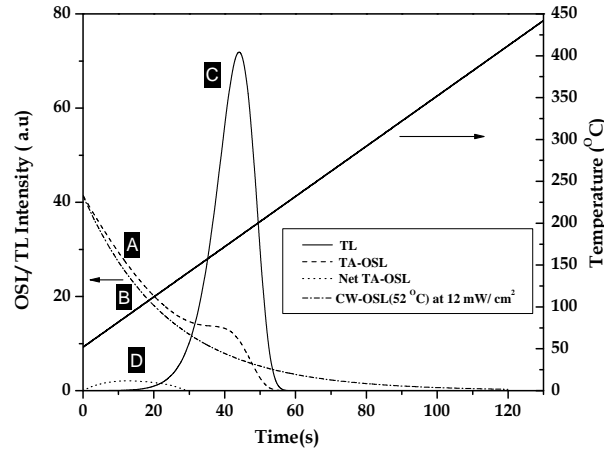
Fig. 2.12   Using experimentally determined value E_A=0.03 eV, σ_o = 4.24 $\times$ 10^{-18} cm^2, E=1.1 eV and S= 2.5 $\times$ 10^{11} s^{-1} numerical simulated curves for α-Al$_2$O$_3$: C. The Curve (A) is TA-OSL signal recoded with CW stimulation and linear heating of 3K/s. Curve (B) is the CW-OSL recorded at 52 °C temperature with 12 mW/cm^2 stimulation light. The curve (C) is a TL glow curve. Curve (D) is the subtraction of curves D= A- B - ςC is resultant net TA–OSL.

The comparison of the net TA-OSL signal numerically generated using experimentally determined values of TL and OSL parameters as shown in Fig. 2.12, curve (D) for 12 mW/cm^2 optical stimulation with corresponding TA-OSL signal measured experimentally are in good agreement (Fig. 2.5). These results show the validity in assumption of considering Arrhenius nature of temperature dependence of photo-ionization cross-section in dosimetry OSL traps of α-Al$_2$O$_3$: C. The above results have been published in the international journal [9].

2.4. Conclusions

This chapter presented the theoretical formulation for TA-OSL and the same has been used to analyze the thermal assistance nature of dosimetry traps in α-Al$_2$O$_3$: C. The thermal assistance energy associated with dosimetry OSL trap in α-Al$_2$O$_3$: C was measured using two different methods and found to agree within experimental limitations. The simulation of numerically generated TA-OSL signal using experimentally determined values of thermally assistance energy and pre-exponential factor of α-Al$_2$O$_3$: C is in good agreement with experimentally recorded TA-OSL signal. The present study highlighted the effects of Arrhenius nature observed in temperature dependence of photo-ionization cross-section of OSL dosimetry traps in α-Al$_2$O$_3$: C. The results also concluded that the TA-OSL and hence the OSL signal increases with temperature. This effect of temperature on the OSL intensity can be used to probe the deeper defects in the material to make them applicable for dosimetry, which essentially forms the basis of the next chapter.

References

1. Spooner, N. A. 1994. *Radiat. Meas. 23* 593-600

2. Chruścińska, A. 2010 *Radiat. Meas. 45* 991-999

3. McKeever, S .W.S., Bφtter-Jensen, Agersnap Larsen, N, and Duller, G.A.T., 1997. *Radiat. Meas.* 27, 161-170.

4. Grimmeiss, H. G., Ledebo ,L-A. 1975 *J. Phys. C: Solid State Phys. 8* 2615-226

5. Alexander, C. S., Morris M F, Mackeever, S. W. S. 1997 *Radiat. Meas. 27 2 153*-159

6. Kulkarni, M. S., Mishra, D. R, Sharma, D. N. 2007 *Nul Inst, Method in Phys*. B 262 2 384-356.

7. Akselrod, M.S., Agersnap Larsen, N., Whitley, V. and McKeever, S.W.S., 1998. *J Appl. Phy.* 84, 3364-3373.

8. Mishra, D. R., Kulkarni, M. S., Muthe, K. P., Thinaharan, Roy. M., Kulshreshtha, S. K., Kannan, S., Bhatt, B. C., Gupta, S. K., Sharma, D. N. 2007 *Radiat. Meas. 42 2* 170-176.

9. Mishra, D. R., Soni, A., Rawat, N.S., Kulkarni, M.S., Bhatt, B. C., Sharma, D. N. 2011. *Radiat. Meas. 46,* 635-642.

Chapter 3

Extension of Dose response of

α-Al$_2$O$_3$:C

This chapter will delve into the formalism of a novel experimental technique to access the signal from deep traps of α-Al$_2$O$_3$:C using TA-OSL phenomenon. It will describe the theoretical simulation and experimental validation of the suggested method. Further, it will present the through characterization of deeper defects using the suggested method which has resulted in the extended dose response of α-Al$_2$O$_3$:C and hence the application of the phosphor for high dose dosimetry. The technique also overcomes the limitation of OSL of requirements of dark conditions. In the end, it also throws some light on the nature of such deep defects.

3.1. Introduction

Anion deficient α-Al$_2$O$_3$:C has shown increasing popularity for use as an optically stimulated luminescent (OSL) radiation dosimeter. The F (two electrons trapped in oxygen vacancy) and F$^+$ (one electron trapped in oxygen vacancy) centers are the main luminescence centers in the phosphor [1, 2]. At room temperature, for stimulation with green or blue light, the OSL comes from the intermediate energy level defects, also termed as dosimetric traps. These dosimetric traps however show sub-linear dose response for doses > 1Gy and hence put limitations for high dose applications like accidental dosimetry and dosimetry for food irradiation. As Al$_2$O$_3$ has large band gap, there exists the possibilities of deep energy level defects [3], which cannot be accessed either by visible light or by temperature during stimulation in conventional TL/OSL reader systems. In α-Al$_2$O$_3$:C (TLD-500) single crystals, the deeper defects were found to give their presence at 873K and 1173 K respectively [4]. These deep traps have been reported to have substantial influence on the dosimetric properties of α-Al$_2$O$_3$:C, in particular, their sensitivity to light and ionizing radiation, dose dependence, linearity and other parameters that change after exposure to ionizing radiation at higher doses. Yukihara et al. [5] have studied the effect of high dose irradiation in α-Al$_2$O$_3$:C on the OSL sensitivity and on the shape of the CW-OSL decay curve. The OSL decay curve becomes faster with dose while change in OSL sensitivity during step annealing procedure is due to the filling of deep traps. Molnar et al. have reported TL peaks in Al$_2$O$_3$:C at 310, 460 and 675 °C for heating rate of 2 K/s using UV interference filters [6]. Yukihara et al. [7] have also studied the influence of deep traps on the changes in TL sensitivity and in peak shape of 177 °C TL peak with dose, type of irradiation and temperature of heating. Their investigation demonstrated that sensitization/desensitization (increase/decrease of sensitivity for subsequent irradiation) effects in α-Al$_2$O$_3$:C can be explained by competition process introduced by presence of deep hole and deep electron traps with delocalization

temperatures of 773K and 1173K respectively. Such deep traps having large thermal trap depth are difficult to access by TL method using commercially available TL readers. Secondly, at such higher temperatures the loss of signal due to very high thermal quenching [8] and interference of high infrared background makes such TL measurements difficult beyond 750 °C. Apart from this, the conventional OSL technique using various available visible light sources at room temperature is also incapable of accessing such deep traps, as the photoionization cross-section of these traps is expected to be very low at room temperature (RT). Thus, if a method becomes available to exploit and reliably measure the information from the deep traps using the conventional TL/OSL reader, new vistas in the field of luminescence dosimetry may emerge to overcome the limitations of OSL for α-Al$_2$O$_3$:C in high dose dosimetry. Further advancements have been made in use of thermally assisted OSL (TA-OSL) by exploiting deeper traps [9]. In their work the OSL readout was taken at elevated temperature for 1000 s which may have limitation for adoption of this technique for routine dose measurements. The present work describes a new experimental method to access the signal from deep traps without heating the sample to temperatures higher than 400 °C and limiting the readout time up to 120 s. However, it should be noted that the α phase of Al$_2$O$_3$:C does not undergo phase transition at such temperature range. In this method, blue light is used to stimulate the traps which does not irradiate the traps. UV light of specific wavelength (203 nm), which is the excitation wavelength for the F-center in α-Al$_2$O$_3$:C, do irradiate the sample which leads to OSL. This part of the spectrum in the Led is blocked by placing GG-435 optical filter in front of the blue LED. To understand the origin of TA-OSL, it is important to study the nature of the traps which are responsible for TA-OSL signal. Umisedo et al. [10] have recently reported that the 190 °C peak is due to F-center emission, but that due to 675 °C peak is less clear. It could be F-center or impurity (e.g Ti) emission as well. These results of F and F$^+$-center emissions at high

75

temperatures should be viewed in the light of the important results of quenching of F and F$^+$ emissions around 150-200 °C in Al$_2$O$_3$C [8]. Also the assignment of F center (due to F$^+$ + e$^-$ to F transformation) for 675 °C TL seems to be contradicting with the previous optical annealing measurements [4]. In the current work, TA-OSL measurements have been used to identify the nature of these deep energy level defects in α-Al$_2$O$_3$:C powder (Landauer Inc.) and also to evaluate their TA-OSL parameters.

3.2. Materials and Methods

Commercially available α-Al$_2$O$_3$:C powder (Landauer Inc.) was used to carry out the TA-OSL studies on its deep traps. The powder sample was annealed at 900 ^{o}C to remove any prior existing signal. This annealing removes the hard to bleach OSL components which may interfere with TA-OSL measurements [7]. The annealed sample (10mg) was coated on 0.5 mm thick stainless steel disk and the calibrated 2.2MeV ^{90}Sr/^{90}Y beta source was used to irradiate the samples. The TA-OSL measurements were performed using a programmable integrated TL/OSL reader system [14]. The TL and TA-OSL curves were recorded at a constant heating rate of 4 K/s and all OSL measurements were performed in the Continuous Wave (CW- OSL) mode. The light intensity at the sample position was measured approximately to be 48.8 mW/cm^2.

3.3. Results and Discussion

3.3.1 Generation of TA-OSL signal

The prepared sample was irradiated to an absorbed dose of 500 mGy and the TL was recorded up to a temperature of 400 °C, to deplete the signal due to 185 °C main dosimetry TL peak in α-Al$_2$O$_3$:C, which is also associated with the basic OSL traps. Fig. 3.1 shows the energy level diagram representing the electronic transition involved in the photo-transfer process from various traps reported in α-Al$_2$O$_3$: C [7]. The proposed model for TA-OSL has been given in Fig. 3.2

which shows the vibrational level of deep energy level defects participating in thermally assisted OSL.
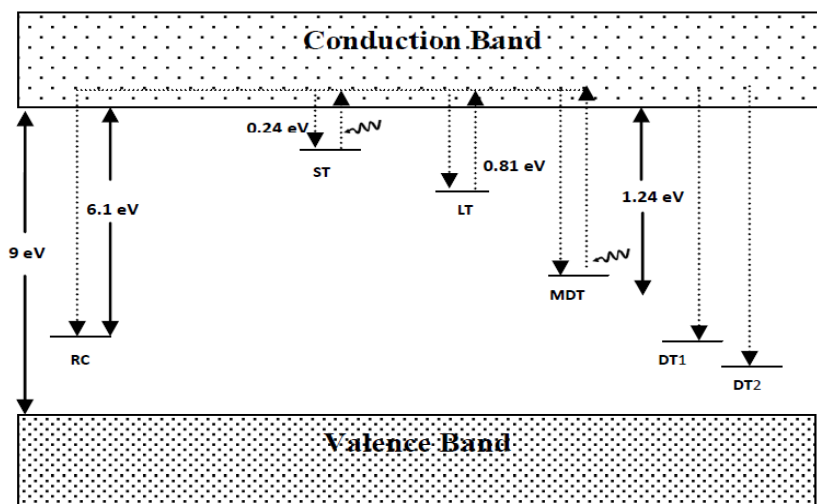
Fig. 3.1. Energy level diagram representing the electronic transition involved in the photo-transfer process from various traps in α-Al₂O₃: C powder.
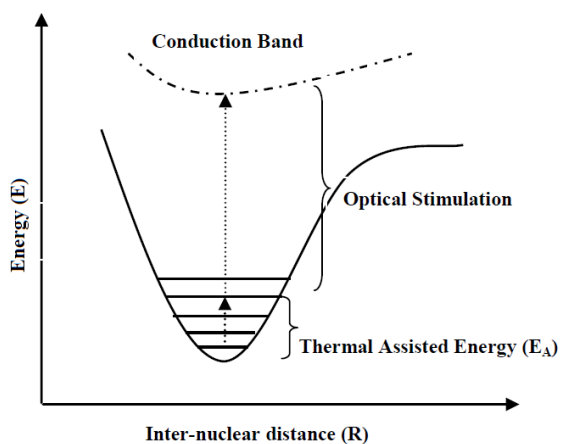
Fig. 3.2. Configuration coordinate diagram representing the thermally assisted optical stimulation process from deep traps in α-Al₂O₃: C powder.

The deeper energy level defects, having relatively lower photoionization cross-section for blue

(470 nm) LED stimulation light source at room temperature give slow, exponentially increasing

OSL signal on subsequent CW-OSL readout as shown in Fig. 3.3. (C1), which otherwise should

have given exponential decay curve on CW-OSL readout [15] (Bos et al., 2009), if the optical

cross-section of these traps was comparable to that for dosimetric traps. This kind of CW-OSL

behavior can also be explained by a photo-transfer mechanism in which the electrons from the

first deep trap DT1 are transferred to conduction band on stimulation (Fig.3.1).
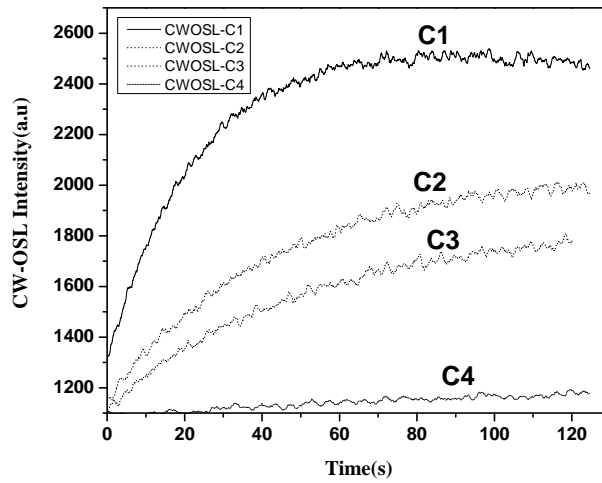
Fig.3.3. CW-OSL readout from deep traps. C1 is the CW-OSL readout following the first TL readout upto 400ᵒC after a beta dose of 500mGy. C2 is Subsequent CW-OSL readout after the second TL readout upto 400ᵒC, and so on, up to C4.

The main dosimetric traps (MDT) responsible for 180 °C TL peak are empty at the start of OSL

readout, due to the initial TL readout, offer competition to recombination centers for capturing

the free electrons from the conduction band. Therefore, the initial OSL signal is low. However,

as the trapping centers are filled, the equilibrium is established between charge capture and

charge stimulation from these trapping centers. As the system approaches equilibrium and the

main OSL traps compete less for the capture of free electrons, the OSL signal increases,

approaching a constant equilibrium level. Here we have considered both the deep traps (DT1 & DT2) as electron traps and the experimental justification for this is given in the results and discussion-section D. However, Akselrod and Gorelova had earlier reported two types of traps in α-Al$_2$O$_3$:C single crystals - deep hole traps which are emptied at 600 °C and deep electron traps getting bleached at 900 °C [4].
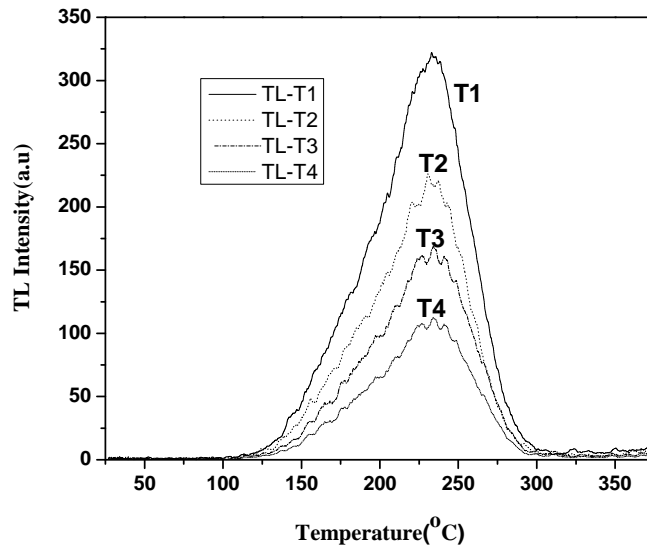
Fig.3.4. Subsequent TL readouts after each CW-OSL readouts (i.e., C1, C2, C3 and C4 in Fig. 3.3) of Al₂O₃:C sample.

The phototransfer process described above is further supported by TL measurements carried out immediately after CW-OSL readout (Fig. 3.4 (T1)). As the first TL readout of irradiated sample was taken up to 400 °C prior to CW-OSL, no TL peak in this region is expected to appear in the absence of phototransfer. However, due to phototransfer from deeper traps, TL peaks appeared at slightly higher temperature (~245 °C) as shown in Fig. 3.4(T1). Similar results in α-Al$_2$O$_3$:C powder have also been observed by earlier investigators [10]. Now, the second TL readout of the above sample will deplete the main dosimetric traps and subsequent

CW-OSL readout will result in refilling of main dosimetric traps, though to a lesser extent, gives same exponentially increasing pattern with slightly lesser intensity (Fig. 3.3. (C2)), as compared to previous CW-OSL readout after the TL readout of the initially exposed sample. Fig. 3.3 and 3.4 give results on subsequent sequential CW-OSL and TL readout on the sample. However, no CW-OSL is observed from the irradiated sample annealed at 700 °C as first trap bleached out on annealing at 700 °C. This indicates that the exponential increasing signal from the sample treated up to 400 °C (i.e after TL readout) comes from the first deeper trap by stimulation with blue light. The phototransfer mechanism is in agreement with previous observations of phototransfer thermoluminescence in Al₂O₃:C, which shows that deep traps can be stimulated with light of shorter wavelength, including blue light [10]. In order to explain the results on thermally assisted OSL in Quartz, Spooner (1994) postulated the existence of an array of available states in the ground state of the trap [12]. The upper levels of these traps are accessed at higher temperatures with an activation energy requiring a smaller optical energy to excite the charges to delocalized band.

Therefore, in order to record the TA-OSL response of deep traps, after taking first TL readout, the sample was subsequently subjected to CW-OSL readout along with simultaneous application of temperature profile at a linear heating rate at 4K/s. The TA-OSL signal increases with increasing the temperature as predicted by 1st exponential term in Eq. (2.7) described in chapter 2 and later the depletion of charges dominate and 2nd exponential term in Eq. (2.7) starts showing effect on the TA-OSL intensity. As a result two well-defined TA-OSL peaks at 121 °C and at 232 °C occur in time as well as temperature domain which are different from the main dosimetric TL peak which occurs at ~ 185 °C (Fig. 3.5a, 3.5b). Since both the TA-OSL and TL peak are recorded at the same heating rate (4K/s), the occurrence of these TA-OSL peaks at different

temperatures confirms the existence of distinct deeper defects in dosimetry grade α-Al$_2$O$_3$:C powder.
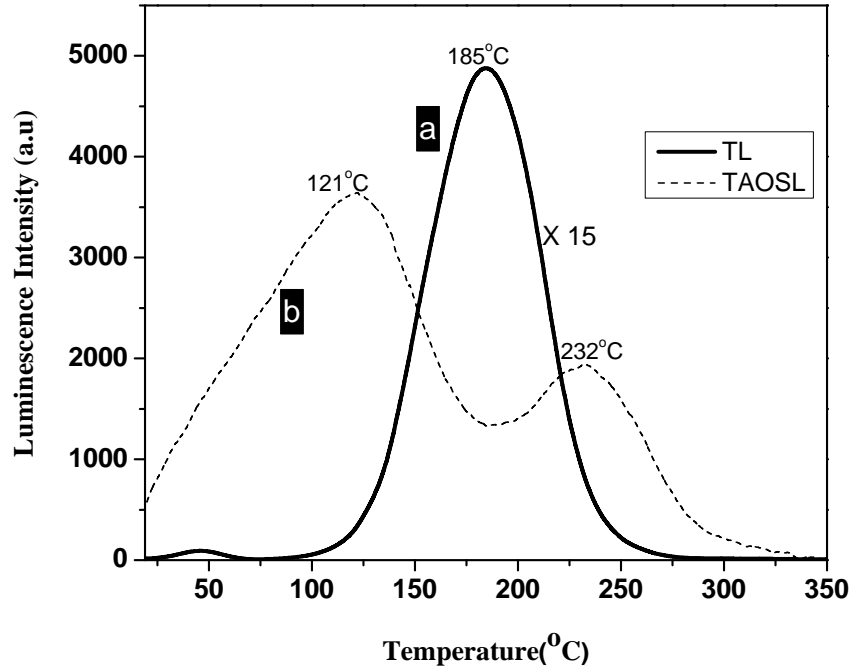
Fig. 3.5 (a) TL glow curve recorded just after irradiation 500 mGy of β dose.

(b) TA-OSL curve taken after TL readout recorded at 48mW/cm² stimulation light along with TL heating at 4 k/s.

The shift in TA-OSL peak position (experimental and simulated) with heating rate β is shown in Fig. 3.6. For given stimulation intensity, TA-OSL peak temperature T_m increases with heating rate β as expected from Eq. (2.11). The numerical fitting of experimentally evaluated TA-OSL curve is done by using Eq. (2.13a) as shown in Fig. 3.7. Slight mismatch between the experimental and fitted data and also the evaluated parameters may be attributed to the simplified assumptions in the theoretical TA-OSL equations.
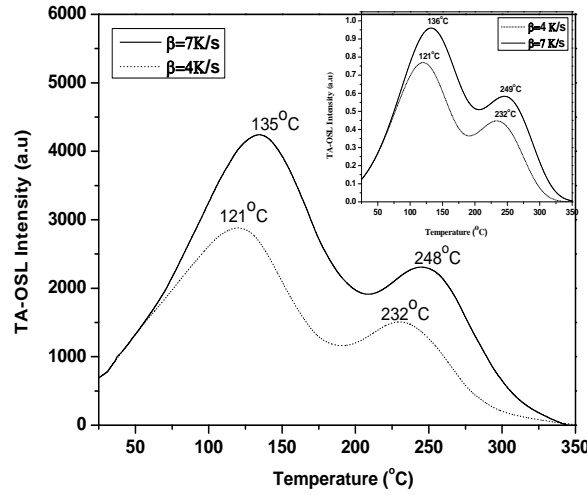
Fig.3.6. Experimental TA-OSL curve for different heating rate under CW stimulation intensity of 48 mW/cm^2. The inset figure shows numerically simulated TA-OSL signal v/s temperature plot for various heating rates β with CW-stimulation intensity $φ_o$ = 48.8 mW/cm^2, E_A=0.2648, $σ_o(λ)$= 1.8 ×10^{-15} cm^2 of first peak and E_A=0.4865, and $σ_o(λ)$= 3.3 ×10^{-14} cm^2 of second peak of 470 nm light.
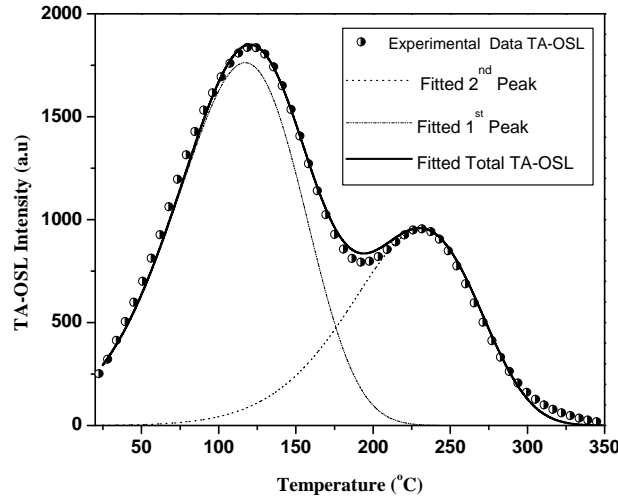
Fig.3.7. Individual peak fitting using TA-OSL equation in experimental TA-OSL. For first peak with β=4 K/s, E_A=0.268, $σ_o(λ)$= 1.1 ×10^{-15} cm^2 and b=1.1 For second peak with β=4 K/s, E_A=0.4857, $σ_o(λ)$=

1.3 ×10^{-14} cm^2 and b=1with CW stimulation intensity ϕ_o= 48.8 mW/cm^2 of 470 nm light and n$_{o1}$/n$_{o2}$= 0.86 for first and second peak respectively.

3.3.2. Measurement of TA-OSL parameters

3.3.2.1 Thermal Quenching Factor

The slope of integral plot of TA-OSL intensity vs. *1/kT* gives the value of thermal assistance energy E_A associated with the array of available excited states of ground level of deep traps in OSL meta-stable defects for stimulation with blue light. This E_A is nothing but the sum of series of quanta of all possible vibrational energy states associated with the ground state of deep OSL traps at elevated temperature of TA-OSL measurement. The thermal quenching of F-center is reported at higher temperature (>130°C) in Al$_2$O$_3$:C [8] and can be expressed in terms of luminescence efficiency w.r.t. temperature and can be expressed as

$$\eta = \frac{1}{1+\tau_o v \, exp \, (-\frac{W}{kT})} \tag{3.1}$$

Therefore, the effect of thermal quenching of F-center in TA-OSL measurement has been determined for the sample under study by using elevated temperature CW-OSL measurement of dosimetric trap (185 °C TL peak) for same absorbed dose and fixed stimulation intensity of 40mW/cm^2. Appropriate corrections for partial loss of OSL signal at elevated temperature due to isothermal TL have been incorporated. The Fig. 3.8 shows the total TA-OSL and elevated temperature normalized CW-OSL intensity for various temperatures revealing the presence of strong thermal quenching of F-center in the temperature range 130 °C - 220 °C in α-Al$_2$O$_3$:C. The inset of Fig. 3.8 shows the numerical fitting of Eq. (3.1) to the experimental data with the measured value of W (1.1eV) and $\tau_o v$ (1.8 ×10^{12}) which are in good agreement with the studied by other researchers. It is found that thermal quenching starts dominating above 130 °C. Thus the

thermal quenching effect will be similar in TA-OSL as it is in TL measurements for heating upto same temperature. However, it should be noted that TA-OSL methods reduces the heating temperature from 600 & 900 to 122 and 232 °C to probe the deep traps as compared to TL method. Thus the quenching effect has been reduced to some extent using TA-OSL. Further, the sensitization problem due to heating has not been reported so far in Al₂O₃:C.
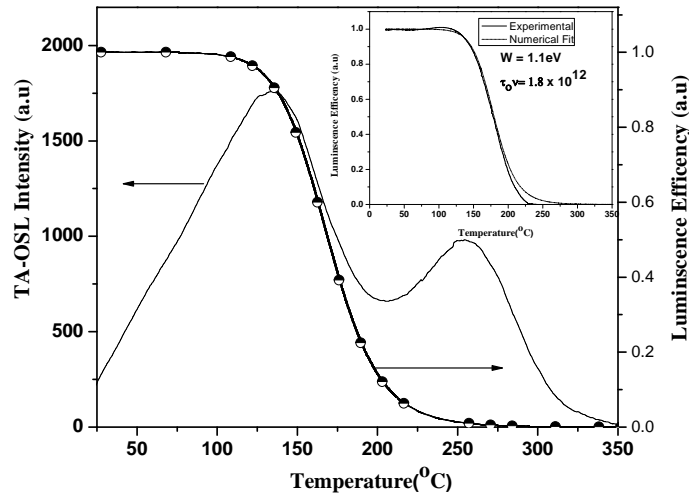
Fig. 3.8. TA-OSL signal vs temperature for 250 mGy of β dose. Inset fig shows the luminescence efficiency measured using elevated temperature CW-OSL vs temperature revealing the decrease in luminescence efficiency.

3.3.2.2 TA-OSL Analysis of first peak

The evaluation of E_A for the first peak is performed by applying initial rise method on it. As the thermal quenching factor is negligible below 130 °C, the method of initial rise is well within the applicability limit for determination of activation energy of first TA-OSL peak which is occurring at 121°C, without the need to apply any correction for the effect of thermal quenching. Since the initial rising part of TA-OSL is governed by 1st exponentially increasing part of Eq. (2.7) and under weak stimulation product of $n_o f_o$ and the second exponential term can be

assumed to remain constant. Therefore, the under these assumptions, the Eq. (2.7) can be expressed as

$$I_{TA-OSL} = A\,e^{-\frac{E_A}{kT}} \tag{20}$$
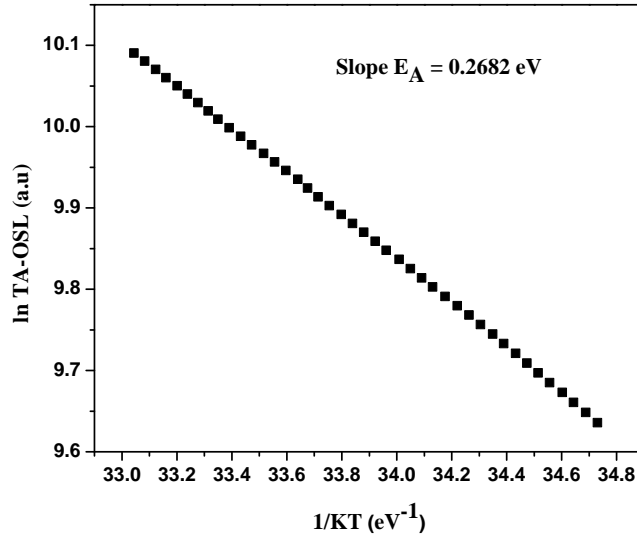
Fig. 3.9. Natural logarithm TA-OSL intensity of first peak vs 1/ kT plot gives slope (Activation Energy(E_A)) of first deep trap = 0.2682 ± 0.0151 eV.

Where A is a constant and the plot of ln(I_{TA-OSL}) vs *1/kT* gives linear plot with slope as thermal assistance energy (E_A) (Fig. 3.9). For the measurement of TA-OSL signal from the first deep trap at 121°C, for stimulation with blue light, the thermal assisted energy associated with the trap is found to be $E_A= 0.265$ eV. With this value of E_A, the corresponding σ_o was calculated by using Eq.(14) which comes out to be 1.88×10^{-15} cm². The corresponding photoionization cross-section at room temperature, i.e, $\sigma(300K, \lambda)$ was calculated by using Eq. (2.1), which comes out to be 5.82×10^{-20} cm² by using the above calculated values of E_A and σ_o.

3.3.2.3 TA-OSL Analysis of second peak

As the two TA-OSL peaks are overlapping in nature, to find out the activation energy of the second peak, the first peak was thermally bleached out by annealing the sample at 700 °C and then its TA-OSL was recorded, which gives only the second TA-OSL peak. Alternatively, the optical bleaching of irradiated sample to 100 mW/cm² for 10 hours has also been found to remove first TA-OSL peak of 121 °C. TA-OSL recorded after removal of first peak shows distinct nature of 2nd TA-OSL peak as shown in Fig 3.10.
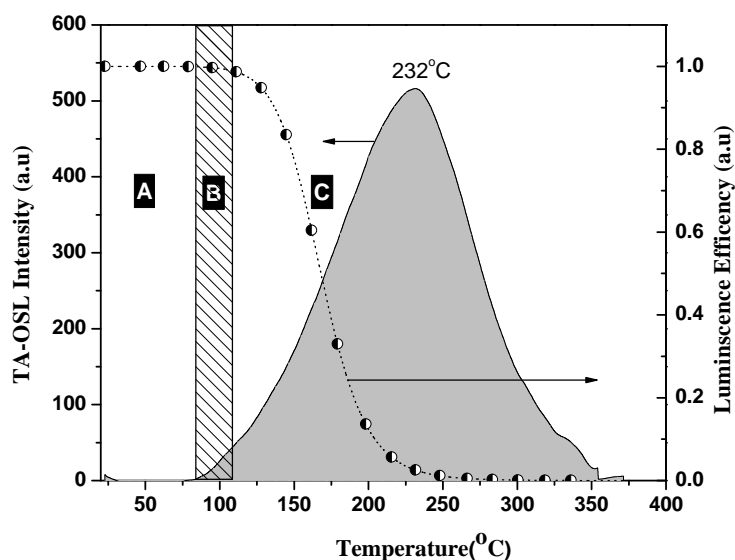
Fig. 3.10. TA-OSL vs temperature of second peak obtained after thermally filtering out the first peak, along with measured thermal quenching w.r.t temperature. Region A (25 °C to 80 °C) - No thermal quenching, region B (80 to 110 °C)-negligible thermal quenching, region C (110 to 250 °C) - dominating thermal quenching.

The second method (optical bleaching of irradiated sample) gives relatively more intense TA-OSL peak than the first method (thermal annealing at 700 °C), as at such high temperature annealing, partial annealing of second peak cannot be ruled out. The initial rise method has been

applied to the region B (80 to 110 °C) of the TA-OSL curve shown in Fig. 3.10 where thermal quenching effect is nearly absent and stars domination above this temperature region. Hence, under these circumstances, the initial rise method will able to give estimation of activation energy with reasonable accuracy. The TA-OSL parameters for the 232 °C peak are found to be: E_A=0.485 eV (Fig. 3.11), with corresponding σ_o = 5.43 x10^{-14} cm^2 and σ(300K, λ)= 3.70 x10^{-22} cm^2. Table 3.1 shows the TA-OSL parameters of the deep traps in α-Al₂O₃: C.
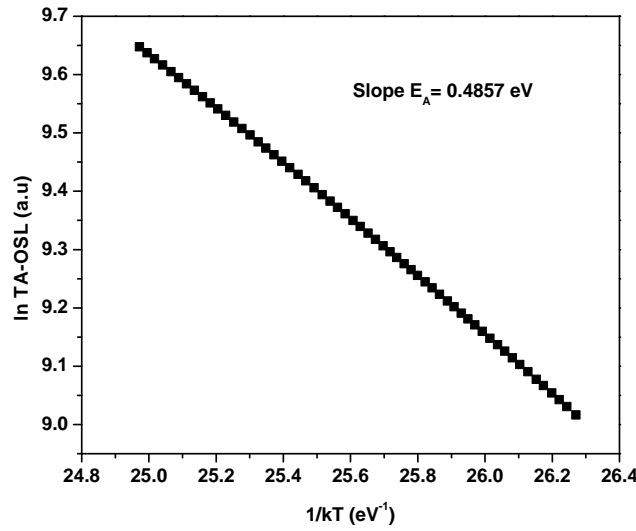
Fig. 3.11. Natural logarithm TA-OSL intensity of second peak vs 1/ kT plot with slope (Activation Energy (E_A)) of second deep trap =0.4857 ± 0.0132 eV

Table 3.1: TA-OSL parameters of deep traps of α-Al₂O₃:C.

Type of defect	*TA-OSL peak (°C)*	*Activation Energy E_A (eV)*	*Pre-exponential factor $\sigma_o(\lambda)$ (cm^2)* $\sigma_o(\lambda)=\dfrac{E_A\beta}{\phi_o k\, T_M^2}e^{\frac{E_A}{k\,T_M}}$	*Photo-ionization cross-section (cm^2) at (T=300K)* $\sigma(T,\lambda)=\sigma_o(\lambda)\,e^{-\frac{E_A}{KT}}$	*Photo-ionization cross-section (cm^2) at temperature corresponding to TA-OSL peak*
DT1	121	0.2648	1.88×10^{-15}	5.82×10^{-20}	7.61×10^{-19}
DT2	232	0.4857	5.43×10^{-14}	3.70×10^{-22}	7.64×10^{-19}

3.3.2.4 Simulation of TA-OSL

Numerically simulated TA-OSL intensity for deeper traps is plotted by summing up the two individual TA-OSL peaks generated using Eq. 2.7 of chapter 2. For this, experimentally evaluated values of $E_A = 0.268$ eV, $\beta = 4$ K/s and $\sigma_o(\lambda) = 1.8 \times 10^{-15}$ cm^{-2} for first peak and $E_A = 0.487$ eV, $\beta = 4$ K/s and $\sigma_o(\lambda) = 3.3 \times 10^{-14}$ cm^{-2}, for second peak respectively, with CW stimulation intensity $\phi_o = 48.8$ mW/cm^2 of 470 nm light, were used in Eq. 2.7 as shown in Fig. 3.12
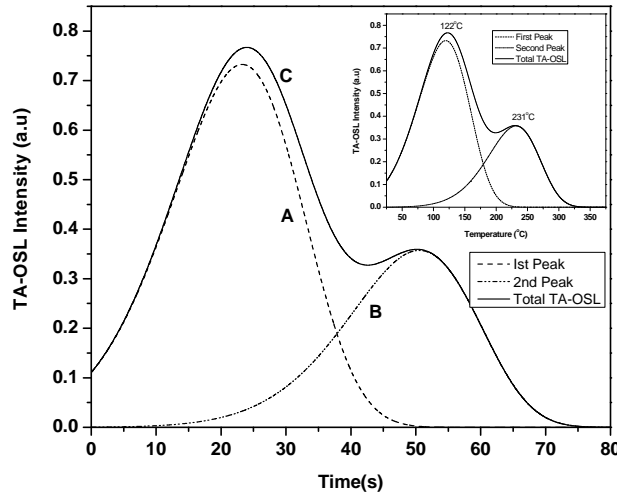
Fig.3.12. Numerically simulated TA-OSL signal v/s time plot. (A)For first peak with β=4 K/s, E_A=0.268, σ_o(λ)= 1.8 ×10^{-15} cm² with CW stimulation intensity φ_o=48.8 mW/cm² of 470 nm light. (B) For second peak with β=4 K/s, E_A=0.4857, σ_o(λ) = 3.3 ×10^{-14} cm² with CW stimulation intensity φ_o= 48.8 mW/cm² of 470 nm light. (C) Total TA-OSL signal.

3.3.2.5 Specific Advantage over Dosimetric trap

The photoionization cross-section $\sigma(300K, \lambda)$ of dosimetric traps was 1.8×10^{-18} cm^2 (Chapter 2) as compared to that of two deeper traps having values 5.82×10^{-20} cm^2 and 3.70×10^{-22} cm^2

respectively. Hence, these deep traps, having lower photoionization cross-section at room temperature as compared to that of the dosimetric traps, can retain the absorbed dose information even for storage of the sample in room light conditions. This is in contrast to significant fading of OSL signal reported from the dosimetric traps in α-Al₂O₃:C, due to the leakage of light through the nearly light tight cassette of Landauer Inlight personnel dosimetry badges during its exposure to daylight conditions for 45 days [16]. Thus, for the deeper trap to have the same photoionization cross-section as that of the dosimetric trap at RT, i.e, to access them by light as OSL signal at RT, the stimulation intensity should be about 1.2 W/cm^2 for the first trap and about 192 W/cm^2 for the second trap, which is not practically achievable in the commercial OSL reader systems. Apart from this, at such high optical power, non-linear optical phenomenon starts playing its role and optical heating of sample will takes place. Hence these deep traps are stable in room light conditions, having an average light intensity of tens of mW/cm^2. Further at 121 °C, the photoionization cross-section of first trap becomes 7.61 x10^{-19} cm^2 while for the second trap it becomes 7.64 x10^{-19} cm^2 at 232 °C, which are comparable to that of the main dosimetric trap at room temperature. Therefore, by increasing the temperature simultaneously along with constant light stimulation, the photoionization cross-section (σ) of these deeper traps increases due to the temperature dependence of OSL [12,18], thus making them accessible for stimulation by blue (470nm) light at the measurement temperatures of 121 and 232 °C respectively.

3.3.3. *Dosimetric properties of TA-OSL signal*

3.3.3.1 *Dose vs TA-OSL response*

The linearity of the integrated TA-OSL signal has been measured as a function of absorbed dose and found to be linear in the dose range of 0.1 to 10 kGy as shown in Fig. 3.13. The measured TA-OSL signal can be used to extend the applicability of α-Al₂O₃:C OSL phosphor for high dose

dosimetry upto 10 kGy, such as food irradiation, retrospective/accident dosimetry in nuclear and radiological emergencies, in harsh conditions of light exposure and temperatures such as fire accident. This is in contrast to applicability of α-Al$_2$O$_3$:C using conventional CW-OSL up to dose of 10 Gy. Later, other investigators have reported the dose response from deep traps of α-Al$_2$O$_3$:C upto 100 kGy using TL technique, though TA-OSL has been acknowledged as better and advanced technique [19]. The dose threshold was found to be 10 mGy using the in-house developed TL/OSL reader [14]. However, it can be further improved on improving the sensitivity of the reader system by using UV enhanced PMT.
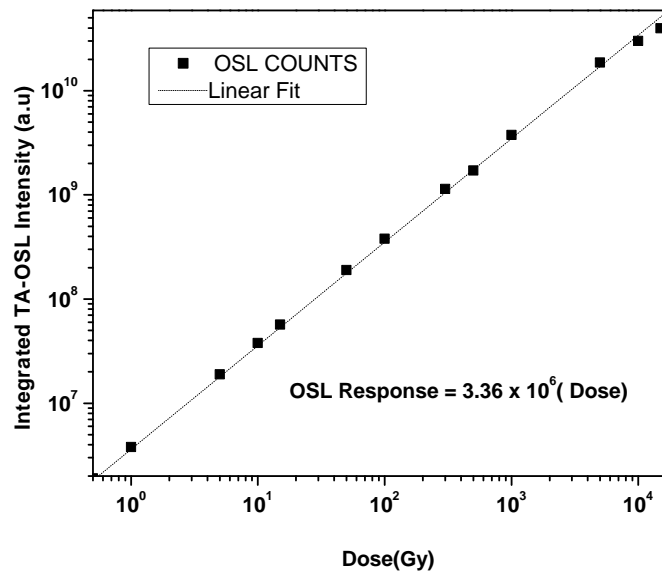
Fig. 3.13. Integrated TA-OSL dose response from deep traps of α-Al₂O₃:C.

3.3.3.2 Multiple TA-OSL readout

It was found that only 43% of total TA-OSL signal gets bleached out on first readout, while in the second readout the depletion of the signal is by 19.8% of the total TA-OSL. Hence by using this method one can have multiple readout of TA-OSL signal from deep traps. Fig. 3.14 shows

the results for successive readouts of TA-OSL signal while the inset of Fig. 3.14 shows the decay

pattern of this signal as a function of number of readouts. It also shows the percentage signal

which gets depleted in first and successive readouts. It was found that to erase the OSL signal

from these defects one must apply thermal treatment at temperature of ∼ 400 °C along with high

intensity of light stimulation power or otherwise the sample has to be annealed at 900 °C,

however, the former is preferred from the practical considerations. Therefore, even in extreme

environment of temperature of about 400 °C, these deep traps were found to hold the stored

information, if not exposed to intense light.
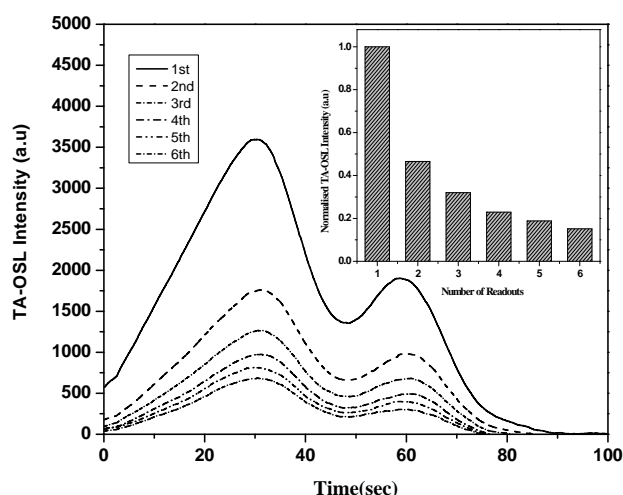
Fig. 3.14. Successive TA-OSL readout vs time with 200 mGy of β dose. Inset fig shows the Number of readouts vs normalized TA-OSL intensity showing the decay pattern of the signal on successive readouts.

Hence, handling of these samples in room light does not affect appreciably the signal from

deeper traps. Due to these properties of deep traps, the TA-OSL technique can be used to assess

the dose from previously irradiated dosimeter even if the main OSL traps have been

inadvertently bleached due to heat or light, thus proving its capability for accidental and

retrospective dosimetry. Further, using TA-OSL method these deep traps are accessible at 121 and 232 °C, which otherwise could be detected by Phototransfered TL (PTTL) [3], or direct TL measurement up to 600-650 °C for the first deep trap and up to 900 °C for second deep trap, but due to the very high thermal quenching in α-Al₂O₃:C and high infrared background at such higher temperatures, it is very difficult to record these high temperatures TL peaks by direct TL measurement. However, the TA-OSL measurements require normal TL-OSL reader [14], having simultaneous TL and OSL readout facility which is also available in commercial Risø reader [17]

3.3.4. *Nature of deep energy level defects*

The nature of deep traps in α-Al₂O₃:C powder was investigated by TA-OSL measurements. The samples were exposed to 10 Gy of gamma dose and then annealed at different temperatures in the range 400 to 900 °C, each for 10 minutes.
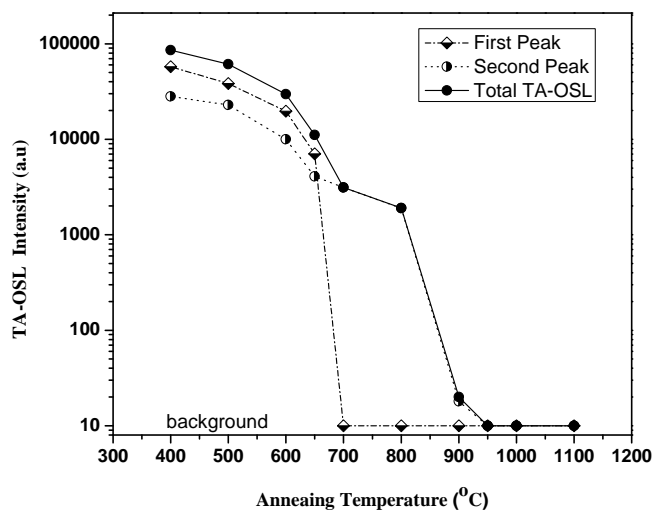
Fig.3.15. TA-OSL intensity variation of individual deconvoluted peaks and total TA-OSL on the annealing temperature after gamma irradiation of 10 Gy.

The samples thus annealed at different temperatures were subjected to TA-OSL measurement. It was found that there are two different deep traps being emptied at about 650 °C and 900 °C respectively. The temperature dependence of intensity of deconvoluted two individual peaks and total TA-OSL is shown in Fig. 3.15 which shows that TA-OSL intensity reduces with annealing treatment in the range 400 to 950 °C. The decrease in TA-OSL intensity for thermal treatment at 500°C may be due to the combined effect of decrease of 460 °C peak (as detected by Molnar et al., 2002) and 650 °C TL peaks. However, the first peak disappears in the sample annealed at 700 °C and only second peak remains in the TA-OSL glow curve as shown in Fig. 3.16.
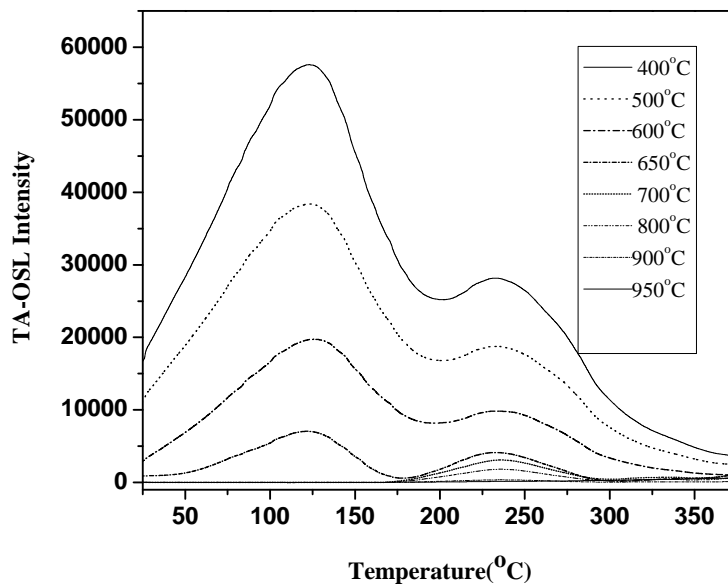
Fig. 3.16. TA-OSL intensity variation of α-Al₂O₃:C powder on the annealing temperature after gamma irradiation of 10 Gy, showing bleaching of both peaks at different temperatures.

Further, the sample annealed at 900 °C shows neither significant TA-OSL signal nor the peak in TA-OSL readout indicating that the second deep trap also gets emptied at 900 °C (Fig. 3.16).

In this TA-OSL method, sample is heated upto 400 °C along with simultaneous optical stimulation to deplete the signal from deeper traps. The samples can be reused after giving the

93

heat/annealing treatment upto 900 °C for complete resetting of the dosimeter. Heating the material upto 900 does not affects the defect levels/carbon impurity concentration. The alternative to above annealing treatment is elevated temperature (at 400 °C) optical bleaching (470 nm light) at high optical power for 2 hours to reset the dosimeter. This treatment will further avoid the effect (if any) on the sensitivity/reusability of the material is case of annealing treatment.

The 900 °C annealed sample, which shows no TA-OSL output, was irradiated with UV light of 203 nm to find out the nature of such traps. The UV irradiation with 203 nm light preferentially results in the release of electrons from F-centers to the conduction band and populates the different traps in the phosphor [6]. The irradiated sample was subjected to TL readout up to 400 °C to empty the dosimetric traps and then TA-OSL measurement was carried out, which again results in two well-defined TA-OSL peaks as shown in Fig. 3.17, similar to that observed in gamma irradiated sample in which both holes and electrons are formed due to effect of ionization by high energy gamma rays in the phosphor material. Hence, the appearance of two TA-OSL peaks from deep traps, which get populated due to electron released from F-center during shining of UV radiation of 203 nm on the sample and no holes are generated, suggests that the nature of both the types of deep traps is electron.
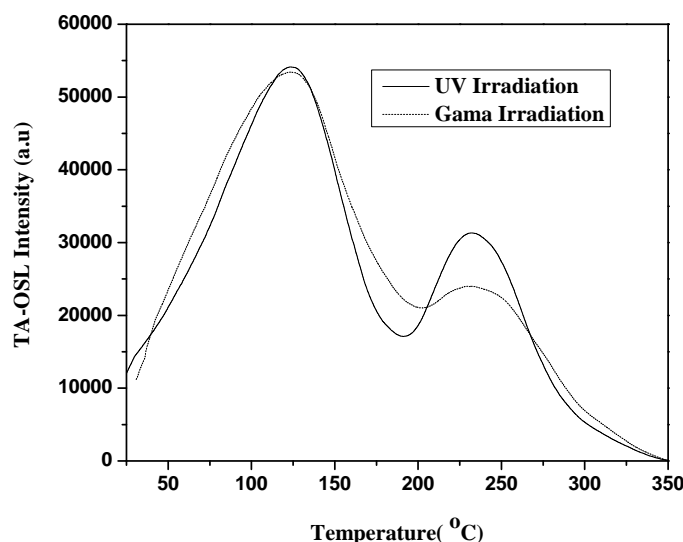
Fig. 3.17. Comparison of TA-OSL glow curve of α-Al₂O₃:C powder gamma irradiated by 10 Gy of gamma and equivalent dose of 203 nm of UV light.

 Further, as the first trap gets emptied at 650 °C, while the second trap is stable at this temperature and get depleted at 900 °C, suggests that both are due to different electron traps and accordingly get emptied at different temperatures. The sample annealed at 700 °C having only second peak was irradiated with UV light of 310 nm for 30 s which does not excite the F and F$^+$-center electrons. It regenerates the first peak along with the second peak in TA-OSL readout of this sample as the 310 nm light transfers few of the electrons from the second trap to first deep trap. It also suggests that both the deep traps in α-Al₂O₃:C powder are electron trap in nature because if the trap ~ 650-700 °C was hole in nature, only one peak would have appeared on such treatment. However, the detailed experimental results of Akselrod and Gorelova [3] and Yukihara et al. [5,6] demonstrated that in α-Al₂O₃:C crystals the 650 °C might be a hole trap. This contradiction with our results may be because of the reason that the effect of UV exposure on TA-OSL is not sufficient to reach a conclusion as both 203 and 310 nm exposure may lead to electron transition from the valence band to the impurity level and produce free holes. Thus,

95

more detailed studies involving direct measurement of F and F$^+$-centers along with TA-OSL in Al$_2$O$_3$:C would be required to assign the nature of deep traps. All the above results have been published in the international journal [20].

3.3.5 Reusability and Phase stability

The reusability of the sample was tested after heating it upto 900°C. The variation in the sensitivity was found to be less than 1% in repeated readout (Fig. 3.18). The samples can be reused after giving the heat/annealing treatment upto 900°C for complete resetting of the dosimeter. Heating the material upto 900°C does not affects the defect levels/carbon impurity concentration. The α phase of Al$_2$O$_3$:C does not undergo phase transition at such temperature range. The XRD was performed on fresh samples as well as those used five times (and annealed at 900°C after each readout). The results show no change in its phase and peak position (Fig 3.19).
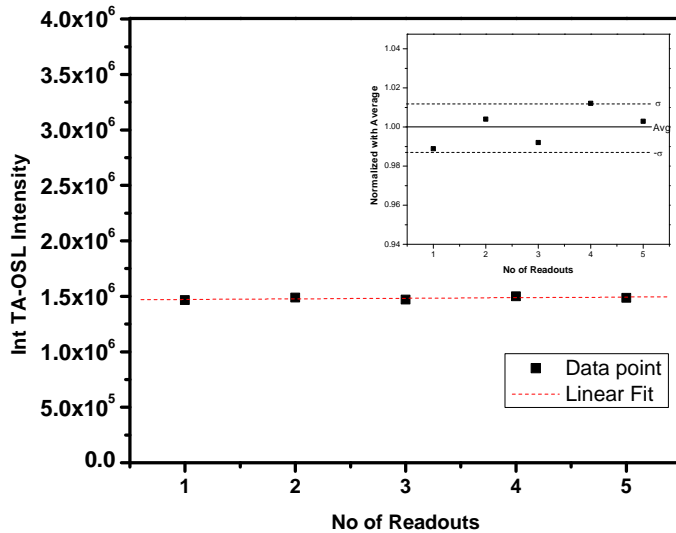
Fig. 3.18: Variation in TA-OSL readout (sensitivity of the material) with number of readouts. Inset shows the statistical variation in the sensitivity.
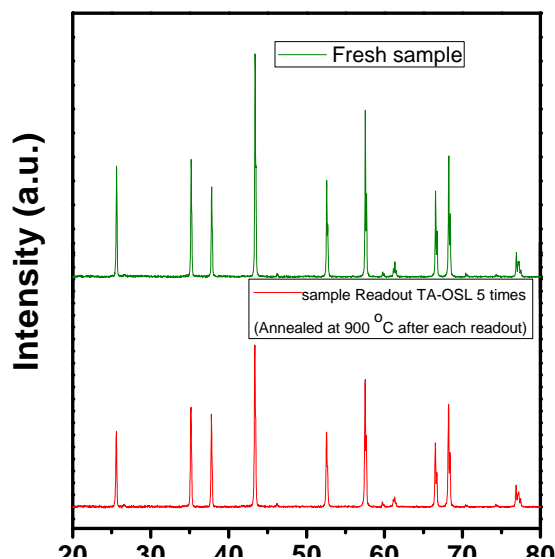
Fig. 3.19: XRD of fresh sample as well as those used five times (and annealed at 900°C after each readout).

Further, in this method, blue light is used to stimulate the traps which does not irradiate the traps. UV light of specific wavelength (203 nm), which is the excitation wavelength for the F-center in α-Al₂O₃:C, do irradiate the sample which leads to OSL. This part of the spectrum in the Led is blocked by placing GG-435 optical filter in front of the blue LED.

3.4. Conclusions

This chapter presented the novel method of accessing the deep energy level defects of α-Al₂O₃:C phosphor by stimulating with visible light at elevated temperatures, but at significantly lower temperatures than their respective TL peak temperatures, due to increase in their photoionization cross-section at such temperatures. It also revealed that TA-OSL signal from these traps can be used to extend the use of α-Al₂O₃: C phosphor in high dose dosimetry applications such as retrospective dosimetry, accidental dosimetry, and irradiation of food

products. Using TA-OSL method, one can make multiple readouts from the deep defects in an irradiated phosphor material, thus can be used for confirmation/re-estimation of the measured dose in the certain exposure cases. The dosimetric properties and nature of deep traps have been studied. Both the deep traps have been found to contribute to TA-OSL peaks at 121 and 232 °C, respectively with delocalization temperatures of about 650 and 900 °C. By using the method suggested in this chapter, further study on material such as quartz and feldspar will help in extending the dose range of these materials for archaeological and geological dating applications. The measurement of E_A and pre-exponential factor is important to understand the change in value of photoionization cross-section with LET of incident charge particle such as β, α and HCP (Heavy Charge particles). Next chapter will discuss the utilization of TA-OSL technique for the improvement of dose threshold of α-Al₂O₃:C which can be applied on others phosphors too.

References

1. Evans, B. D. and Stepelbroek, M., 1978. *Phys. Rev. B* 18, 7089-7098.

2. Lee, K. H. and Crawford, J. H., 1979. *Phys. Rev. B* 19, 3217-3221.

3. Bulur, E., Goksu, H. Y., and Wahl, W., 1999. *Radiat. Meas.* 30, 203-206.

4. Akesrold, M.S., and Gorelova, E.A., 1993. *Nucl. Tracks Radiat. Meas.* 21, 143-146.

5. Yukihara E. G., Whitley. V.H., McKeever, S.W.S., Akselrod, A.E., Akselrod, M.S., 2004. *Radiat. Meas.* 38, 317-330.

6. Molnar, G., Benabdesselam, M., Borossay, J., Iacconi, P., Lapraz, D.and Akselrod, M. 2002. *Radiat. Proc.Dosi* 100, 139-142.

7. Yukihara E. G., Whitley. V.H., Polf, J.C., Klein, D.M., McKeever, S.W.S., Akselrod, A.E., Akselrod, M.S., 2003. *Radiat. Meas.* 42, 627-638.

8. Akselrod, M.S., Agersnap Larsen, N., Whitley, V. and McKeever, S.W.S., 1998. *J Appl. Phy.* 84, 3364-3373.

9. Polymeris, G. S., Raptis, S., Afouxenidis, D., Tsirliganis, N.C., Kitis, G., 2010. *Radiat. Meas.* 45, 519-522.

10. Umisedo, Nancy., K Elisabeth, M. Yoshimura, Patricia, B.R., Gasparian, Yukihara E.G., 2010. *Radiat. Meas.* 45, 151-156.

11. Hütt, G., Jaek, I., Tchonka, J., 1988. *Quaternary Sci. Rev.* 7, 381-385.

12. Spooner, N. A., 1994. *Radiat. Meas.* 23, 593-600.

13. Mishra, D.R., Soni, Anuj., Rawat. N. S., Kulkarni, M.S., Bhatt. B. C., and Sharma, D.N., 2011. *Radiat. Meas.* 46, 635-642.

14. Kulkarni, M.S., Mishra, D.R. and Sharma, D.N., 2007. *Nul. Ins., Method in Phys. B.* 262, 384-356.

15. Bos, A. J. J. and Wallinga, J., 2009. *Phys. Rev. B* 79, 195118.

16. Benevides, L., Romanyukha, A., Hull, F., Duffy, M., Voss, S., Moscovitch, M., 2010. *Radiat. Meas.* 45, 523-526.

17. Bøtter-Jensen, L., Bulur, E., Duller, G.A.T., Murray, A.S., 2000. *Radiat. Meas.* 32, 523–528.

18. McKeever, S .W.S., Bφtter-Jensen, Agersnap Larsen, N, and Duller, G.A.T. 1997. *Radiat. Meas.* 27, 161-170.

19. Kortov, V., Ustyantsev, Yu. *Radiat. Meas.* 56 (2013) 299-302.

20. Soni, Anuj., Mishra, D.R., Bhatt. B. C., Gupta, S.K., Rawat. N. S., Kulkarni, M.S., and Sharma, D.N., 2012. *Radiat. Meas.* 47, 111-120.

Chapter 4

Improvement in MDD of

α-Al$_2$O$_3$:C

This chapter illustrates the influence of electron-phonon interaction on the shape of the OSL decay curve of α-Al$_2$O$_3$:C and improvement in its minimum detectable dose (MDD) using TA-OSL. It presents the theoretical formulation and experimental validation of the method used for improvement in MDD and comparison with other existing techniques.

4.1. Introduction

The optical methods of stimulating luminescent materials have gained new ideas in last decade with introduction of Pulsed-OSL, using monochromatic, short duration ($\approx$ 300 ns) laser,

pulsed stimulation is performed and luminescence is recorded between such series of stimulation pulses separated by few hundred microseconds interval and the light detection is gated during such pulsed stimulation. This gives the fastest readout and high signal to noise ratio (S/N) and thus strongly recommended for personnel monitoring with fast readout time and high throughput. However, the traditional way of stimulating phosphor is continuous wave (CW)-OSL mode, where the stimulation light intensity is held constant with respect to time and decay of OSL signal thus recorded. The decay constant of such a CW-OSL curve under first order kinetics contains information about photo-ionization cross-section of traps participating in OSL phenomenon. Mishra et al (2011) suggested that non-linearly (particularly for parabolic profiles) modulated NL-OSL technique provides better signal to noise ratio compared to LM-OSL technique [1]. Wallinga and A.J.J. Bos 2008 measured the continuous wave (CW), linearly modulated (LM), as well as hyperbolically modulated (HM) OSL responses to β-dose on a range of samples from different provenance and with different dominance of OSL components [2]. They suggested that the CW-stimulation is the method of choice for dating phosphors as it allows the fastest readout among these techniques with the highest signal to noise ratio. The data reported in the paper was for non-pulsed readout. The relatively long time of CW-OSL recording generates considerable amount of background counts due to scattering of stimulating light from sample holder, LED light leakage due to inadequate optical filtration of the stimulated light by optical filter combination. This results in degradation of overall signal to noise ratio. The overall background in the recorded OSL signal can be expressed as [1]

$$OSL\ counts\ (N_{OSL}) = \quad N_{PMT} + N_{sc} + N_e \tag{4.1}$$

Where,

N_{PMT} : Dark counts of PMT,

N_{sc} : background signal generated due to scattering of stimulation light from sample / sample holder and inadequate optical filter action which does not fully cut off stimulation wavelength.

N_e: Background counts contributed due to electronics hardware / circuit used for stimulation as well as detection of PMT output signals at amplifier and pre-amplifier.

The dark counts of PMT (N_{PMT}) can be reduced by properly controlling the bias voltage, providing adequate cooling to PMT, shielding it against external magnetic field by μ-shielding material [3] (Baiccker J. A., 1960). The major background component in OSL reader systems is the counts originated due to leakage of stimulation light (Nsc). It has dependence on many factors; most important among them is selection of cut-off optical filters. For example, most of OSL readers used to study the α-Al$_2$O$_3$: C, contain combination of optical filters across blue LED and PMT, e.g., GG-435 + UG-1 or GG420+Hoya (U)-340. Since both these combinations of filters have partially overlapping transmission band across 400-440 nm, the incident blue (470nm) light after leakage through the filter combination system, scattering from sample / sample holder reaches PMT photocathode. Apart from this both Schott UG-1 and Hoya U-340 optical filters have considerable transmission in red (>690 nm) spectrum, which transmits the low intensity red components of blue LEDs and contributes to unwanted background signal. However, due to low quantum efficiency of bi-alkali photocathode PMT in the red region, the background counts due to this wavelength range are less important as compared to the background counts contribution due to blue overlapping wavelength range. The contribution of these background signals increases with increase in the value of stimulation intensity and reflectivity of sample/sample holder. The contribution of this signal can be reduced substantially by reducing the reflectivity of sample holder and statistically stabilizing the stimulation intensity, so that the large part of this background signal can be subtracted as constant background. Therefore, in brief, the background counts generated due to scattering of stimulation light N$_{sc}$ can

be reduced if the total integrated stimulation flux incident on sample during readout is reduced without compromising on total OSL signal.

In the traditional CW-OSL method, it is not possible to achieve lower total integral flux without compromising on total OSL signal as the total integral flux required to take out complete OSL signal is fixed for the given dose for the given material. The aim of present investigation is to improve signal to noise ratio for α-Al₂O₃: C using CW-OSL readout by taking the advantage of temperature dependence of photoionization cross-section. The temperature dependence of photoionization cross-section on the decay constant and its application for the improvement in the dose threshold is discussed.

4.2. CW-OSL at Elevated Temperatures

In the chapter 2 the theory TA-OSL was formulated for recording OSL along with linear heating of the material. The TA-OSL equation for taking CW-OSL at constant elevated temperature can be found by incorporating Eq. (2.3) into Eq. (1.11), and solving for n_o, we get temperature dependent CW-OSL as :

$$I_{TA-OSL} = n_o \, \phi_o \, \sigma_o(\lambda) \, e^{-\frac{E_A}{k \, T}} e^{-\phi_o \sigma_o(\lambda) \, e^{-\frac{E_A}{k \, T}} t} \qquad (4.2)$$

4.2.1 Temperature dependence of decay constant

Fig. 4.1 shows numerically simulated temperature dependent CW-OSL intensity using Eq. (4.2) at various temperatures. The values of parameters in the simulations were used which were evaluated experimentally in chapter 2 i.e $E_A = 0.039$ eV, $\beta = 4$ K/s and $\sigma_o(\lambda)= 5.5 \times 10^{-18}$ cm^{-2}, with a fixed CW stimulation intensity $\phi_o= 48$ mW/cm^2 of 470 nm light. These CW-OSL curves show the change in CW-OSL decay constant as a function of temperature.
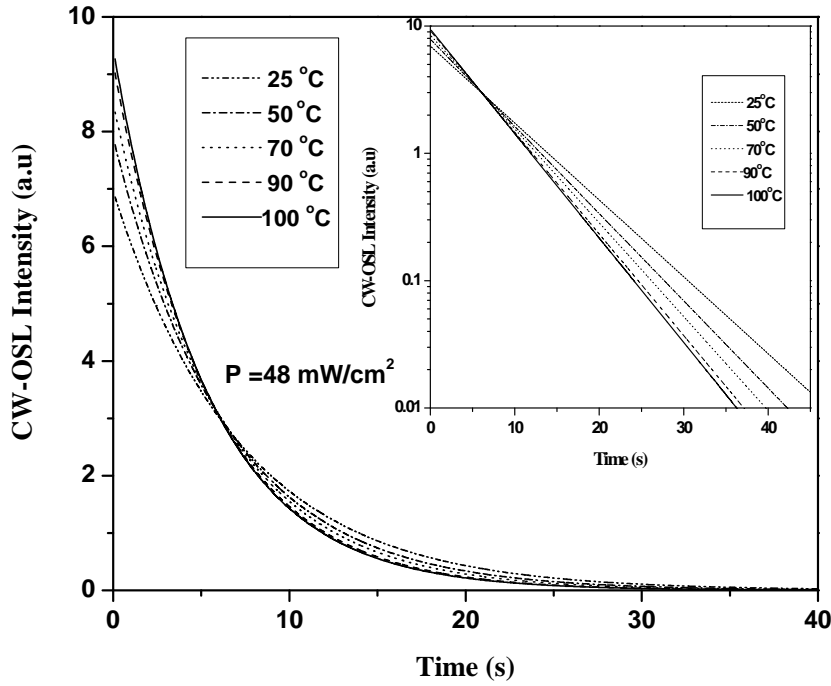
Fig. 4.1: Numerically simulated CW-OSL at various temperatures for a given set of experimentally evaluated values in chapter 2 as $E_A = 0.039$ eV, $\beta = 4$ K/s and $\sigma_o(\lambda) = 5.5 \times 10^{-18}$ cm⁻², with fixed CW-stimulation intensity $\phi_o = 48$ mW/cm² of 470 nm light. Inset figure shows the same in log scale.

4.2.2 Stimulation intensity dependence of decay constant

Similarly, Fig. 4.2 shows numerically simulated CW-OSL intensity at various CW stimulation intensities, at 25 °C using the same set of experimentally evaluated values. These CW-OSL curves show the change in CW-OSL decay constant as a function of stimulation intensity. The temperature required to increase the decay constant at a particular stimulation intensity can also be given by incorporating Eq. (2.3) in Eq. (2.1) as

$$T = \frac{E_A}{K \ln \dfrac{\varphi \sigma_o}{f}} \qquad (4.3)$$

104
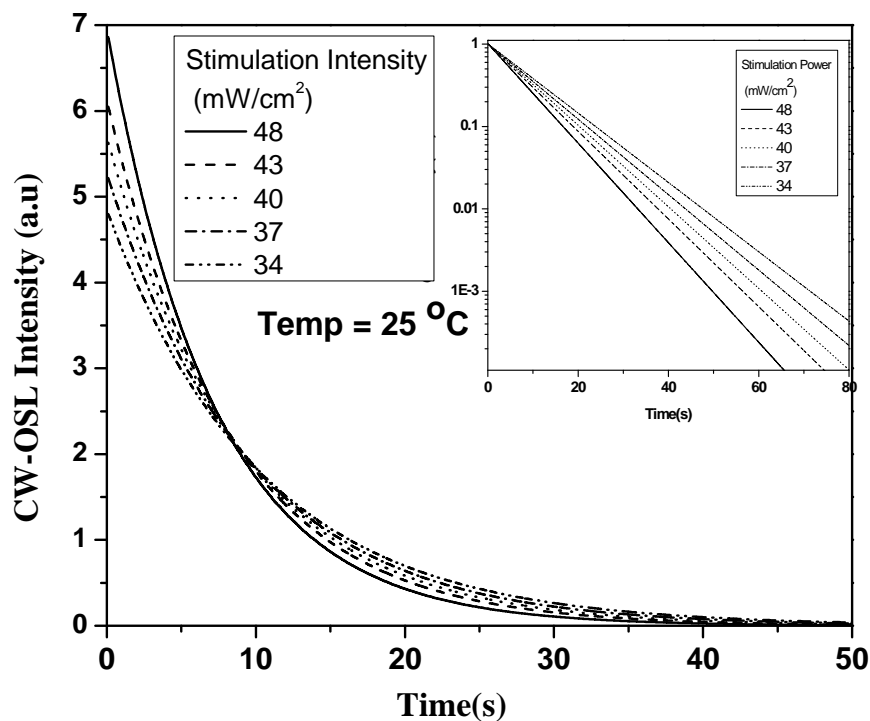
Fig. 4.2: Numerically simulated CW-OSL for various stimulation intensities of 470 nm light for a given set of experimentally evaluated values E_A = 0.039 eV, β = 4 K/s and $σ_o(λ)$= 5.5 ×10 $^{-18}$ cm^{-2}, at fixed stimulation temperature 25 °C. Inset figure shows the same in log scale.

Table 4.1 shows theoretically evaluated temperature as well as experimentally required temperature at various stimulation intensities for obtaining same decay constant. Slight mismatch between the experimentally and theoretically evaluated values may be attributed to the simplified assumptions in the theoretical TA-OSL equation.

Table 4.1: **Pairs of values of stimulation intensity and OSL readout temperature for obtaining same decay constant.**

Power (mW/ cm^2)	Decay Constant (f= σφ) (s^{-1})	Temperature (^{o}C) (Theoretical)	Temperature (^{o}C) (Experimental)
48	0.192	25	25
43	0.192	49	40
40	0.192	60	50
37	0.192	70	60
35	0.192	85	75
30	0.192	100	85

4.3 Theoretical Formulation for MDD Improvement

For the *S/N* consideration, we have to compare the *S/N* for higher stimulation intensity to that at lower stimulation intensity at room temperature (RT)

$$\frac{^{RT}\left(S_H / N_H\right)}{^{RT}\left(S_L / N_L\right)} = k \tag{4.4}$$

Where S_H/N_H and S_L/N_L are the signal to noise ratio for higher and lower stimulation intensity respectively. However, assuming the first order decay and acquisition of complete area lead to same amount of signal ($S_H=S_L$) i.e., the dose is same for both the cases, the values of k which is the measure of figure of merit is given by:

$$\frac{^{RT}\left(S_H / N_H\right)}{^{RT}\left(S_L / N_L\right)} = k = \frac{^{RT}N_L}{^{RT}N_H} \tag{4.5}$$

So the value of k is nothing but the ratio of noise at lower stimulation intensity to that at higher stimulation intensity. The differential noise for any stimulation intensity at RT is given by

$$\frac{^{RT}dN}{dt_R} = N_{sc} + N_{PMT} + N_e$$

$$^{RT}N = \int_0^{tR} \left(N_{sc} + N_{PMT} + N_e \right) dt_R$$

$$^{RT}N = t_R \left(N_{sc} + A \right)$$

Where $A = N_{PMT} + N_e$, which is independent of stimulation intensity whereas N_{sc} is a function of stimulation intensity and t_R is total time of readout. Therefore, the value of k is given by

$$\frac{^{RT}N_L}{^{RT}N_H} = \frac{t_{RL} \left(N^L{}_{sc} + A \right)}{t_{RH} \left(N^H{}_{sc} + A \right)}$$

Where, $N^L{}_{sc}$ and $N^H{}_{sc}$ are the scattering noise for lower and higher stimulation intensity respectively and t_{RL} and t_{RH} are the time of readout for lower and higher stimulation intensity respectively. As $N_{sc} >> A$, therefore, the value of k can be written as

$$\frac{^{RT}N_L}{^{RT}N_H} = \left(\frac{t_{RL}}{t_{RH}} \right) \left(\frac{N^L{}_{sc}}{N^H{}_{sc}} \right)$$

$$k = \eta * \xi \tag{4.6}$$

where,

$$\eta = \left(\frac{t_{RL}}{t_{RH}} \right) \quad and \quad \xi = \left(\frac{N^L{}_{sc}}{N^H{}_{sc}} \right)$$

Where ξ is independent of temperature while η is a function of temperature. At RT $\eta > 1$ ($t_{RL} > t_{RH}$) for taking complete signal and $\xi < 1$ as reported in the literature [1].

Evaluating the value of k for 48 mW/cm^2 and 30 mW/cm^2 at RT from Eq (4.6) by putting $t_{30} = 90$ s, $t_{48} = 70$ s, N_{sc} (P_{30}) = 220 and N_{sc} (P_{48}) = 380 from Fig. 3 of Mishra et al., 2011, we get $k = 0.74$.

Therefore, the signal to noise ratio (at RT) at higher stimulation intensity is slightly better than that at lower stimulation intensity. This value of k is for commercial reader (having highest detection threshold) where one will get almost same signal ($S_H = S_L$) for two values of stimulation intensities so we canceled the S term in Eq. 4.5. However, for moderate sensitivity reader system (laboratory reader system) signal S never come same ($S_H \neq S_L$) for two different values of stimulation intensities due to the problem of detection threshold of PMT. In such cases, one cannot cancel S in Eq. 4.5 for two different intensities. S will be more for higher stimulation intensity as compared to that at lower stimulation intensity. Thus, for practical reader system k is slightly more than 1 due to $S_H > S_L$. So for such reader system we get higher signal to noise ratio at higher stimulation intensities.

Now considering the effect of temperature in Eq 4.6, the value of $\eta \sim 1$ at elevated temperature i.e, ($^{TH}t_{RL} = t_{RH}$) due to temperature dependence of photoionization cross-section (where, $^{TH}t_{RL}$ is time taken to take complete signal at lower stimulation intensity with higher temperature). As the signal increases at high temperature due to thermally assisted OSL, we have ($^{TH}S_L \sim S_H$). Therefore, the value of k at higher temperature will only depend on ξ which is <1. Thus, the signal to noise ratio with lower stimulation intensities at elevated temperature is better than the one with higher stimulation intensities at lower (or room) temperature.

4.4. Materials and method

The dosimetry grade single crystal of α-Al$_2$O$_3$: C (TLD 500; 5 mm dia, 0.8 mm thick) was irradiated using a calibrated ^{90}Sr/^{90}Y beta source to an absorbed dose of 40 mGy and used for recording CW-OSL signals. The CW-OSL was recorded at various temperatures and various stimulation intensities for the irradiated samples in a laboratory developed integrated TL/OSL measurement set-up [3].

4.5 Results and Discussion

4.5.1 Measurements of background scattering signal during CW-OSL

The comparison of signal-to-noise ratio (S/N) in all CW-stimulation cases is required to measure scattering counts recorded during the CW-OSL stimulation, with an un-irradiated OSL sample. This scattering contributes to the background signal, which is termed previously as N_{sc}. The relation of this background counts with stimulation intensity (P) has been shown in Fig.4.3.
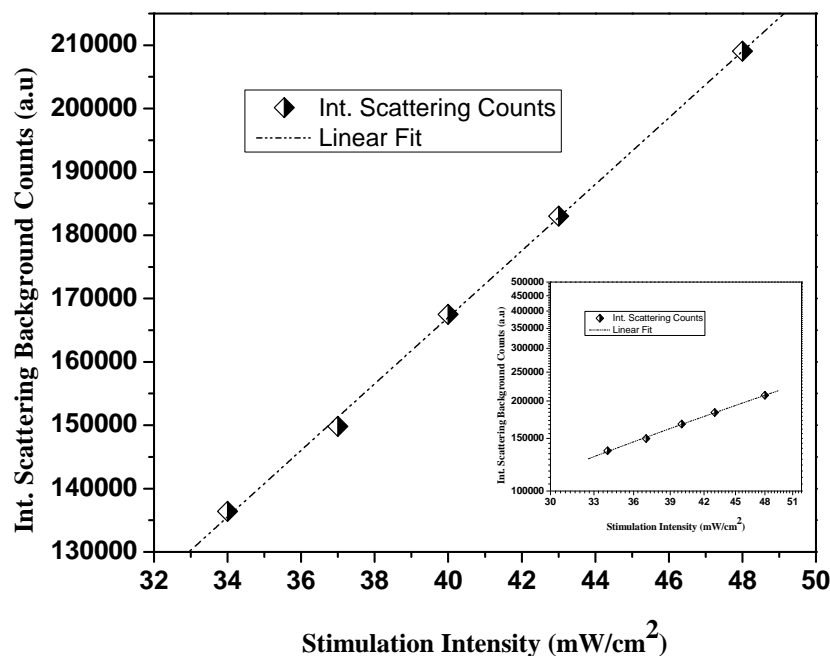
Fig. 4.3. Background count due to CW-Stimulation light detected by PMT with sample stimulated for various final intensities and fixed time at 25 °C. Inset figure shows the same in log scale.
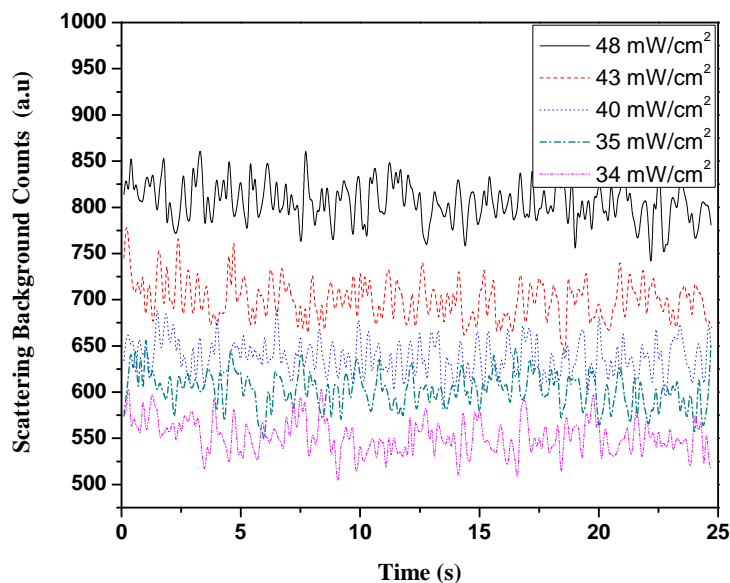
Fig. 4.4. Variation of scattered background signal recorded in PMT for various stimulation intensities and fixed time at 25 °C.

The background counts due to scattering of stimulation light can be expressed as

$$N_{sc} = \chi P^{m} \tag{4.7}$$

Where N_{sc}: signal due to leakage of scattered light, from the filter assembly and detected by PMT, expressed in terms of counts, which correspond to current / charge generated in PMT due to photons falling on the photocathode.

χ : is a constant which depends on reflectivity, geometrical considerations- solid angle cone seen by photocathode from sample position, the focusing of stimulation light on sample position and the set of cutoff filters used across PMT & LED stimulation light source. Therefore, this factor varies with sample to sample and optical surface quality of OSL sample under readout.

P: is the optical stimulation intensity expressed in mW/cm^2.

m: dimensionless constant which measures the degree of linearity of N_{sc} for given range of optical stimulation intensity (P). The values of χ and m have been determined for the present OSL reader system as 9.1 and 0.98, respectively. Since the present value of m (≈ 0.98) shows that the N_{sc} is directly proportional to optical stimulation power, as expected, any reduction in optical stimulation power will directly lead to reduction in noise contributed due to this stimulation light scattering. The experimentally recorded value of N_{sc} in CW-OSL stimulation mode with single crystal α-Al₂O₃:C has been shown in Fig. 4.4. The net integral counts due to the scattering stimulation noise N_{sc} has been extracted from total background signal in the presence of bare sample. The reduction in stimulation light scattering reduces the standard deviation in the total background signal. Fig. 4.5 shows the variation in standard deviation in background count as a function of CW-stimulation light intensity with sample stimulated for fixed time at 25 °C.
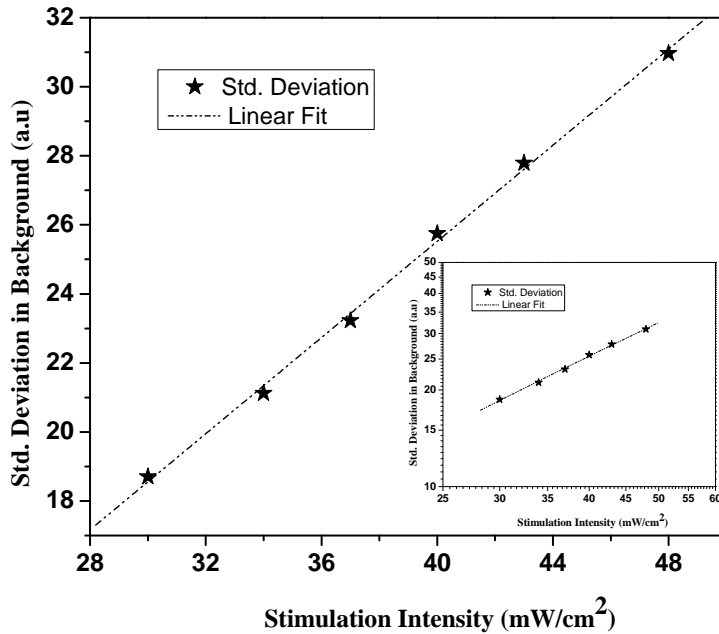
Fig. 4.5. Standard deviation in background count vs CW-stimulation light intensity with sample stimulated for fixed time at 25 °C. Inset figure shows the same in log scale.

4.5.2 Improvement in MDD

The CW-OSL of α-Al$_2$O$_3$:C was recorded at various stimulation intensities for same beta dose of 20 mGy. It is clear from Fig. 4.6 that the decay constant of CW-OSL reduces on reducing the stimulation intensity and it takes more time to take the complete signal at lower intensities. In case of OSL measurement, the background signal is due the scattering of the stimulation light intensity from the planchet.
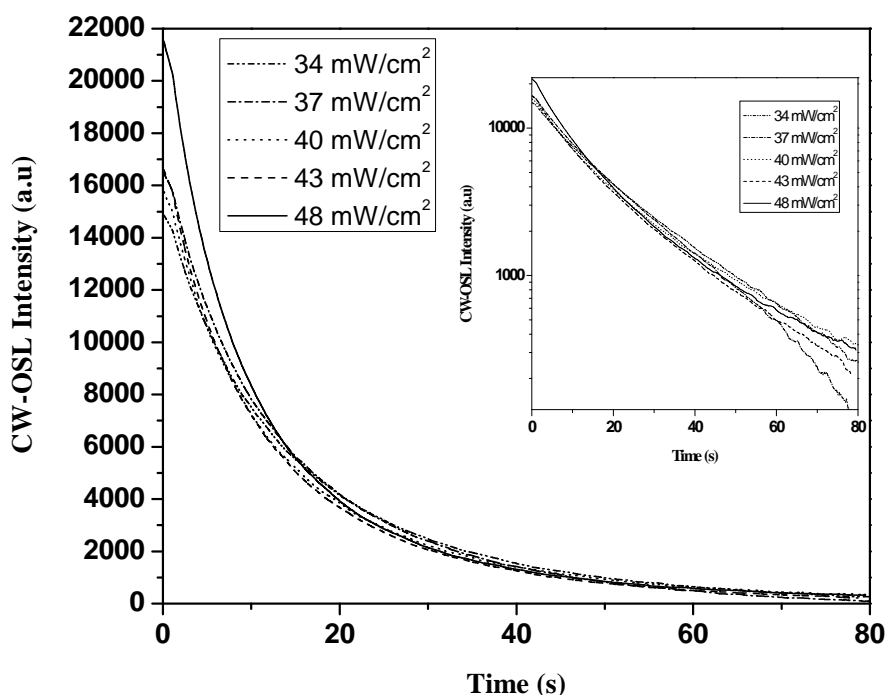
Fig. 4.6: Experimentally evaluated CW-OSL of Al₂O₃:C for various Stimulation intensities of 470 nm light at fixed stimulation temperature 25 °C. Inset fig shows the same in log scale.

At lower stimulation light intensities, the scattering component and thus the standard deviation of the background signal reduces considerably but the readout time increases as the decay constant of OSL signal increases. The dose threshold of phosphor depends on the standard deviation of the background signal which affects the signal to noise ratio of the instrument. The

decay constant also depends on the photoionization cross-section of the OSL active traps in the phosphor participating in OSL phenomenon and thus on the readout temperature due to the temperature dependence of photoionization cross-section. Hence, the CW-OSL of α-Al$_2$O$_3$:C was also recorded at various temperatures at stimulation intensity of 48 mW/cm^2 as shown in Fig. 4.7.
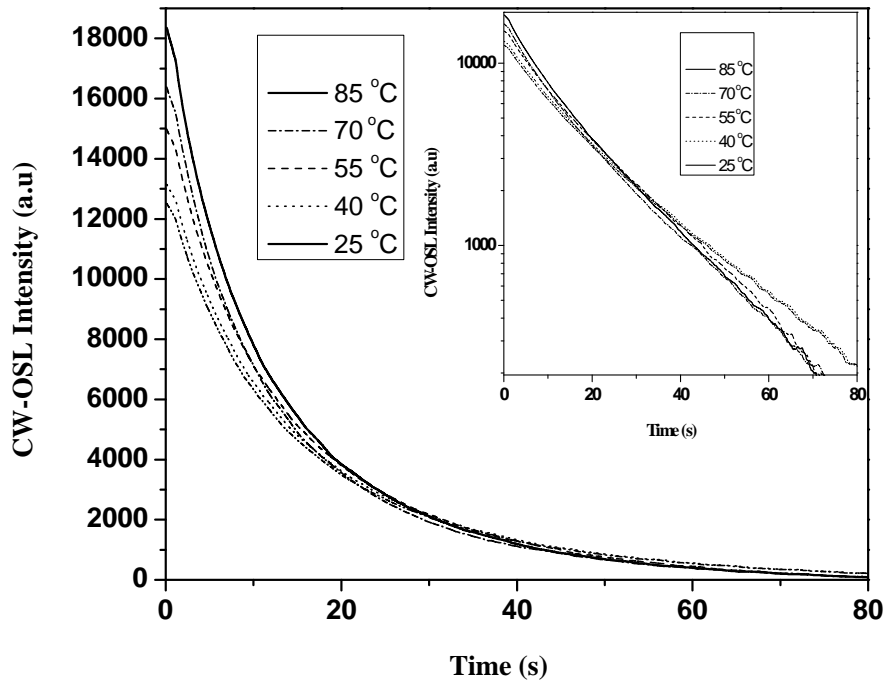
Fig. 4.7: Experimentally evaluated CW-OSL of Al$_2$O$_3$:C at various temperatures for a fixed stimulation intensity 48 mW/cm^2 of 470 nm. Inset fig shows the same in log scale.

Henceforth, this technique will be referred to as thermally assisted CW-OSL (TA-CW-OSL). In addition, the increase of readout temperature does not affect the standard deviation in the background signal of OSL readout. The background signal was measured 10 times, consecutively. The evaluation of standard deviation in the total signal was done by measuring 10 different samples. The optimized elevated temperature for α-Al$_2$O$_3$:C was found to be 85 °C as

its 57 °C TL peak being not OSL sensitive but the main dosimetric peak (184 °C) which is OSL sensitive, starts giving signal from 90 °C onwards. (Fig. 4.8 shows the TL glow curve of α-Al₂O₃:C taken at 4K/s).
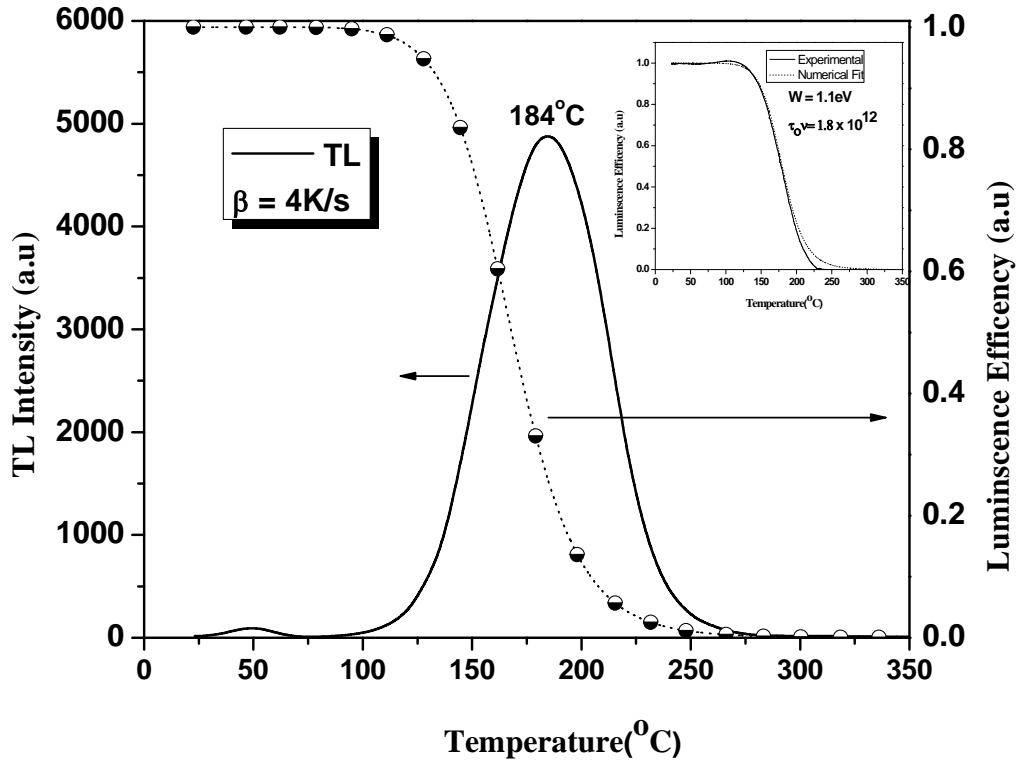
Fig. 4.8: TL glow curve of α-Al₂O₃:C for a beta dose of 100 mGy showing that the main dosimetric peak starts giving signal at 95 °C onwards. Inset figure shows the luminescence efficiency measured using elevated temperature CW-OSL vs temperature, which reveals decrease in luminescence efficiency from 120 °C onwards.   Region (25 to 100 °C) - No thermal quenching, region (100 to 120 °C)- negligible thermal quenching, region (120 to 250 °C) - dominating thermal quenching.

The thermal quenching of F-center is reported at higher temperature (>130 °C) in Al₂O₃:C [4] and can be expressed in terms of luminescence efficiency with respect to temperature as:

$$\eta = \frac{1}{1 + \tau_o \nu \exp\left(-\dfrac{W}{kT}\right)} \qquad (4.8)$$

Therefore, the effect of thermal quenching of F-center in CW-OSL measurement has been determined for the sample under study by using elevated temperature CW-OSL measurement of dosimetric trap (185 °C TL peak) for same absorbed dose and fixed stimulation intensity of 48mW/cm² [5]. Appropriate corrections for partial loss of OSL signal at elevated temperature due to isothermal decay of TL signal have been incorporated. The Fig. 4.8 shows the total TL and elevated temperature normalized CW-OSL intensity for various temperatures revealing the presence of strong thermal quenching of F-center in the temperature range 130 °C - 220 °C in α-Al₂O₃:C. The inset of Fig. 4.8 shows the numerical fitting of Eq. (4.8) to the experimental data with the measured value of W (1.1eV) and $\tau_o\nu$ (1.8 ×10¹²) which are in good agreement with those reported by other researchers. It is found that thermal quenching starts dominating above 130 °C. Therefore, the decay constant of the CW-OSL was increased without compromising on the total OSL signal. Fig. 4.9 shows the CW-OSL readout of α-Al₂O₃:C at two different stimulation intensities 30 and 48 mW/cm² at 25 °C, showing the change in the CW-OSL decay constant as a function of stimulation intensity.
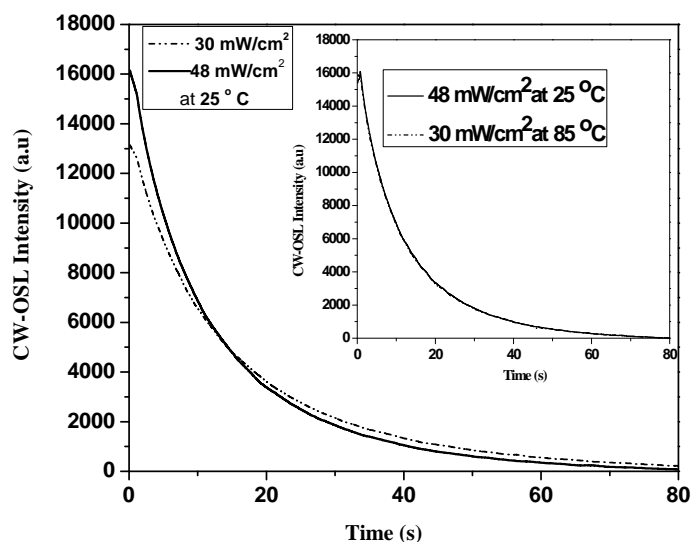
***Fig. 4.9: Experimentally evaluated CW-OSL of α-Al₂O₃:C at two different stimulation intensities at 25
•C, showing the change in the CW-OSL decay constant as a function of stimulation intensity. Inset
figure shows the effect of temperature to achieve the same CW-OSL decay constant at different
stimulation intensities***
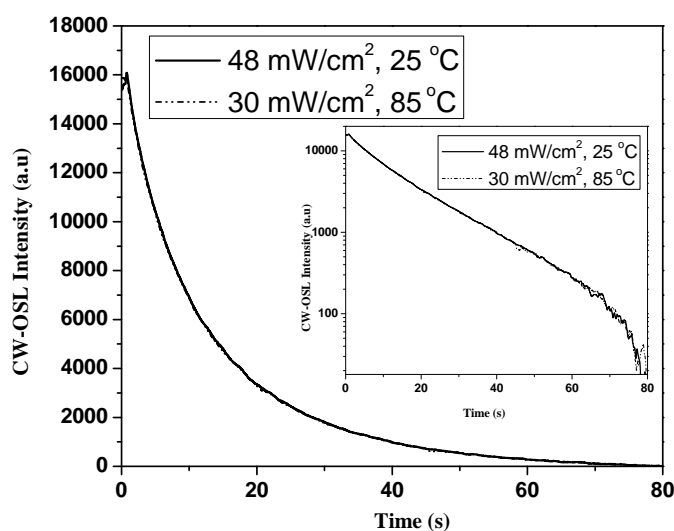
***Fig 4.10: CW-OSL of α-Al₂O₃:C at different stimulation intensity with optimized temperatures to make
achieve same decay constant.***

The CW-OSL signal taken at 30 mW/cm^2 stimulation intensity takes more time to decay to the same level when as compared to that at higher intensity. In order to achieve the same decay constant i.e. to take the OSL measurement in the same time at 30 mW/cm^2 stimulation light intensity as that at 48 mW/cm^2 light intensity, the temperature of measurement for α-Al₂O₃:C was raised (Fig. 4.10). Table 4.2 shows the variation of decay constant at various temperatures and optical power.

Table 4.2: Variation of Decay constant at various temperatures and optical power. (CW-OSL and TA-CWOSL method).

Power (mW/ cm²)	Decay Constant (f= σφ) (s⁻¹)				Std Dev. In Bkg	Improve ment factor in MDD	MDD of Al₂O₃:C (µGy)	Respective temperatures (°C) for same decay constant
	25°C	**45°C**	**60°C**	**85°C**				
48	**0.192**	0.221	0.245	0.258	30.96	1	20.00	25
43	0.181	0.210	0.232	0.249	28.79	1.07	18.79	35
40	0.151	0.183	0.208	0.221	25.65	1.20	16.66	50
35	0.123	0.151	0.182	0.203	21.23	1.45	13.79	65
30	0.113	0.130	0.161	**0.191**	17.69	1.75	11.40	85

As a result of lowering the stimulation intensity (30 mW/cm^2) at higher temperature (85 °C), the standard deviation in the background signal was found to be improved. Therefore, the overall dose threshold of α-Al₂O₃:C was improved by 1.8 times to that measured at higher intensity (48 mW/cm^2) at 25 °C. As a results, the MDD of α-Al₂O₃:C is reduced from 20 µGy to 11.4 µGy

using integrated TL/OSL reader. Fig. 4.11 shows the improvement in MDD as a function of stimulation intensity and experimentally evaluated values of decay constant at various combination of readout temperature and stimulation intensity.
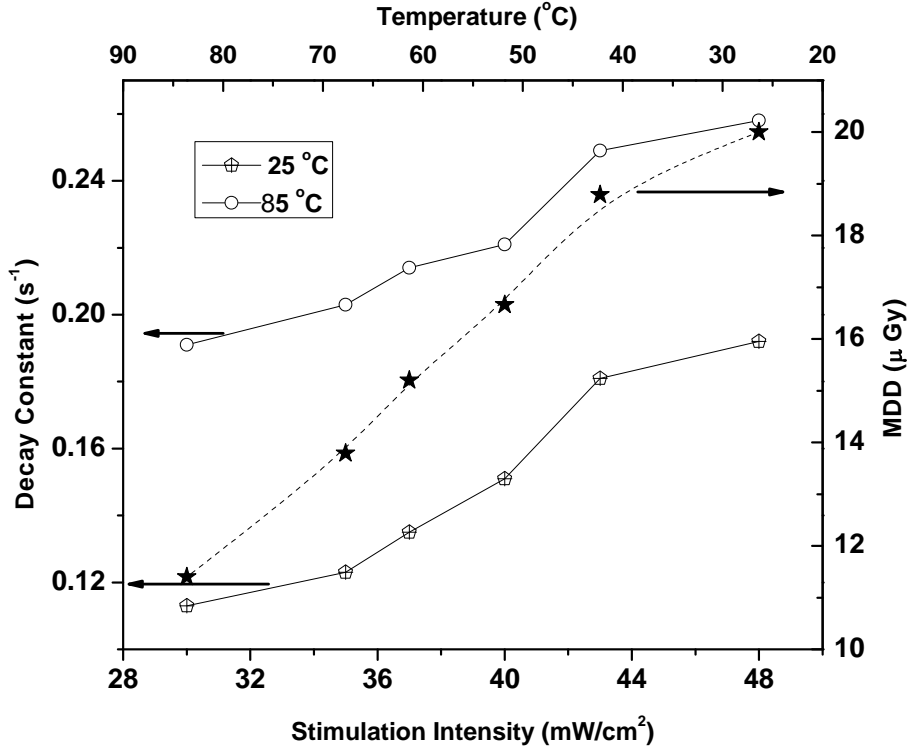
Fig. 4.11: Experimentally evaluated CW-OSL decay constant of α-Al₂O₃:C at various stimulation intensities and two different temperatures(25 ºC, 85 ºC) showing the change in the CW-OSL decay constant as a function of stimulation intensity. The other graph shows the improvement in MDD as a function of stimulation intensity.

The Dose threshold was measured by following way

       a. Measurements of background on six freshly annealed, unirridiated Al₂O₃:C detectors to determine 3 standard deviations of the background signal (X).

b. Expose six annealed crystals to a dose of 500 μGy. Determine mean output of these detectors (Y/**μGy**).

c. Calcúlate MDD as

$$\text{MDD (μGy)} = \text{X*μGy / Y} \tag{4.15}$$

4.5.3 Comparison of MDD for various techniques

Table 4.3 shows the comparison of dose threshold and respective OSL readout time for various stimulation techniques. It is clear that POSL gives the best signal to noise ratio and thus the dose threshold [6]. LM-OSL was recorded for same final stimulation intensity and integration time as for CW-OSL stimulation and readout. It is estimated that LM-OSL gives lower detection threshold as compared to CW-OSL by a factor of 1.3 (Fig. 4.12). Further, NL-OSL has been reported to give 1.2 times better detection threshold as compared to LM-OSL [1].
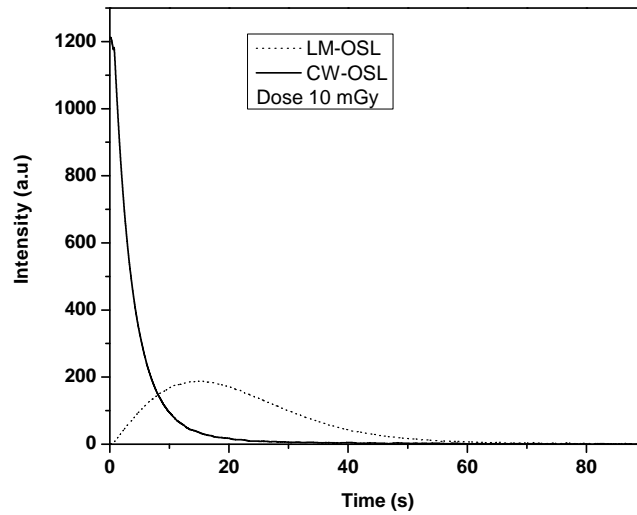
Fig 4.12: CW-OSL vs LMOSL of α-Al₂O₃:C at same final stimulation intensity for same dose and same readout time.

Table 4.3: Stimulation Techniques and Dose threshold with respective OSL readout time. (MDD for NL-OSL and POSL and are reported in [1, 6])

Stimulation Techniques	Low Dose limit (µ Gy)	Readout Time (s)	Power Used (mW/cm^2)
CW-OSL	20.00	90	48
POSL	5.00	1	48
LM-OSL	15.38	90	48
NL-OSL	12.80	90	48
TA-CW-OSL	11.40	90	30

All the above results have been published in the international journal [7, 8]. The technique was tested on the same material for the reusability. Fig 4.12 shows the reusability of the material using this technique at low doses.
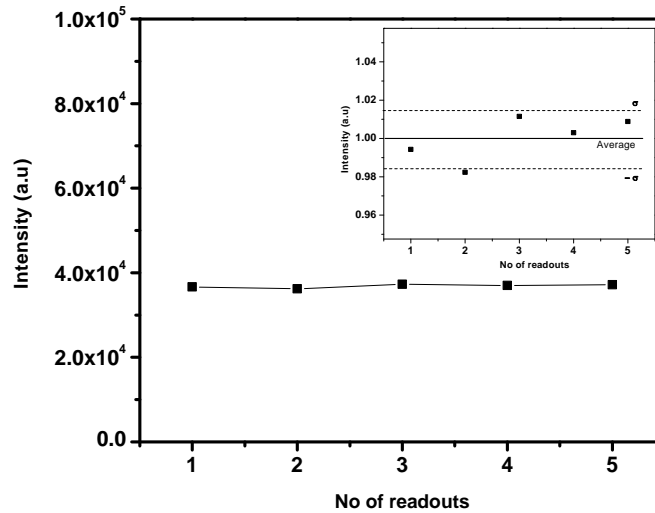
Fig. 4.13: Variation in TA-OSL readout (sensitivity of the material at low dose (20 mGy)) with number of readouts. Inset shows the statistical variation in the sensitivity.

4.5.4 Conclusions

The dose threshold was found to improve by factor of 1.8 using TA-CWOSL. In α-Al$_2$O$_3$:C the main dosimetric TL peak starts showing signal from 90 °C onwards so the elevated temperature measurement were restricted upto 85 °C only. But for those phosphors in which the TL peaks occurs at higher temperature one can go to even higher elevated temperature readouts and thus making it feasible to use even at lower stimulation intensities to further improve the dose threshold using this method. Next chapter deals with the study of TA-OSL phenomenon on the other side of the temperature scale (i.e below room temperature) and related instrumentation.

References

1. Mishra, D.R., Kulkarni, M.S., Rawat, N.S., Soni, Anuj., Bhatt, B.C., Sharma, D.N. 2011. *Radiat. Meas.,* 46, 1462-1468.

2. Wallinga, J., Bos, A.J.J., Duller, G.A.T. 2008. *Radiat. Meas*. 43, 742-747.

3. Kulkarni, M.S., Mishra, D.R., Sharma, D.N. 2007. *Nucl. Instrum. Method. Phys. Reasch. B* 262, 348-356

4. Akselrod, M.S., Agersnap Larsen, N., Whitley, V. and McKeever, S.W.S. 1998. *J Appl. Phy.* 84, 3364-3373.

5. Soni. A., Mishra, D.R., Bhatt, B. C., Gupta, S.K., Rawat, N. S., Kulkarni, M.S., and Sharma, D.N. 2012. *Radiat. Meas*. 47, 111-120.

6. McKeever, S .W.S., Akselrod, M . S and Murkey, B. G., 1996. *Radiat. Prot Dosimetry.* 65, 267-272

7. Soni. A., Mishra, D.R., Bhatt, B. C., Gupta, S.K., Rawat, N. S., Kulkarni, M.S., and Sharma, D.N. 2012. *Radiat. Meas*. 49, 67-72.

8. Soni. A., Mishra, D.R., Bhatt, B. C., Gupta, S.K., Rawat, N. S., Kulkarni, M.S., and Sharma, D.N. 2013. *Geochronometria.* 40, 258-265.

Chapter 5

Development of Low Temperature

TL/OSL reader

The earlier chapters discussed about the temperature dependence of photo-ionization cross-section of OSL active traps at above room temperature. This chapter will delve into the TA-OSL phenomenon at below room temperature. For this, chapter begins with the design and development of the cryostat integrated TL/OSL reader and its operational aspects. The later section deals with the studies on α-Al_2O_3:C using the developed reader system.

5.1 Introduction

Thermoluminescence (TL) studies provide vital clues in connection with the mechanism of trap formation, concentration and nature of the traps as well as the modifications occurring into this nature associated with variations in process parameters. For a radiation phosphor generally, dose readout is carried out at the temperatures that are much higher than normal room temperature where shallow traps are ineffective and as such cannot contribute to the TL response. In OSL based dosimetry, however, the measurement is usually carried out at room temperature, where these shallow traps can significantly affect the OSL response. The TL record at low temperature may gives the useful information about shallow TL traps which may be having metastable life-time order of $\approx$ few ms at room temperature. It has been observed that these traps exercise a decisive influence over the OSL response of samples as they lead to a delayed optically stimulated luminescence (D-OSL) in which charges released from dosimetric traps, upon optical stimulation get re-trapped at shallow traps. Since these shallow traps are having lifetime of the order of ms to few seconds and hence delay the OSL signal in time scale, particularly in Pulsed Optically Luminescence (POSL) measurements. There are good possibilities that these low energy shallow traps give rise to TL peaks in low temperature range (far below room temperature) Therefore, study of the TL peaks in this temperature range may add collateral information that may find application in engineering of dosimetrically pertinent defects which is an integral part development of a typical phosphor. Apart from this, such shallow defects can play crucial role in OSL based online dosimetry in low temperature ambient conditions.

In order to investigate such defects, cryostat integrated TL/OSL reader system is in great demand in all the research and academic institutions for their applications in radiation dosimetry, dating of archeological and geological samples using thermo-optical investigations. However, very few

such readers have been developed [1]. Hence, it is required to design in-house TL/OSL reader system for study of doped phosphors over wide temperature range (-100 °C to +150 °C). Considering above need, a cryostat integrated TL/OSL (CITOR) reader system has been designed and developed for studying the TA-OSL phenomenon at low temperature in various OSL phosphors.

5.2 Desired features in cryostat integrated TL/OSL reader system

Scope and deliverables of integrated cryostat TLOSL reader system are as follows:-

(a) TL measurements with a linear heating rate of 0.1 - 2 K/s and temperature range (-150 °C to +350 °C).

(b) Facility for TL, OSL (CW-OSL, LM-OSL) or combined readout (TA-OSL) with blue light.

(c) MS Windows based control software.

(d) A Cryostat unit capable of storing upto 5 litres of liquid nitrogen.

5.3 CITOR Reader Setup

The reader system consists of two parts. The first part or sub unit is a liquid nitrogen based cryostat unit with a planchet assembly along with a PMT housing mounted on top of the planchet for TL/OSL signal collection. The second part is the control unit of the reader system. A conceptual sketch diagram of the instrument is shown in Fig 5.1.
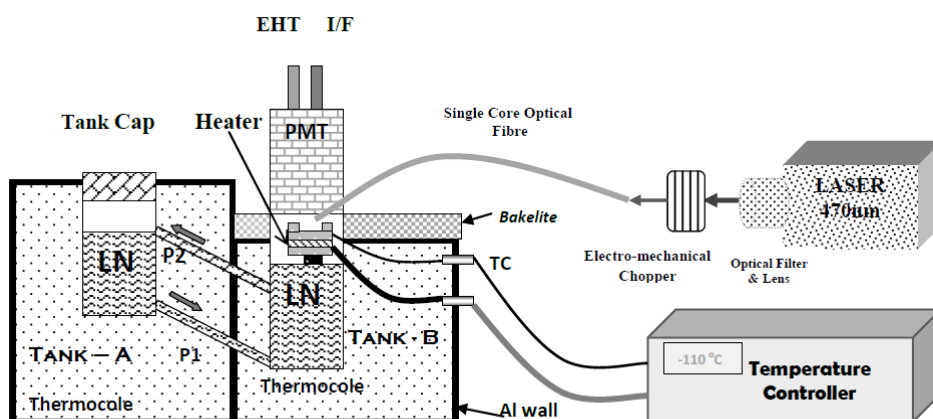
Fig. 5.1: Diagram of Laser based Cryostat integrated TL/OSL reader system.

5.3.1 Cryostat Unit

Cryostat unit design comprises of two chambers made of high quality stainless steel, one of which serves as a storage tank for liquid nitrogen and the other one houses the planchet assembly. The cryostat unit filled with liquid nitrogen brings the temperature of the planchet down to -150 °C. During the course of experiment, the liquid nitrogen keeps getting consumed due to flow around the two chambers and escape to environment through exit openings provided in bigger chamber. Fig 5.2 shows the design cryostat unit along with filling of liquid nitrogen.
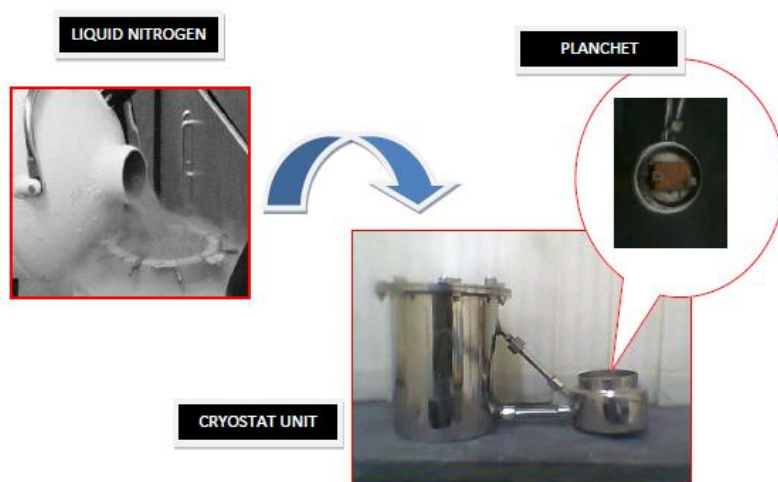
Fig. 5.2 Design of Cryostat unit along with filling of liquid Nitrogen

5.3.1.1 Analytical calculations involved with cryostat unit

Cryostat unit is required to hold liquid nitrogen. The salient features of liquid nitrogen are:-

➤ Density = 0.807 g/ml

➤ Boiling temp = 77K (-196 °C) at atmospheric pressure

➤ Non-toxic, odorless, colorless, relatively inert & non-flammable

The liquid nitrogen can be stored in the cryostat unit if it is appropriately insulated from ambient heat. Depending on the size and design, the holding time of container ranges for few hours. In order to have least possible heat transfer through unit, several metals were compared in terms of their thermal conductivity.

Table 5.1 Thermal conductivity of various materials

Material	Thermal conductivity (kW/mK) at 25 °C
Aluminum	250
Aluminum Brass	121
Brass	109
Copper	401
Stainless steel	16
Iron	80

Stainless steel (SS) having least thermal conductivity amongst all possible options was preferred over others. Its conductive heat transfer was evaluated and compared with iron and aluminium for performance analysis. The conductive heat transfer through a flask wall is given as:

$$q / A = k \, dT / s$$

where, q / A = heat transfer per unit area (W/m^2); k = thermal conductivity (W/mK); dT = temperature difference (°C); s = wall thickness (m)

Conductive heat Transfer for temperature difference 200 °C and wall thickness 2mm through SS flask, Al flask and Iron flask was found to be is 1600, 25000, 8000 kW/m^2 respectively.

Thus, in terms of conductive heat transfer, SS qualifies as a best material for construction of cryostat unit. Since liquid nitrogen is inert and non corrosive, corrosive strength of cryostat unit material was not taken into consideration.

5.3.1.2 Planchet assembly

Smaller chamber of cryostat unit houses a planchet assembly on which the sample under analysis is placed. Planchet assembly primarily consists of two copper plates clamped to each other with help of SS clamps as shown in Fig 5.3. As the thermal conductivity of copper is 401 (kW/mK) at 25 °C which is highest amongst all compared materials, a planchet made of copper was used. Heating of planchet assembly is obtained with the help of a Nichrome coil extracted from heater plate used in household iron**.** Between both the copper plates Nichorme coil is sandwiched with the help of mica sheets serving as electrical insulators as shown in Fig 5.3. A Teflon sheet was added between Nichrome coil and lower copper plate of planchet assembly to block heat conductivity mediums between two copper plates. Additionally, stainless steel clamps were also clamped with a cotton cloth strip over copper plates. In case of TL analysis from low temperatures, the heat lost by copper based planchet assembly will be gained by the liquid nitrogen circulating in the cryostat unit. Fig 5.4 shows the planchet assembly at room temperature and at low temperature. It is clear from this Fig that water/ice gets formed on the planchet/sample at low temperature due to humidity. To solve this problem, the planchet was allowed to cool at

low temperature and whatever ice/water was formed on it was removed manually in the current setup and then sample was placed on it. The setup was then immediately closed which avoids condensation from external air. This problem can be removed by having a provision of evacuation using vacuum pump. This provision will be incorporated in the future design of the setup.
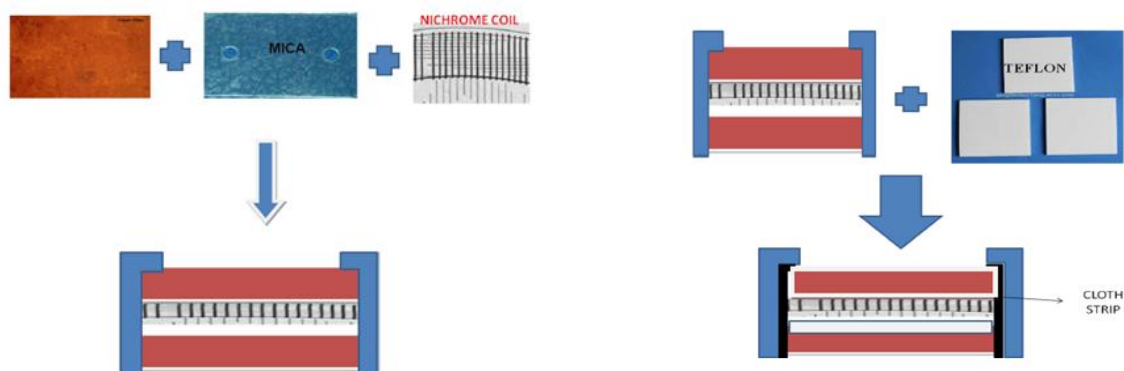
Fig. 5.3. a) Planchet assembly b) Planchet assembly with modified setup
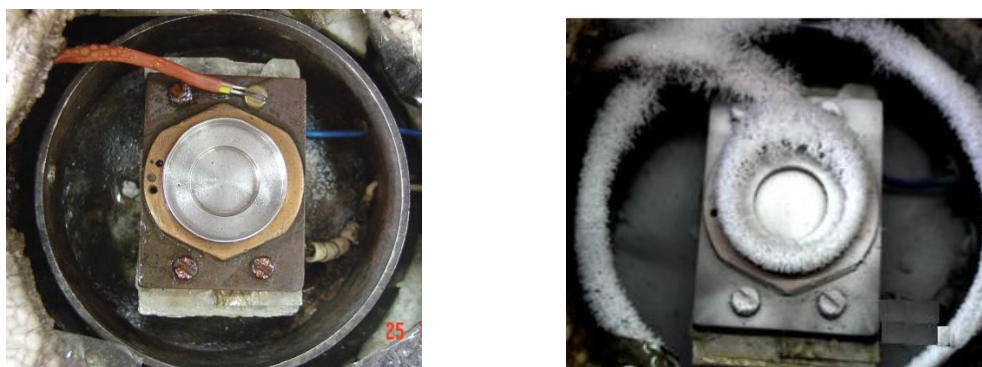
Fig 5.4: (a) Sample holder at 25 °C (b) Sample holder at -110 °C

5.3.1.3 Heat lost by Copper planchet during cooling

The heat lost by copper planchet can be determined using the following relation

$Q_c = m \times Cp \times dT$

Where, Q_c = heat lost by the planchet (Calories); m = mass of the planchet (50 gm); C_p = specific heat (Cu : 0.092 (kcal/kg °C)); dT = change in temperature (°C); 1 calorie = 4.18J

Thus, for a 100 °C (say) fall in the temperature during cooling, the amount of heat lost by copper planchet is:

$Q_c = m \ x \ Cp \ x \ dT = $ 50 x $10^{-3} \times 0.092 \times 100 = 460$ cal $= 460$ x $4.18 = $ **1.923 KJ**

The amount of liquid nitrogen required for this can be calculated as

$Q_n = m_n \ x \ L$

Where, Q_n = heat gained by nitrogen*;* m_n = mass of liquid nitrogen; L = latent heat of vaporization of liquid nitrogen (45 cal/g).

$m_n = Q_n/L = 460 / 45 = 10.22$ g (neglecting heat losses from walls & container block)

Volume of liquid nitrogen required $= 10.22/.807 = $ **12.66 ml** (density of liquid nitrogen (ρ) = 0.807 g/ml). Thus, 12.66 ml of liquid nitrogen will bring down temperature of planchet by 100 °C and with experiments under process liquid nitrogen due to boiling and evaporation gets consumed leading to refill requirements.

5.3.1.4 Temperature Sensor

K-type thermocouple placed in a small cavity at centre of upper copper plate of the planchet assembly was used to measure the temperature of the planchet. Type-K (chromel {90% nickel and 10% chromium} alumel {95% nickel, 2% manganese, 2% Al and 1% silicon}) is the most common general purpose thermocouple as shown in Fig 5.5. It is inexpensive, temperature range of −200 °C to +1250 °C with sensitivity 5 mV/ °C. Wire color standard is yellow (+) and red (-).

Fig 5.5. Standard thermocouple with connector

5.3.2 Control unit of CITOR

The control unit of the reader system is based on P89V51RD2 microcontroller and the basic hardware consists of 12 bit digital to analog converters (DAC) (MAX-539), 12 bit analog to digital converter (ADC) (MAX-1241) and MAX-232 for serial transfer of data from reader system to PC. A heater temperature control circuit is designed and developed for TL measurements and a constant current driver circuit connected to LED for OSL measurements. A high voltage supply module (EHT) for the PMT along with normal DC power supply circuit and a current to frequency converter board are also incorporated in the control unit. Fig. 5.6 shows the front and back view of the control unit.

Fig 5.6. Control unit of low temperature TL/OSL reader system.

5.3.2.1 Power supply board

The power supply board is BR-1010 based which is a silicon bridge rectifier used to convert input ac supply into dc form. The essential requirement of power supply board is to provide a stable and regulated voltage to other circuits and device of control unit. The power supply board was designed to supply +5V,-5V,+12V,-12V to the system using input ac supply of 230V,50 Hz. Various voltage regulator ICs have been used to maintain constant supply. Keeping heat dissipation and temperature management under consideration, all ICs have been mounted with heat sinks on rear panel of control unit as shown in Fig. 5.7.

Fig 5.7. Voltage regulator IC's mounted on the back panel of the unit

The efficiency of the developed power supply board was measured with the help of Load regulation. Load regulation of constant-voltage power supply lines is:-

% regulation = $(V_{NL} - V_{FL} / V_{NL}) \times 100$

Where, V_{NL} = Voltage output at no load and V_{FL} = Voltage output at full load

In case of +12V supply; % regulation = ((12.04 − 11.98)/12.04) x 100 =0.498%

In case of +5V supply;   % regulation = ((4.98 − 4.93)/4.98) x 100 = 1.004%

In case of -12V supply; % regulation = ((-12.00 − (-11.86)/-12.00) x 100 = 1.16%

In case of -5V supply line; % regulation = ((-5.01 − (-4.92)/-5.01) x 100 = 1.79%

Thus, overall a variation of less than upto 2% is found to be satisfactory one resulting in more than 98% regulation output in voltage lines. The step-down Toroidal transformer was used in the

power supply board, which offers many advantages over standard laminated power transformers. Toroidals provide quiet, efficient operation with very low stray magnetic fields. Their small size and weight support a package that is easy to design into any application. Fig. 5.8 shows the power supply board and the Toroidal transformer coupled below it.
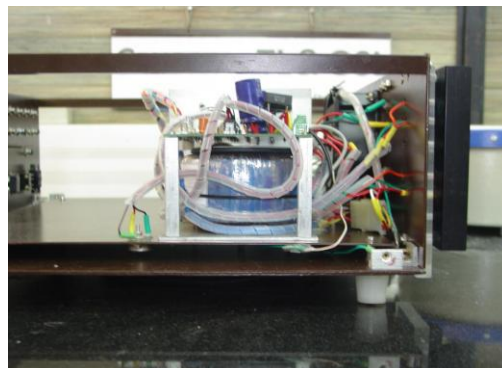
Fig 5.8 a) Power supply board b) Toroidal transformer coupled below power supply board

5.3.2.2 Temperature control board for TL

The proportional type temperature controller circuit was designed and developed which can control the temperature of the planchet within ± 1ºC. Block diagram of temperature control board is shown in Fig 5.9.
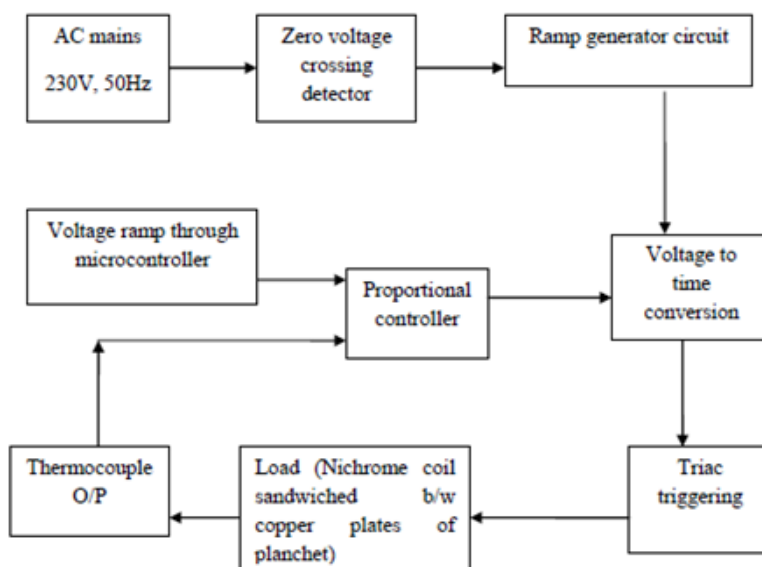
Fig 5.9. Block diagram of temperature control board

Sub modules of heater temperature control unit are as following:-

5.2.2.2a Proportional Control

Accurate control of temperature can be achieved by causing heater power to be simply switched on and off according to an under and over temperature condition respectively. Ultimately, the heater power will be regulated to achieve a desired system temperature but refinement can be employment to enhance the control accuracy.
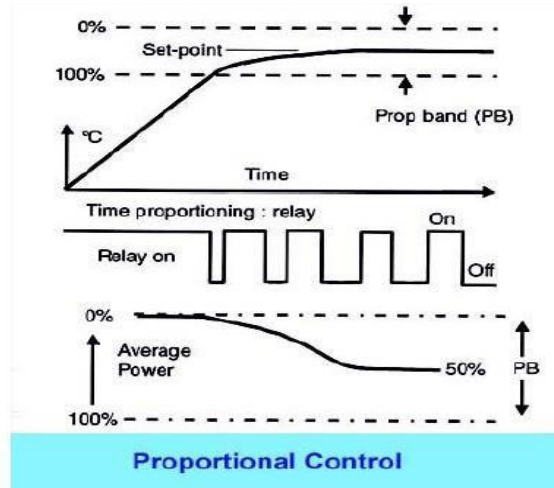
Figure 5.10. Temperature controller response without P control

A P-type controller attempts to correct the error between a measured process variable and a desired set-point by calculating and then outputting a corrective action that can adjust the process accordingly as shown in Fig 5.10. Variations are more smoothly corrected but an offset will occur (between set and achieved temperatures) as applied power is proportional to the error between sensor temperature and set point (usually by time proportioning relay switching). The region over which power is thus varied is called the Proportional Band (PB) it is usually defined as a percentage of full scale. Offset is the deviation of the sensor temperature from the desired value (set-point). The further fine tuning can be done by incorporating I(integral) and D (Derivative) term.

5.2.2.2b Zero voltage crossing detector.

The rectified DC voltage is fed to Opto-isolator (IC 4N25) which isolates the temperature control board from input AC mains and associated noise It also produces time pluses corresponding to all zero voltage crossing instants (i.e when AC mains crosses zero). These zero crossing pulses are fed to mono-stable multi-vibrator(IC 74221) to make them TTL and the desired pulse time of 50 μs.

5.2.2.2c *Ramp generator*

The ramp generation is obtained by using integrator circuit. The TTL zero crossing pulses from the multi-vibrator are fed to the ramp generator circuit which provides upward and downward ramp of 0–3V range. These ramp waveforms are compared with the proportional output. The output of comparator circuit is time pulses of <50 μs duration whose pulse width keeps on varying with difference in desired and set temperature range depicting different firing angles. The output pulses of voltage to time conversion circuit are fed to TRIAC firing circuit for controlling the firing angle of heater transformer (9V rating) to control the temperature of the planchet.

5.2.2.2d **Phase control with TRIAC**

Effective and widely used method of controlling the average power to a load through a TRIAC is by phase control. Phase control is a method of utilizing the TRIAC to apply the ac supply to the load for a controlled fraction of each cycle. It is a two directional electronic switch that can conduct current in both directions when it is triggered (turned on). Either a positive or a negative gate can trigger the TRIAC voltage. This makes the TRIAC a convenient switch for AC circuits. Applying a trigger pulse at a controllable point in an AC cycle allows one to control the percentage of current that flows through the TRIAC. The TRIAC is held in an ON and OFF condition at a time in the AC cycle determined by the control circuitry as shown in Fig 5.11
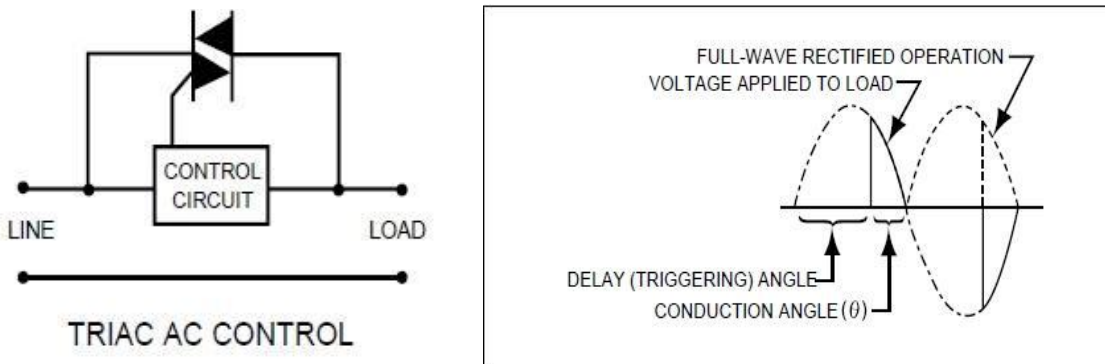
Fig 5.11. AC Phase Control by using TRIAC

During the first portion of each half cycle of the ac sine wave, an electronic switch is opened to prevent the current flow. At some specified phase angle, this switch is closed to allow the full line voltage to be applied to the load for the remainder of that half cycle. Varying phase angle will control the portion of the total sine wave that is applied to the load (shaded area), and thereby regulate the power flow.
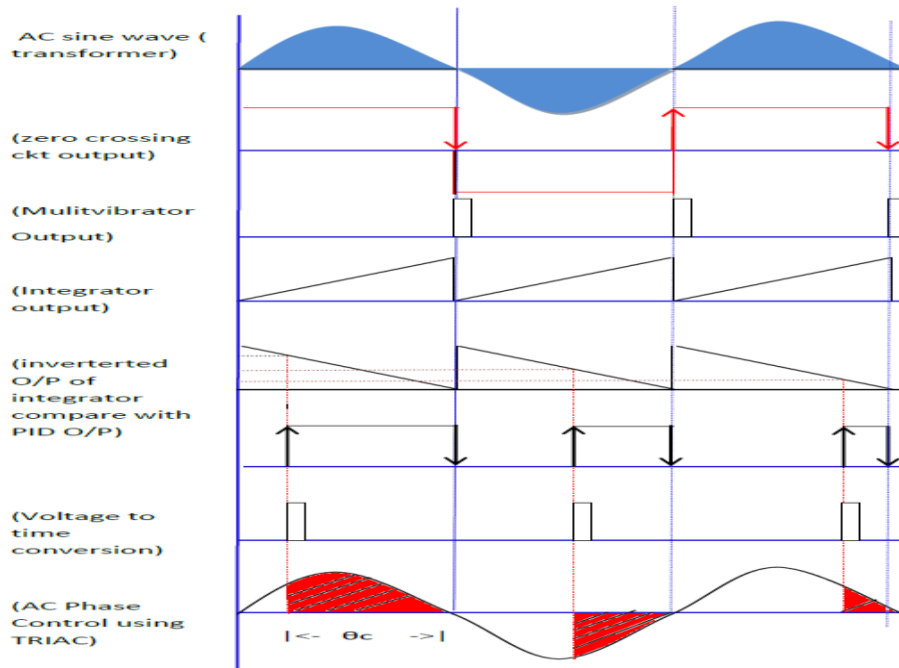
Fig 5.12. Timing diagram of Temperature control board

5.3.2.3 OSL Measurement Setup

The OSL measurement setup consists of following sub assemblies:

5.3.2.3a. Stimulation Assembly

The optical stimulation assembly consists of light stimulation unit based on blue LEDs having peak wavelength $\lambda p = 470$ nm. These high power LEDs can generate the maximum optical power of 100 mW/cm^2 at the sample position using appropriate lenses. The user can select the blue or

green light stimulation depending on the OSL sample under study. The current to the LED is controlled with the help of LED constant current driver circuit. A GG-435 color glass filter is fixed in front of a blue LED to cut off the stimulation wavelengths below 430 nm (for green light a GG-495 filter is used). An UG-1 optical color glass filter has been used across the PMT to prevent the stimulating light from reaching the PMT. Fig 5.13 shows the % transmission of color glass filters which are used with the reader system for recording selective luminescence from different samples.
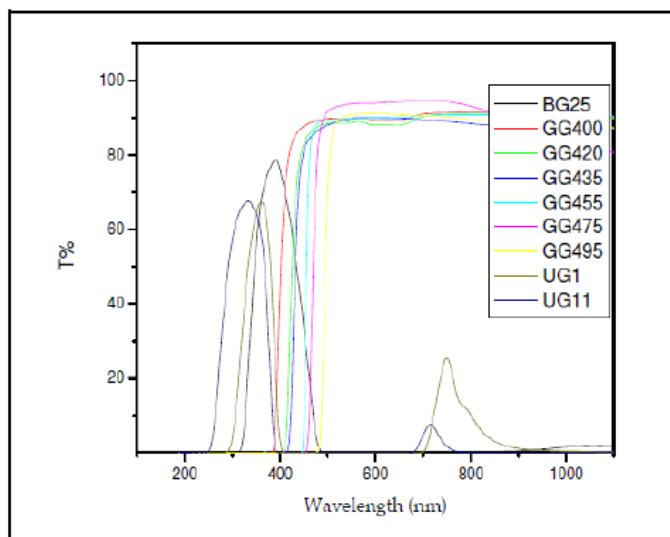
Fig 5.13. Transmission percentage of various color glass filters.

5.3.2.3b. Detection Assembly

The photomultiplier tube (PMT) (Hamamatsu R-669) has been used as a light detector for luminescence measurements. It is a vacuum tube that includes a photosensitive cathode, a number of electron multiplying dynodes and an anode normally held at about 1000 volts. Light photons interact with the photoelectric cathode material (e.g. potassium-cesium) causing the emissions of electrons that are then attracted to the positive voltage of the first dynode which emits further

electrons which are multiplied by other dynodes (Fig. 5.14). Thus, a light photon reaching the photocathode is converted to an electrical pulse at the anode. In our developed system, PMT is operated in analog mode which gives DC current signal that is proportional to the number of photons reaching the photocathode. This DC signal may be digitized using a current-to-frequency converter (I to F) which allows a wide response range of the order of 7 decades, and the possibility of off-setting the dark current to zero.
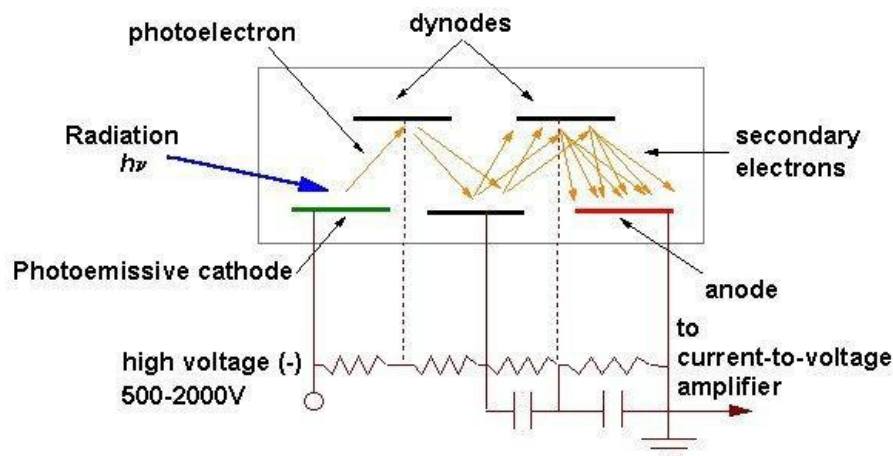
Fig 5.14. Structure of photomultiplier tube (PMT).

The dark count (intrinsic background signal in the absence of any light source) of light detector module PMT (Hamamatsu R-669) was studied for various applied voltage at EHT. It is clear from Fig 5.15 that the dark count of the PMT increases non-linearly with the applied voltage. The advantage of this PMT module is that it has the maximum applied voltage rating is 1500 V as compared to normal bi-alkali PMT in which the maximum applied voltage is 1200 V.
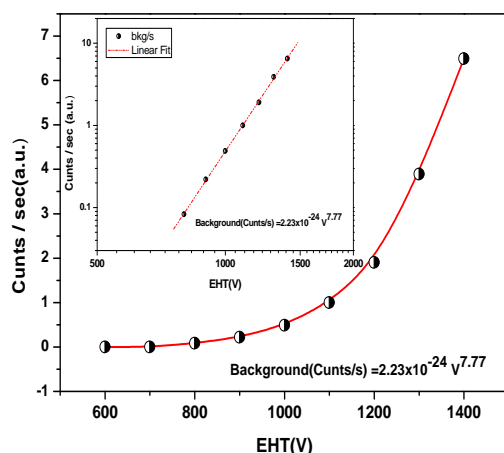
Fig. 5.15. Variation of background signal (dark count) of PMT at room temperature with increase in applied voltage to PMT. Inset shows the same in log scale.

Similarly, the gain of the PMT was studied using a constant light source (plastic scintillator) at various applied EHT voltage. It is clear from Fig 5.16 that the PMT has maximum gain at 1500 V and similar to the dark count, the gain also varies non-linearly with the applied EHT voltage.
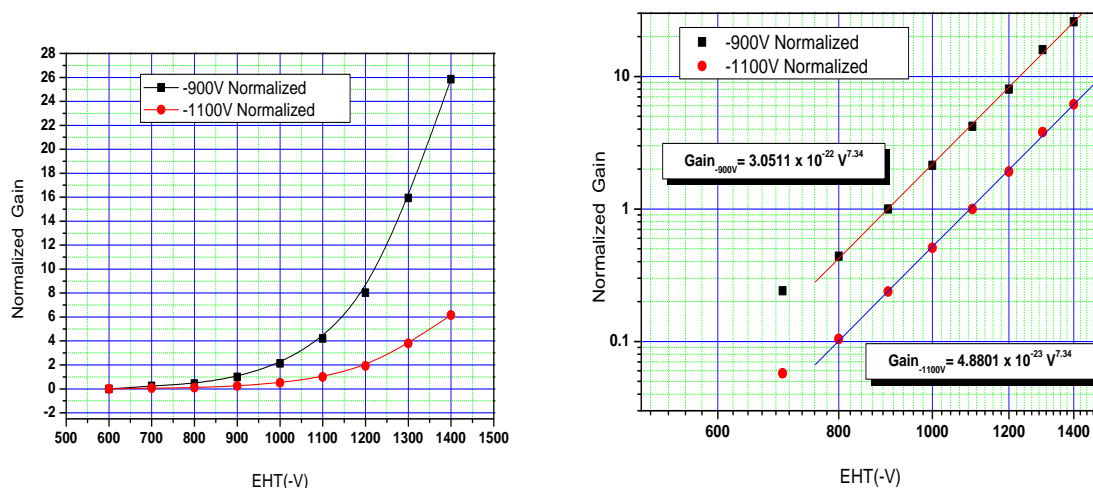
Fig. 5.16 a) Gain of PMT module using constant light source signal at various applied EHT voltage. b) Shows the same in log scale.

139

5.3.2.4 Software design

The software to control the system was developed using C language through (KEIL IDE), compiler and run on the P89V51RD2 microcontroller with help of FLASH Magic software (Fig. 5.17). The operation of the entire reader system can be done by giving command from the computer. Upon selection of a particular mode of operation (TL / OSL), the software generates the user defined voltage function in time domain. A basic internal delay has been generated using the interrupt overflow of programmable logic array (PLA). The track of the program cycle time and the set readout time are measured with respect to this internal timer. The software displays the parameters of the reader such as temperature of the heater strip, the intensity of the stimulation light source. The software gives the facility of recording TL in linear, non-linear or at elevated temperatures. Similarly in OSL user can take CW-OSL and LM-OSL with desired stimulation intensity.
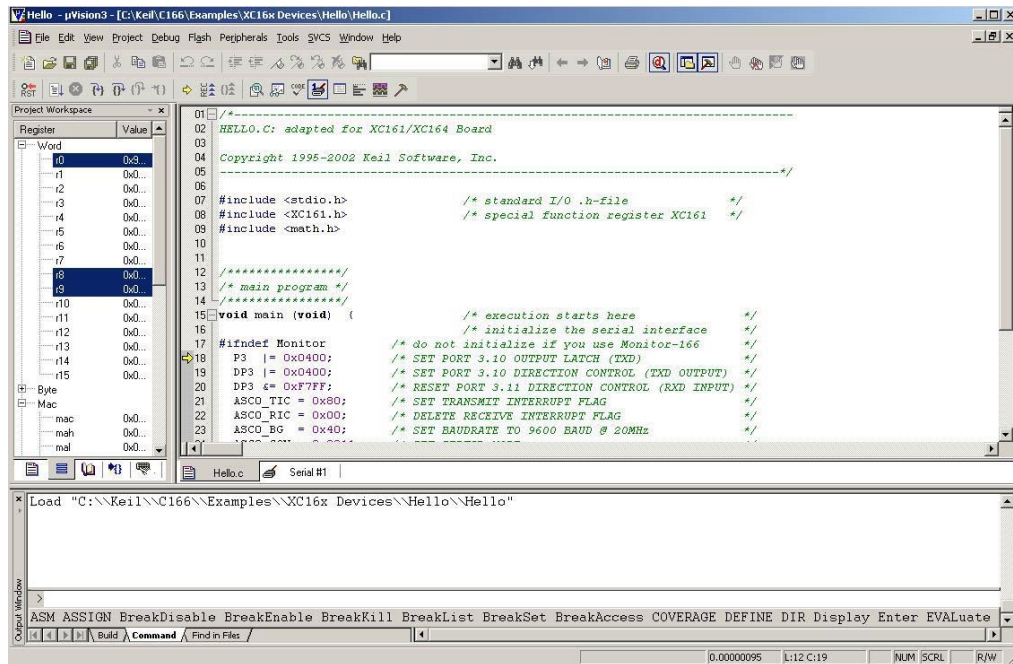
Fig 5.17. Programming using Keil Software

5.4 Low Temperature TL/OSL studies

This section describes the study of low temperature TL/OSL defects on commercially available α-Al$_2$O$_3$:C using the developed cryostat TL/OSL reader system. The phosphor was characterized using various luminescence techniques such as TL, CW-OSL, POSL and TA-OSL.

5.4.1 Introduction

The TL glow curve of α-Al$_2$O$_3$:C single crystals commercially grown in Russia as TLD-500K consists of two clearly separated TL peaks one occurring at ~200 °C and another one at low temperature viz. ~50 °C. It has been reported that it is possible to engineer dosimetrically relevant defects in α-Al$_2$O$_3$ crystals by annealing them in a composite ambience of vacuum and graphite using post growth thermal impurification (PGTI) method [2]. Further, earlier researchers have shown that it is possible to selectively enhance and freeze low temperature shallow traps [3]. In the following section we have investigated TL/OSL response of commercial α-Al$_2$O$_3$:C phosphor in the temperature domain (-100 °C to 300 °C), with the objective of recording TL peaks if any, due to these shallow traps. Effect of temperature on the OSL decay from such traps and their possible role in radiation dosimetry has also being studied.

5.4.2 Materials and methods

The TL/OSL measurements were carried out in an indigenously built low temperature TL/OSL reader set up described in earlier section. For POSL measurement, the Nd:YAG 532 nm laser was used for stimulation of samples. The continuous wave (CW) Laser beam was chopped by using speaker coil and Cu thin plate attached to it along with pairs of convex lenses used to guide the laser bean in optical fiber. This pulsed laser beam is incident on OSL sample and using

Photomultiplier tube (PMT) along with UG filter, luminescence signal was recorded. The POSL setup thus made can generate minimum 900 μs pulse width at maximum 1 kHz repetition rates. The commercially available α-Al$_2$O$_3$:C powder, weighing 5 mg each was subjected to irradiation by UV light on the heater planchet held at (-100 °C) for 5 minutes so that the electrons excited from the F-center can be trapped at shallow traps (since these traps becomes stable at this low temperature). The F-center gets excited by 203 nm of UV spectrum and the excited state of F-center lies in the bottom of conduction band in α-Al$_2$O$_3$:C. The sample was heated from the -100 °C to 300 °C in the reader system at different heating rates (0.1 to 0.3 K /s).

5.4.3 *Results and Discussion:*

5.4.3.1 *Low Temperature TL Studies:*

Fig 5.18a shows the TL glow curve of commercial α-Al$_2$O$_3$:C samples at different heating rates. The α-Al$_2$O$_3$:C shows TL peaks at 12.5°C and 55°C for 0.3 K /s heating rate. It is clear from Fig 5.18 b, that for 0.3 K/s heating rate, the 12.5 °C peak arrives early (in time domain) as compared to that at low heating rate of 0.1 K/s and the area under glow curve remains conserved for different heating rate. Further this peak, being observed in α-Al$_2$O$_3$:C developed by PGTI method (Figs 5.19 a & b), can be taken as one of the important signatures for the formation of α-Al$_2$O$_3$:C phosphor. The study also reveals that the defects formation in α-Al$_2$O$_3$:C single crystals, by processing in vacuum at 1500 °C in graphite ambience (PGTI method), are of same type as that in the commercial phosphor developed by melting of polycrystalline α-Al$_2$O$_3$:C in graphite ambience. Al$_2$O$_3$:C was irradiated by UV light at -100 °C and then its TL was recorded upto 250 °C. The TL glow curve consists of peak at 8, 47 and 173 °C respectively suggesting the filling of all the traps existing in the material including shallow, intermediate and deep traps. By irradiation with UV light, the electrons from the F-centers get excited and go to conduction band. This will cause filling of the traps. The

shallow traps giving their presence at 8 °C suggest that they are not stable at RT (25 °C) and hence material should be irradiated at low temperatures in order to record signal from them. The TL/OSL studies at RT or at some ambient temperatures will not cause the trapping of electrons in shallow traps. Further the traps stable at temperature higher than irradiation temperature, will give their presence in TL glow curve. Fig. 5.20 shows the entire TL glow curve of commercial α-Al$_2$O$_3$:C at heating rate of 0.05K/s having three peaks in at -8, 31and 173 °C respectively. The -8 °C TL peak in commercially available Al$_2$O$_3$:C single crystals is found to have thermal trap depth of $E = 0.24$ eV which is much lesser than that of dosimetric trap (1.1eV), and half life ≈ 5 ms at room temperature, hence unstable at room temperature (RT) and does not show its presence in TL measurements carried out at RT. Therefore, these shallow traps which become stable at low temperatures will also contribute to the total OSL signal used for OSL radiation dosimetry in low temperature ambient conditions, thus may improve the detection threshold, particularly in online OSL radiation dosimetry. When the pre-irradiated sample was subjected to intense bleaching at low temperature using blue light, TL glow curve does not show the low temperature peak (-8 °C), confirming the OSL sensitivity of the peak. The 32 °C TL peak is found to be sensitive in TL mode only but the (-8 °C) TL peak is found to be sensitive in OSL mode as well. Table 5.2 shows the measured TL parameters on the processed and commercial α-Al$_2$O$_3$:C samples. The order of kinetics b was determined using the method based on glow curve shape analysis using the geometrical shape factor μ$_g$. These results have been published in the journal [4].
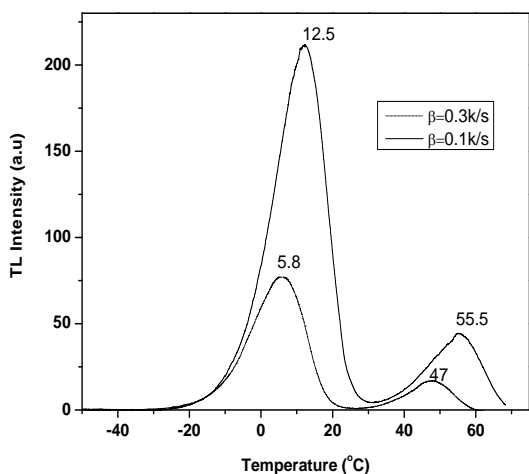
Fig.5.18a. TL Glow curve of Commercial α-Al₂O₃:C at different heating rate showing shift in peak temperature.
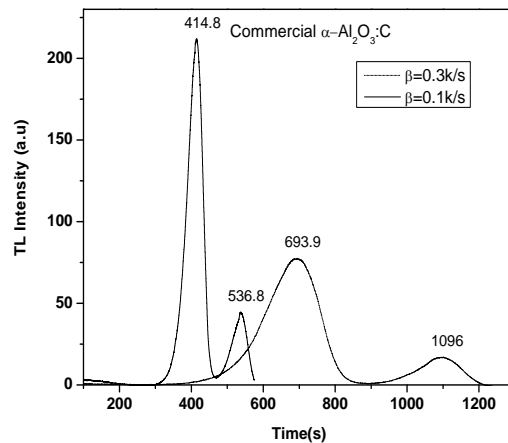
Fig.5.18b. TL Glow curve of Commercial α-Al₂O₃:C at different heating rate showing shift of peak temperature in time scale.
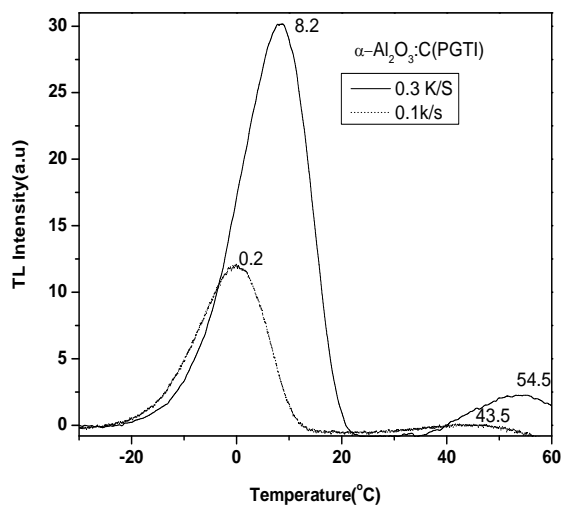
Fig.5.19a. TL Glow curve of developed (PGTI) α-Al₂O₃:C at different heating rate showing shift in peak temperature.
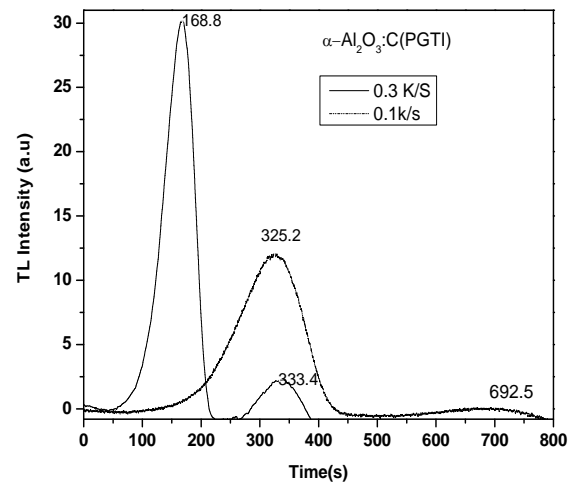
Fig.5.19b. TL Glow curve of developed α-Al₂O₃:C at different heating rate showing shift of peak temperature in time scale.
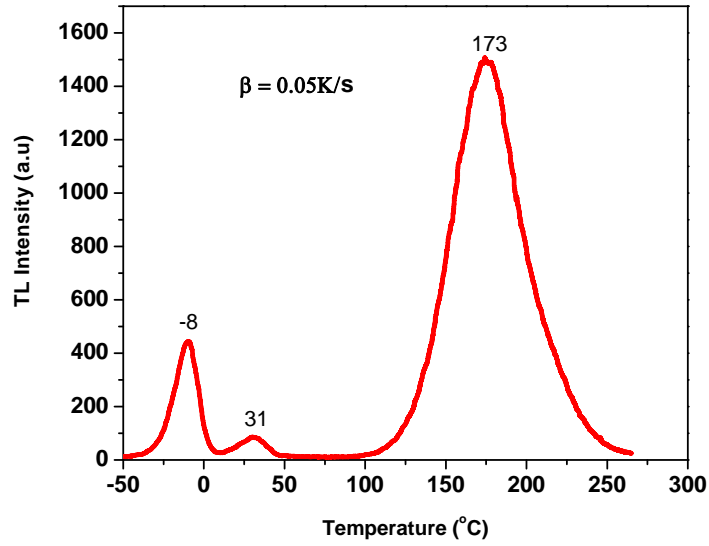
Fig. 5.20. TL glow curve of α-Al₂O₃:C at heating rate of 0.05K/s shows three peaks in at (-8 °C) 31 °C and 173 °C respectively.

The thermal trap-depth (E) of the TL peaks is determined using variable heating rate method as follows:

$$E = k \frac{T_{m1} T_{m2}}{T_{m1} - T_{m2}} \ln \left[\frac{\beta_1}{\beta_2} \left(\frac{T_{m2}}{T_{m1}} \right)^2 \right]$$

(1)

The condition of TL maxima is used for the evaluation of frequency factor *S* for first order kinetics as

$$S = \frac{\beta E}{k T_m^2} \exp \left(\frac{E}{k T_m} \right)$$

(2)

The mean-life τ (in s) of TL traps for each peak for a given temperature *T* is determined by

$$\tau = S^{-1} \exp \left(\frac{E}{k T_m} \right)$$

(3)

For the second order kinetics following relation was used to evaluate S

$$S = \frac{\beta E}{kT_m^2 \left(1 + \frac{2kT_m}{E}\right)} \exp\left(\frac{E}{kT_m}\right)$$

(4)

Table 5.2: TL parameters of Commercial and α-Al$_2$O$_3$:C

Measured TL Parameters	*Commercial α-Al$_2$O$_3$:C*	
	-8 °C TL Peak	*33 °C TL Peak*
E$_m$(eV)	0.243	0.845
S (sec^{-1})	1.02×10^6	1.02×10^{11}
b	1	2
$\tau_{1/2}$ (at 25°C)	5ms	1.5 minute

5.4.3.2 Low Temperature CW-OSL Studies

In order to investigate the OSL sensitivity of the low temperature TL peak in α-Al$_2$O$_3$:C, the sample after the irradiation to UV light was exposed to intense blue light (470 nm LED at 48 mW/cm^2) for 15 minutes and then it's TL from -100 °C to 60 °C was recorded in which only 33°C peak was observed which is not OSL sensitive as shown shaded region of Fig 5.21.The (-8 °C) TL peak is found to be OSL sensitive as it gets bleached on optical stimulation. Interestingly, the main dosimetric peak in α-Al$_2$O$_3$:C also doesn't get bleached completely on optical stimulation for 15 minutes at -40 °C. It can be attributed to the temperature dependence of the photo-ionization cross-section of this peak. The photo-ionization cross-section gets lower at lesser temperature (-40 °C) and the trap is not as accessible as it was at room temperature. Thus, in case of OSL based dosimetry, the calibration temperature of the OSL dosimeter must be taken into
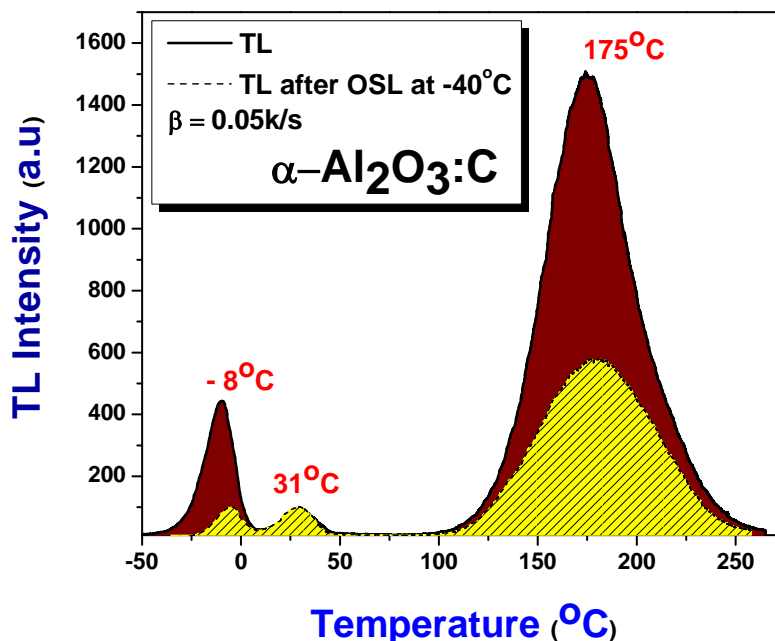
Fig. 5.21. TL glow curve of α-Al$_2$O$_3$:C at heating rate of 0.05K/s shows three peaks in at (-8 °C), 31 °C and 173 °C respectively. The shaded region shows the TL glow curve recorded after the OSL readout at (-40 °C).

consideration in the readout protocol of the OSL dosimeter based on Al$_2$O$_3$:C phosphor. This temperature effect becomes even more apparent while recording CW-OSL at even lower temperatures. Fig. 5.22 shows the CW-OSL decay of α-Al$_2$O$_3$:C recorded at various low temperatures. It is also clear from Fig 5.21 that at very low temperatures, the photo-ionization cross section of main dosimetric peak becomes so low that it acts like deeper trap and does not contribute to the OSL. The net OSL is due to the shallow TL peak which is also OSL sensitive.
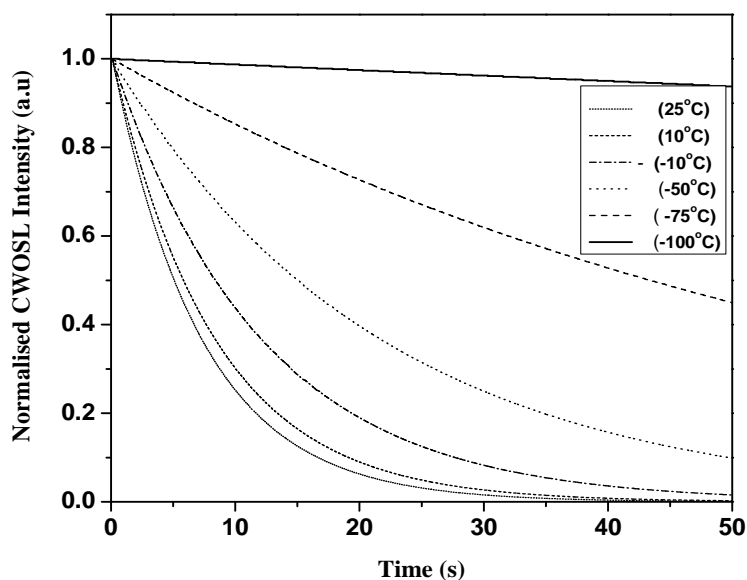
Fig.5.22. CW-OSL decay of α-Al₂O₃:C at various low temperatures with fixed CW stimulation intensity ϕ_o= 48 mW/cm² of 470 nm light.

5.4.3.3 Low Temperature TA-OSL Studies

Fig 5.23a shows the numerically simulated values of increase in photo-ionization cross-section with temperature for α-Al₂O₃:C temperatures using the values of TA-OSL parameters evaluated in earlier chapters. The photo-ionization cross-section continues to increases after (-100 °C) upto 1200 °C. However, the TA-OSL signal is experimentally found to decrease sharply from 100 °C as shown in Fig 5.23b, which can be attributed to dominating thermal quenching in this region which takes over the increase in TA-OSL signal. Table 5.3 shows the photo-ionization cross section of TL peaks α-Al₂O₃:C at various temperatures.

148
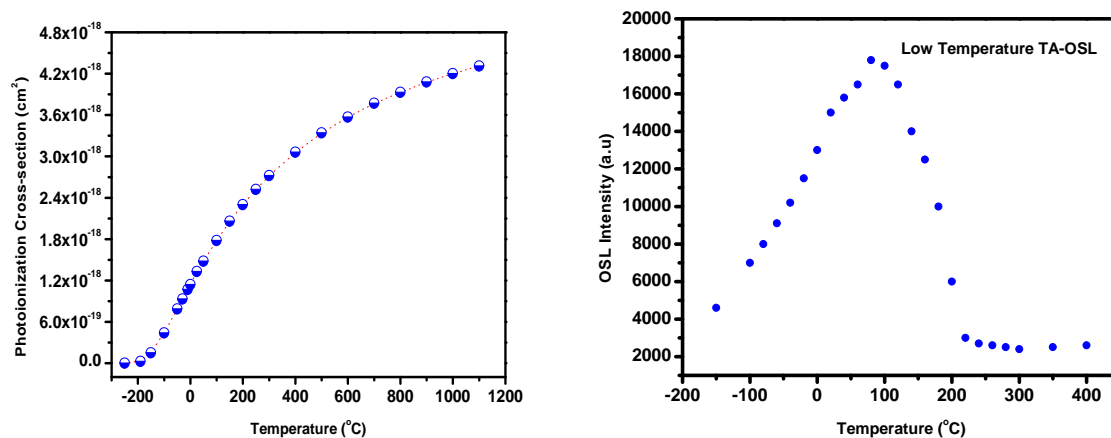
Fig. 5.23a. Variation of numerically simulated values of photoionization cross-section with temperature.

b. Variation of TA-OSL signal of α-Al$_2$O$_3$:C at various temperatures.

Table 5.3: Photo-ionization cross-section of TL peaks at various low temperatures

Temperature (^oC)	*Photoionization Cross-section (cm^2)*		
	Dosimetric Trap (180 $^\bullet C$)	*Deeper Trap1 (650 $^\bullet C$)*	*Deeper Trap2 (900 $^\bullet C$)*
-100	4.38×10^{-20}	5.18×10^{-21}	3.08×10^{-23}
-50	9.30×10^{-19}	6.12×10^{-21}	7.10×10^{-23}
-30	7.87×10^{-19}	9.12×10^{-21}	8.30×10^{-23}
-10	1.07×10^{-18}	2.57×10^{-20}	1.77×10^{-22}
0	1.14×10^{-18}	1.01×10^{-20}	2.14×10^{-22}
25	1.33×10^{-18}	5.82×10^{-20}	3.70×10^{-22}
125	9.33×10^{-17}	1.47×10^{-18}	5.82×10^{-20}
230		-	1.33×10^{-18}

5.4.3.4 Low Temperature POSL Studies

In order to investigate the extent of the small life time component from shallow defects, POSL curve was recorded by cooling the pre-irradiated OSL sample to around liquid nitrogen temperature. The sample was irradiated at low temperature by 203 nm UV light. Fig. 5.24 shows the POSL signal of α-Al$_2$O$_3$:C samples at different temperatures. During the 2000 ms, the laser beam was incident on the sample. In this period, each datum corresponds to the measured POSL from the samples between each laser pulse. We observe an initial increase in POSL intensity as an equilibrium population of excited luminescence sites (i.e. F-centers) is established. After this, a slow, gradual decrease in intensity is observed with continued laser exposure as the source traps are depleted. At the end of 2 s, the laser stimulation was stopped and the luminescence decays. This component represents the DOSL signal, which follows the last laser stimulation pulse. The room temperature POSL curve gives the 35 ms life time of faster component and the delayed component of 235 ms. However, the low temperature POSL measurement shows no change in lifetime (35 ms) of the faster component which is temperature independent. Thus, low temperature POSL results also confirm the presence of these shallow traps as the slower component of the OSL was found to be temperature dependent as at such low temperature the shallow traps become stable and contributes to delayed signal in POSL called as DOSL. However, shallow trap component shows relatively larger lifetime of about 2s. Similar experiment was performed at room temperature.
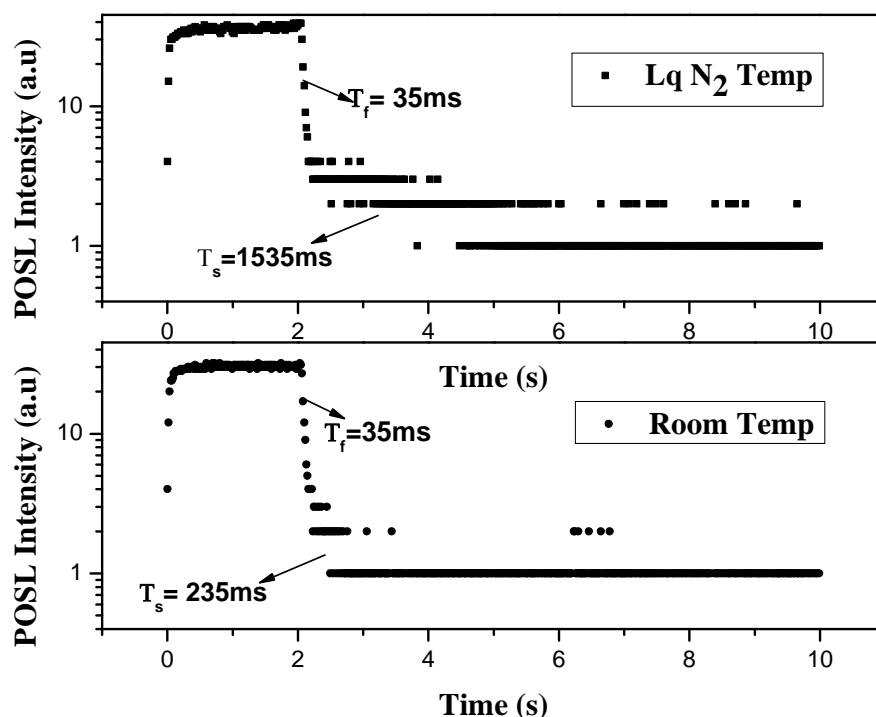
Fig. 5.24. POSL studies on α-Al₂O₃:C at different temperatures showing the effect of temperature on the life time of shallow traps.

5.5. Conclusions

The developed low temperature integrated TL/OSL reader is capable of extracting TL from very low temperature -125 °C to 300 °C. The low temperature TL studies on commercial and indigenously developed α-Al₂O₃:C samples reveal that the vacuum annealing in graphite ambience of α-Al₂O₃ single crystals leads to the formation of same types of defects as in case of commercial α-Al₂O₃:C single crystals. Hence the PGTI method in which the grown single crystal α-Al₂O₃ is treated at 1500 °C which is well below its melting point at reducing environment in graphite ambience is equivalent to conventional method in which the crystal is grown from

melting, which involves sophisticated technique. Further, as the low temperature peak being OSL sensitive it plays essential role in radiation dosimetry and can increase detection threshold. The TA-OSL studies suggest that the readout protocol of the OSL dosimeter based on Al_2O_3:C phosphor must consider the calibration temperature of the OSL dosimeter. Next chapter deals with the application of TA-OSL phenomenon on other oxide based OSL phosphors to ascertain the wider applicability of the technique.

Reference

1. Blair, M.W., Yukihara, E.G., McKeveer. 2006. *Radiat. Proc. Dosim.* 119, 454-457.

2. Kulkarni, M.S., Mishra, D.R., Muthe, K.P., Singh, A., Roy, M., Gupta, S.K., Kannan, S. 2005. *Radiat. Meas*. 39, 277.

3. Mishra, D.R., Kulkarni, M.S., Muthe, Thinaharan, C., Roy, M., Kulshreshtha, S.K., Kannan, S., Bhatt, B.C., Gupta, S.K., Sharma, D.N. 2007. *Radiat. Meas*. 42, 170–176.

4. Soni, A., Mishra, D.R., Kulkarni, M.S., Muthe, K.P., Gupta, S. K., Sharma, D.N. 2011. *Radiation Protection and Environment.* 34, 29-31.

Chapter 6

Universality of TA-OSL in OSL

phosphors

6.1 Permeable

The applicability and advantage of TA-OSL on α-Al_2O_3:C has been described in earlier chapters. This chapter presents the universality of TA-OSL technique on various other OSL phosphors such as $BaSO_4$:Eu^{2+}; Dental Enamel ($Ca_{10}(PO_4)_6(OH)_2$); Al_2O_3: Si, Ti; Al_2O_3: Mg, Y and Mg_2SiO_4:Tb to ascertain wider applicability of the technique. These phosphors have been characterized using various other luminescence techniques also to have better understanding of the defects involved.

6.2 Investigation on BaSO$_4$:Eu^{2+}

6.2.1 Introduction

Eu^{2+} - doped phosphors have been investigated for their TL and OSL response. This is possibly due to the allowed nature of 4f^{6}5d $\rightarrow$4f^7 transition on Eu^{2+} ion. Also, the emission spectra of Eu^{2+} doped phosphors lie in the peaking region of the response of commonly available photomultiplier tubes (PMTs). Therefore, Eu^{2+} -doped phosphors yield good PL and TL. In Eu^{2+} - doped CaSO$_4$ and BaSO$_4$ phosphors, the TL intensity of the most prominent peak is higher in Eu^{2+} -doped samples than that in the corresponding Eu^{3+} - doped samples [1, 2]. This could be partly due to better detector efficiency of PMT for the blue emission in Eu^{2+}-doped phosphors than that for the Eu^{3+} -doped samples, as most of the commercial TL readout systems give peak emission sensitivity in the region 400 - 420 nm. Okamoto et al. (1986) reported the development of BaSO$_4$:Eu^{2+} TL phosphor powder and phosphor embedded Teflon TL sheets for study of hadronic and electromagnetic cascade showers in ultra high energy interactions [3]. The BaSO$_4$:Eu^{2+} (Japan) Teflon TL sheet was reported as an effective detector because of its high sensitivity for detection of cascade showers (around 1 TeV), high position resolution of about 50 μm, wide dynamic dose range and little thermal fading of stored TL signal. Azorin et al. (1991) studied TL characteristics of BaSO$_4$:Eu embedded Teflon TL discs cut out from the TL sheet (Japan) [4]. The TL glow curve exhibits essentially a single glow peak at around 540 K for a heating rate of 7.1 K/s. They reported that the TL sensitivity of BaSO$_4$:Eu embedded Teflon disc was 3-4 times than that of CaSO$_4$:Dy embedded Teflon discs. Bhatt et al.(1997) studied the TL and ultraviolet (UV) response of BaSO$_4$:Eu^{2+} embedded Teflon TL discs (Japan) [5]. TL sensitivity of BaSO$_4$:Eu embedded Teflon discs was about 5.8 times that of CaSO$_4$:Dy embedded Teflon discs, whereas its intrinsic response to UV (254 nm) was 3378 times that of CaSO$_4$:Dy embedded Teflon discs.

Shinde et al. (1996) synthesized $BaSO_4$: Eu and $BaSO_4$:Eu, P phosphors for studying their gamma-ray and ultraviolet (UV) response [6]. With the objective of understanding the TL process in $BaSO_4$:Eu, P, Gundu Rao et al. (1995, 1996) investigated TL, ESR and fluorescence correlation [7,8]. Annalakshmi et al. (2012) prepared $BaSO_4$:Eu^{2+} by solid-state diffusion method involving sintering at 1173 K in reducing atmosphere of NH_3 for 3 h [9]. The phosphor showed a dominant single peak at ~ 513 K (240 °C) and TL sensitivity 3 - 4 times that of $CaSO_4$:Dy. Krystek, 1980 has stated that $BaSO_4$: Eu resembles $CaSO_4$: Dy in that the emission peaks correspond to the release of holes, he identified these traps to be the SO_4^-, and SO_2^- defects, or barium vacancies associated with a neighboring SO_4^- radical ($\mathbf{V}_{Ba}$-SO_4^- hole traps) [10]. The TL process in $BaSO_4$:Eu was reported by several investigators [7,10,11,12]. It is reported that nanophosphors of $BaSO_4$:Eu exhibit lesser TL sensitivity than that of the microcrystalline sample at low doses, while it is more at higher doses. The nanophosphor exhibits a linear/sub-linear TL response to γ-radiation over a very wide range of exposures (0.1Gy to 7 kGy), which is much wider compared to that of the microcrystalline counterpart (0.1–50 Gy) [13,14]. Eu^{2+} - doped $BaSO_4$ phosphors have been reported to be highly sensitive TL phosphors [3,4,5,6,9]. Though, $BaSO_4$:Eu has been used for dosimetry of ionizing radiation as well as for UV dosimetry, its OSL and TA-OSL response was not reported so far. Therefore, it is thought worthwhile to investigate OSL and TA-OSL in Eu doped $BaSO_4$ phosphors.

Materials and method

6.2.2.1 TL/OSL Measurements

The samples used in the present work were $BaSO_4$:Eu^{2+} powder and Teflon embedded discs received from Nemoto and Co. Ltd. Japan. $BaSO_4$:Eu^{2+} powder was used for PL studies and

comparison of sensitivity with other phosphors ($CaSO_4$:Dy and α-Al_2O_3:C (Landauer Inc.)), while the phosphor impregnated Teflon embedded discs were used for other TL/OSL characterization. Samples were annealed at 400 °C before irradiation. Luminescence measurements were performed using the RISØ TL/OSL reader (model TL/OSL-DA-15) equipped with a blue LED array light source used for stimulation (470 nm, FWHM 20 nm, delivering up to 25 mW/cm^2 at the sample position). Irradiations were carried out using the 40 mCi (dose rate : 0.018 Gy/s) ^{90}Sr/^{90}Y β-source built into the Risø reader. The reader is fitted with a 9635QA PM Tube. The detection optics consisted of a 7.5 mm Hoya U-340(λ_p ~340 nm, FWHM 80 nm) filter; this was used for all luminescence measurements. All TL measurements were performed using a heating rate of 2 °C/s in order to avoid significant temperature lag and unless otherwise stated, to a maximum temperature of 500 °C. All OSL measurements were performed in the continuous-wave OSL (CW-OSL) mode, and the power level was software controlled and set at 90% of the maximum stimulation intensity for blue LEDs.

6.2.2.2 Lifetime Measurements

All steady-state luminescence and lifetime measurements were carried out at room temperature by using an Edinburgh Instruments FLSP 920 system (Livingston, UK), having a 450 W Xe lamp and a microsecond flash lamp as the excitation sources. Around 20 mg sample was mixed with one ml methanol, made into a slurry and spread over a quartz plate and dried under ambient conditions prior to luminescence measurements. All emission spectra were corrected for the detector response and all excitation spectra for the lamp profile. Emission measurements were carried out with a resolution of 2 nm. Average lifetime values ($\tau_{average} = \Sigma x_i \tau_i / \Sigma x_i$) were calculated by summing the values obtained by multiplying each lifetime component (τ_i) with corresponding

percentages (x_i) and then dividing the sum by 100 (i.e. Σx_i) and the mean lifetime values were calculated using $\tau_m = \Sigma x_i \tau_i^2 / \Sigma x_i \tau_i$.

6.2.3 Results and Discussion

6.2.3.1 Photoluminescence Studies

PL spectra are useful in identifying the valence state of the Eu ion. Eu^{3+} gives characteristic emission in the orange-red region of the spectrum corresponding to the transitions $^5D_0 \rightarrow {}^7F_j$. These transitions are parity forbidden. Eu^{2+} emission, on the other hand, is lattice dependent and it originates from the lowest band of $4f^6 5d^1$ configuration to $^8S_{7/2}$ state of $4f^7$ configuration. The excitation arises from the transition from $^8S_{7/2}$ state of $4f^7$ configuration to the states belonging to $4f^6 5d^1$ configuration. The ground state electronic configuration of Eu^{2+} is $4f^7$. This results in a $^8S_{7/2}$ level for the ground state. The most commonly observed emission is the dipole and spin allowed d-f emission starting from the relaxed $4f^6 5d^1$ level. Due to allowed nature of the transition, d-f emission is intense. In case of $BaSO_4:Eu^{2+}$ it is known to occur around 375 nm [15]. PL excitation and emission measurements are shown in Fig.6.1 and 6.2 respectively. In the unirradiated sample, the emission of Eu^{2+} corresponding to 375 nm was seen for an excitation wavelength of 320 nm. Very weak emission around 612 nm (corresponding to excitation wavelength of 394 nm) was observed.

6.2.3.2 Luminescence lifetime studies

Luminescence lifetime measurement carried out on both irradiated and unirradiated samples. The luminescence decay curves corresponding to relaxed $4f^6 5d^1$ level of Eu^{2+} ions in Eu-doped $BaSO_4$ as shown in Fig 6.3.
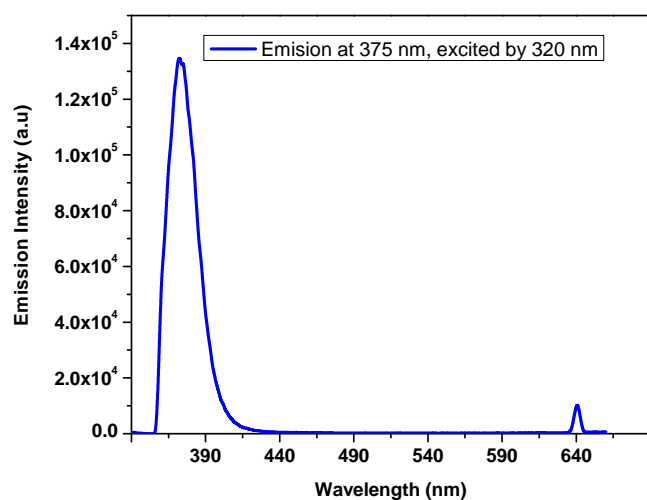
Fig.6.1 PL emission spectrum of Eu²⁺ in BaSO₄:Eu²⁺ showing the emission at 375 nm when excited by 320nm.
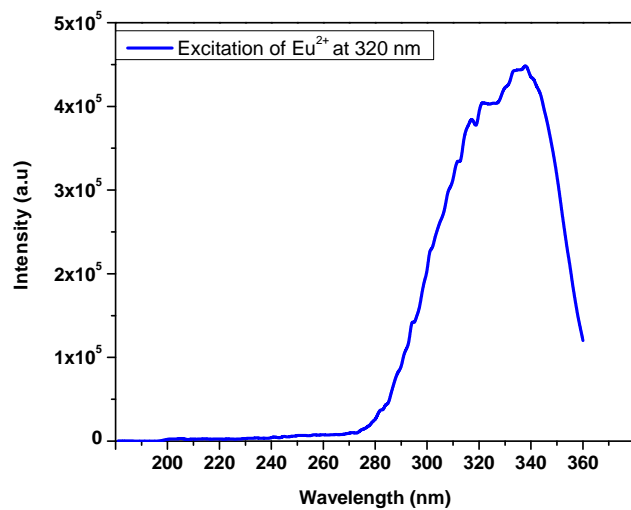
Fig.6.2 PL excitation spectrum of Eu²⁺ in BaSO₄:Eu²⁺ showing the excitation at 320 nm for emission at 375 nm.
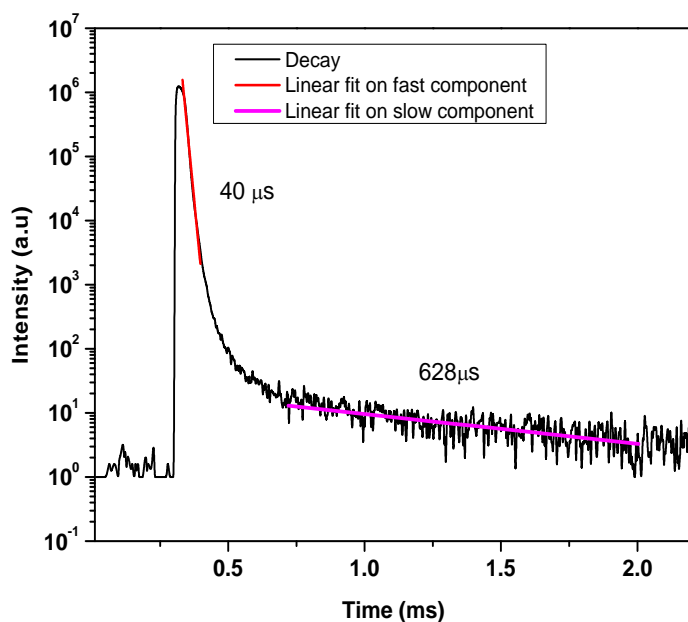
***Fig 6.3. Luminescence lifetime of Eu^{2+} in BaSO$_4$:Eu^{2+} estimated as 40µs*.**

The decay is found to be bi-exponential and could be fitted with short (45 µs) and long lifetime (628 µs) components, as can be seen in Table 6.1. The luminescence lifetime (τ_1 and τ_2), average lifetime (τ_{avg}) and mean lifetime (τ_m) of Eu^{2+} ions of unirradiated, gamma irradiated and UV (253.7 nm) irradiated samples are given in Table 6.1.

Table 6.1: Lifetime Measurement of BaSO$_4$:Eu^{2+}

Sample	τ_1 *(µs)*	τ_2 *(µs)*	χ^2	τ_{avg}*(µs)*	τ_m*(µs)*
Un-irradiated	45 (45.56%)	628 (54.44%)	0.886	362.38	595.01
UV-irradiated	62 (30.04%)	689 (64.96%)	1.088	466.19	663.95
Gamma-rradiated	48 (30%)	789 (70%)	1.915	566.70	770.17

6.2.3.3 TL Characterization

The $BaSO_4:Eu^{2+}$ phosphor was studied for its TL/OSL defects. Its TL glow curve consists of various peaks at 130, 190, 230, 280 and 330 °C. Fig 6.4 shows the typical glow curve of $BaSO_4:Eu^{2+}$ and its comparison with $CaSO_4:Dy$ and commercial α-$Al_2O_3:C$ (TLD-500) irradiated to the same dose. It is found to be 6 times more sensitive than $CaSO_4:Dy$ and 4 times more sensitive (area wise) than α-$Al_2O_3:C$ in TL mode. However, for UV exposure, its TL sensitivity is only 9 % to that of α-$Al_2O_3:C$ whereas $CaSO_4:Dy$ gives negligible TL response (2.2e-5 times of α-$Al_2O_3:C$). Earlier studies have also reported TL comparison of $BaSO_4:Eu^{2+}$ with other materials [5]. The minimum detectable dose (MDD) has been found to be 0.3µGy as compared to 2µGy to that of $CaSO_4:Dy$ [16].
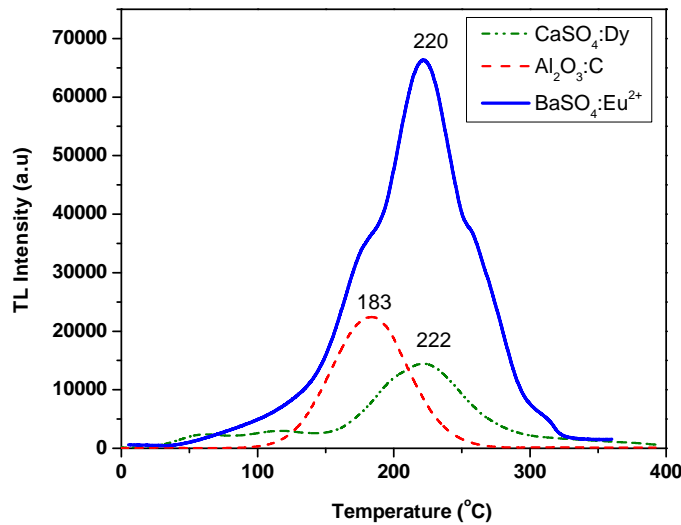
Fig 6.4. Comparison of TL intensity of CaSO₄:Dy, α-Al₂O₃:C and BaSO4:Eu²⁺ phosphors for 100 mGy beta dose with heating rate 4 K/s. BaSO₄:Eu²⁺ is found to be 4 times more sensitive to α-Al₂O₃:C.

The TL glow curve was resolved using a Computerized Curve De-convolution Analysis (CCDA) for TL peaks at 130, 190, 230, 280 and 330 °C. The single glow-peak equation of general order kinetics was used in the case of discrete trap distributions:

$$I(T) = I_m \cdot b^{\frac{b}{b-1}} \exp(\frac{E}{kT} \frac{T-T_m}{T_m}) \cdot [(b-1)(1-\Delta)\frac{T^2}{T_m^2} \exp(\frac{E}{kT}\frac{T-T_m}{T_m}) + Z_m]^{-\frac{b}{b-1}}$$

(6.1)

where

$\Delta = 2kT/E$, $\Delta_m = 2kT_m/E$ and $Z_m = 1 + (b-1) \Delta_m$. (6.2)
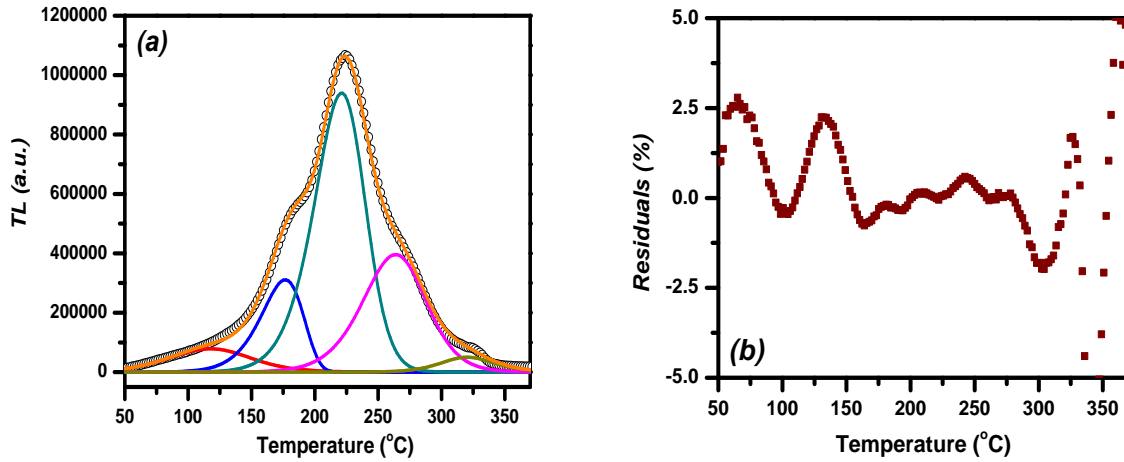
Fig. 6.5. (a) TL glow curve of BaSO₄:Eu²⁺ de-convolved into its five individual components according to equations corresponding to discrete general order kinetics trap distribution. Open circles experimental points and solid lines the fit and each individual TL glow peak. (b) Residuals of the fitting.
Equation (6.1), suggested by Kitis et al., (1998), is an analytical expression that could be used for CCDA in the case of single-value energy trap depth associated with the localized states, with each crystalline phase of a TL material, corresponding to a discrete trap distribution [17]. All curve fittings were performed using the software package Microsoft Excel, with the Solver utility [18]

(Afouxenidis et al., 2012), while the goodness of fit was tested using the Figure of Merit (FOM) of Balian and Eddy (1977) [19]. The obtained FOM values were better than 1.5%.

Based on the related theory presented in these aforementioned citations, it becomes easy to decide the choice of the total number of peaks/components as well as the decision upon the selection of the appropriate order of kinetics for each one. The software could enable determination of the application of one among the first, second and general order of kinetics. Therefore, the excel software, in conjunction with the solver add-in was applied for all de-convolution analyses of the dissertation.

The number of TL peaks required for best fitting could be easily identified based on the number of points indicating maximum intensity as well as change of curvature at the glow curve. Nevertheless, always the least number of peaks required for a good fitting based on the FOM index is adopted. However, in principle, the sample could have more number of peaks than used in analysis, this will be difficult to analyze within scope of this thesis.

The increasing trend of activation energies, in conjunction with the low FOM values provides additional evidence towards the not arbitrary selection of the number of components. Ordinary, a number of related measurements is required, in order to get useful hints for selecting both the number of TL peaks as well as the order of kinetics, such as isothermal TL (ITL), fractional glow technique (FGT) and/or various heating rates. Nevertheless, the de-convolution procedure could reveal useful hints towards selecting the order of kinetics, since the applied equations were yielded using also peak shape methods.

Fig.6.5a presents a typical TL glow curve de-convolved into its individual peaks. A total of 5 individual TL peak-components were used; this was the minimum number of peaks required in order to perform a quality fit. Fig. 6.5b gives the residuals of the fitting. Table 6.2 gives the TK kinetics parameters of the material by peak fitting method.

Table 6.2: TL kinetics parameters of BaSO$_4$:Eu^{2+} by peak fitting method.

Measured TL	*BaSO$_4$:Eu^{2+}*				
Parameters	*130 °C*	*190 °C*	*220 °C*	*280 °C*	*330 °C*
E$_m$(eV)	0.5	1	1.2	1.19	2
S (sec^{-1})	4.6×10^5	3.7×10^{10}	3.7×10^{11}	3.03×10^{10}	2.5×10^{16}
μ$_g$	0.48	0.42	0.48	0.48	0.52
b	1.5	1.001	1.5	1.5	2

6.2.3.4 CW-OSL Characterization

The sample was studied for its OSL response using blue LED stimulation (470 nm). Figure 6.6 shows the typical CW-OSL response of BaSO$_4$:Eu^{2+} for 200 mGy beta dose. It is found to possess three OSL components having photoionization cross-sections of 1.4×10^{-17}, 1.2×10^{-18} and 5.2×10^{-19} cm^2 respectively. The 3rd order exponential fit on the decay curve shows the presence of three components. Its OSL sensitivity for beta/gamma exposure is found to be 75% of commercial α-Al$_2$O$_3$:C (Fig.6.7), while for UV exposure of 254 nm, it is 25 % to that of α-Al$_2$O$_3$:C. Table 6.3 gives the comparison of TL/OSL sensitivities for beta as well as UV exposure. The sample has been found to give linear dose response upto 30 Gy in OSL mode (Fig.6. 8).
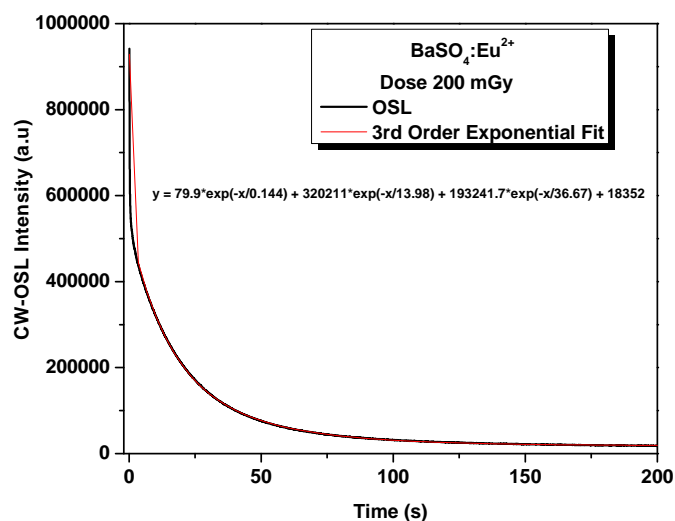
Fig 6.6. CW-OSL response of BaSO$_4$:Eu^{2+} for 200 mGy beta dose. The 3rd order exponential fit on the decay curve shows the presence of three components.
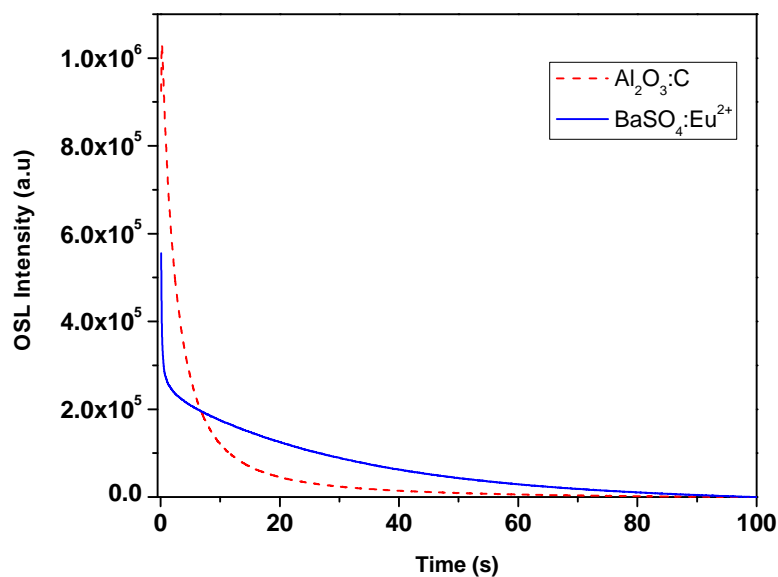
Fig 6.7. Comparison of OSL signal for Al$_2$O$_3$:C and BaSO$_4$:Eu^{2+} phosphors. OSL from BaSO$_4$:Eu^{2+} is 60% to that of α-Al$_2$O$_3$:C.

The figure shows a log-log plot of CW-OSL Intensity (a.u) versus Dose (Gy) with legend "OSL COUNTS" and "Linear Flt", and annotation:

OSL Response = 4.51 x 10^7(Dose)
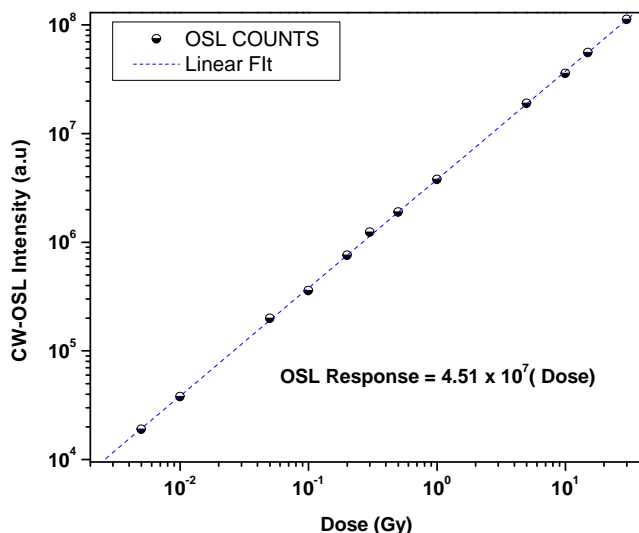
Fig.6.8. Dose vs OSL intensity for BaSO$_4$:Eu^{2+} phosphor.

Table 6.3: Comparison of TL/OSL sensitivities of various phosphors

Phosphors	*TL Sensitivity*		*OSL Sensitivity*	
	beta	*UV*	*beta*	*UV*
CaSO$_4$:Dy	0.76	2.2E-5	-	-
α-Al$_2$O$_3$:C	1	1	1	1
BaSO$_4$:Eu^{2+}	4.3	0.09	0.74	0.25

6.2.3.5 Qualitative correlation of OSL & TL

In order to find the OSL active traps i.e., the TL peaks contributing the OSL signal, sample was subjected to OSL readout at various readout temperatures by pre-heating the sample up to the preset temperatures as shown in Fig.6.9. It clear from Fig.6.9 that the phosphor gives OSL even after its TL readout up to 380 °C suggesting the existence of deeper defects.
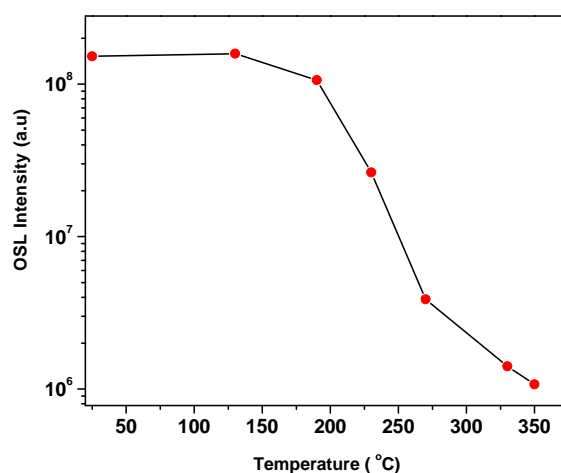
Fig 6.9. OSL intensity of BaSO₄:Eu²⁺ at various readout temperatures by pre heating the sample up to the pre-set temperatures. It is clear that OSL is not zero even at 350 °C suggesting the presence of deep defects.

6.2.3.6 Analysis of faster component of CW-OSL

Out of three OSL components, one has very fast photoionization cross-section and decays in 2 s for stimulation with 48 mW/cm^2 while the slower components take very long time to decay out. In sedimentary quartz, Wintle and Murray (1997) reported a linear correlation between the loss of TL from the rapidly bleaching peak at 310 °C and integrated OSL, by using stimulation times between 0.1 and 100 s [20]. Similar studies have been reported by Koul et al. (2014) [21]. Hence, in order to find out the peak/traps responsible for fastest component, the beta-irradiated sample was subjected to blue light stimulation for various stimulation time durations of 1, 5, 10, 100, 500, 1000 and 2000 s followed by subsequent TL (Fig.6.10a). Fig.6.10b shows the increase of OSL signal and decrease in TL signal as a function of stimulation time.
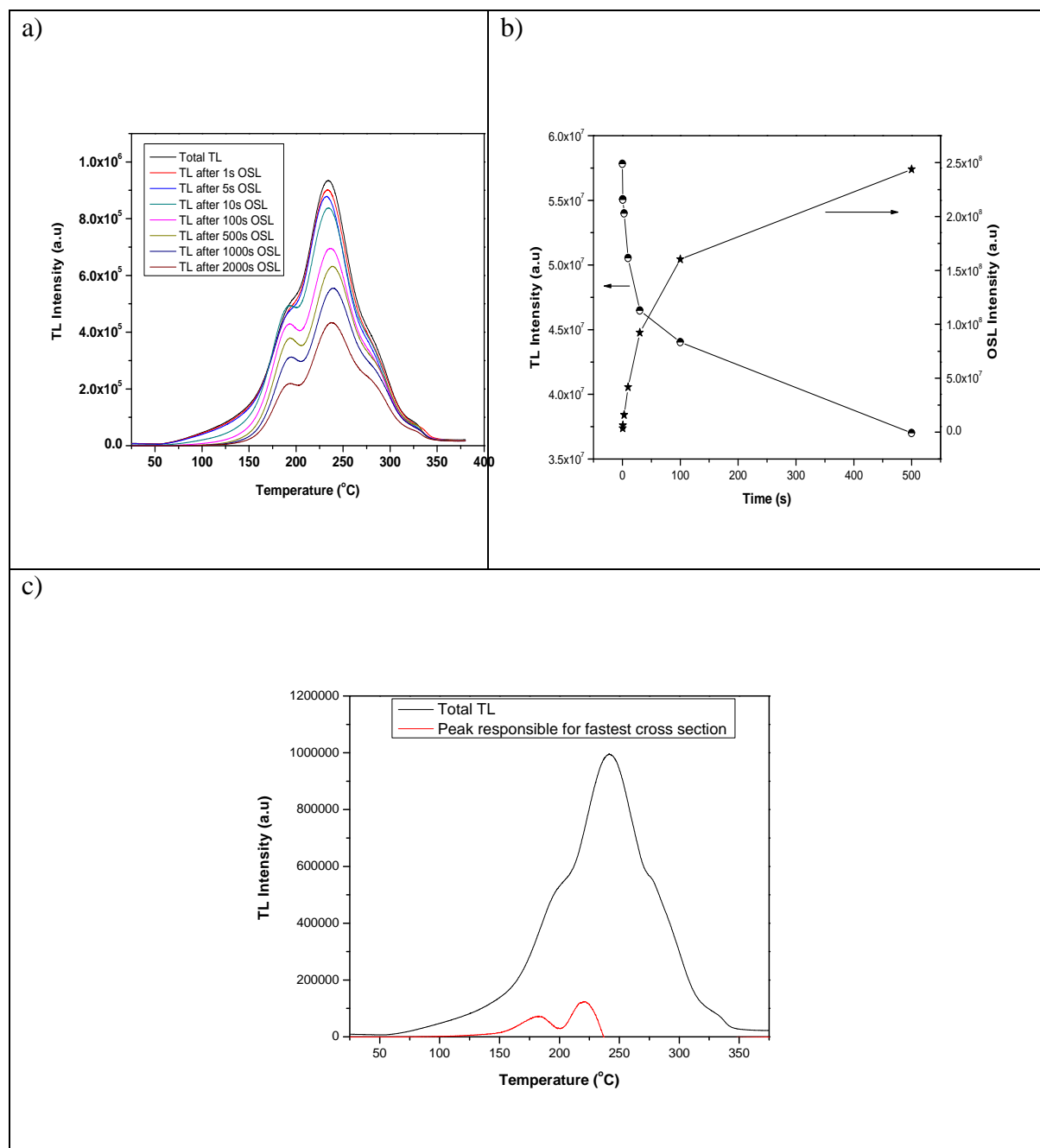
Fig.6.10 a). TL glow curve of BaSO₄:Eu²⁺ after OSL stimulation for various time intervals. b) Shows the increase of OSL signal and decrease in TL signal as a function of stimulation time. c) Shows the TL peaks, responsible for fast OSL component in BaSO₄:Eu²⁺, found by subtracting the TL after 1s OSL from total TL.

It is clear from Fig.6.6 that the faster component decays out in 1s. However, taking OSL for 1s to erase the fast component may also affect the other components, but their contribution will be negligibly

small (it is seen that rate of OSL signal from other components is too slow Fig 6.6), hence by subtracting the TL taken after I s of OSL from the total TL will give the information about the traps responsible for fast component. It was found that 190 and 230 °C peaks are responsible for fast component (Fig.6.10 c).

6.2.3.7 LM-OSL Characterization

The CW-OSL only suggests about the multiple components but it does not reveal the exact contribution and number of the traps responsible for total OSL signal. On the other hand, the linearly modulated optically stimulated luminescence (LM-OSL) is expected to separate out the different peaks having the well separated values of photo-ionization cross sections [22]. However, in the case of the present study LM-OSL record does not give well defined LM-OSL peaks, even with slowest possible LM stimulation rate. Once again, de-convolution is required. The LM-OSL curves were analyzed through a Computer Curve De-convolution Analysis (CCDA) using a general order kinetics expression proposed of Bulur (1996) and later modified by Polymeris et al., (2006) and Kitis and Pagonis (2008) onto an expression containing only the peak maximum intensity I_m and the corresponding time t_m [22,23,24]. These two variables can be extracted directly from the experimental OSL curves. The modified expression used in our computerized procedure is:

$$I(t) = I_m \frac{t}{t_m} \left(\frac{b-1}{2b} \left(\frac{t}{t_m} \right)^2 + \frac{b+1}{2b} \right)^{\frac{b}{1-b}}$$

(6.3)

Where, b is the order of kinetics. The background signal was simulated by an equation of the form:

$$\text{BKG}_{\text{LM}} = a + ct$$

(6.4)

168

where *a* is the average in the initial few seconds of a zero dose LM-OSL measurement, and *c* is a

constant, which was included as fitting parameter.

The non-zero intensity value at $t = 0$ in the LM-OSL was considered in the CCDA analysis in

order to accomplish best fit. Hence, the un-wanted initial signal in this work is attributed to the

signal arising from the decay of extremely shallow traps that decay in RT. Since these traps decay

in RT and do not require optical stimulation. Therefore, adopting the suggestion of Kitis et al.

(2010) that this non-zero intensity value could be attributed to the presence of phosphorescence, a

first order phosphorescence component of the form, $I(t) = I_0 exp(-A \cdot t)$ was included in the CCDA

analysis [25].
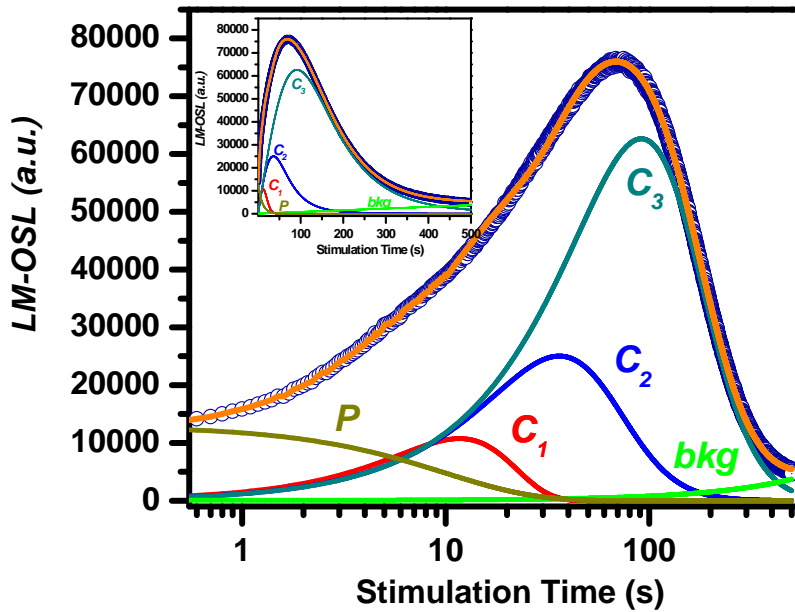
Fig 6.11. LM-OSL curve of $BaSO_4:Eu^{2+}$ de-convolved into its three individual components, a background signal and a phosphorescence component. Open circles experimental points and solid lines the fit and each individual LM-OSL component. The logarithmic axis for the stimulation time was deliberately chosen in order to verify the quality of the fitting. (Inset shows the same in normal scale.)

The decay rate, *A*, was included as a fitting parameter. Further, a near estimation of its value was obtained experimentally, by performing the OSL measurements at various short times duration in between irradiation and measurement. The decay of the intensity of the signal at $t = 0$ s provides a measure for the value of the *A* parameter. To ascertain exact number of peaks is always difficult, but our analysis provides minimum number of peaks. Once again, all curve fittings were performed using the software package Microsoft Excel, with the Solver utility [18] (Afouxenidis et al., 2012), while the goodness of fit was tested using the Figure of Merit (FOM) of Balian and Eddy (1977) [19]. Fig.6.11 presents an example of RT LM-OSL curve de-convolved into each individual component. Three LM-OSL components are recognized in the OSL glow curve, along with the background signal (*bkg*) and the phosphorescence component (*P*). The logarithmic axis for the stimulation time was deliberately chosen in order to verify the quality of the fitting. Interestingly, the kinetic values for the three OSL components, being 1, 1.5 and 1.5, directly correlating to TL peaks 190, 220 and 280 °C.

6.2.3.8 NL-OSL Characterization

These three components were further confirmed and quantified by nonlinearly modulated optically stimulated luminescence (NL-OSL) measurements. In this method, the stimulation intensity profile on the sample is modulated non-linearly with respect to time during the OSL readout. NL-OSL is expected to give more useful results for the very closely overlapping OSL peaks originating from the traps having very close values of photoionization cross-sections [26]. The sample was given 50 Gy of beta dose for taking NL-OSL readout. The NL-OSL readout of $BaSO_4:Eu^{2+}$ along with corresponding stimulation profiles is recorded for (time base power) TBP

(l=2.5) with fixed final stimulation intensity (φ_o) of 100 mW/cm^2 for fixed time 12000 s as shown Fig.6.12. The time required to reach the maximum value of NL-OSL intensity can be given as

$$^l_1 t_{max} = \left[\frac{l}{\sigma \gamma'} \right]^{\frac{1}{l+1}}$$

(6.5)

Where σ (cm^2) is photo-ionization cross-section of the OSL active traps and γ' is a constant having dimensions cm^{-2} s$^{-(l+1)}$ and l is the parameter which can take values in the range: $0 < l \leq \infty$ (like 0.1, 0.5, 1, 2,… etc.), the value of l determines the power of light modulation in the time domain [27]. It is clear from NL-OSL readout that the OSL in BaSO$_4$:Eu^{2+} consists of three well defined components having the photo-ionization cross-sections 3.17×10^{-17}, 2.52×10^{-18} and 6.52×10^{-19} cm^2 respectively, evaluated using NL-OSL method. Table 4 gives the OSL components BaSO$_4$:Eu^{2+} measured by various independent methods.
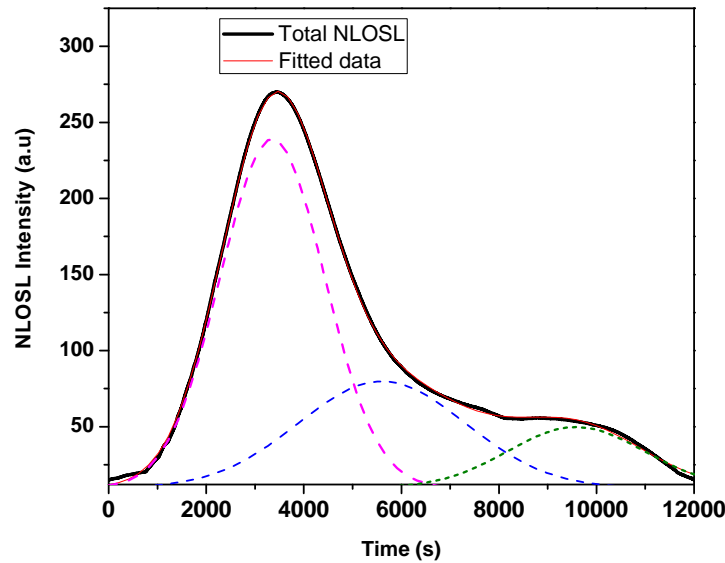
Fig.6.12. NL-OSL curve of BaSO$_4$:Eu^{2+} for 12000 s resolving three components.

Table 6.4: OSL parameters of BaSO₄:Eu²⁺.

Stimulation Techniques	*σ (cm²) of Faster component*	*σ (cm²) of Intermediate component*	*σ (cm²) of Slower component*
CW-OSL	1.4×10^{-17}	1.2×10^{-18}	5.2×10^{-19}
NL-OSL	3.17×10^{-17}	2.52×10^{-18}	6.52×10^{-19}

6.2.3.9 TA-OSL Characterization

In past two decades, researchers have emphasized on various aspects of TA-OSL to investigate the temperature dependence of decay constant in CW-OSL measurement [28,29,30,31,32]. The temperature dependence of OSL was studied in order to see the effect of stimulation temperature on the OSL intensity. OSL intensity has been reported to increase with temperature due to the temperature dependence of photo-ionization cross-section in a number of published papers. The slope of integral plot of TA-OSL intensity vs. $1/kT$ gives the value of thermal assistance energy E_A associated with the array of available excited states of ground level of traps in OSL meta-stable defects for stimulation with blue light. This E_A is nothing but the sum of series of quanta of all possible vibrational energy states associated with the ground state of OSL traps at elevated temperature of TA-OSL measurement. Therefore, under weak stimulation, TA-OSL intensity can be expressed as [32,33]:

$$I_{TA-OSL} = A e^{-\frac{E_A}{kT}} \qquad (6.6)$$

Where A is a constant and the plot of ln(I_{TA-OSL}) vs $1/kT$ gives linear plot with slope as thermal assistance energy (E_A). In the current studies, the irradiated sample was subjected to the multiple short pulses of 0.3 s on every 20 °C at low stimulation power of 10 mW/cm² with simultaneous

TL up to 500 °C at a heating rate of 4 K/s. Hence, the OSL intensity at different temperatures has been obtained in a single readout. It is expected that the short time and low power illumination does not deplete the signal significantly. This type of measurement, called thermo-optical luminescence (TOL) by Duller and co-workers [34,35], was first proposed by Hutt et al.,1988 [36] who used the data to support a mechanism for IRSL in feldspar. Yukihara et al., 2004 has done somewhat similar studies on α-Al$_2$O$_3$:C by measuring OSL with a combination of low power and short-period stimulations [37]. The samples were heated at 5 K/s until 100 °C, and then cooled to room temperature for a new measurement of the OSL signal with a short light pulse. The sequence
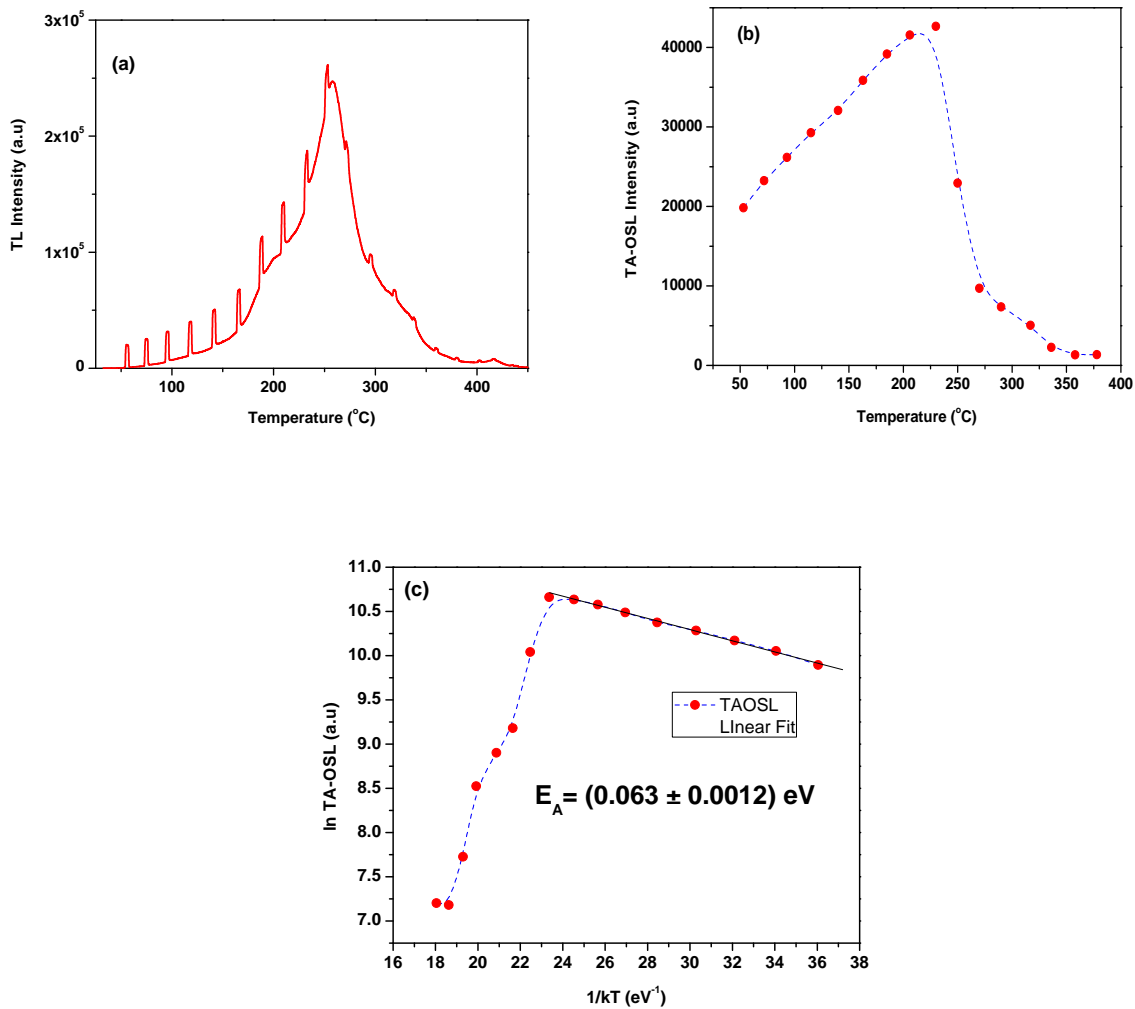
Fig.6.13a) TOL measurements of TL and OSL signal obtained with short (0.3 s) and low power illumination (20% LED power) (for every 20 °C when heating at 4K/s) of a sample previously irradiated to 50 Gy. b) TA-OSL signal obtained with short (0.3 s) and low power illumination (20% LED power) i.e, the pulse height of Fig a vs temperature. c) Arrhenius analysis of the integrated TA-OSL signal from Fig.b. The straight line fit yields the activation energy for the thermally assisted OSL (TA-OSL) process $E_A= 0.063\pm0.0012$ eV.

was repeated each time increasing the end temperature of the heating from 100 °C to until 500 °C in 20 steps. Yoshimura et al. (2006) also performed similar studies on spinel [38]. However, the difference between their method and the method used in our current study is that we have measured the OSL intensity at different temperatures in a single readout by using the linear temperature ramp at 4 K/s up to 500 °C and the short pulses of low LED power were used simultaneously during the temperature ramp (Fig.6.13a). The OSL signal emitted in each step was plotted against temperature, as seen in the (Fig.6.13 b). Fig.6.13c shows the Arrhenius analysis for the integrated TA-OSL signal during the optical stimulation period. From the straight line fit of the data between stimulation temperatures of 50 to 250 °C in Fig.6.13c, an estimate of the activation energy for the TA-OSL process was obtained as $E_A= 0.063\pm0.0012$ eV using Eq. (6.5). This represents the activation energy for the TA-OSL process in phosphor during the short blue light pulses used in this experiment. The continuous increase of the OSL signal with temperature up to 250 °C can be attributed to the existence of thermally assisted OSL in this region. After that, the OSL intensity continues to decrease in a more or less continuous way with increasing temperatures up to 500 °C due to the less availability of trapped charges or may be due to thermal quenching. This increase of OSL at elevated temperature can be employed for enhancing the sensitivity of phosphor for retrospective dosimetry. Pagonis et al. (2013) also found similar results in α-Al$_2$O$_3$:C but in that case the decrease in OSL intensity after 150 °C was attributed to the

existence of thermal quenching in α-Al$_2$O$_3$:C [39]. In their studies, the sample was stimulated optically using blue LED at variable stimulation temperatures between 20 and 240 °C, in steps of 10 °C. A single TR-OSL pulse was recorded for the 0.5 s duration of the optical stimulation period, and the TR-OSL signal was recorded for an additional relaxation time period of 2.5 s after the termination of each such single pulse.

6.3 Investigations on Dental Enamel

6.3.1 Introduction

Nowadays, ionizing radiation is used in various fields including medical, nuclear power/weapon, and industrial applications etc. As a consequence, the possibility of radiological accidents cannot be ruled out despite considerable precautionary measures. In addition, a terrorist act or the uses of a strategic nuclear weapon that both may lead to various degrees of large-scale radiation exposures are possible. Thus, reliable methods for the estimation of the dose received by individuals exposed to ionizing radiation under nuclear / radiological emergency are required, when no active or passive dosimeter is worn. There are various physical and biological methods available to estimate the absorbed dose in accidental exposure situations. Among these methods those that use any material which is part of the exposed individual are of particular value. In particular, human calcified tissues such as tooth enamel are of special interest for retrospective dosimetry. Basically enamel consists of hydroxyapatite (Ca$_{10}$(PO$_4$)$_6$(OH)$_2$) and the basic mineral species is crystalline calcium phosphate((Ca$_3$(PO$_4$)$_2$). Tooth enamel as a radiation detector is known for almost four decades [40] and electron paramagnetic resonance (EPR) spectroscopy of human tooth enamel has been well established for the reconstruction of individual doses [41,42,43]. In-vivo EPR instruments such as benchtop EPR spectrometers with very good sensitivity, require only few mg samples and are field deployable for radiological accidents and

are noticeable recent developments [44,45]. However, the costs of such instruments are very high and the weight of the magnet and its power supply for an in-vivo EPR reader as reported by Swartz et al. 2006 is 80 kg which is intended for vehicular transportation [46]. Hence, for large-scale triage situation, availability of such EPR reader system still remains to be a challenge.

Retrospective dosimetry based on optically stimulated luminescence (OSL) can be an alternative to the EPR technique as it also requires only small amount masses while at the same time being comparatively more sensitive. OSL measurements and their analysis are much simpler and the instruments used are more compact having a mass of only about ~5 kg (e.g. portable Microstar OSL reader, Landauer Inc. USA), therefore being easily deployable in difficult field conditions. Hence, the availability of a portable, cost effective, and light-weight OSL reader would be an asset for quick screening of the affected people for triage. In addition, measurements could be made in-vivo from the tooth using optical fibres without the need for extracting it [47,48]. Optical fibres based OSL reader systems have been reported for their application in in-vivo dosimetry [49,50,51]. Moreover, an in-vivo OSL measurement (sample preparation and extraction not required) takes lesser time for dose assessment than EPR measurements – this is important because it also accelerates dose reporting to decision makers during triage for further action. Of late, various OSL based measurements have been reported on dental enamel and several attempts have been made to improve the sensitivity of OSL compared to that of EPR [48,52,53,54,55]. Further, the ceramic materials employed in dental prosthetics and repairs have also been characterized using TL/OSL and infrared stimulated luminescence (IRSL) techniques [56]. The OSL of dental enamel was observed using infrared (IR), blue and green stimulation, but out of these, blue stimulation was found to give better sensitivity than the others [53].

Unfortunately, there are many challenges for the development of the OSL technique as a tool for retrospective dosimetry using dental enamel, which include the thermal and optical stability of the OSL signal, i.e, fading of the OSL signal in dark conditions. The information regarding the luminescence lifetime of the dental enamel is needed for implementation of the pulsed optically stimulated luminescence (POSL) technique to enhance its sensitivity for retrospective dosimetry application [48]. Photoluminescence (PL) studies will provide information about detection filters to be used for an OSL reader to enhance the overall sensitivity of the system. Minimum detectable dose (MDD) needs to be improved using advanced TL/OSL techniques such as thermally assisted OSL (TA-OSL) and highly sensitive compact instruments need to be developed. We have recently shown that TA-OSL can improve the MDD of OSL phosphors [57]. In this regard, the present study characterizes the OSL and TA-OSL active defects using different techniques (POSL, PL, NL-OSL, TA-OSL, etc) for a better understanding of the defects responsible for the OSL signal from tooth enamel.

6.3.2 Materials and Method

6.3.2.1 Sample preparation

The teeth sample used in this study were extracted by dentists from patients during their medical treatment then they were disinfected and stored under controlled conditions. The method used for sterilization of extracted teeth is the use of about 1–5% sodium hypochlorite for 24 hours. The enamel part was separated from the dentine by mechanical and physico-chemical method [54]. Enamel fragments were crushed using an agate mortar and pestle and sieved into grain sizes of 70-110 μm range. After crushing the enamel part, samples were cleaned with acetone for 5 min in a sonicator which helped in removing the spurious signal caused due to mechanical stress. The

OSL dosimeter from 5 mg powder was made by fixing the powder on 8 mm diameter steel disc with silica glue as shown in Fig.6.14a. Before pasting the enamel powder on the disc, the bare disc and disc with glue were checked for any possible luminescence signal from it but no signal was observed neither from bare disc nor from the glue. The developed sample was irradiated using a 2.2 MeV (peak energy with dose rate 1.2 Gy/min) ^{90}Sr/^{90}Y beta source for various absorbed doses such as 50 Gy for TL and NLOSL measurement, 20 Gy for POSL and CWOSL measurements.
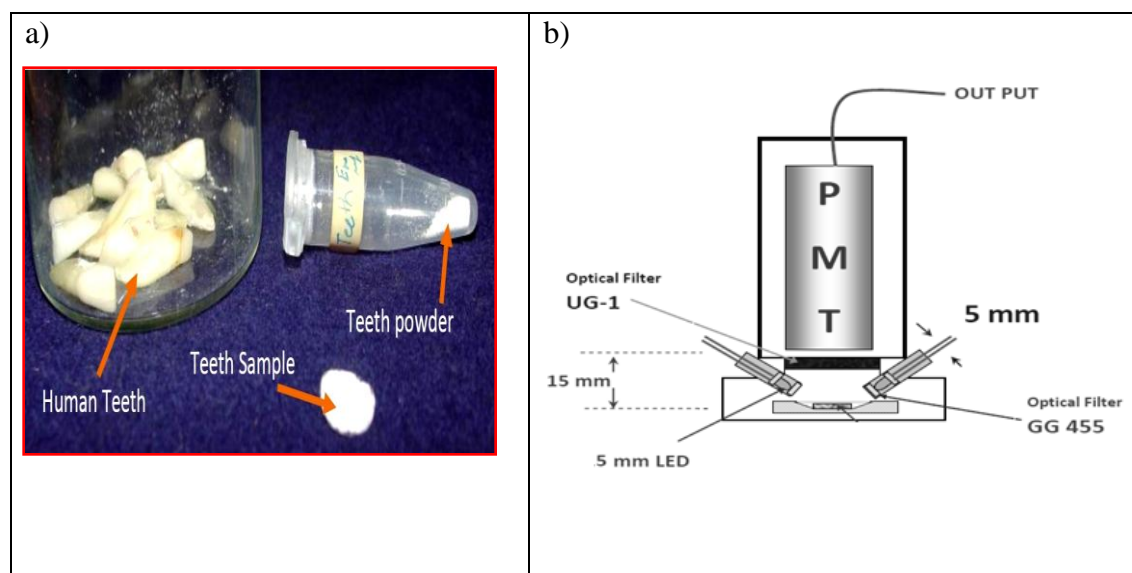
Fig.6.14 a) Powder sample of dental enamel with grain size of 70-110 μm range. b) Sketch of the highly sensitive OSL reader used for the present OSL measurements of dental enamel

6.3.2.2 TL and TA-OSL Measurements

The TL and TA-OSL measurements were performed using a programmable integrated TL/OSL reader system [58]. The same photon counting module (P25232) PMT with RS232 output was also used to detect the luminescence emission. The GG-435 and UG-1 optical filters were used across the LED cluster and PMT, respectively to prevent the stimulating light from reaching the PMT. The calibrated samples were optically bleached by 470 nm light for 10 minutes, before the

irradiation. In the present study, the TL curve was obtained by heating the enamel sample up to 450 ^{o}C at a 4 ^{o}C/s heating rate. To measure the MDD for TL method, background was measured on six un-irradiated enamel samples to determine 3 standard deviations of the background signal (X); then these six samples were exposed to a dose of 5 Gy to determine the mean TL output of these samples (Y/Gy); finally, MDD was calculated as MDD (Gy) = X * Gy / Y

The TL glow curve was resolved using a Computerized Curve De-convolution Analysis (CCDA). Following single glow-peak equation of general order kinetics suggested by Kitis et al., (1998) was used for the de-convolution of glow curve [17]:

$$I(T) = I_m \cdot b^{\frac{b}{b-1}} \exp(\frac{E}{kT} \frac{T-T_m}{T_m}) \cdot [(b-1)(1-\Delta) \frac{T^2}{T_m^2} \exp(\frac{E}{kT} \frac{T-T_m}{T_m}) + Z_m]^{-\frac{b}{b-1}} \qquad (6.7)$$

where

$$\Delta = \frac{2kT}{E}, \Delta_m = \frac{2kT_m}{E}, Z_m = 1 + (b-1)\Delta_m \qquad (6.8)$$

Where E is the trap depth, b is the order of the kinetics, k is the Boltzmann's constant, and T_m is the peak temperature. The software package Microsoft Excel, with the Solver feature [18] (Afouxenidis et al., 2012) has been used for all the curve fittings. The fit is based on Eq. (6.7) which directly gives the TL kinetics parameter such as E and b. The goodness of fit was checked using the Figure of Merit (FOM) [19] (Eq. 6.9) (Balian and Eddy 1977).

$$FOM = \sum_i \frac{|Y_{Exp} - Y_{Fit}|}{A} \qquad (6.9)$$

Where, A is the area of the fitted curve, Y_{Exp} is the data point on the experimental curve and Y_{Fit} is the data point on the fitted curve. The FOM values were found to be more than 1.5%. The condition of TL maximum is used for the evaluation of the frequency factor s (Eq. 6.10).

$$s = \frac{\beta E}{kT_m^2} \exp\left(\frac{E}{kT_m}\right) \tag{6.10}$$

where β is the heating rate. The order of kinetics b was determined by means of glow curve shape analysis using the geometrical shape factor (μ_g).

The TA-OSL measurements were carried out by stimulating the irradiated sample with multiple short pulses of blue LED light (470 nm). This was done for 0.3s after every 20 °C temperature interval at a very low power of 10 mW/cm^2 with simultaneous TL upto 500 °C at a heating rate of 4K/s. The stimulation intensity and the time period of the optical pulses were chosen as low as possible so that the TL glow curve and the trapped charges were not affected. In this way, the temperature dependence of OSL at each temperature was obtained. This type of measurement was first reported by Hutt et al. (1988) on feldspar. Yukihara et al. 2004 have also reported similar studies on α-Al$_2$O$_3$:C by heating the samples upto 100 °C, exposing the sample with a low power optical pulse and recording the OSL signal [37]. The sample was allowed to cool to room temperature. The same procedure was repeated up to 700 °C in 20 steps. However, unlike their method, we have measured the OSL intensity at different temperatures in a single step by heating the sample upto 500 °C and the short pulses of low LED power were incident simultaneously during the temperature ramp. In case of very low stimulation power, the TA-OSL intensity can be expressed as Eq. 6.11 [33]

$$I_{TA-OSL} = A e^{-\frac{E_A}{kT}} \tag{6.11}$$

Where A is a constant and the plot of ln(I_{TA-OSL}) vs 1/kT is linear with a slope expressed by the thermal assistance energy (E_A).

6.3.2.3 OSL instrumentation

As the radiation sensitivity of dental enamel is very low, we have developed a highly sensitive compact OSL reader, to carryout the CW-OSL, NL-OSL and MDD measurements. The reader consists of a blue LED (diameter: 5; $\lambda_p = 470$ nm), as a stimulating light source. As the diameter of the LED is only 5 mm, the distance of the photomultiplier tube (PMT) from the sample has been reduced to 15 mm as compared to that of the integrated TL/OSL reader described by Kulkarni et al. (2007) [58] in which the LEDs are at 50 mm from the sample. (Fig.6.14b). Hence, the light collection efficiency is increased (due to increase in solid angle) and thus the sensitivity of the reader is increased by a factor of 10. The combination of 12 such LEDs generates a maximum of 48 mW/cm^2 (each LED is capable of generating 4 mW/cm^2 at 30 mA current) at the sample position. The light intensity at the sample position was measured using a Si photodiode (OSD-5). A photon counting module (P25232) PMT with RS232 output has been used to detect the signal coming from the sample. The GG-435 optical color glass filter was used across the LED cluster to cut the stimulation wavelength below 435 nm. An UG-1 UV band-pass filter (Schott AG, Mainz, Germany) with maximum transmittance at ≈ 360 nm having a transmittance ≈ 0.02 at 420 nm, was used across the PMT to prevent the stimulating light from reaching the PMT.

6.2.3.4 OSL measurement procedures

In the present work, the CW-OSL response, dose linearity and MDD measurements were carried with highly sensitive compact OSL reader system described above, as the MDD does not only depend on the material but also on the instrument used for readout. The CW-OSL response of dental enamel of 20 Gy was taken at a fixed stimulation intensity of 48 mW/cm^2 of 470 nm LED light. The background from the un-irradiated samples was subtracted from the actual readings. For

calculating MDD for the OSL method, the same procedure as that described for the TL method earlier was used.

The OSL components from the CW-OSL decay curve were evaluated using a second order equation (Eq. 6.12) [31].

$$I_{CWOSL} = I_{10} \exp\left(-\frac{t}{\tau_1}\right) + I_{20} \exp\left(-\frac{t}{\tau_2}\right) + c \tag{6.12}$$

Where I_{CWOSL} is the CWOSL intensity, τ_1 and τ_2 are the decay constants of two different components respectively, I_{10} and I_{20} are the initial intensities of these components, t is the time taken for OSL readout and c is a constant. From the decay constants of the two components, the photoionization cross-section was calculated using (Eq. 6.13).

$$f = \sigma\varphi \tag{6.13}$$

where f (s^{-1}) is the excitation rate (1/τ), σ the photoionization cross-section (cm^2) and φ the stimulation flux (photons/cm^2/s).

The NL-OSL method was also used to evaluate the OSL components in dental enamel. In this method, the stimulation intensity profile on the sample is modulated non-linearly with respect to time during the OSL readout. NL-OSL is expected to separate out closely overlapping OSL peaks having similar values of photo ionization cross-sections [26]. The photoionization cross-section σ (cm^2) of the OSL active traps can be evaluated using Eq. 6.14.

$$_1^l t_{max} = \left[\frac{l}{\sigma\,\gamma'}\right]^{\frac{1}{l+1}}$$

(6.14)

Where t is the time required to reach the maximum value of NL-OSL intensity and γ' is a constant with dimension cm^{-2} s$^{-(l+1)}$, and l is the parameter which determines the power of light modulation

in the time domain; *l* can take values in the range: $0 < 1 \leq \infty$ such as 0.1, 0.5, 1, 2,… etc [26,27]. The sample was given 50 Gy of beta dose for taking NL-OSL readout for 6000s. The NL-OSL readout of dental enamel along with the corresponding stimulation profiles is recorded for Time base power (TBP) (*l*=2.5) with fixed final stimulation intensity (φ_o) of 100 mW/cm^2 for a fixed time of 6000 s.

6.3.2.5 Emission and Excitation Spectra

The excitation and emission spectra were recorded on the un-irradiated dental samples using a Hitachi F-4500 fluorescence spectrometer. The fluorescence spectrometer consists of a 150 W xenon lamp in a self-deozonating lamp house as light source, a PMT as a light detector, and a large aperture stigmatic concave diffraction grating as monochromator on the excitation and emission sides. Wavelength accuracy of the instrument is within ± 2.0 nm.

There is little information available on the OSL emission spectrum of dental enamel. Generally, PL studies provide information about the enamel luminescence centers involved in the TL/OSL process. They also give an idea regarding the use of appropriate optical filters to be used to maximize transmission of OSL emission and to appreciably cut the stimulating light in the OSL reader to enhance the overall sensitivity of the system. Around 5 mg of sample was mixed with one ml methanol, producing slurry which was spread over a quartz plate and dried under ambient conditions prior to luminescence measurements. In photoluminescence (PL) measurements, luminescence centers of an un-irradiated sample are excited by light and their subsequent emission is recorded, thus the sample was not exposed to any dose for this measurement. An un-irradiated sample (to avoid OSL interference) was studied for the excitation and emission characteristics of luminescence centers. In order to get the excitation and emission spectra of the sample (when no information is available about the excitation and emission wavelength of the

luminescence centers), successive excitation and emission spectra were recorded for various set of parameters including different emission windows (800- 300 nm) and scanning the excitation wavelength. Once the excitation wavelength was known, the emission spectrum was scanned for that fixed excitation wavelength.

6.3.2.6 Lifetime Measurements

For carrying out the POSL studies, a separate setup was developed in which the continuous wave (CW) diode pump solid state laser beam was chopped (Laser Quantum Ciel, Sr. no: 0904C, Power: 50 mW, wavelength: 473 nm, beam diameter: 0.9 ± 0.2 mm). The chopper consists of an electromagnetic shutter (speaker coil) with an attached thin Cu plate. Pairs of convex lenses were used to guide the laser beam in an optical fiber. The pulsed laser beam was incident on the OSL sample and the luminescence signal was recorded using a photon counting module PMT (Sens-Tech, Package-P30CWAD5 and Type- 9125B84) with TTL output. This module contains a built-in high voltage supply and does not include any means to gate its diodes. Hence, an AND gate (DM7408) was used for gating the output of PMT as shown in Fig 6.16a. A UG-1 filter was used across the PMT for preventing the stimulating light from entering the PMT. This was also important to enable the PMT during laser pulses though its output will not be recorded during that time in the present setup. The POSL setup thus installed allows generation of at least 90 μs pulse width at maximum 1 kHz repetition rates. The timing synchronization is shown in Fig 3a where the pulse frequency is 800 Hz (corresponding to 1.25 ms), T_1 (Pulse width) is 90 μs, T_2 (dead time during which PMT output is gated off) is 190 μs, and T_3 (acquisition time) = is 1.25ms -190 μs = 1060 μs. The PMT output was gated 50 μs before and after the pulse (also shown in Fig 3b). The total dead time for the 0.9 s stimulation period and 800 Hz frequency is 800×190 μs = 237 ms.

The total acquisition period is 663 ms. The luminescence lifetime (τ) was measured by fitting the luminescence decay curve with an exponential function (Eq.6.15).

$$I = A\exp\left(\frac{t}{\tau}\right) + C \tag{6.15}$$

Where *I* is the luminescence intensity, *t* is the time following the laser pulse, *A* is a constant and *C* is the offset.

6.3.3 Results and Discussion

6.3.3.1 Photoluminescence (PL) Studies

The dental sample showed an emission spectrum at 412 nm when excited at 324 nm as shown in Figs 6.15a and 6.15b. To the best of the authors' knowledge this result has not been reported yet in the literature. Emission at 412 nm is quite similar to that of α-Al_2O_3: C; thus no modification was required in the filter assembly of the compact OSL reader. As the Schott UG-1 UV band-pass filter with maximum transmittance at about 360 nm shows a transmittance of only about 0.02 at 420 nm, most of the signal is not recorded.
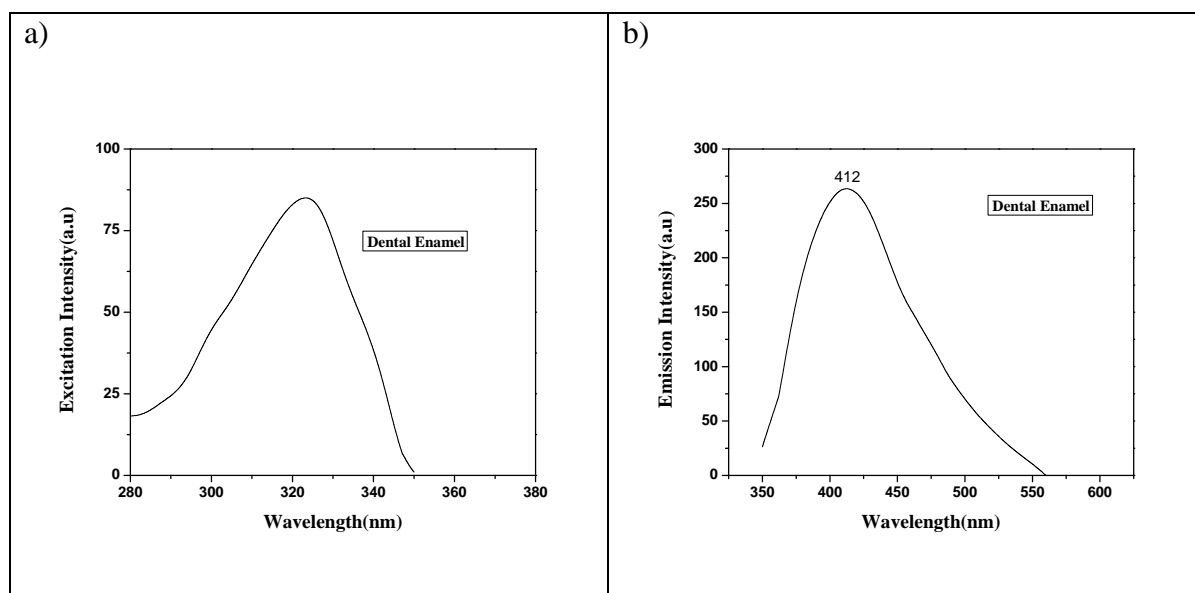
Fig. 6.15a) Excitation spectrum of a dental enamel sample with emission at 412 nm. b) Emission spectrum of dental enamel sample when excited by 324 nm.

This limitation is due to the interference with the stimulation wavelength (470 nm) used for the enamel sample. If the filter assembly is chosen for maximum transmittance at about 410 nm, then the background due to scattering of the 470 nm stimulation wavelength will be too high, and the signal-to-noise ratio will become very poor, because the filter will also allow the 410 nm components of the stimulation wavelength to be transmitted, which will be very high as compared to the signal from the sample.

6.3.3.2 Luminescence Lifetime Measurement

The implementation of POSL technique to enhance the sensitivity for it to be used for retrospective dosimetry using dental enamel requires the information about the role of shallow traps and the lifetime of recombination centers. There is no information available in the literature about the luminescence lifetime of recombination centers in dental enamel. The POSL technique is more advanced and fast method of measuring absorbed dose from phosphors as it allows maximum signal to noise ratio as compared to other dosimetric techniques [59]. It is suitable when the lifetime of the luminescence centers in the material is longer than the period of the stimulation pulses. The POSL curve is supposed to give an estimate of luminescence lifetime of recombination center along with delayed POSL luminescence component originating from low order shallow defects trap levels. The POSL has been recorded at 50mW/cm^2 at pulse width of 90 µs at 800 Hz at room temperature. After the stimulation for 0.8 s, decay of the luminescence centers has been recorded in the absence of any stimulation light. The POSL curve of dental enamel is shown in Fig. 6.16b and luminescence lifetime was measured using Eq. 6.15. Taking log of Eq. 6.15 (i.e., putting POSL intensity in log scale), the inverse of the slop (by linear fitting)

of the two components will directly give the luminescence lifetime as shown in Fig. 6.16c. The POSL results show 32 ms as the luminescence lifetime oriented of the main recombination center and a slow component having lifetime 350 ms.
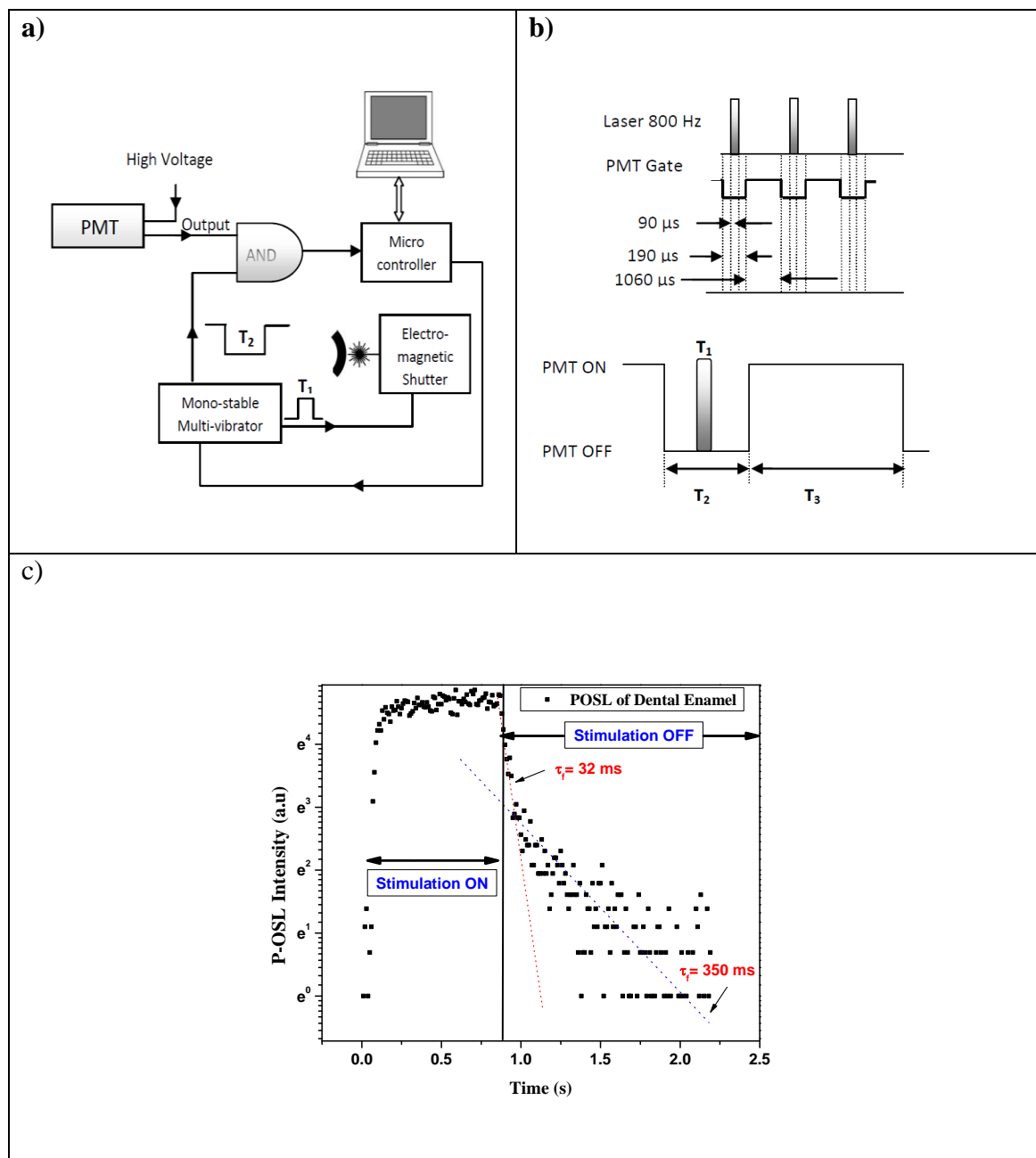
Fig. 6.16a) Sketch of the gating mechanism at PMT output. The output of PMT is not recorded for T_2 (190 μs) using AND gate. b)) Timing diagram of POSL measurement: The stimulation pulses having a 90 μs pulse-width and an 800 Hz frequency were ON for 0.9 s and after that stimulation was switched

off.   c) POSL response of a dental enamel sample exposed at 20 Gy showing two distinct components of

32ms and 350 ms respectively

6.3.3.3 TL Characterization

TL studies provide vital clues on the nature and types of the traps and the thermal stability of the OSL signal can be estimated by the peak temperatures of TL peaks. However, the application of TL for retrospective dosimetry using teeth has its limitation, as organic tooth constituents decompose and emit light - a process called chemiluminescence - upon heating during TL measurements [60].   In the present study, the investigated enamel showed a broad and structureless TL curve from 100 to 450 °C for a 4 °C/s heating rate (Fig. 6.17a). The curve can be attributed to the recombination of several radiation-induced CO_2^- radicals generated from surface CO_2^- impurities in hydroxyapatite [61]. The MDD from TL response of dental enamel was found to be 150 mGy. As the enamel sample starts decomposing and converting into other compounds at higher temperatures (> 400 °C) [62], data upto 400 °C in Fig. 4a were integrated for MDD calculation. The TL glow curve was resolved using a CCDA for TL peaks having multiple peaks at 115, 185, 260, 330, 380 and 410 °C. Figure 6.17a presents a typical TL glow curve de-convolved into its individual peaks. A total of six individual TL peak-components were used; this was the minimum number of peaks required in order to perform a quality fit. Figure 6.17b gives the residuals of the fit. Table 6.5 shows the measured TL parameters of the different peaks of the TL glow curve. It gives the information regarding the frequency factor, order of kinetics and thermal trap depth/thermal stability of the traps.
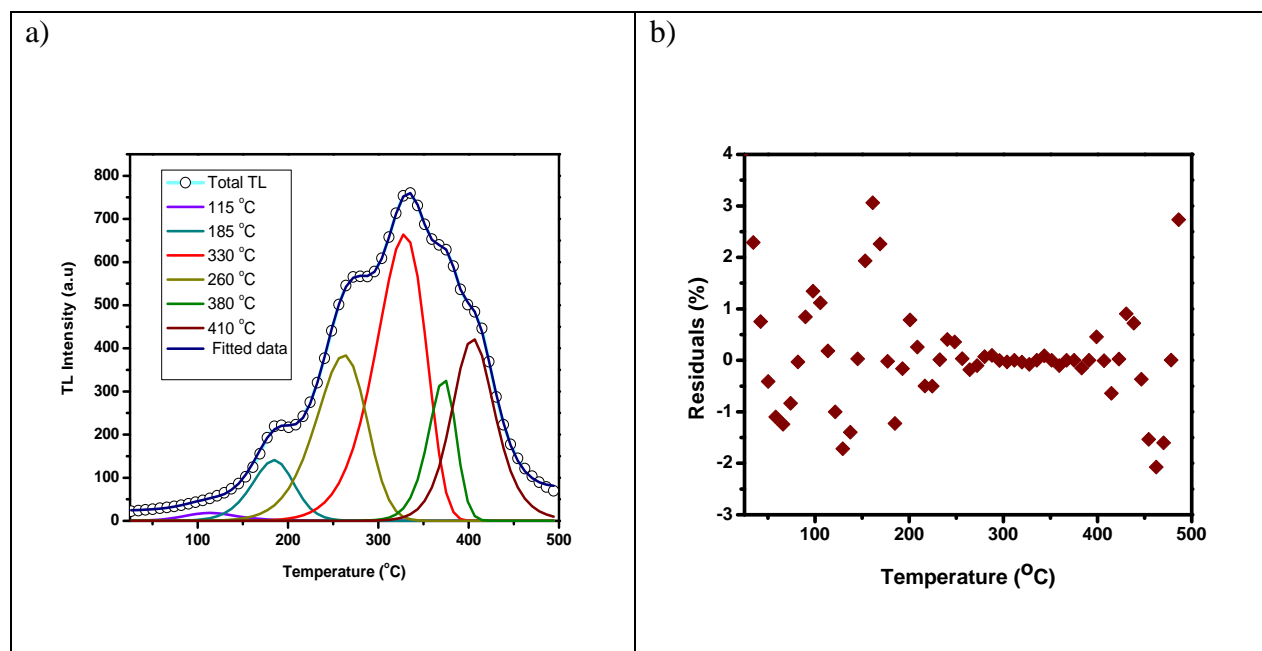
Fig. 6.17a). TL glow curve of dental enamel de-convolved into its six individual components according to discrete trap distribution for general order kinetics; for 50 Gy beta dose. Open circles represent experimental points and solid lines the fit and each individual TL glow peak; b) Residuals of the fitting

Table 6.5. The kinetics parameters of dental enamel after the deconvolution into single peaks of the TL curve.

Measured TL parameters	115 ^{o}C TL Peak	185 ^{o}C TL Peak	260 ^{o}C TL Peak	330 ^{o}C TL Peak	380 ^{o}C TL Peak	410 ^{o}C TL Peak
E_m(eV)	0.6	1.19	1.29	1.42	1. 6	1.8
S (sec^{-1})	5.08×10^9	7.58×10^{11}	2.74×10^{11}	5.8×10^{12}	4.36×10^{12}	5.04×10^{13}
b	2	1.41	1.14	1.14	1.22	2

E= Thermal trap depth, s= frequency factor, b= order of kinetics.

6.3.3.4 CW-OSL Studies

Earlier studies reported that the CW-OSL response of dental enamel for doses of less than 1.4 Gy was indistinguishable from background and that a statistically significant dose response was observed above 1.4 Gy [53]. Figure 6.18 shows the CW-OSL response of dental enamel of 20 Gy at a fixed stimulation intensity of 48 mW/cm^2 of 470 nm LED light. The samples show a linear dose response up to a dose of 500 Gy (Fig. 6.19). The MDD, corresponding to the 3σ limit of the variation of the output of the un-irradiated samples, was estimated to be 100 mGy for blue light stimulation.
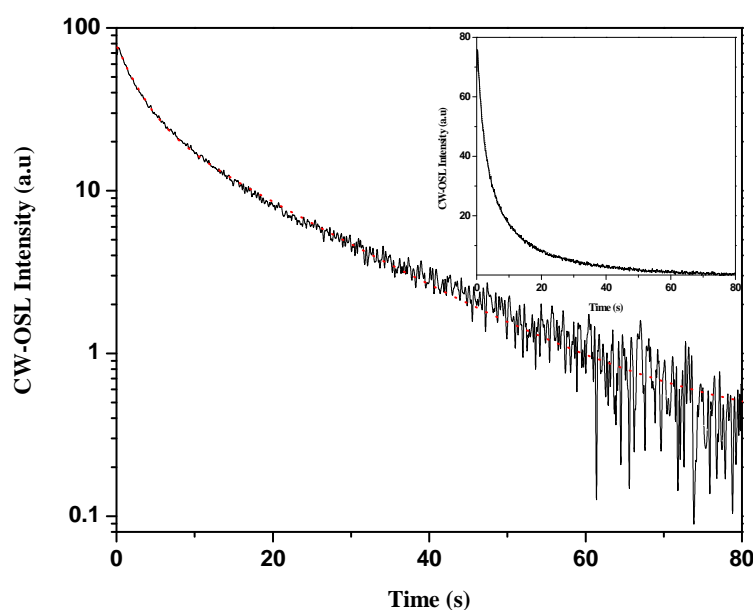
*Fig. 6.18. CW-OSL response of dental enamel exposed to an absorbed dose of 20 Gy at a fixed stimulation intensity of 48 mW/cm^2 of 470 nm LED light. The CW-OSL decay was found to be best fitted by a second order exponential fit (I_{CWOSL} = 4869 * exp(-80/2.74) + 2879 * exp(-80/15.92) + 31.88). Inset shows the same curve but for a linear y-scale*

In the present study, the CW-OSL decay of dental enamel was found to be best fitted by a second order exponential fit ($I_{CWOSL} = 4869 * \exp(-80/2.74) + 2879 * \exp(-80/15.92) + 31.88$) as shown in Fig.6.18. The photo-ionization cross-sections of the two components were determined as 3.17×10^{-18} and 5.52×10^{-19} cm^2, respectively for 48 mW/cm^2 stimulation intensity using Eqs. 6 and 7. The stimulation flux φ for 48 mW/cm^2 was 1137.12×10^{14} photons/cm^2/s (1 mW/cm^2 (470 nm) = 23.69×10^{14} photons/cm^2/s). Godfrey-Smith (2008) also reported the existence of two OSL components in dental enamel [53].
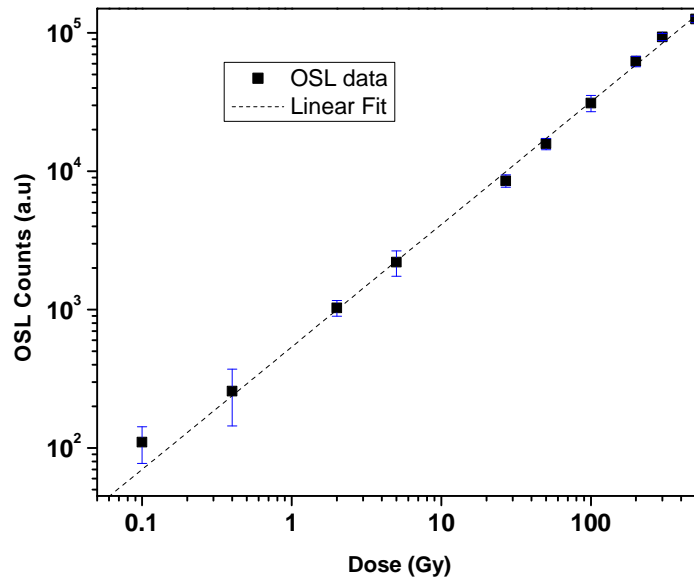
Fig. 6.19. Dose vs. CW-OSL response of dental enamel. The OSL dose was evaluated using the entire area under the CW-OSL curve (i.e, including both the fast and the slow component). Every point represents an average of 5 different samples; the error bars represents one standard deviation

To investigate the optical nature of the TL traps, the CW-OSL signal was taken for different preheating temperatures (Fig. 6.20). It is clear that all the traps are contributing to the OSL signal

i.e, all the TL traps are OSL active traps. However, the OSL signal doesn't become zero even if the sample is heated upto 420 °C, suggesting the existence of deeper traps in dental enamel, which is further confirmed by TA-OSL studies described in the next section.
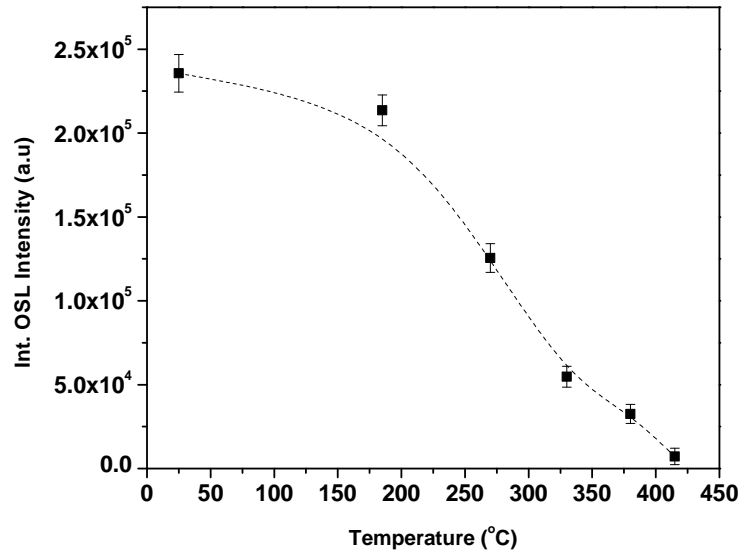
Fig. 6.20. Integrated CW-OSL response of dental enamel: five samples were preheated at various temperatures and subsequently the CW-OSL was taken at room temperature; the error bars represents one standard deviation.

6.3.3.5 NLOSL studies

The CW-OSL response of dental enamel suggests the existence of multiple components. On the other hand, the method of linearly modulated optically stimulated luminescence (LM-OSL) does separate out different peaks with the well separated photo-ionization cross-sections. However, for a system with closely overlapping OSL components, even the LM-OSL record will not provide well-defined LM-OSL peaks, even with the slowest possible LM simulation rate suggesting very close values of the photo-ionization cross-sections responsible for total OSL (Fig. 6.21).
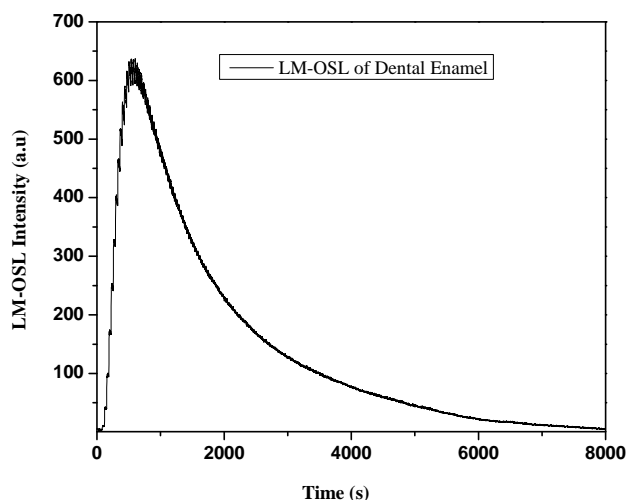
Fig. 6.21. LM-OSL response of dental enamel sample for 8000 s for an absorbed dose of 50 Gy.

In the present study, an enamel sample was investigated by means of NL-OSL to further confirm and quantify the two distinct components. It is clear from NL-OSL readout shown in Fig. 6.22 that the dental enamel consists of two well defined components. Based on Eq. 8, the photo-ionization cross-sections of the two OSL components were found to be 6.09×10^{-18} and 8.25×10^{-19} cm^2 respectively. Table 6.6 gives the photo-ionization cross-sections of OSL components of dental enamel measured by different methods.

Table 6.6 OSL parameters of dental enamel.

Stimulation Techniques	σ (cm^2) of Faster component	σ (cm^2) of Slower component
CW-OSL	3.17×10^{-18}	5.52×10^{-19}
NL-OSL	6.09×10^{-18}	8.25×10^{-19}
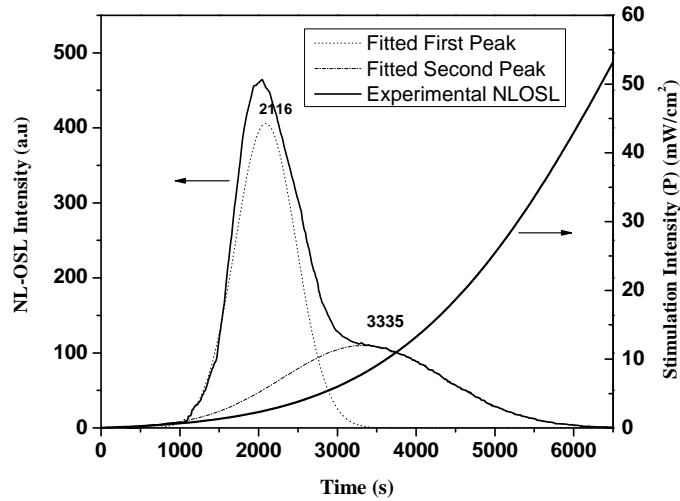
Fig. 6.22. NL-OSL response of dental enamel for a TBP (time base power) value of (l=2.5) for the sample showing two distinct components, and having photoionization cross-section of 6.09×10⁻¹⁸ and 8.25×10⁻¹⁹ cm², respectively

6.3.3.6 TA-OSL Studies

The temperature dependence of OSL was studied, in order to investigate the effect of the stimulation temperature on OSL intensity. OSL intensity has been reported to be increased with temperature, due to the temperature dependence of the photo-ionization cross-section, in a number of publications [31,32]. Fig 6.23a is the TL glow curve superimposed with the recurrence of narrow peaks due to the multiple short OSL pulses (0.3 s after every 20 $^{\circ}$C interval) with simultaneous TL readout. Before irradiation, the sample was subjected to pulses of blue light of the same intensity and for the same time as for the actual measurement along with simultaneous TL readout, and the OSL+TL background thus obtained was subtracted from the finally obtained pulse height. The resulting OSL signal (pulse height subtracted from OSL+TL background) emitted in each step was plotted against temperature (Fig. 6.23b).

194
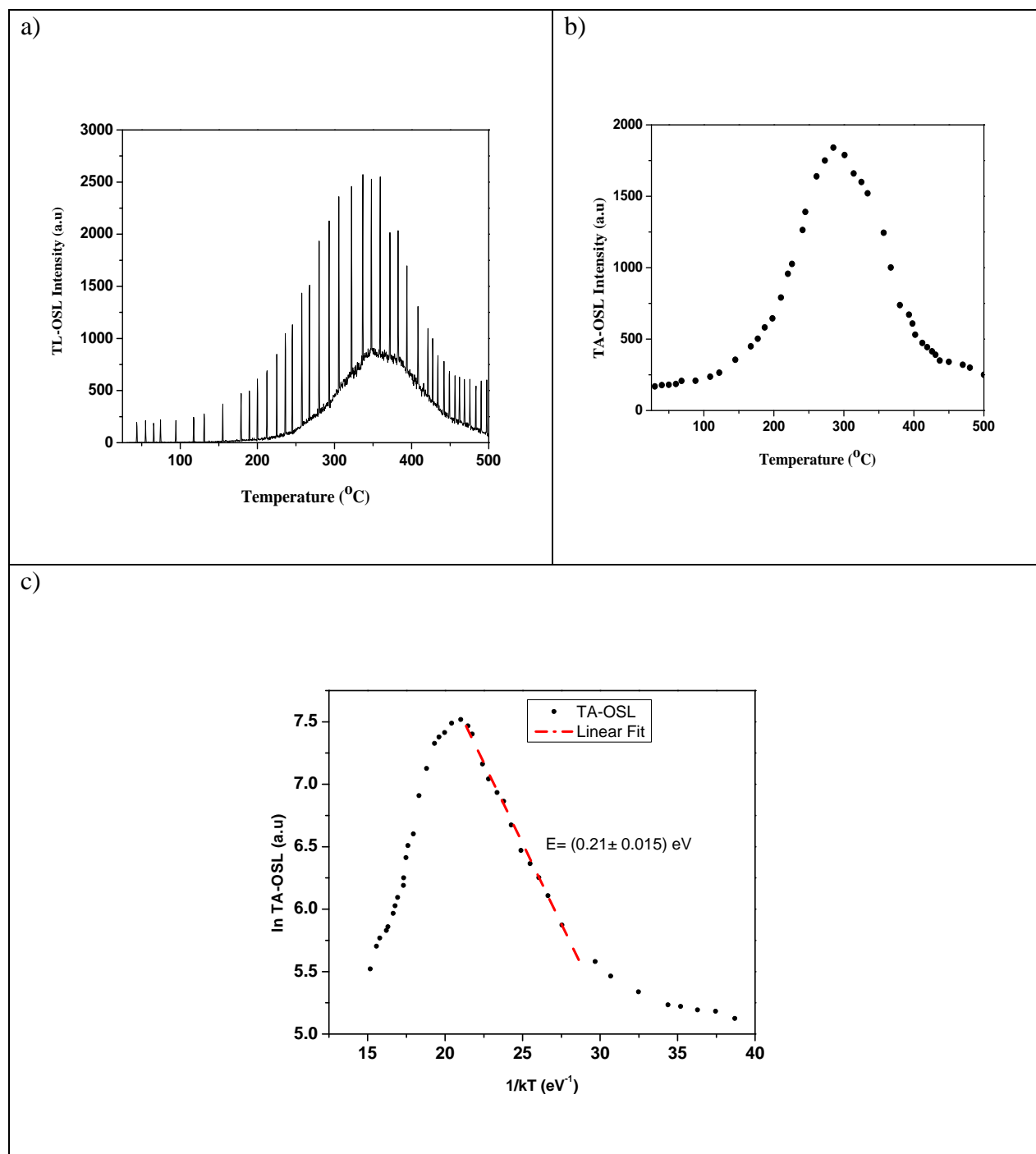
Fig. 6.23a TA-OSL measurements of dental enamel sample with short (0.3 s) and low power stimulation pulses (20% LED power) for every 20 °C when heating at 4K/s of a sample previously irradiated to 50 Gy. b) TA-OSL signal obtained i.e, the pulse height of Fig 6.23a vs temperature. c)

Arrhenius analysis of the integrated TA-OSL signal from Fig. 6.23b. The straight line fit yields the activation energy for the thermally assisted OSL (TA-OSL) process $E_{th}= 0.21\pm0.015$ eV.

Figure 10c shows the result of an Arrhenius analysis for the integrated TA-OSL signal. The activation energy of the thermal assistance was found to be $E_A = 0.21 \pm 0.015$ eV by linear fitting of the data between stimulation temperatures of 120 °C to 250 °C using Eq. 5 (Fig. 6.23c). The increase in OSL signal with temperature up to 300 °C can be attributed to the temperature dependence of photoionization in this region. The temperature dependence was tested using different samples and the result obtained (nature of the OSL dependence on temperature) was found to be similar. In principle, this increase of the OSL signal with increasing temperature can be used for enhancing the sensitivity of dental enamel for retrospective dosimetry. However, this might not be applicable for an in-vivo method. Beyond 300 °C, the OSL intensity starts decreasing with increasing temperature, due to the depletion of trapped charges or perhaps due to thermal quenching. However, the OSL signal is still present even if the sample is heated upto 500 °C (Figs. 6.23a and 6.23b) suggesting the existence of deeper traps in dental enamel.

6.3.2.5 Fading Studies

Samples stored at room temperature in the dark have been studied for their fading properties. For this, nine sets of different samples (each set containing 10 samples) were prepared. All the samples were irradiated with the same dose (20 Gy) at the same time. The first set of samples was measured immediately for its CW-OSL decay after exposure. These samples were taken as a reference while the remaining sets were stored in dark conditions. These sets of samples were measured after 1, 3, 5, 12, 24, 48, 100, and 200 hours respectively. All measurements were conducted at room temperature only, and no preheat treatments were given to the samples before

or after storage. The CW-OSL data used for the fading study was integrated for 80 s for all the samples (i.e until it reached the background signal).
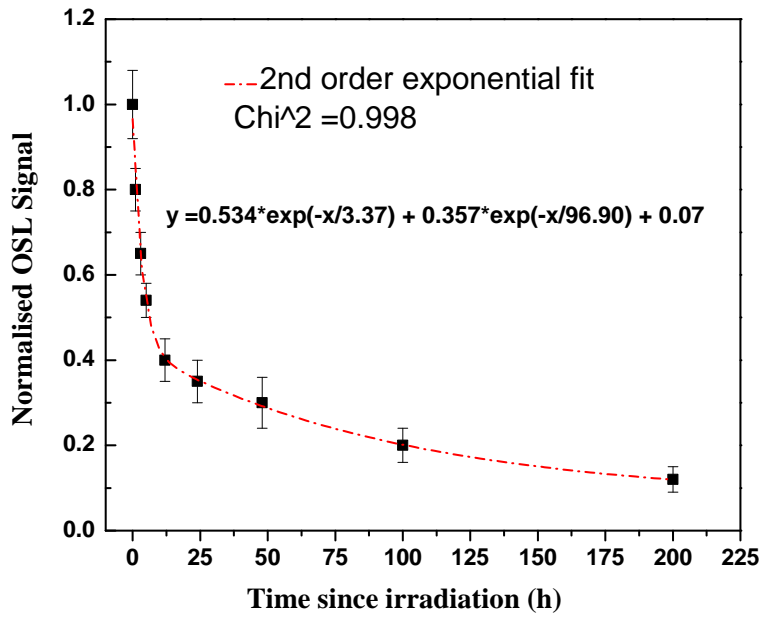
Fig. 6.24 Fading studies of dental enamel samples. Every point is an average of measurement of 10 different samples. All data were normalized to the corresponding values of signal in samples immediately after irradiation; the error bars show the standard deviations.

It was found that fading consisted of two components resulting in a fast fading of 60-65 % of the signal in 24 hours, then fading due to a slow took over (Fig. 6.24). The best fit was obtained with a second order exponential function ($y = 0.534 * \exp(-x/3.37) + 0.357 * \exp(-x/96.90) + 0.07$) with decay time constants of 3 h and 96 h respectively. Sholom et al. (2011) studied the fading properties of tooth enamel and discussed how a calibration could be carried out in-vivo [55]. They presented the hitherto lowest minimum detectable absorbed dose, which they termed minimum measurable dose (MMD), for multiple teeth samples: the MMD they obtained was 27 mGy for the most sensitive sample and 0.64 Gy for the least sensitive sample. They concluded that UV light

197

was not useful for in-vivo calibration purposes regarding exposures to ionizing radiation from photons and electrons. Future work on deep traps of dental enamel can improve the problem of fading associated with intermediate traps of dental enamel, because such deep traps should be very stable in ambient light. We have recently studied the thermal and optical stability of deep traps of α-Al$_2$O$_3$:C using TA-OSL and showed that they are stable even in room light [32].

6.3.4 Challenges for its application in Accident Dosimetry

Ex-vivo and in-vivo approaches each have their own advantages and disadvantages. The problem encountered in in-situ dose reconstruction is the difficulty in re-irradiating the tooth for calibrating its radiation response (although using pencil X-ray tube or a well collimated beta source it could be done), which calls for an alternate way of calibration. Swartz et al. (2006) have suggested to measure the dose in radiation therapy patients who received accurately known doses, and to create a library of response-to-dose conversion factors for prompt estimates [46]. They gave a detailed description of the in-vivo EPR method along with the instrumentation to be used for dose reconstruction from dental enamel. They already measured the responses of a large number of teeth to a range of doses, to create a library that can be used to estimate the dose directly. This may also overcome the problem of variation of radiation sensitivity from sample to sample as reported by Sholom et al. (2011) [55]. The other problem with in-vivo measurements reported recently by Geber-Bergstrand et al. (2012) is the reduction of sensitivity of tooth enamel irradiated in wet condition [63]. Hence, the sensitivity of any in-vivo OSL reader must be very high for immediate dose measurements using tooth enamel. However, there was no effect of wet condition on the OSL sensitivity of external ceramic material fitted as dental crowns [63]. Further, because a large part of the adult population has some dental repair material in their teeth, such materials can

be utilized for in-vivo/ex-vivo accident dosimetry as these materials are easier to extract as compared to tooth enamel. Since tooth enamel is OSL sensitive, ambient light can affect the OSL signal. Therefore, precautions should be taken while handling of dental samples. As OSL processing and sample preparation are always carried out in red light (highest visible wavelength, lesser energy), OSL measurements for retrospective dosimetry should be carried out in red /dim light in case of an in-vivo approach. Extraction of tooth samples, their storage and sample preparation should also be done in red /dim light in case of an ex-vivo approach because the red light has lesser energy as compared to blue light (stimulation wavelength) and is therefore not expected to bleach the OSL signal present in any irradiated tooth. Hence, the dentist should also extract the teeth in such condition or with the aid of an infrared dental mouth camera.

6.4. Investigations on Al_2O_3:Si, Ti

6.4.1 Introduction

Al_2O_3:Si,Ti prepared by sintering in air, is reported as a sensitive thermoluminescent material with multiple TL peaks with emission in blue region (420 nm) [64,65,66]. Titanium is reported to be present in the Ti^{4+} state under the highly oxidizing conditions used in the preparation of Al_2O_3:Si,Ti [67,68]. TL peak at 250 °C was observed to be most intense having a detection threshold of 0.01mGy. Detailed TL studies on Al_2O_3:Si,Ti, such as dose vs. TL response, phototransferred thermoluminescence (PTTL), ultraviolet (UV) induced TL and radiation-induced sensitization, had been reported earlier by Mehta and Sengupta [64,65,69]. The TL peaks at 250 and 475 °C are reported to exhibit radiation-induced sensitization due to the influence of the traps related to the 625 °C TL peak [64]. Recently, Bhatt et al., (2008) reported the TL and OSL characteristics of Al_2O_3: Si,Ti [70]. Its TL and OSL sensitivity was found to be 1/9th and 1/20th

respectively compared to that of commercial α- Al_2O_3: C phosphor. Its dose vs OSL response was found to be linear upto 5 Gy. Its emission was reported at 410 nm for excitation at 240 nm which matches the emission reported in the literature for Ti^{4+} ions in Al_2O_3. No F and F^+ center was found in its PL measurements. In the present investigation, we report the TA-OSL characteristics of Al_2O_3: Si,Ti along with TL glow curve to see the effect of temperature on the OSL intensity and its effect to improve the sensitivity of the material.

6.4.2 Materials and methods

The Al_2O_3:Si,Ti phosphor was prepared according to the procedure described by Mehta and Sengupta (1976a) and McKeever et al. (1995). All the samples used in the present study contained 300 ppm Si and 10 ppm Ti. The phosphor in the grain size range 100–200 mesh was selected for the present work. Samples were annealed at 400 °C before irradiation. TL/OSL and TA-OSL measurements were performed using the same RISØ TL/OSL reader.

6.4.3 Results and Discussions

6.4.3.1 TL Characterization

Fig 6.25 shows the TL glow curve of Al_2O_3:Si, Ti at 4K/s for 200 mGy β-dose. Its glow curve consists of multiple peaks at 80 175, 280, 350 °C respectively.
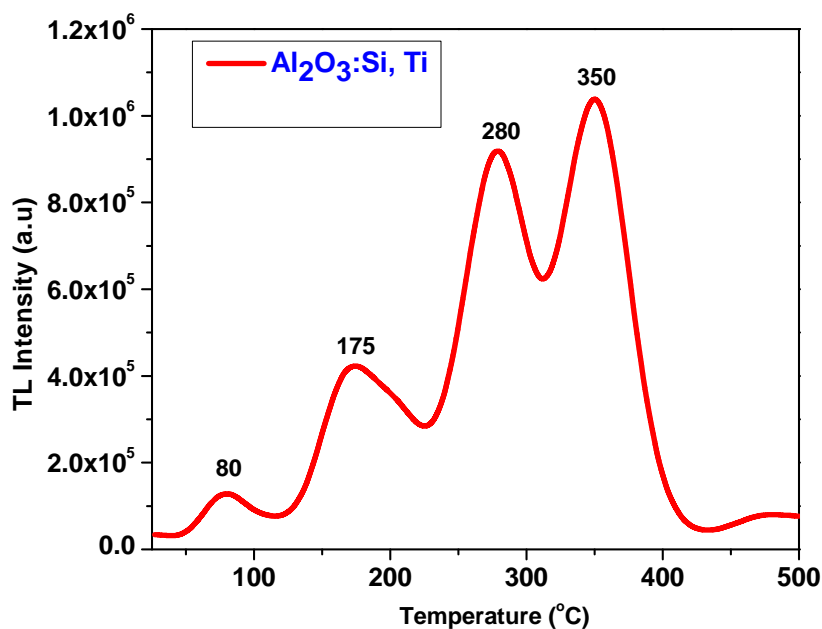
Fig. 6.25. TL glow curve of Al₂O₃: Si, Ti at 4 K/s for 200 mGy dose showing TL peaks at 80, 175, 280, 350 °C.

6.4.3.2 TA-OSL Studies

In order to investigate the effect of the stimulation temperature on OSL intensity of Al$_2$O$_3$:Si, Ti, TA-OSL studies was carried out. Fig 6.23a is the TL glow curve superimposed with the recurrence of narrow peaks due to the multiple short OSL pulses (0.3 s after every 5 °C interval) with simultaneous TL readout. Before irradiation, the sample was subjected to pulses of blue light of the same intensity and for the same time as for the actual measurement along with simultaneous TL readout, and the OSL+TL background thus obtained was subtracted from the finally obtained pulse height. The resulting OSL signal (pulse height subtracted from OSL+TL background) emitted in each step was plotted against temperature (Fig. 6.23b).
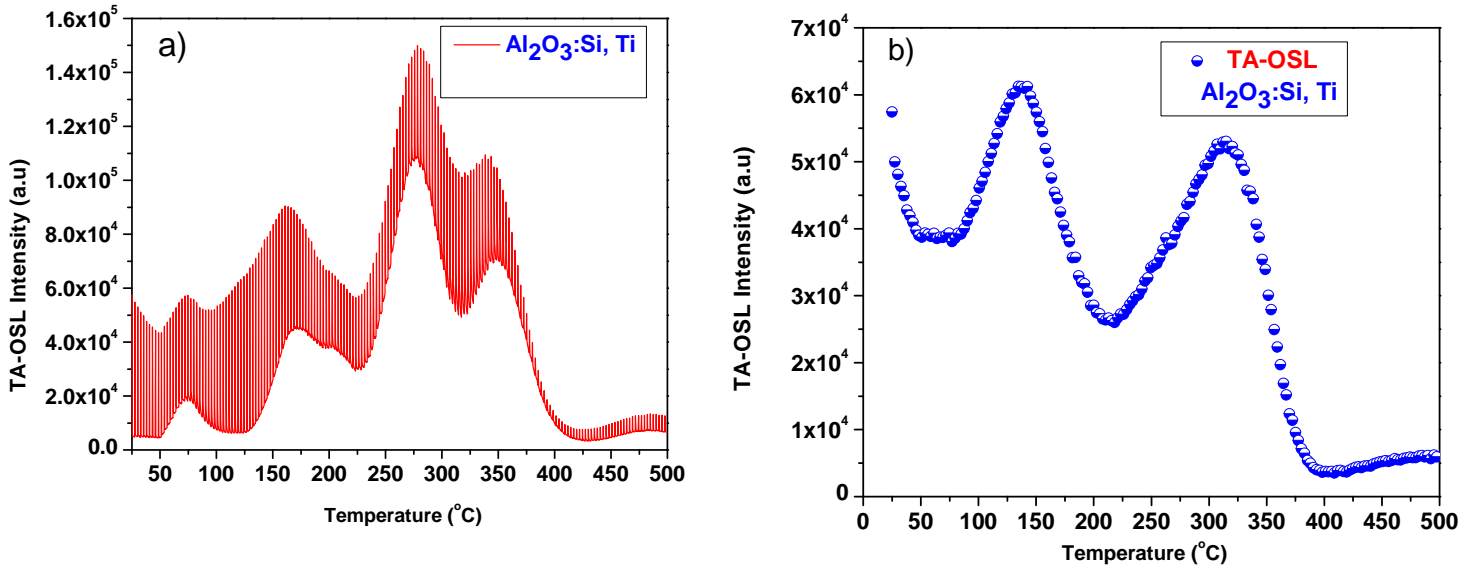
Fig. 6.26 a) TA-OSL measurements of Al_2O_3: Si, Ti sample with short (0.3 s) and low power stimulation pulses (20% LED power) for every 5 °C temperature interval when heating at 4K/s of a sample previously irradiated to 200 mGy. b) TA-OSL signal obtained i.e, the pulse height of Fig 6.26a vs temperature.

Figure 6.26b shows the TA-OSL signal obtained i.e, the pulse height of Fig 6.26a vs temperature. It is clear from the Fig 6.26b that TA-OSL intensity and hence the OSL signal decreases initially upto 70 °C then it increases upto 120 °C. This initial decrease upto 70 °C is expected as there is no trap/TL peak in this region, thus no increase in photoionization cross-section is associated in this region. On the other hand, the increase in TA-OSL signal upto 120 °C can be attributed to the temperature dependence of photoionization cross-section of OSL active traps in this region. Figure 6.27a shows the Arrhenius analysis of the integrated TA-OSL signal from Fig. 6.26b. The straight line fit between 75 to 90 °C yields the activation energy for the thermally assisted OSL (TA-OSL) process E_A= 0.13±0.0021 eV. Further increase in temperature upto 200 °C results in decrease in TA-OSL intensity and can be attributed to the TL peaks in this region which are not

OSL sensitive. However, the TA-OSL intensity increases on further increase in temperature upto 300 °C due to increase in the photoionization cross-section of OSL active traps in this region. The straight line fit between the 200 and 300 °C yields the activation energy for the thermally assisted OSL (TA-OSL) process E_A= 0.20±0.0026 eV. The decrease in TA-OSL intensity from 300 to 400 °C may due to the less availability of trapped charges i.e., depletion of the charges. However, TA-OSL signal again increases slightly upto 500 °C whose activation energy has been found to be E_A= 0.38±0.0023 eV.
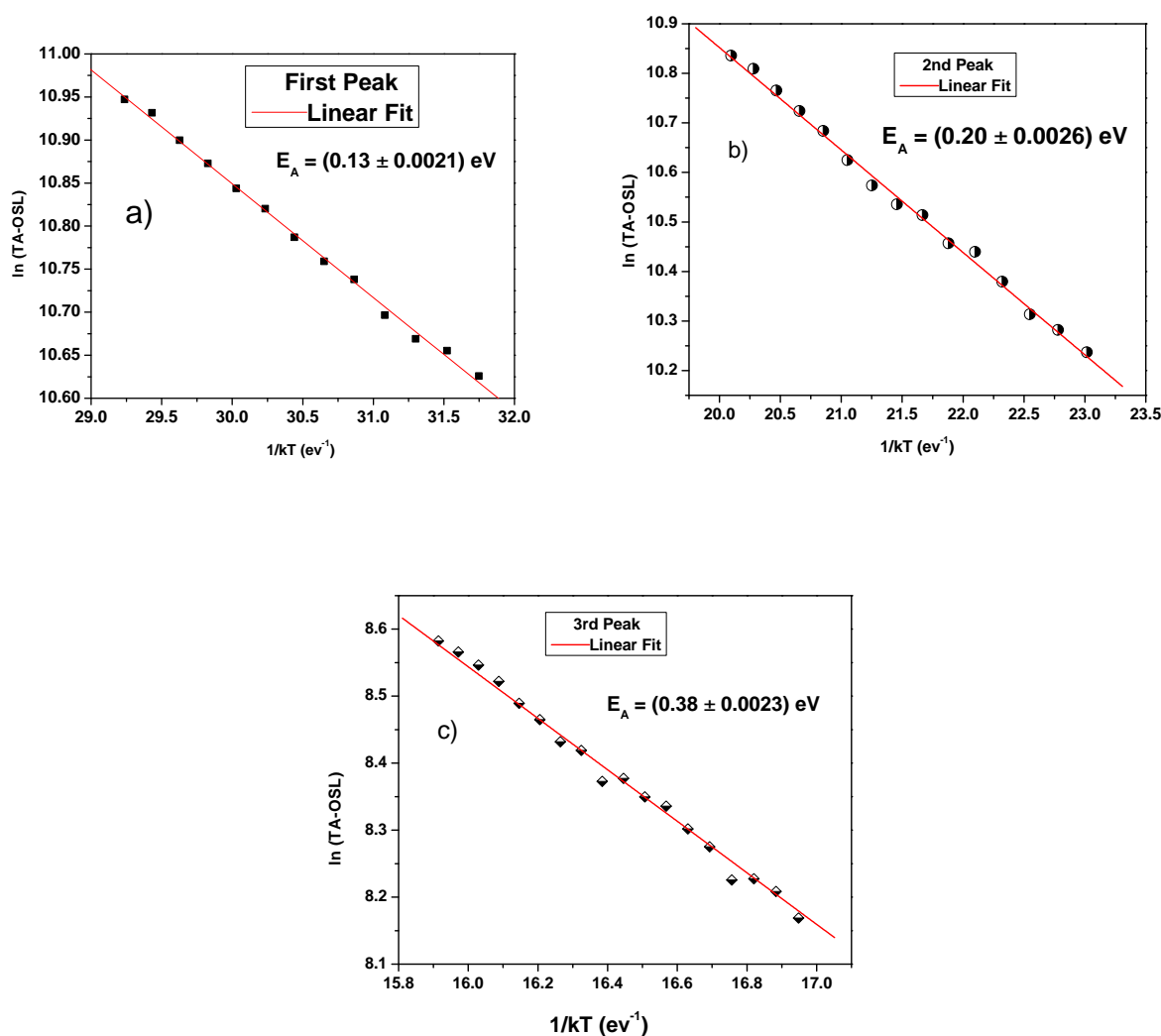
Fig. 6.27 a) Arrhenius analysis of the integrated TA-OSL signal from Fig. 6.26b. The straight line fit between 75 to 90 °C yields the activation energy for the thermally assisted OSL (TA-OSL) process E_A= 0.13±0.0021 eV. b) Activation energy for the thermally assisted OSL (TA-OSL) process in the region 200 - 300 °C (E_A= 0.20±0.0026 eV) c) Activation energy for the thermally assisted OSL (TA-OSL) process in the region 400 - 500 °C (E_A= 0.38±0.0023 eV)

It is clear from fig 6.26b that maximum increase in OSL signal OSL occurs at 120 °C and hence one can conclude that the OSL output will be more at 120 °C as compared to that at 25 °C. It is obvious from the above analysis that as the trap depth/ TL peak temperature increases, thermally assisted energy/ thermal assistance required also increases.

6.5 Investigations on Al_2O_3: Mg, Y

6.5.1 Introduction

Al_2O_3 was one of the materials initially used as a TL phosphor. The TL properties of different forms of pure and doped Al_2O_3 have been investigated for a long time [71]. A systematic survey of the effect of different dopants on the dosimetric properties of Al_2O_3 phosphors has lead to the development of new Al_2O_3: Mg, Y TL material [72]. Osvay et al., 1980 reported its linear dose response upto 10 kGy in TL mode. Later its photo induced TL (PTTL) and photo transferred TL (PTTL) response were reported to determine the possibility of their re-estimation [73]. Recently, it was used to measure photon and fast neutron (>7 MeV) doses in the mixed radiation field of research reactor. [74]. However, it's OSL and TA-OSL studies have not been reported so far. In the present work investigated the temperature dependent of OSL intensity and its effect on the sensitivity of the material.

6.5.2 Materials and methods

In the current work, Al_2O_3: Mg, Y, TL dosimeters grown by the Institute of Isotopes and Surface Chemistry, Hungary were used. TL/OSL and TA-OSL measurements were performed using the same RISØ TL/OSL reader.

6.5.3 Results and Discussions

6.5.3.1 TL Characterization

Fig 6.28 shows the TL glow curve of Al_2O_3: Mg, Y at 4K/s for 200 mGy β-dose. Its glow curve consists of three TL peaks at 112, 210 and 390 °C respectively.
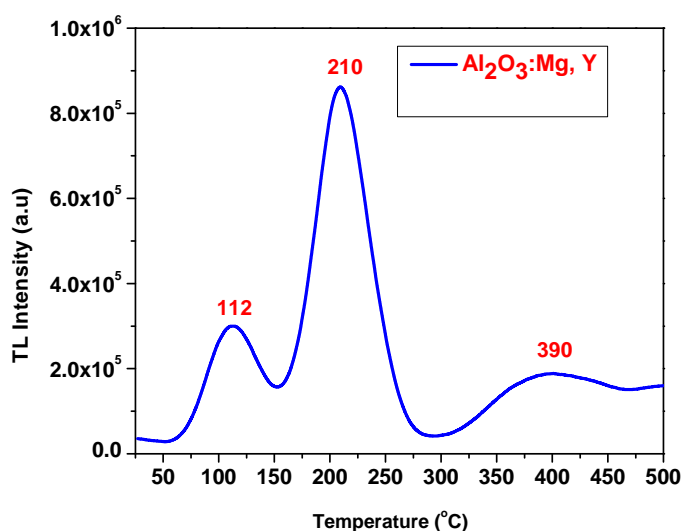
Fig. 6.28. (a) TL glow curve of α-Al_2O_3: Mg, Y at 4 K/s for a dose of 200 mGy showing three TL peaks at 112, 210 and 390 °C respectively.

6.5.3.2 TA-OSL Studies

In order to investigate the effect of the stimulation temperature on OSL intensity of Al_2O_3:Mg, Y TA-OSL studies was carried out. Fig 6.29a is the TL glow curve superimposed with the

recurrence of narrow peaks due to the multiple short OSL pulses (0.3 s after every 5 ^{o}C interval) with simultaneous TL readout. Figure 6.29b shows the TA-OSL signal obtained i.e, the pulse height of Fig 6.29a vs temperature. It is clear from the Fig 6.26b that TA-OSL intensity and hence the OSL signal decreases initially upto 50 °C then it increases upto 100 °C.
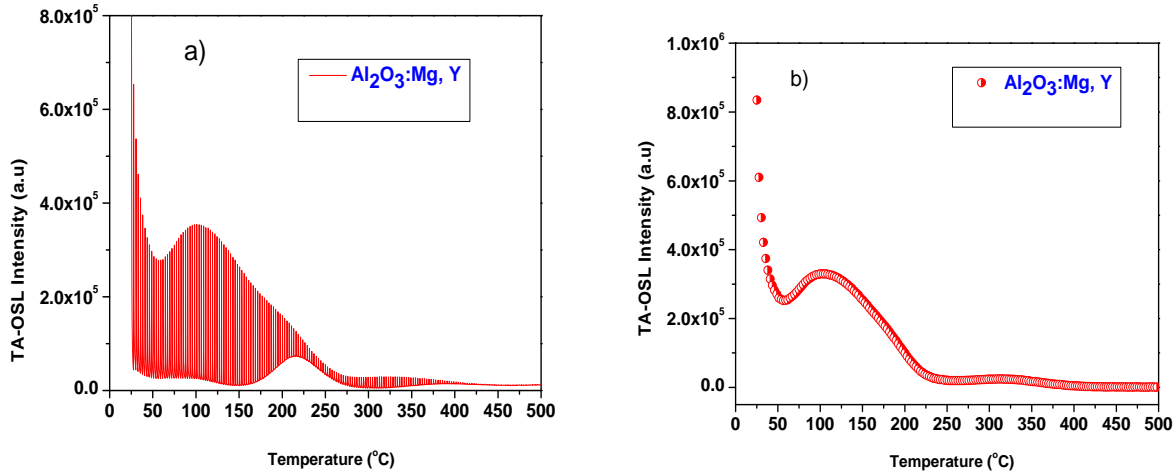

Fig. 6.29 a) TA-OSL measurements of Al₂O₃:Mg, Y sample with short (0.3 s) and low power stimulation pulses (20% LED power) for every 5 •C when heating at 4K/s of a sample previously irradiated to 200 mGy. b) TA-OSL signal obtained i.e, the pulse height of Fig 6.26a vs temperature.

This initial decrease upto 50 °C is expected as there is no trap/TL peak in this region, thus no increase in photoionization cross-section is associated in this region. On the other hand, the increase in TA-OSL signal upto 120 °C can be attributed to the temperature dependence of photoionization cross-section of OSL active traps in this region. Figure 6.30a shows the Arrhenius analysis of the integrated TA-OSL signal from Fig. 6.29b. The straight line fit between 50 to 100 °C yields the activation energy for the thermally assisted OSL (TA-OSL) process $E_A=$ 0.09±0.0021 eV. Further increase in temperature upto 220 °C results in decrease in TA-OSL intensity and can be attributed to the huge thermal quenching of F and F^{+} center in this region

which is a known feature of such luminescence centers. This type of thermal quenching is also reported in other alumina host base phosphors such as Al_2O_3:C. However, the TA-OSL intensity increases slightly on further increase in temperature upto 300 °C due to increase in the photoionization cross-section of OSL active traps in this region. The straight line fit between the 220 and 300 °C yields the activation energy for the thermally assisted OSL (TA-OSL) process E_A= 0.14±0.0040 eV.
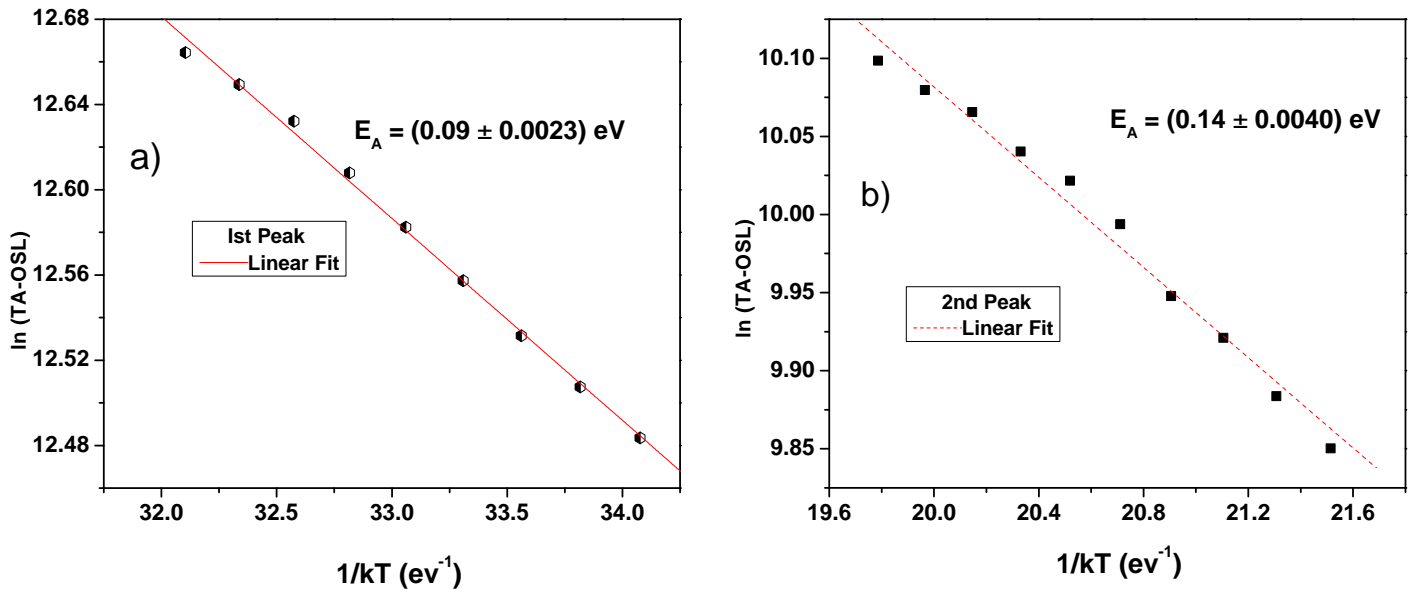
Fig. 6.30 a) Arrhenius analysis of the integrated TA-OSL signal from Fig. 6.26b. The straight line fit between 75 to 100 °C yields the activation energy for the thermally assisted OSL (TA-OSL) process E_A = 0.09±0.0023 eV. b) Activation energy for the thermally assisted OSL (TA-OSL) process in the region 250 - 300 °C (E_A = 0.14±0.0040 eV)

6.6 Investigations on Mg₂SiO₄:Tb

6.6.1 Introduction

As described in chapter1, Mg_2SiO_4:Tb has been studied for its TL/OSL response by various groups. Recently, Yoshimura and Yukihara have reported OSL of Mg_2SiO_4:Tb sintered discs (0.5 mm thick, 5 mm diameter) produced by Kasei Optonix Ltd., Japan [75]. They report that after an OSL readout of 300s, using blue light (470nm, 20mWcm^{-2}), entire TL glow curve is affected. This resulted in reduction of ~ 80% of the first two TL peaks. However, no detailed results were presented by them. The aim of the present investigation is to study OSL and TA-OSL characteristics of Mg_2SiO_4: Tb produced by Kasei Optonix Ltd., Japan.

6.6.2 Materials and methods

Mg_2SiO_4:Tb powder, having grain size ~ 170 μm, was obtained from Kasei Optonix Ltd., Japan. The phosphor was annealed at 600 °C for 1h to erase the entire induced TL signal. TL and OSL and TA-OSL measurements were carried out using the same Riso Reader. The TL glow curves were recorded at a constant heating rate of 4°C/s.

6.6.3 Results and Discussions
6.6.3.1 TL Characterization

Fig. 6.31 shows TL glow curve of Mg_2SiO_4: Tb for a gamma-ray dose of 200 m Gy. It consists of TL peak at 152, 274 and 360 °C.
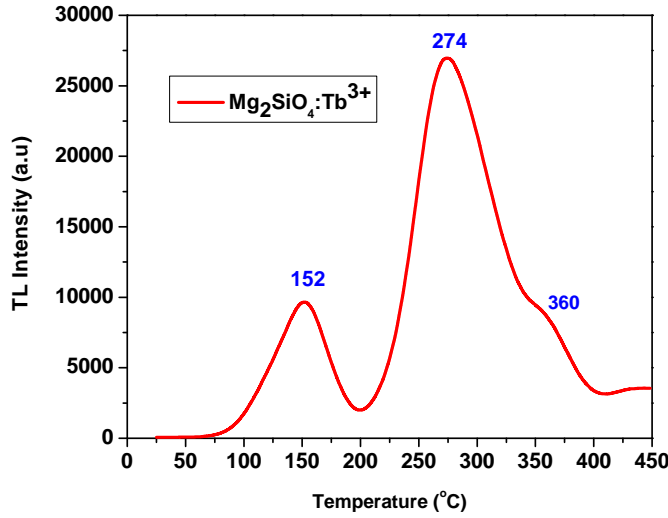
Fig. 6.31. TL glow curve of Mg₂SiO₄:Tb at 4K/s for 200 mGy dose showing TL peaks at 152 and 274 °C respectively.

6.6.3.2   CW-OSL Characterization

Fig. 6.32 shows CW-OSL decay curves of Mg$_2$SiO$_4$:Tb for an absorbed dose of 200 mGy at a constant stimulation power of 48 mWcm^{-2}. The Blue OSL curves were de-convolved by using the general order kinetics (GOK hereafter) expression for OSL theory (Bøtter-Jensen et al., 2003; Kitis and Pagonis, 2008):

$$I_{CWOSL} = (1 + (b-1).\frac{t}{\tau})^{\frac{1}{b-1}}, b \neq 1 \tag{6.16}$$

where $I_{CW\text{-}OSL}$ is the CW-OSL intensity as a function of time, $\tau = 1/\lambda$ (s) is the life time (λ being decay constant), t is the time taken for OSL readout and b is the order of kinetics. For the case of general order kinetics the value of kinetic order b was left to vary freely in the range between 1.00001 and 2. In practise, a sum of three components was applied in all cases except the case of the OSL curves received at RT. Once again, the quality of fit was tested by checking the FOM values obtained, being better than 0.90 %. All three components were of second order of kinetics. The decay constant for each component was calculated using $\lambda = 1/\tau$ (s^{-1}); for the three components of the present study the values yielded for the decay constants, λ_i, were 8.844, 0.789

and 0.039 s^{-1} for the fast, medium and slow component respectively. The error for each value, expressed in percentage, was 0.9%, since this error coincides with the FOM value parameter. Thus, assuming first-order kinetics of OSL decay, and using the equation $\tau_1 = 1/\sigma_1\phi_1$, From the decay constants, the photoionization cross-section was calculated using (Eq. 6.17).

$$f = \sigma\varphi \tag{6.17}$$

where f (s^{-1}) is the excitation rate $(1/\tau)$, σ the photoionization cross-section (cm^2) and φ the stimulation flux (photons/cm^2/s). The photo-ionization cross-sections of the three components were determined as 7.7×10^{-17} cm^2, 6.93×10^{-18} cm^2, and 3.42×10^{-19} cm^2, respectively for 48 mW/cm^2 stimulation intensity using Eqs. 6.16 & 6.17. The stimulation flux φ for 48 mW/cm^2 was 1137.12×10^{14} photons/cm^2/s (1 mW/cm^2 (470 nm) = 23.69×10^{14} photons/cm^2/s).
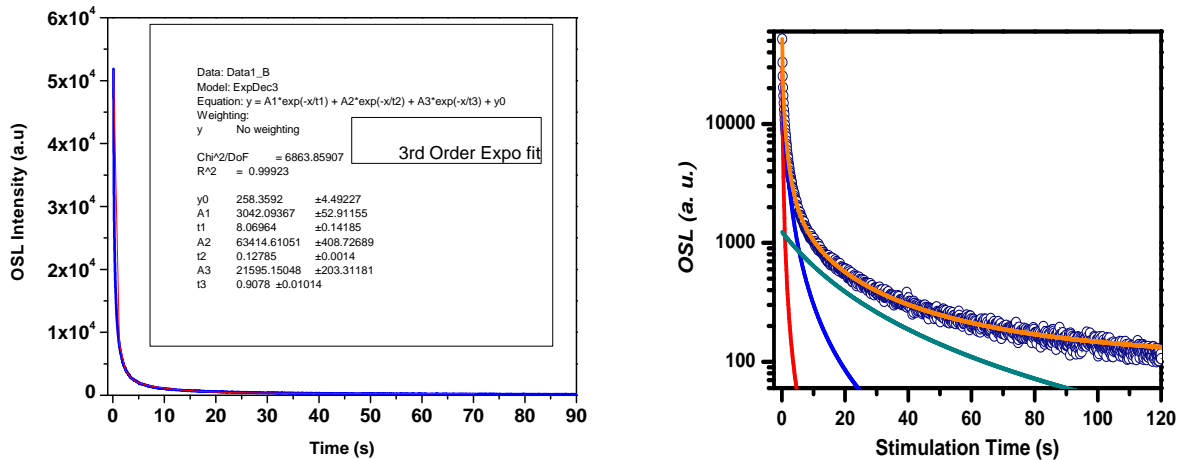
Fig. 6.32.a) CWOSL decay of Mg$_2$SiO$_4$:Tb for 200 mGy beta dose. The 3rd order exponential fit on the decay curve shows the presence of three components. b) De-convolution of the decay curve using CCDA analysis found to be best fitted with three components. The values of three decay constants λ_i, were 8.844, 0.789 and 0.039 s^{-1} for the fast, medium and slow component respectively.

Fig 6.33 shows the integrated TL and OSL of Mg$_2$SiO$_4$:Tb at each respective temperature for 200 mGy beta dose. The sample was heated at various temperatures 120, 230, 310, 360, 400 °C and

subsequently its CW-OSL was recorded. It shows that all the TL peaks are OSL sensitive and OSL doesn't come to complete zero even at 400 °C suggesting the existence of deeper traps which is again evident from the TA-OSL studies in the next section.
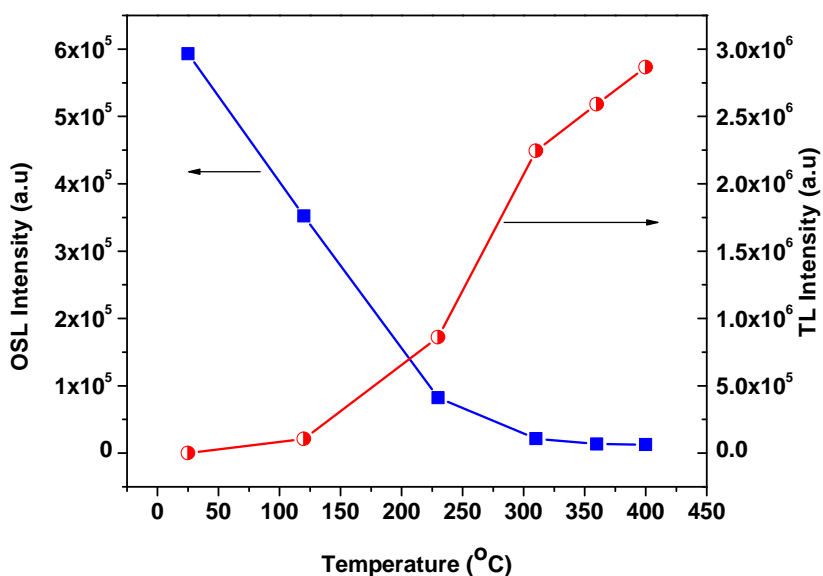
Fig. 6.33. Integrated TL and OSL of Mg$_2$SiO$_4$:Tb at each respective temperature for 200 mGy beta dose.

Mg$_2$SiO$_4$:Tb phosphor (Kasei Optonix Ltd.), when exposed to 150 mGy of [90]Sr β-rays, did not show any fading of the OSL signal six hours after storage in dark as compared to the corresponding sample measured 30 min after storage in dark. Whereas, it is reported by Mittani et al that in Mg$_2$SiO$_4$:Tb sintered samples (developed at the Institute of Nuclear Sciences, Vinca, Belgrade) faded nearly 30% in dark in the first 10h of storage, remaining approximately constant afterwards. It is possible that sintered material, prepared by slightly different method may show somewhat different characteristics than the Mg$_2$SiO$_4$:Tb powder sample.

6.6.3.3 TA-OSL Studies

The TA-OSL studies showed that integrated TA-OSL and thus OSL signal initially decreases with readout temperature upto 150 °C, suggesting that the effect of temperature on the OSL is not dominating in this region. However the signal increases appreciably after 250 °C due to the temperature dependence of photo-ionization cross-section. On the other hand, the OSL signal, if taken at room temperature (after the sample is heated upto 250 °C) , decreases as shown in Fig 6.33. Thus, the OSL signal in this region enhances on the presence of temperature. The thermally assisted energy E_A associated with this increase in signal is found to be $E_A = 0.26 \pm 0.0043$ eV.
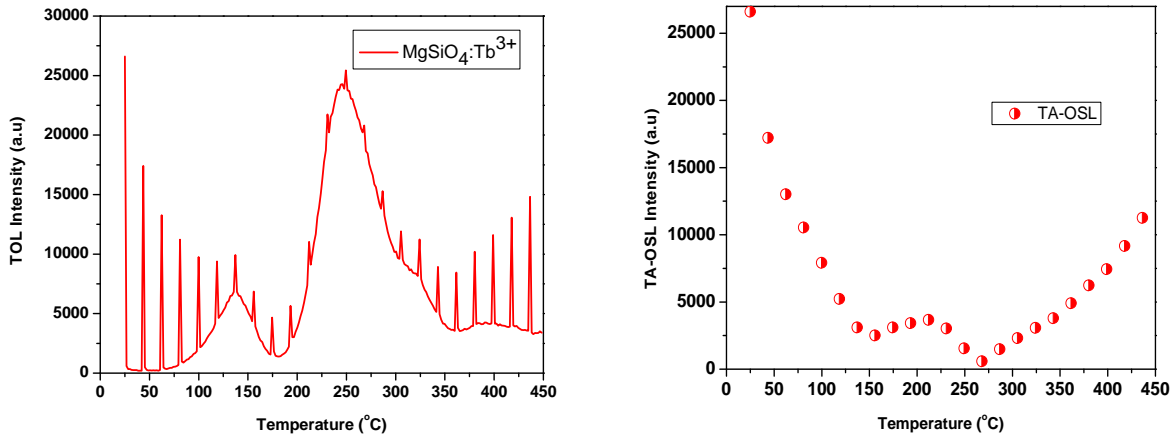
Fig. 6.34 a) TA-OSL measurements of Mg$_2$SiO$_4$:Tb sample with short (0.3 s) and low power stimulation pulses (20% LED power) for every 20 °C when heating at 4K/s of a sample previously irradiated to 200 mGy. b) TA-OSL signal obtained i.e, the pulse height of Fig 6.34a vs temperature.

6.7. Conclusions

This chapter was about the application of TA-OSL technique on various oxide based OSL phosphors. It was found that TA-OSL is not only α-Al$_2$O$_3$:C specific, instead can be applied to other phosphors also for the improvement of the OSL sensitivity. Next chapter will discuss the

novel technique of Pulse Frequency Modulation (PFM) based CW-, LM-, NL-, and TA-OSL techniques using constant Laser light source.

References

1. Dhopte, S.M., Muthal, P.L., Kondawar, V.K, Moharil, S.V., 1991. J. Lumin. 50, 187-195.

2. Atone, M. S., Dhoble, S. J. And S. V. Moharil. 1993. Radiation effects and defects. 127, 225-230.

3. Okamoto, Y., Kawaguchi, S., Kino, S., Miono, S., Kitajima, T., Misaki, A., Saito, T., 1986. Nucl. Instrum. Meth. Phys. Res. A243, 219-224.

4. Azorin, J, Furetta, C., Gutierrez, A., Gonzalez, P., 1991. Appl. Radiat. Isot. 42, 861-863.

5. Bhatt, B.C., Sanaye, S.S., Shinde, S.S., Srivastava, J.K., 1997. Radiat. Prot. Dosim. 69, 105-110.

6. Shinde, S. S., Bhatt, B. C., Srivastava, J. K., Sanaye, S. S., 1996. Radiat. Prot. Dosim. 65, 305−308.

7. Gundu Rao, T. K., Shinde, S. S., Bhatt, B. C., Srivastava, J. K. and Nambi, K. S. V., 1995. J. Phys. Condens. Matter. 7, 6569-6581.

8. Gundu Rao, T. K., Shinde, S. S., Bhatt, B. C., Srivastava, J. K. and Nambi, K. S. V., 1996. Phys. Stat. Sol.(a) 157, 173-179.

9. Annalakshmi, O., Jose, M. T., Madhusoodanan, U., 2012. Phosphor. Radiat. Prot. Dosim. 150, 127–133.

10. Krystek, M., 1980. Phys. Stat. Sol.(a) 57, 171-178.

11. Luthra, J.M., Gupta, N.M., 1974. J. Lumin. 9, 94-103.

12. Fox, P.J., Akber, R.A. Prescott, J.R., 1988. J. Phys. D: Appl. Phys. 21, 189-193.

13. Lochab, S.P., Sahare, P.D., Chauhan, R.S., Salah, N., Ranjan, R. Pandey, A., 2007. J. Phys. D: Appl. Phys. 40, 1343–1350.

14. Salah, N, Habib, S.S., Khan, Z.H., Al-Hamedi, S., Lochab, S.P., 2009. J. Lumin. 129, 192–196.

15. Yamashita, N., Yamamoto, I., Ninagava, K., Wada, T., Yamashita, Y, Nakao, Y., 1985. Jpn. J. Appl Phys. 24, 1174-1180.

16. Yamashita, T., Nada, N., Onishi, H., and Kitamura, S., 1971. Health Phys. 21, 295-300.

17. Kitis, G., Gomez, J. M., and Tuyn, J. W. N., 1998. J. Phys. D: Appl. Phys. 31**,** 2636–2641.

18. Afouxenidis, D., Polymeris, G. S., Tsirliganis, N. C. and Kitis, G., 2012. Radiat. Prot. Dosim. 149, 363–370.

19. Balian, H. G. and Eddy, N. W., 1977. Nucl. Instrum. Methods 145(2), 389–395.

20. Wintle, A. G., Murray, A. S., 1997. Radiat. Meas. 27, 611-624.

21. Koul, D.K, Patil, P.G, Oniya, E.O, Polymeris, G.S., 2014., Radiat. Meas. 62, 60-70.

22. Bulur, E., 1996. Radiat. Meas. 26, 701-709.

23. Polymeris, G.S., Tsirliganis, N.C., Loukou, Z., Kitis, G., 2006. Phys. Status Solidi A 203 (3) 578-590.

24. Kitis, G., Pagonis, V., 2008. Radiat. Meas. 43, 737-741.

25. Kitis, G., Kiyak, N., Polymeris, G.S., Tsirliganis, N.C., 2010 J. Lumin. 130 (2), 298-303.

26. Mishra, D. R., Kulkarni, M. S., Rawat, N. S., Muthe, K. P., Gupta, S. K., Bhatt, B. C. Sharma, D. N., 2008. Radiat. Meas. 43**,** 1177-1186.

27. Mishra, D. R., Kulkarni, M. S., Rawat, N. S., Soni, A., Bhatt, B. C., Sharma, D. N.,2011a. Radiat. Meas. 46, 1462-1468.

28. Chruścińska, A., 2010 Radiat. Meas. 45, 991-999.

29. Spooner, N. A., 1994. Radiat. Meas. 23, 593-600.

30. Kuhns, C.K., Agersnap, Larsen and McKeever, S.W.S., 2000. Radiat. Meas. 32,   413-418.

31. McKeever, S .W.S., Bϕtter-Jensen, Agersnap Larsen, N, and Duller, G.A.T., 1997. Radiat. Meas. 27, 161-170.

32. Soni, A., Mishra, D. R., Bhatt. B. C., Gupta S. K., Rawat. N. S., Kulkarni, M. S., and Sharma, D.N., 2012. Radiat. Meas. 46, 635-642.

33. Mishra, D.R., Soni, Anuj., Rawat, N.S., Kulkarni, M.S., Bhatt, B.C., Sharma, D.N. 2011b. Radiat. Meas., 46, 635-642.

34. Duller, G.A.T., Wintle, A. G., 1991. Nucl. Tracks Radiat. Meas. 18**,** 379-384.

35. Duller, G. A. T., Botter-Jenson, L., 1993. Radiat. Prot. Dosim. 47**,** 683-688.

36. Hutt, G., jack, I., Tchonka, J., 1988. Quat. Sci. Rev. **7**, 381-385.

37. Yukihara, E. G., Whitley, V. H., McKeever, S. W. S., Akselrod, A. E., Akselrod, M. S., 2004. Radiat. Meas. 38**,** 317–330.

38. Yoshimura, E. M. and Yukihara, E. G. 2006. Radiat. Meas. 41, 163-169.

39. Pagonis V., Ankjaergaard. C., Jain. M., Chen. R. 2013. J. Lumin. 136, 270-277.

40. Brady J.M., Aarestad N.O., Schwartz H.M., 1968. Health Phys., 15, 43-47.

41. Wieser A. and El-Faramawy N., 2002. Radiat. Prot. Dosim. 101, 545–548.

42. Wieser, A., and Darroudi, F. (2014a). Radiat. Prot. Dosim. 101, 217–220

43. Wieser, A., Vasilenko, E., Aladova, E., Fattibene, P., Semiochkina, N., Smetanin, M. 2014b. Radiat. Environ. Biophys. 53, 321–333.

44. Williams, B. B., Dong, R., Flood, A. B., Grinbergm O., Kmiecm M., Lesniewskim P. N., Matthews, T. P., Nicolalde, R. J., Raynolds, T., Salikhov, I. K., Swartz, H. M. 2011. Radiat. Meas. 46(9), 772-777.

45. Benjamin, B. W., Flood, A. B., Salikhov, I., Kobayashi, K., Dong, R., Rychert, K., Du G, Schreiber, W., Swartz, H. M. 2014. Radiat. Environ. Biophys. 53, 335–346.

46. Swartz, H. M., Iwasaki, A., Walczak, T., Demidenko, E., Salikhov, I., Khan, N., Lesniewski, P., Thomas, J., Romanyukha, A., Schauer, D., Starewicz, P. 2006. Radiat. Prot. Dosim. 120(1–4),163–170.

47. Pass, B., Godfrey-Smith, D. I., Scallion, P. 2003. In: Proceedings of the 36th Midyear Topical Meeting "Radiation Safety Aspects of Homeland Security and Emergency Response," 2003. Health Physics Society, San Antonio, Texas, January 27–29, McLean, Virginia: Health Physics Society. 210–217.

48. Yukihara E.G., Mittani. J., McKeever. S.W.S., Simon.S.L. 2007. Radi. Meas.42,1256-1260.

49. Huston, A. L., Justus, B. L., Falkenstein, P. L., Miller, R. W., Ning, H., Altemus, R.. 2001. Nucl Instrum. Methods Phys. Res. B 184, 55– 67.

50. Polf, J. C., McKeever, S.W.S, Akselrod, M.S., Holmstrom, S. 2002. Radiat. Prot. Dosim. 100,301–304.

51. Klein, D.M., McKeever, S.W.S., 2008. Radiat. Meas. 43, 883-887.

52. Godfrey-Smith, D.I., Pass, B. 1997. Health Phys. 72(5),744 –749.

53. Godfrey-Smith, D.I. 2008 Radiat. Meas. 43, 854-858.

54. DeWitt, R., Klein, D M., Yukihara, E G., Simon, S L., McKeever, S W. S. 2010. Health Physics 98, 432-439.

55. Sholom, S., DeWitt, R., Simon, S..L., Bouville, A., McKeever, S.W.S., 2011. Radiat. Meas.46 778-782.

56. Bailiff, I. K., Correcher, V., Delgado, A., Goksu, Y., Hubner. S. 2002. Radiat. Proc. Dosim. 101, 519-524.

57. Soni, A., Mishra, D. R., Bhatt. B. C., Gupta S. K., Rawat. N. S., Kulkarni, M. S., and Sharma, D.N., 2013. Radiat. Meas. 49, 67-72.

58. Kulkarni, M.S., Mishra, D.R., Sharma, D.N. 2007. Nucl. Instrum. Method. Phys. Res. B. 262 348-356.

59. Akselrod, M. .S., and McKeever, S.W.S. 1999. Radiat. Prot. Dosim. 81, 167-175.

60. Shimano, T., Iwaski, M., Miyazawa, C., Miki, T., Kai, A and Ikeya M., 1989. Appl. Radiat. Isot. 40, 1035-1038.

61. Secu, C.E., Cherestes, M., Secu, M., Cherestes, C., Paraschiva, V. and Barca, C. 2011. Radiat. Meas. 46, 1109-1112.

62. Anderle, H., Stefaan, I., Wild, E., Bermanec, V., Sővegjarto, F., 1998. Radiat. Meas. 29, 531-551.

63. Geber-Bergstrand, T., Bernhardsson, C., Mattsson, S. L., Rääf, C. 2012. Radiat. Environ. Biophys. 51, 443–449.

64. Mehta, S.K., Sengupta, S., 1976a. Phys. Med. Biol. 21, 955–964.

65. Mehta, S.K., Sengupta, S., 1976b. Health Phys. 31, 176–177.

66. Mehta, S.K., Sengupta, S., 1977. Phys. Med. Biol. 22, 863–872.

67. McKeever, S.W.S., Moscovitch, M., Townsend, P.D. (Eds.), 1995.Nuclear Technology Publishing, Ashford, UK, pp. 117–159.

68. Molnar, G., Benabdesselam, M., Borossay, J., Lapraz, D., Iacconi, P., Kortov, V.S., Surdo, A.I., 2001. Radiat. Meas. 33, 663–667.

69. Mehta, S.K., Sengupta, S., 1978. Phys. Med. Biol. 23, 471–480.

70. Bhatt, B. C., Page, P.S., Rawat, N.S., Dhabekar,B.S., Mishra, D.R., Kulkarni, M.S., 2008 Radiat. Meas. 43, 327-321.

71. Summers, G. P. Radiat. Proc. Dosim. (1984) 8, 69-80.

72. Osway, M and Biro, T. Nucl. Instrum. Methods (1980) 175, 60-61.

73. Osway, M, Komor, R., Golder, F. Radiat. Proc. Dosim. (1990) 33, 135-138.

74. Santos, J.P., Marques, G.J., Fernandes, A.C., Osvay, M. Nucl. Instrum. Methods A (2007) 580, 310-313.

75. E.M.Yoshimura and E.G.Yukihara, Nucl. Instru. Meth. Phys.Res.B 250, 337 (2006).

Chapter 7

LASER based NL-TA-OSL Measurement System

The earlier chapters describes the TA-OSL phenomenon based on LED based optical stimulation. The possibility of modulation of CW-LASER beam for LM/NL/TA-OSL intensity will open a set of new potential to accurately measure the photo-ionization cross-section associated with OSL active traps under monochromatic light. This will results in better estimation of order of kinetics associated with OSL charge transfer phenomenon using fundamental OSL rate equations. Using this system, optimization of stimulation profiles (optical + thermal) for TA-OSL has also being established.

7.1 Introduction

There are various modes of optical stimulation with generic names like, Continues Wave (CW)-OSL, Linearly Modulated (LM)-OSL, Non-Linearly Modulated (NL)-OSL) and Pulsed (P)-OSL described in the first chapter. In the POSL mode, generating desirable pulse width of $< \mu s$ with variable output LASER power is more difficult, as this requires mostly LASER in Q-switching mode, which is expensive and possesses limitation on pulse repetition rates. Moreover, the generation of LM/NL-stimulations profiles needs good control on associated instrumentation and principle of light generation mechanism of these light sources. For LEDs, these stimulation profiles can be generated easily by controlling the LED forward bias current with appropriate close loop optical feedback control [1, 2]. However, the generation of LM-stimulation profile has been reported to show considerably sub-linearity in LED forward bias current vs optical output which was attributed to heating of PN-junction due to high forward current which leads to loss of luminescence efficiency [3]. Therefore, some researchers have used pulse frequency modulation (PFM) of LED forward bias current to overcome from such self heating sub-linearity of LED current vs optical power [3]. In this pulse modulation, the duty cycle of LED forward bias current varies linearly, thus producing linear increases in average optical stimulation power delivered at sample position. However, effect of such averaging stimulation intensity on OSL phenomenon has not been explored completely by theoretically and experimentally. Achieving LM /NL stimulation profiles using LASER has added advantage of large dynamic stimulation power range from few μW to hundreds of watt needed for NL-OSL [4] to get better resolution in closely lying OSL components. Beside this, LASER offers great advantage of monochromatic light thus helps in accurately determining the values of photoionization cross-section (PIC) and order of kinetics associated with charge transfer process in OSL phenomenon. However,

generation of such NL/LM -stimulation profiles using LASER source required continuous varying LASER power with respect to time in accordance with NL or LM-stimulation profiles. This is difficult task as it requires appropriate reproducibility of output power stabilizations associated with LASER source design. On contrast in POSL measurement, pulsed LASER has been used due to its high peak power, short duration and narrow bandwidth in energy domain and suitable gating of PMT lead to highest signal to noise ratio among all optical stimulation techniques. To achieve LM /NL intensity from CW-LASER, amplitude modulation techniques can be employed using opto-electric effects based devices [5, 6] and Pockel's effect based modulators. The possibility of modulation of CW-LASER beam for LM/NL intensity will open a set of new potential to accurately measure the PIC associated with OSL active traps under monochromatic light. This will results in better estimation of order of kinetics associated with OSL charge transfer phenomenon using fundamental OSL rate equations. The current chapter describes the pulsed frequency modulation using fast electromagnetic solenoid shutter with associated optical setup designed get desirable CW- LASER beam modulation. This modulated LASER beam has been guided through optical fiber at the sample position and photodiode is used to measure the optical stimulation power at sample position. The LM-OSL, NL-OSL and Pulsed-OSL stimulation profiles have been generated and verified by photo diode in this developed LASER setup. These various profiles were fed to the planchet assembly of TL reader system via optical fiber to study LASER based TA-OSL phenomenon. The OSL measurements of α-Al$_2$O$_3$: C phosphor has been carried out using these frequency modulated optical stimulation profiles.

7.2 Theory of PFM -OSL

In order to generalize PFM theory and mathematical simplification in our further discussion we assume here one-trap/one-recombination center model. For mathematically formulating this frequency modulation method; let's assume the pulse duty cycle variation approach. In this method, the voltage profiles V(t) that generates the desirable frequency modulation, can be expressed as

$$V(t) = \kappa \, t^{\,l} \tag{7.1}$$

Where, κ is constant having unit as V/s^{-l} and can be selected appropriately to generate different non-linear voltage ramps in time domain and l is time base power (TBP). For TBP $(\,l\,) = 1$ gives rise to linear voltage ramp and $l>1$ gives NL-stimulation voltage profiles [1]. The standered voltage to frequency convertor or voltage controlled oscillator (VCO) may be used to achieve pulsed duty cycle modulation keeping pulse active time ' τ_p' as shown in Fig. 7.1, curve A.
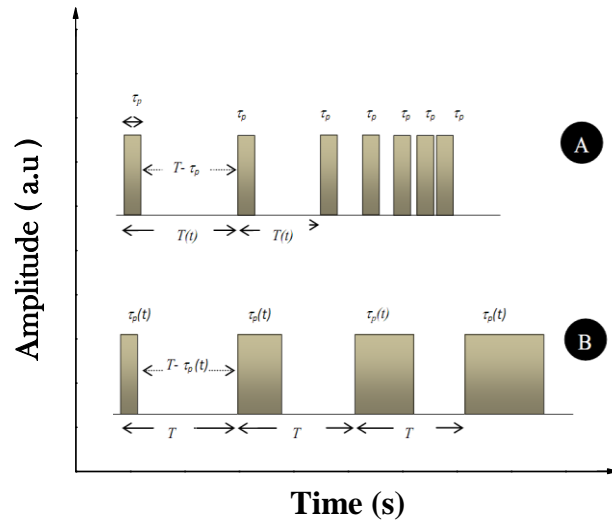
Fig. 7.1 Diagram presenting the duty cycle modulation (A) with constant stimulation active time τ_p and variable frequency $f_m(t)$. (B) frequency modulation with variable stimulation active time $\tau_p(t)$ and constant f_m

In this case, the frequency output of VCO changes, while active pulse width remains constant as τ_p i.e. *Fixed Pulse-width Frequency modulation* (FPFM) and the duty cycle $D(t)$ in this case can be expressed as

$$D(t) = \frac{\tau_p}{T(t)} = \tau_p \, f(t) \qquad (7.2a)$$

Where, $T(t)$ is period of stimulation pulses and it can vary with time for constant pulse duration 'τ_p' as shown in Fig. 7.1(curve A). On the other hand, the duty cycle $D(t)$ can also be varied by keeping frequency $f_m (=1/T)$ constant and varying pulse duration '$\tau_{p(t)}$' i.e. *Variable Pulse-width Frequency Modulations* (VPFM) shown in Fig.7.1, (curve B), and can be expressed as

$$D(t) = \frac{\tau_p(t)}{T} = \tau_p(t) \, f \qquad (7.2b)$$

Where, the time period of frequency modulation T is kept constant and the applied VCO voltage, varies the pulse duration '$\tau_p(t)$'.

For the present discussion, we consider the first case of FPFM expressed in by Eq.(7.2a) as shown in curve A of Fig.7.1. This method will facilitate the selection of different active pulse-width τ_p independent of modulation frequency (f_m) with constrain of $\tau_p < 1/f_{max}$ (f_{max} : maximum modulation frequency). Now for given range of input voltages, VCO generates the modulation frequency 'f_m' that can express by representing Eq.(7.1) as

$$f_m(t) = \varepsilon \, V(t) = \varepsilon \, \kappa \, t^{\,l} \qquad (7.3)$$

Where, ε is the constant expressed in units of (Hz/Volt) and its value depends on the type of the VCO, RC time constant and dynamic frequency range of VCO. The value of ε can be determined as a slope of the line for applied input voltage V(t) v/s generated frequency (f_m). To give better stability against the noise present in applied voltage, the value of ε should be low enough. So that

the (Root Mean Square) RMS ambient noise voltage (~ range of few hundreds of μV) levels of the circuit interferes less on the output modulation frequency of VCO. Furthermore, the variation in duty cycle $D(t)$ for a applied voltage to VCO can be expressed by incorporating Eq.(7.2a) in Eq.(7.3) as

$$D(t) = \tau_p f_m(t) = \tau_p \varepsilon V(t) \tag{7.4}$$

In CW-LASER, the light intensity (ψ_o) measured at input of optical modulator setup remains constant during pulse active time width τ_p, However, the stimulation fluence $(\phi(\lambda))$ at sample position can be varied by varying the modulation frequency. This can be expressed as:

$$\phi(\lambda) = \eta \, \Psi_o \, D(t) \tag{7.5}$$

Where, η the dimensionless parameter takes value < 1and is a measures of the efficiency by which CW intensity (ψ_o) reaches to sample position as modulated stimulation intensity $\phi(\lambda)$ for given values of τ_p and $f(t)$.

Incorporating Eq.(7.3) and Eq.(7.4) in Eq.(7.5) , we get:

$$\phi(\lambda) = \eta \, \Psi_o \, \tau_p \, f(t) = \eta \, \Psi_o \tau_p \, \varepsilon V(t) = \eta \, \Psi_o \tau_p \, \varepsilon \, \kappa \, t^l \tag{7.6}$$

The value of γ' given by Eq. (1.36) in chapter 1 can be derived by comparing Eq.(7.6) with Eq.(1.36) as

$$\phi(\lambda) = \gamma' \, t^l = \eta \, \Psi_o \tau_p \, \varepsilon \, \kappa \, t^l \tag{7.7}$$

This gives the relation for dynamic rate of stimulation γ' as

$$\gamma' = \eta \, \Psi_o \, \tau_p \, \varepsilon \, \kappa \tag{7.8}$$

The LM-stimulation intensity rate γ (described in chapter 1) can be derived using Eq.(7.7) as

$$\gamma = \frac{d\phi(\lambda)}{dt} = l\gamma' \, t^{l-1} = \eta \, \Psi_o \, \tau_p \, \varepsilon \, \kappa \, l \, t^{l-1} \tag{7.9}$$

The γ can also be expressed by putting *l=1* in Eq.(7.9) as

$$\gamma = \frac{d\phi(\lambda)}{dt} = \eta\ \Psi_o\ \tau_p\ \varepsilon\ \kappa \tag{7.10}$$

Therefore, the value of rate of change of stimulation intensity γ in case of LM-stimulation is independent of time and increase/decreases with PFMS parameters τ_p, η, ε, ψ_o and TBP (*l*) as shown in Eq.(7.9). This gives freedom of selecting different values of γ' by setting different values of pulse width τ_p while keeping all other parameters of Eq.(7.8) constant. However, for given hardware, the value of ε depends on VCO characteristics and RC time constant used in VCO. On the other hand, the value of η depends on overall optical focusing geometry of the PFMS setup, more specifically on optical design properties of fast optical modulating shutter.

7.2.1 Analysis for CW-OSL

The conventional method of generation of CW-stimulation is to keeping light source intensity constant with respect to time at sample position and recording decay of OSL signal. However, in frequency modulation method the CW-OSL can be imagined as constant average stimulation power at sample position which remains constant with respect to time. The can be achieved by applying the constant voltage to VCO input in Eq.(7.1) as

$$V(t) = V_o \tag{7.11a}$$

Therefore, the VCO output frequency remains constant as

$$f_m(t) = \varepsilon\ V(t) = \varepsilon\ V_o$$

As the excitation rate f_o can be expressed as

$$f = f_o = \sigma(\lambda)\ \phi_o(\lambda) \tag{7.11b}$$

Now incorporating Eq.(7.6) and (7.11a) in Eq.(7.11b),

$$f = f_o = \sigma(\lambda) \; \eta \; \Psi_o \tau_p \; \varepsilon \; V_o \tag{7.11c}$$

Let's considering the one trap / one recombination center model and first-order kinetics, the CW-OSL intensity I_{CW-OSL} given in chapter 1 as:

$$I_{CW-OSL} = n_o f_o \, e^{-f_o t} \tag{7.12a}$$

Incorporating Eq.(7.11c) in it as

$$I_{CW-OSL} = n_o [\sigma(\lambda) \; \eta \; \Psi_o \tau_p \; \varepsilon \; V_o] \, e^{-[\sigma(\lambda) \; \eta \Psi_o \; \tau_p \; \varepsilon \; V_o] \; t} \tag{7.12b}$$

Therefore, the CW-OSL intensity in this case is expressible in term of PFMS parameters of stimulation profile. In order to get well defined CW-OSL intensity, the luminescence lifetime (τ_R) of recombination charges should obey the following conditions $\tau_R > \tau_p$ and $\tau_R > 1/f_m$. In case of failure to follow these conditions, lead to fragmented CW-OSL decay intensity that would not depict well defined decay nature of CW-OSL phenomenon. The inset of Fig. 7.2 curve A shows the series of CW-OSL curves corresponding to every stimulation pulse width τ_p. The more detailed look of such CW-OSL signal shown in the inset of Fig.7.2 in μs range (Curve B).

The basic CW-OSL consists of two parts, primarily the CW-OSL phenomenon as given in Eq.(7.12a) and followed by exponential decay with recombination life time of R_{Decay} as discussed effectively by Yukihara [4]. The summing function over a time of stimulation or number of such stimulation pulses $f(I_{R_{CW}} \, e^{-\frac{\tau_p}{R_{Decay}}})$ can be expressed in terms of CW-OSL intensity as

$$I_{CW-OSL} = f(I_{R_{CW}} \, e^{-\frac{\tau_p}{R_{Decay}}}) = n_o f_o \, e^{-f_o t} = n_o [\sigma(\lambda) \; \eta \; \Psi_o \tau_p \; \varepsilon \; V_o] \, e^{-[\sigma(\lambda) \; \eta \Psi_o \; \tau_p \; \varepsilon \; V_o] \; t}$$
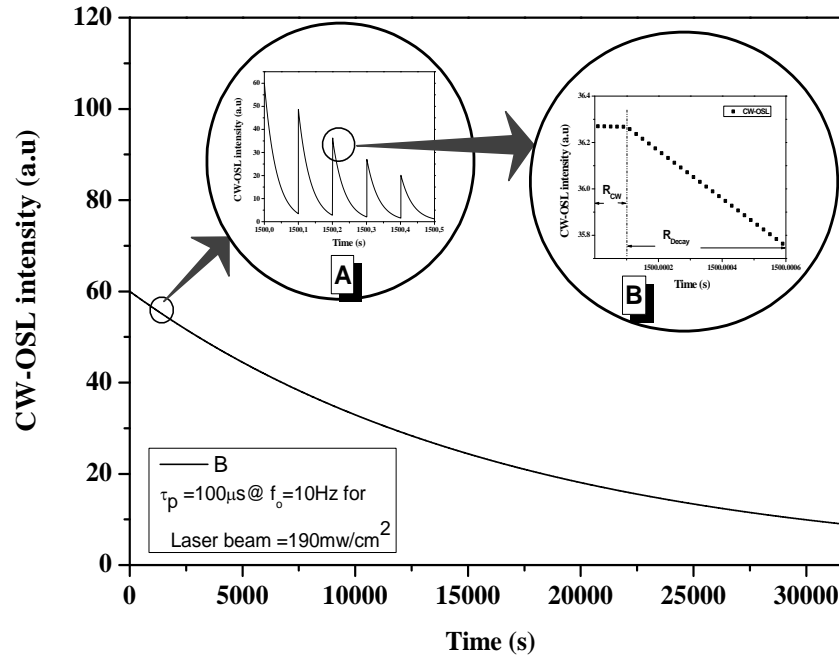
Fig.7.2.   Numerically simulated CW-OSL intensity for active stimulation pulse width τ_p =100 μs at 10Hz for intensity of 190 mW/ cm². Inset -A shows the expanded tine scale of section in ms resolution. Inset B shows the expanded scale of inset A in μs range with Rcw(as shown in inset curve B) time of stimulation pulse periods τ_p

In general order of kinetics, we assume probability of re-trapping of optically released charges and consider this by defining a re-trapping parameter *b*. For *b*=2, the order of kinetics is 2, i.e. the case of equal probability of re-trapping of optically released charge carriers, and *b=1* would lead to the case of first-order kinetics. Therefore, a more general approach would be to consider general- order kinetics and solve CW-OSL equation with incorporation of Eq.(7.11b) as

$$^{b}I_{CW-OSL} = -\frac{dn}{dt} = f_o \frac{n^b}{n_o^{b-1}} = \frac{\sigma(\lambda) \ \eta \ \Psi_o \ \tau_p \ \varepsilon \ V_o}{n_o^{b-1}} \tag{7.13a}$$

Where, ${}^{b}I_{CW\text{-}OSL}$ is the CW-OSL intensity with order of kinetics 'b'. Further solving Eq.(7.13a) for n, we get final CW-OSL intensity under general order of kinetics b as

$$ {}^{b}I_{CW-OSL} = n_o \, \sigma(\lambda) \, \eta \, \Psi_o \, \tau_p \, \varepsilon \, V_o \left\{ 1 + (b-1) \left[\sigma(\lambda) \, \eta \, \Psi_o \, \tau_p \, \varepsilon \, V_o \, \right] t \right\}^{b/1-b} \tag{7.13b} $$

The Eq.(7.13b) gives the CW-OSL intensity for general order of kinetics in terms of PFMS parameters $\psi_o, \kappa, \varepsilon$, and η.

7.2.2 Analysis for NL-OSL

Mishra et al. has reported detailed theoretical description of NL-OSL phenomenon [1, 2] using the one trap / one recombination center model. Considering first-order of kinetics with NL-stimulation intensity given in Eq.(7.7). The NL-OSL intensity can be expressed by incorporating the value of f_o and $\varphi\ (\lambda)$ using Eq.(7.7) and Eq.(7.11b) in general equation of OSL given in chapter 1 and solving as

$$ {}_{l}I_{NL-OSL} = -\frac{dn}{dt} = nf_o = n \, \sigma(\lambda) \, \eta \, \Psi_o \, \tau_p \, \varepsilon \, \kappa \, t^l \tag{7.14a} $$

Where, ${}_{l}I_{NL\text{-}OSL}$ is NL-OSL intensity under PFMS under 1st order of kinetic.

After solving Eq.(7.14a) for 'n' we get

$$ {}_{l}I_{NL-OSL} = n_o \, \sigma(\lambda) \, \eta \, \Psi_o \, \tau_p \, \varepsilon \, \kappa \, t^l \, e^{-\left(\frac{\eta \, \Psi_o \, \tau_p \, \varepsilon \, \kappa}{l+1} \right) t^{l+1}} \tag{7.14b} $$

The condition of maximum can be derived by considering the following condition

$$ \left(\frac{d({}_{l}I_{NL-OSL})}{dt} \right)_{t=t_{max}} = 0 \tag{7.15a} $$

$$_l t_{\max-NL-OSL} = \left[\frac{1}{\sigma \eta \ \Psi_o \ \tau_p \ \varepsilon \ \kappa} \right]^{\frac{1}{l+1}} \tag{7.15b}$$

Where, $_l t_{\max-NL-OSL}$ is the time required to reach peak intensity in NL-OSL curve for TBP value

of 'l 'under first-order kinetics in terms of PFMS. The value of $_l t_{\max-NL-OSL}$ decreases with

increase in PFMS parameters. Considering the general-order kinetics as b and solving NL-OSL

under PFMS, we get the NL-OSL intensity for given values of l and b as

$$_b^l I_{NL-OSL} = -\frac{dn}{dt} = f_o \ \frac{n^b}{n_o^{b-1}} = \frac{\sigma(\lambda) \ \eta \ \Psi_o \ \tau_p \ \varepsilon \ \kappa t^{\ l}}{n_o^{b-1}} \tag{7.16a}$$

$$_l^b I_{NL-OSL} = n_o \ \sigma(\lambda) \ \eta \ \Psi_o \ \tau_p \ \varepsilon \ \kappa t^{\ l} \left[1 + (b-1) \left(\frac{\eta \ \Psi_o \ \tau_p \ \varepsilon \ \kappa}{l+1} \right) t^{\ l+1} \right]^{\frac{b}{1-b}} \tag{7.16b}$$

Eq.(7.16.b) represents the NL-OSL intensity under PFMS for the general-order kinetics (i.e. $b >$

0 and $b \neq 1$). The time required to reach the maximum $_b^l t_{NL-OSL-\max}$ can be obtained by taking the

time derivative of Eq.(7.16.b) and equating it to zero, we get

$$_l^b t_{NL-OSL-\max} = \left[\frac{l(l+1)}{\sigma \ \eta \ \Psi_o \ \tau_p \ \varepsilon \ \kappa (b+1)} \right]^{\frac{1}{l+1}} \tag{7.17}$$

Increase in the order of kinetics will decrease the value of $_l^b t_{NL-OSL-\max}$ i.e. the OSL peak will

appear in a shorter time for both LM- and NL–OSL processes. (see Figs.2a & 2b; Mishra et al.)

[1]. On the other hand, for a given value of the order of kinetics $_b^1 I_{NL-OSL-\max}$ is found to increase

with increase in 'l'. This is expected in order to conserve the total area under all NL-OSL curves

for same value of n_o (dose). Apart from this, an increase in the order of kinetics results in a

stretching of the LM-OSL curve in the time domain into a long tail [1]. However, $^{b}_{l}t_{NL-OSL-max}$

shows strong dependence on PFMS parameters, as with increase in the value of these parameters

(ψ_{o}, κ, ε, and η) the $^{b}_{l}t_{NL-OSL-max}$ decreases.

7.3. Material and Methods

Fig.7.3. shows the block diagram of PFMS NL-OSL reader system. The Phillips P89C51RD2

microcontroller based embedded system controls the whole hardware / software process. For this

setup, generation of various different voltage profiles, 12 bit serial DAC (MAX539) has been

used. The IC VFC32 as VCO generates the modulating frequencies for time applied DAC

voltage input as shown in Fig. 7.3. The output of VCO is in term of modulated frequency $f_{m}(t)$

which depending upon input voltage (Eq.7.1) as discussed in previous section with Fig. 7.1.

Curve (A).
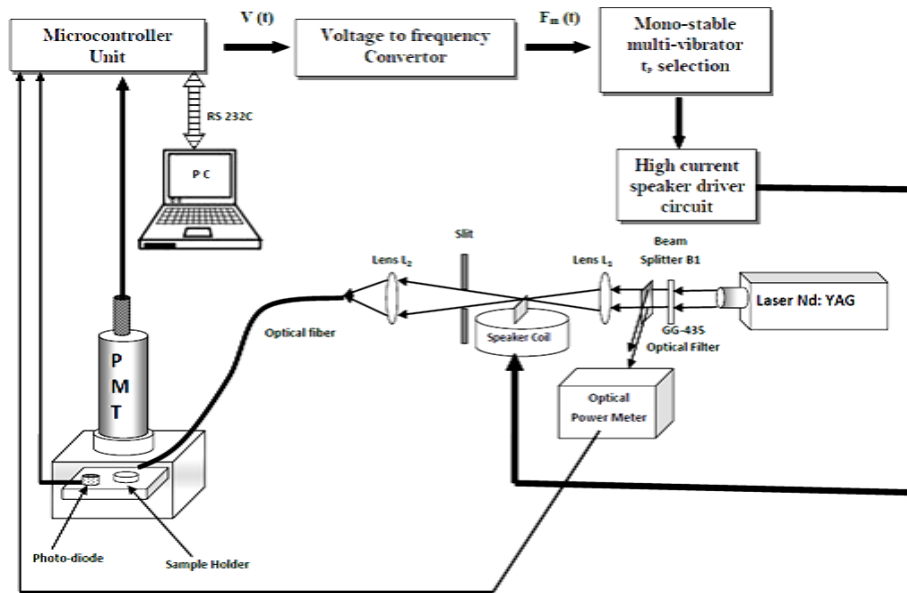
Fig.7.3 Intensity Modulated LASER based OSL Reader System

The IC 74221 based rising input pulse triggered mono-stable multi-vibrator has been used at output of VCO to select different active pulse width τ_p independent of modulated frequency. In order to make fast electromechanical shutter, audio speaker coil has been used.
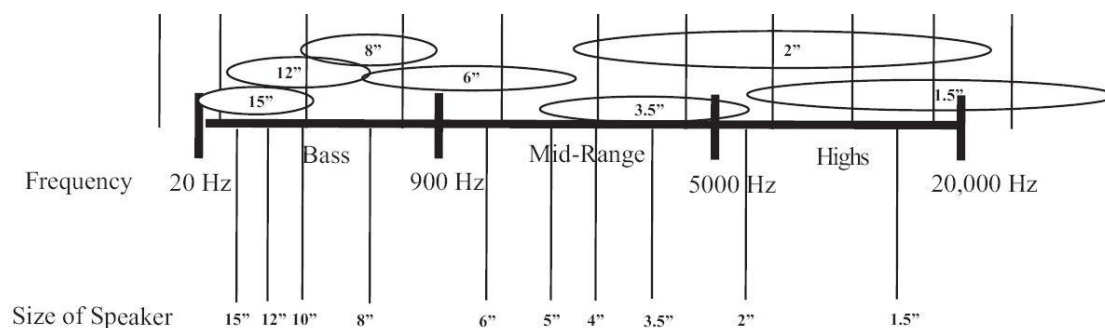
Fig.7.4. Relation of frequency response of speaker with its size.

The selection of speaker has been done on the basis of its frequency response (as shown Fig.7.4) which is inversely proportional to its diaphragm size. In the present experiment, we have selected the speakers in category of subwoofer (pioneer speakers TS-W8102SPL) to have good response in lower frequency range < 2kHz. The typical diagram of speaker is shown in Fig.7.5.
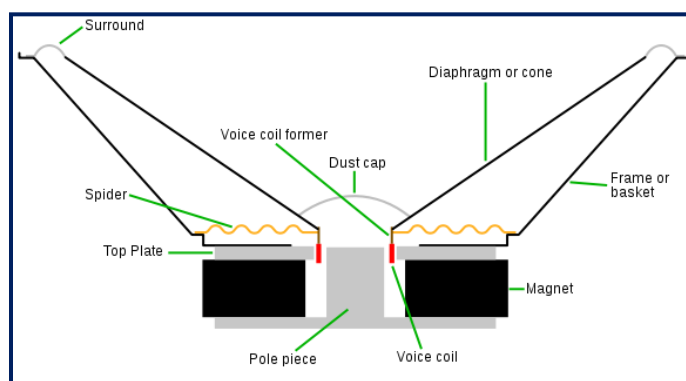
Fig.7.5. Typical construction of speaker system.

However, in the present experiment the diaphragm of speaker has been removed completely to avoid air resistance load from speaker coil. The diaphragm removed speaker coil with frame or basket as shown in Figs.7.6a and 7.6b and the copper thin plate of 12mm x 6mm area, 0.3 mm thick has been fixed to speaker coil.

(a)   (b)
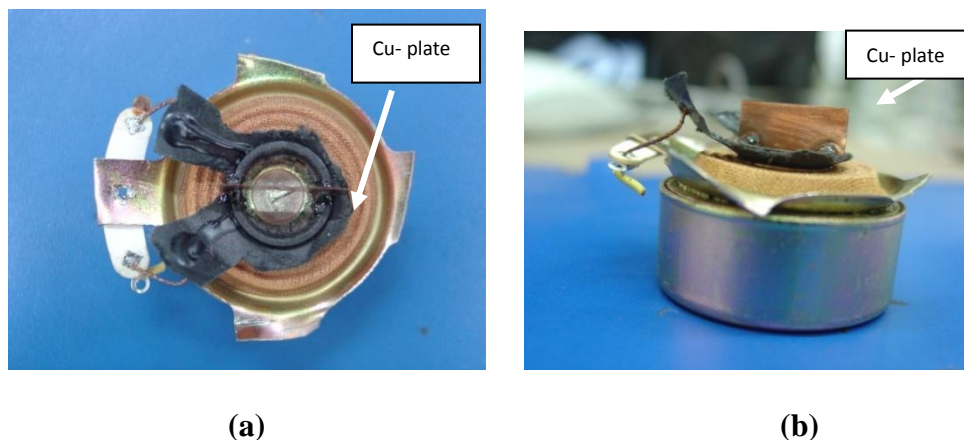
Fig.7.6. Diaphragm cut speaker coil a with attached copper plate (a) vertical view (b) side view.

The movement of this copper plate along with speaker coil acts as the fast optical shutter used to modulate CW-OSL beam as shown in Fig.7.3. In order to drive the high current through speaker solenoid coil, the NPN transistor (BD679) based circuit has been designed which handles peak current of ~10A for driving the solenoid coil. This electromechanical speaker solenoid coil is used to modulate CW-532 nm LASER beam of compact DPSS (LASER Quantum, UK, Ventus 532nm) LASER. The output of LASER beam size is 1.4 mm (dia) with power stability of < 2% RMS. It offers CW mode with a variable power up to 0.5W and is driven by single-phase mains supply and cooled by conduction. The GG-345 optical filter is used across the LASER beam which cuts off < 400 nm harmonics of primary beam. The convex lens L_1 has been used to focus the LASER beam at its focal point at distance of 4 cm (<1mm dia.). It cuts off the LASER beam even with 1 mm vertical movement of Cu-plate due to narrow beam alignment arrangement. This diverged LASER beam after frequency modulation is focused by lens L_2 in single core (1mm dia.) optical fiber. This optical fiber guides the optical PFMS light intensity at the sample position. The beam splitter B1(Fig.7.3) provides the partially refracted optical power (measured using optical power meter) used for monitoring the stability of CW-LASER beam intensity entering in PFM setup. There is also provision of measuring optical stimulation intensity with

OSD-5 photo diode fixed at sample position. This photodiode can measure optical power either in pulsed or average mode using fast Op-Amp AD848 and VFC32 as frequency to voltage convertor. A photon counting PMT module (Sens-tech P30CWAD5) has been used to detect the emitted OSL signal. To study the PFMS OSL phenomenon, commercial α-Al_2O_3:C (5 mm diameter and 0.9 mm thick, Urals Poly-technique Institute, Russia) has been used. All the OSL dosimeters were optically bleached with 50mW/cm^2 light of 470 nm light. These bleached OSL dosimeters were irradiated by a calibrated 5 mCi, ^{90}Sr/^{90}Y (1.2Mev) β-source.

7.4. Results and Discussion

7.4.1 Measurement of PFMS Parameters

For the above discussed OSL setup, it is necessary to determine experimentally PFMS parameters η, ε and κ. The experimental values of these PFMS parameters can be helpful to quantify operational aspect of the setup. The Fig.7.7 shows the measured value of ε as 199.47 Hz/V for present appropriate RC time constant values selected for the present setup.
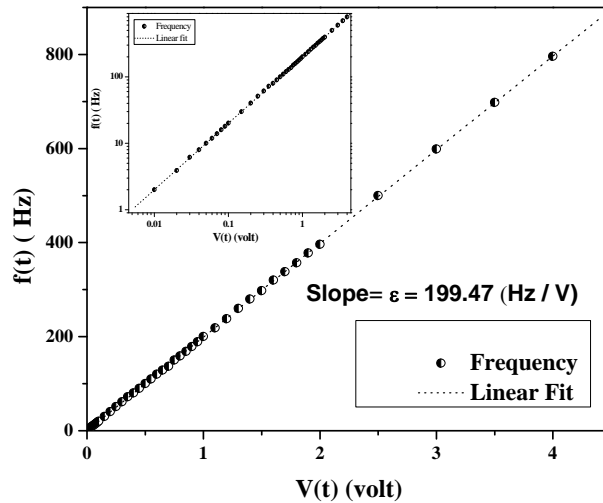
Fig.7.7 The plot of frequency modulation vs applied voltage to VCO used to determine the value of ε =199.47 Hz/V. Inset shows the same in log scale.

The curve is found to be linear within ± 0.1% for maximum modulation frequency range selected (< 1 kHz). Since in the present experiment, subwoofer of low frequency response has been used, therefore there is limitation on the modulation of frequency response (<1 kHz). For a given fixed CW-OSL intensity ψ_o= 100 mW/cm^2 entering in frequency modulation setup at input (right) side of lens L$_1$ for τ_p = 350 μs, the value of η has been determined from the slope of line plotted as optical power measured at sample position vs modulation frequency (f_m). The slope of line (as shown in Fig. 7.8 is $(\psi_o \tau_p \eta)$ = 0.0705 (mW/cm^2/Hz) as expressed in Eq.7.6.
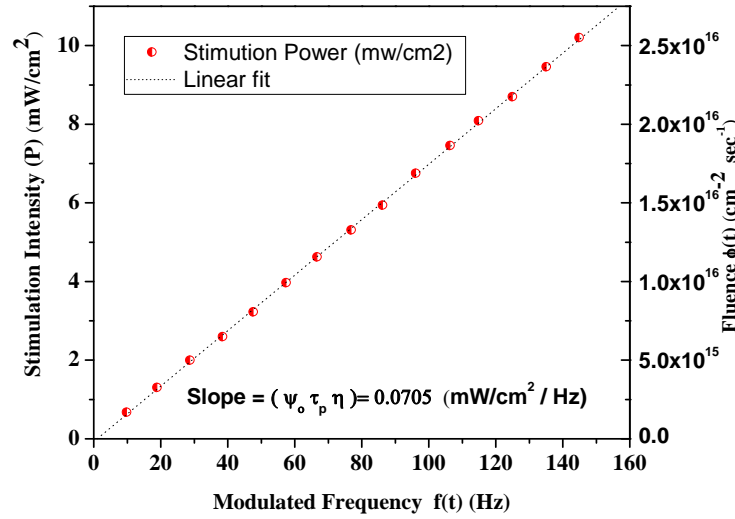
Fig.7.8 Variation of stimulation power at sample position with modulating frequency giving slope as value of η.

The value of η thus determined is found be 0.0227(2.27%). This indicates the considerable loses in efficiency of optical power reaching to sample position due to optical fiber and focusing elements used in PFMS setup system. However, there is considerable scope of improving the efficiency η by further improving optical focusing module.

7.4.2. PFMS-LM-OSL Studies

Fig. 7.9 shows the variation of background signal (i.e. noise due to scattering) by PFMS light as defined by Mishra et.,al. [2] measured for LM –stimulation profile (γ= 0.04 mW/cm^2/s for 20 mW/cm^2 maximum intensity). As expected, the stimulation scattering background found to vary linearly with stimulation light as it depends on reflectivity of sample holder / sample, the set of optical filter combinations used across the PMT and stimulation wavelength [2].
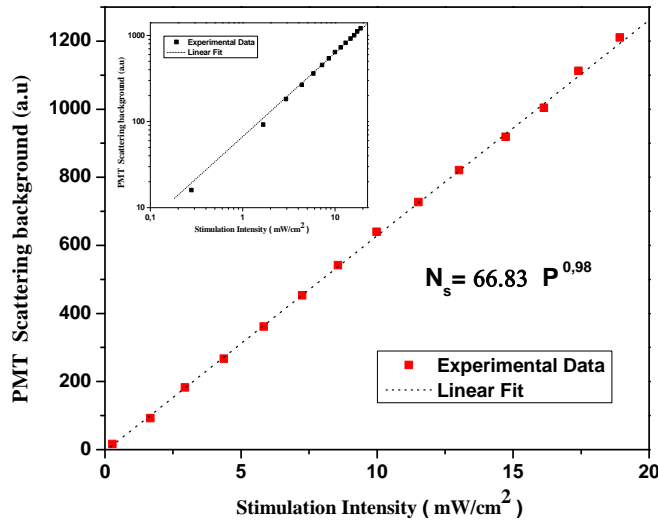
Fig.7.9 Scattering noise background PMT recorded counts due to stimulation intensity.

The PFMS-LM-OSL stimulation response for various values γ (= 0.021 to 0.168 mW/cm^2/s) have been recorded for α-Al$_2$O$_3$:C(as shown in Fig.7.10.a) for absorbed dose of 300 mGy. These PFMS-LM- profile have been generated by selecting different set of PFMS parameters (mostly $\psi_o \tau_p$) keeping fixed value of η and κ. The shift in PFMS-LM- OSL peak is observed with increase in value of intensity ramp rate γ as shown in Fig.7.10a. By assuming nearly 1st order of kinetics, the time required to reach peak in LM-OSL intensity curve can be expressed by taking l=1 in Eq.(7.15b) and incorporating Eq.(7.10) as
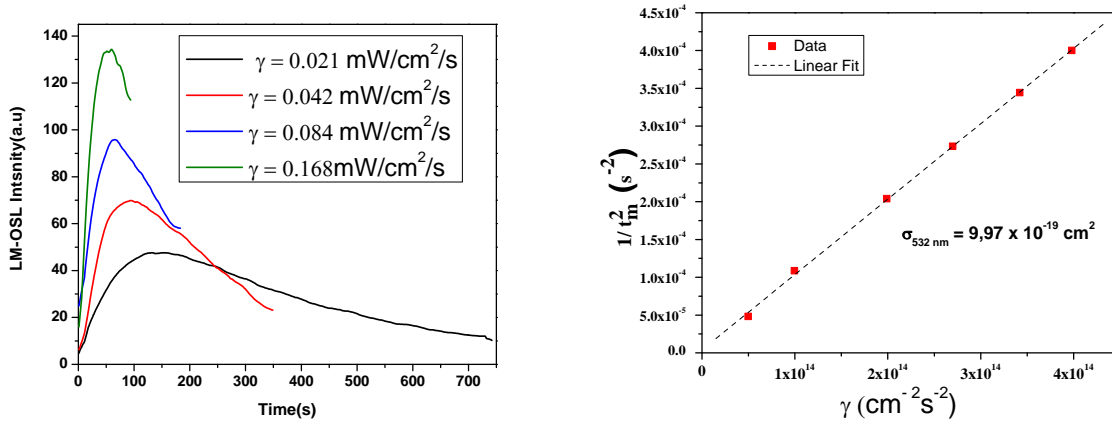
Fig.7.10. a) PFMS LM –OSL recorded of α-Al₂O₃: C recorded for various stimulation ramp rates γ at 300mGy absorbed dose. b) Plot of 1/ t²ₘ Vs various stimulation ramp rates γ for fixed final intensity of 8 mW/ cm². The slope of this line gives value of photo-ionization cross sections σ₅₃₂ ₙₘ.

$$t_m = \left[\frac{1}{\sigma \eta \ \Psi_o \ \tau_p \ \varepsilon \ \kappa} \right]^{\frac{1}{2}} = \left[\frac{1}{\sigma \gamma} \right]^{\frac{1}{2}} \tag{18}$$

The plot of $1/t^2_{max}$ vs stimulation ramp rate γ has been shown in Fig.7.10b. The slope gives as value of photo ionization cross section for 523 nm LASER light as 9.97×10^{-19} cm²; which is ~33% less than the value of photo ionization cross-section measured in chapter 2 for same α-Al₂O₃:C samples to 470 nm blue LED stimulation measured at room temperature [8]. This plot of Fig.7.10b also proves the capability and accuracy of developed PFMS system for generating various stimulation ramp rates (γ).

7.4.2. PFMS-NL-OSL Studies

In order to test the flexibility of developed PFMS system for generating NL- stimulation profiles, NL-stimulation voltage function (as described by Eq.(7.1) and Eq.(7.3)) was given to the frequency modulation system. The Fig.7.11 shows the recorded PFMS NL-stimulation profiles

measured by photodiode placed at sample position for various values of TBP (*l*) by keeping the fixed total stimulation time of 1000 s and fixed final intensity of 8 mW/cm^2 as suggested by Mishra et., al.[6,7].
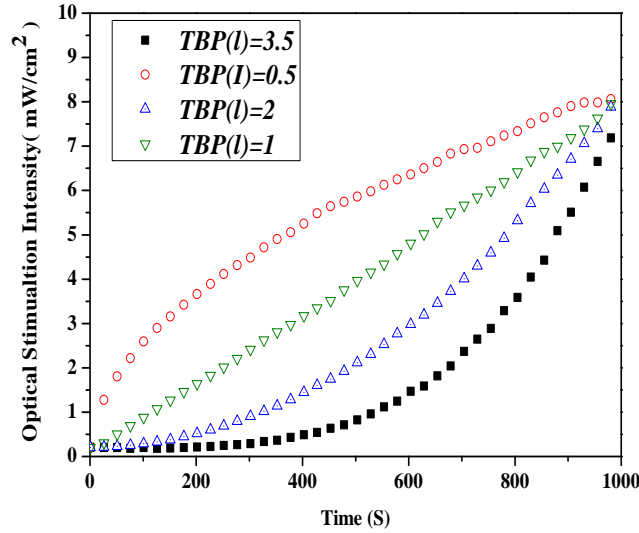
Fig.7.11. Optical stimulation intensity recorded for various stimulation parameter γ' and TBP (l) for fixed final intensity of 8 mW/ cm^2 and time 1000s.

The PFMS NL-OSL of α-Al$_2$O$_3$: C has been recorded for various stimulation profiles TBP (*l*) = 0.5,1,2 and 3.5 as shown in Fig. 7.12 for fixed final intensity of 8 mW/cm^2 and fixed stimulation time of 1000s. The Fig. 7.12 shows that the maximum in PFMS NL-OSL intensity occurs at a longer time with increase in value of TBP as described by Mishra et al.[6,7]. In order to see more detailed effect of PFMS, LM- OSL and NL-OSL (*l*=2) response of α-Al$_2$O$_3$: C has been recorded for 4600s for fixed final intensity ∼ 4.2 mW/cm^2 as shown in Fig.7.13 along with corresponding stimulation profiles. Therefore, potential of the developed PFMS to generate longer and stable NL-stimulation profiles has been depicted in Figs. 7.12 and 7.13.
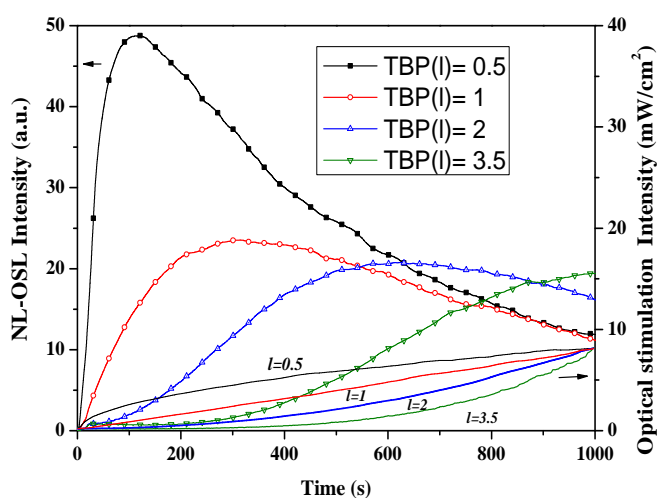
Fig.7.12. PFMS NL–OSL of α-Al₂O₃: C recorded for various stimulation parameter γ' and TBP (l) for fixed final intensity of 8 mW/ cm² and time 1000s at 500 mGy absorbed dose.

This method of generating NL-OSL with frequency duty cycle modulation CW-LASER using electromagnetic shutter is found to be potential method for studying LM-OSL and NL-OSL phenomenon.
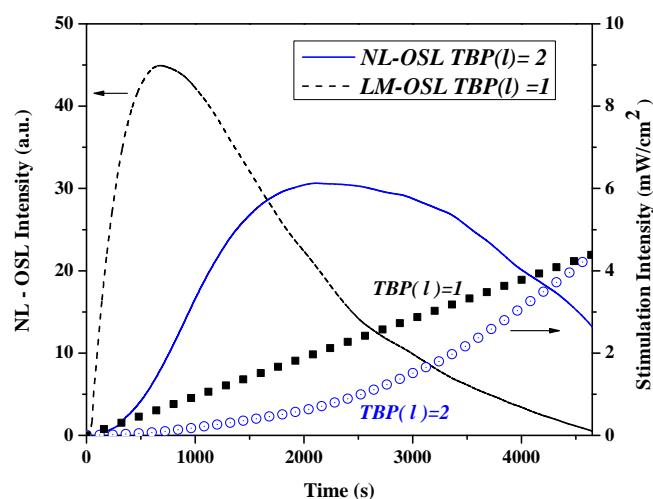
Fig.7.13. PFMS NL-OSL of α-Al₂O₃: C intensity recorded for TBP (l) = 1 and 2 for fixed final intensity of 4.4 mW/ cm² and time 4600 s.

The method provides feasibility to use any type continuous broadband / mono-energetic light source for generating NL-stimulation profiles. It also overcomes from difficulty of warm-up/ stability time requirement for intensity stabilization of such incandesce/ condensed light sources. The different average CW stimulation (as described by Eq.7.12) can also be generated using PFMS method for fixed constant input voltage. The above results have been published in the international Journal [9].

7.4.2. PFMS-TA-OSL Studies

In chapter 3, the deep traps of α-Al_2O_3: C were studied by simultaneous application of constant optical and linear thermal stimulation. The studies resulted in two peaks at 122 and 232 °C respectively. However, the two peaks were not well separated using this combination of stimulation profiles. Therefore, in order to evaluate the TA-OSL parameters of the second peak, first peak was thermally annealed by heating the sample upto 700 °C.
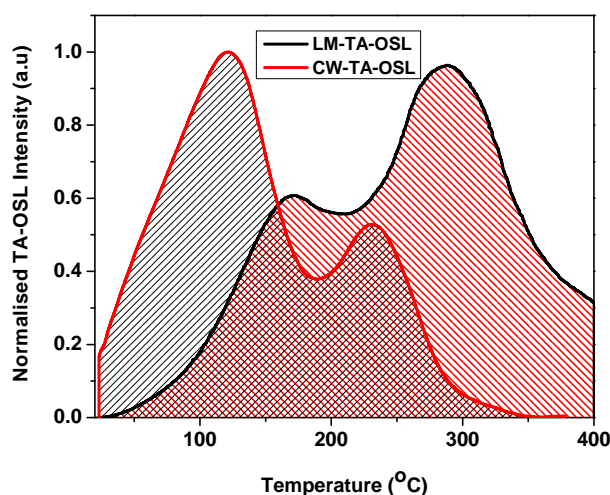
Fig.7.14. Optimization of PFMS based LM-TA-OSL and CW-TA-OSL stimulation profiles for probing the deeper defects of α-Al₂O₃: C.

In the current studies, deep traps of α-Al_2O_3: C were studies by combination of linear optical and linear thermal stimulation (LM-OSL + linear TL) using PFM based system. It is clear from the Fig. 7.14 that the current combination of stimulation profiles found to be better separating the TA-OSL peaks, though the peak positions have been shifted to higher temperatures. It also suggest that the constant optical with linear stimulation profile is the best optimized combination in order to get the information at the lesser temperatures.

7.5. Conclusions

This chapter was about the method of PFM modulation, which is found to be capable of generating different CW-, LM-, NL-stimulation intensity profiles from constant intensity light source. This method has potential to generate greater dynamic NL-stimulation optical power, which may be of great useful in studying very low PIC OSL traps. With incorporation of photo-electric modulator will further refine increase the efficiency of PFMS method. Next chapter will summarize the entire work and also present some of the aspects of the studied materials (particularly α-Al_2O_3:C) that are yet to be explored, setting the tune for the future work.

References

1. Mishra, D.R., Kulkarni, M.S., Rawat, N.S., Muthe, K.P., Gupta, S.K., Bhatt, B.C., Sharma, D.N. 2008. *Radiat. Meas.* 43, 1177.

2. Mishra, D.R., Kulkarni, M.S., Rawat, N.S., Soni, Anuj., Bhatt, B.C., Sharma, D.N. 2011. *Radiat. Meas.,* 46, 1462-1468.

3. Bulur, E., Bøtter Jensen, L., Murray, A.S. 2001. *Nucl. Instr. Meth. in Phys Res. B* 179 151-159.

4. Yukihara, E.G., McKeever, S.W.S. 2011. *A John Wiley and Sons, Ltd., Publication*, p58

5. Haar, H.P., Hauser, M. 1978. *Rev. Sci. Instrum.* 49, 632.

6. Kaminow, L. P., Turmer, E.H. 1966. *Appl. Opt.* 5, 1612

7. Ward, J.F., Frenken, P.A. 1964. *Phys. Rev.* 133, A183

8. Mishra, D.R. , Soni, Anuj., Rawat, N.S., Kulkarni, M.S., Bhatt, B.C., Sharma, D.N. 2011. *Radiat. Meas.* 46, 635.

9. Mishra, D.R., Bishnoi, A.S., Soni, Anuj., Rawat, N.S., Bhatt, B.C., Kulkarni, M.S., Babu, D.A. R. 2015. *Nucl. Inst. Meth. B*. 342, 116-124.

<div align="right">

Chapter 8

</div>

<div align="center">

Summary and Conclusions

</div>

8.1. Summary of the work

The present study has explored the temperature dependence of OSL in oxide based OSL phosphors such as α-Al$_2$O$_3$:C, BasSO$_4$:Eu^{2+} etc. along with their attributes that render them suitable for their application in dosimetry. Although these materials are being developed for their application in OSL domain, their characterization in terms of defects responsible for OSL signal and stability of this signal with time can only be ascertained through TL-OSL correlation studies. Photo-ionization cross-section being the key parameter to judge the dosimetric viability of an OSL phosphor, in this work, its dependence on temperature has been extensively investigated. In addition certain novel experimental techniques which have been specifically devised for TL and OSL characterization of a phosphor have been presented and they constitute an important ingredient of this research work.

<div align="center">243</div>

Temperature dependence of photo-ionization cross-section and determination of thermally assisted energy level in OSL has revealed wealth of information as it is now possible to have an estimate of vibrational energy level of defects. Detailed theoretical simulation and formulation the theory of TA-OSL process has been carried out which matches with the experimental results. The theoretical formulation for determining thermal assistance energy has been very helpful in explaining the thermal assistance nature of OSL dosimetry traps in α-Al$_2$O$_3$: C. The study highlighted the effects of Arrhenius nature observed in temperature dependence of photo-ionization cross-section of OSL dosimetry traps in α-Al$_2$O$_3$: C. Various TA-OSL parameters such as thermally assisted energy, pre-exponential factor, and photoionization cross-section at various temperatures of deeper and dosimetric traps, have been evaluated.

Commercially available α-Al$_2$O$_3$:C powder was studied for deep energy level defects by a newly suggested method using TA-OSL phenomenon. The method involves simultaneous application of CW-OSL as well as thermal stimulation up to 400°C, using a linear heating rate of 4K/s. By using this method, two well defined peaks at 121 °C and 232 °C were observed. These TA-OSL peaks have been correlated to two different types of deeper defects which can be bleached at 650 °C and 900 °C respectively on thermal treatment. These deeper defects, having larger thermal trap depth and relatively lower photoionization cross-section at room temperature for stimulation with blue LED (470nm), are stable up to 500 °C, so they can store absorbed dose information even if the sample is inadvertently exposed to light or temperature. As only a fraction of signal is bleached during TA-OSL readout, multiple readouts could be performed on an exposed sample using this technique. The novel TA-OSL technique enables to measure the signal from deep traps of α-Al$_2$O$_3$:C which were inaccessible using conventional TL and OSL techniques. The technique facilitates the extension the applicability of phosphor up to 10 kGy

utilizing OSL from deeper traps by TA-OSL readout. The phosphor now can be used for high dose dosimetry application such as food irradiation and radiological/nuclear emergencies. The technique has also overcome the limitation of OSL of requirement of dark conditions. Using the technique, nature of deep traps was also identified. The process of thermally assisted OSL has been formulated analytically as well as theoretically for describing the temperature dependence of optical cross-section and evaluation of thermally assisted energy associated with deep traps.

In addition, TA-OSL technique has also been employed to lower the minimum detectable dose (MDD) by a factor of 2 using TA-OSL from filled dosimetry traps. Thus the TA-OSL technique has stretched the dose response and hence the application in both low as well as high dose dosimetry. Besides, MDD has also been demonstrated to be improved significantly by optimizing CW- OSL parameters like stimulation intensity and readout time.

A cryostat integrated TL/OSL reader has been designed and developed to study the temperature dependence of photoionization cross-section at low temperatures. Using this system, TL/OSL studies of α-Al$_2$O$_3$:C have been carried out that showed the existence of low temperature (-8 $^\circ$C) OSL sensitive peak, which can play crucial role in online radiation dosimetry. The low temperature TL studies on commercial and indigenously developed α-Al$_2$O$_3$:C samples reveal that the vacuum annealing in graphite ambience of α-Al$_2$O$_3$ single crystals leads to the formation of same types of defects as in case of commercial α-Al$_2$O$_3$:C single crystals. Hence the PGTI method in which the grown single crystal α-Al$_2$O$_3$ is treated at 1500 °C which is well below its melting point at reducing environment in graphite ambience is equivalent to conventional method in which the crystal is grown from melting, which involves sophisticated technique The studies suggest that the readout protocol of the OSL dosimeter based on Al$_2$O$_3$:C phosphor must consider the calibration temperature of the OSL dosimeter.

$BaSO_4$:Eu^{2+} phosphor has been investigated for its PL, TL, TL kinetics, OSL and TA-OSL response. $BaSO_4$:Eu^{2+} phosphor was found to be 4 times more sensitive than α-Al_2O_3:C in TL mode, and 0.74 times in OSL mode. The temperature dependence of OSL studies showed that integrated TA-OSL signal increases with stimulation temperature between 50 and 250 °C, while between 260 and 450 °C the signal intensity decreases. This behavior is interpreted to arise from competing effects of thermal assistance (activation energy $E_A = 0.063 \pm 0.0012$ eV) and depletion of trapped charges. This increase of OSL at elevated temperature can be employed for enhancing the sensitivity of phosphor for radiation dosimetry. $BaSO_4$:Eu, being high Z material, its good TL and OSL sensitivity and wide dynamic dose range, can be exploited for relative dose measurements for various applications in radiation dosimetry. Similarly, OSL and TA-OSL of dental enamel have also being investigated for possible use of the TA-OSL technique in retrospective dosimetry. The TA-OSL studies showed that integrated TAOSL and thus OSL signal increases with readout temperature between 100 and 250 °C due to the temperature dependence of OSL. The thermally assisted energy E_A associated with this increase in signal is found to be 0.21 ± 0.015 eV. This increase of OSL at elevated temperature can be employed for enhancing the sensitivity of dental enamel for ex-vivo measurements in retrospective dosimetry. The dental sample showed linear OSL dose response up to 500 Gy. The dose threshold is found to be 100 mGy using highly sensitive compact OSL reader with blue LED (470 nm) stimulation. Similar studies were also carried out on Al_2O_3: Si, Ti; Al_2O_3: Mg, Y and Mg_2SiO_4:Tb to ascertain wider applicability of the technique.

The detailed theoretical and experimental approach to novel technique of Pulse Frequency Modulated Stimulation (PFMS) method has been described for OSL phenomenon. The PFMS based LM-, NL-OSL studies have been carried out on dosimetry grade single crystal

α-Al$_2$O$_3$: C. The photo ionization cross section of α-Al$_2$O$_3$: C has been found to be ~9.97 × 10^{-19} cm^2 for 532 nm laser light using PFMS LM–OSL studies under assumption of first order of kinetic. This method of PFMS is found to be potential alternative to generate different stimulation profiles using CW- light sources.

8.2. Challenges and scope of future studies

This research work highlights the temperature dependence of OSL in various oxide based phosphors with great emphasis on α-Al$_2$O$_3$:C. Although sensitivity of α-Al$_2$O$_3$:C is very high but the lacunae associated with this material was that the dosimetric traps show sub-linear dose response for doses > 1Gy and hence put limitations for high dose applications like accidental dosimetry and dosimetry for food irradiation. However, deep traps are supposed to give extended doe response. But, conventional OSL technique using various available visible light sources at room temperature are incapable of accessing deep traps, as the photoionization cross-section of these traps is expected to be very low at room temperature. In other words, the optical energy (470 nm light) is not sufficient enough to reach the deep traps of α-Al$_2$O$_3$:C. To overcome this, additional energy was supplied by thermal mode i.e, simultaneous application of optical as well as thermal stimulation and the dose response was extended.

The thermal energy can also be provided using IR laser or by hot inert gas instead of planchet heating as it would solve two problems, namely, the good thermal contact of the sample with the planchet and other problem of black body radiation. Besides, these deep traps can also be accessed by increasing the optical energy i.e., using UV light, though one has to be careful while choosing the wavelength of the stimulating light, since the emission of the luminescence centers is at 410 nm. Apart from that, the excitation wavelength of F-center lies at 203 while that of F$^+$ center is at 225 and 258 nm respectively. In particular, the excited state of the F–center lies in the bottom of the

conduction band hence 203 nm wavelength cannot be used for stimulation as it will populate the conduction bad instead of detraping the traps. Hence one has to work in between 380- 300 nm to get the maximum response from the material. In this case, thermal assistance might not be required and using high energy, both dosimetric and deep traps can be accessed simultaneously which may lead to the further improvement of MDD of the material. As the dose response of α-Al$_2$O$_3$:C has now been extended upto 100 kGy using TA-OSL, it can be very well tried for food irradiation and compared with conventional dosimeters such as Fricke and Alanine for such application. Recently few TL materials have been tried for temperature sensing. Similarly α-Al$_2$O$_3$:C can also be tried for this application using signal from deep traps.

By using the method suggested for deep traps, further study on material such as quartz and feldspar will help in extending the dose range of these materials for archaeological and geological dating applications. Moreover, photo-ionization cross-section and hence the decay constant in CW-OSL is reported to vary with the LET of the incident radiation. However, the exact cause of it is still not known. As the photo-ionization cross-section depends on two factors namely the pre-exponential factor and the thermally assisted energy, studies can be performed on irradiated α-Al$_2$O$_3$:C for various LET. The measurement of E$_A$ and pre-exponential factor is important to understand the change in value of photoionization cross-section with LET of incident charge particle such as β, α and HCP (Heavy Charge particles).

Apart from this, α-Al$_2$O$_3$:C can also be used to differentiate between the nuclear or conventional blast which is the very urgent requirement these days as one need to have quick answer whether it is normal blast or some kind of dirty bomb. For this, we can make a box of SS (which can sustain thermal shock) in which the α-Al$_2$O$_3$:C will be kept. In case of any nuclear blast, the box and thus the material will not see much temperature in that period of time since the temperature

pulse is of µs only and deeper traps might register the dose and retain the information. Thus, such boxes can be purposely installed at various places which can help us in fighting against nuclear terrorism. Besides, an additional dosimeter can also be placed in the OSLD badge which will be kept in light tight thermally insulated box. It will act like a black box and in case of fire (in the room where all OSLD are kept), dose can be retrieved from it as the deeper traps require both light as well as temperature to gets bleached.

Pulse Frequency Modulated Stimulation (PFMS) method is found to be potential alternative to generate different stimulation profiles using CW- light sources. Future researchers can very well follow its theoretical part and apply on LEDs too and various phosphors can be studied using this technique.